

*Republic of Iraq
Ministry of Higher Education
And Scientific Research
University of Baghdad
College Of Education For
Pure Science Ibn- Al-Haitham
Department of Physics*



*Study and compare influence of the partial
substitution of copper nickel on the physical
properties of superconducting compounds*

A Thesis

*Submitted to University of Baghdad \College of Education for
Pure Science (Ibn-AL-Haitham) in partial Fulfillment of the
Requirements for the Degree of Philosophy Doctorate of
Physics Science*

By

Laheeb Ahmed Mohammed AL-Hamdani

Supervised

by

Prof.Dr . Kareem Ali Jasim

2018 A.D

1439 A.H

بِسْمِ اللَّهِ الرَّحْمَنِ الرَّحِيمِ

اقْرَأْ بِاسْمِ رَبِّكَ الَّذِي خَلَقَ (1) خَلَقَ الْإِنْسَانَ مِنْ عَلَقٍ

(2) اقْرَأْ وَرَبُّكَ الْأَكْرَمُ (3) الَّذِي عَلَّمَ بِالْقَلَمِ

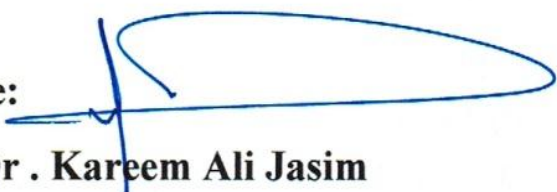
(4) عَلَّمَ الْإِنْسَانَ مَا لَمْ يَعْلَمْ (5)

صدق الله العظيم

سورة العلق

Supervisors Certification

I certify that this thesis "*Study and compare influence of the partial substitution of copper nickel on the physical properties of superconducting compounds*" was prepared by ((**Laheeb Ahmed Mohammed**)) under my supervision at Physics Department, College of Education for Pure Sciences Ibn- Al-Haitham University of Baghdad as partial requirement for the degree Doctor of Philosophy in Physics Science .

Signature: 

Name : Dr . Kareem Ali Jasim

Title : Professor

Address: collage of Education for pure science Ibn-Al - Haitham University of Baghdad

Date : 10/6/ 2018

In view of the available recommendations , I forward this thesis for debate by the Examination Committee .

Signature: S. A. MAKI

Name : Dr . Sameer Atta Makki

Title : Professor

Address : Head of Department of Physics College of Education for pure Science Ibn-Al-Haitham, University of Baghdad .

Date : 10/6/ 2018

Committee Certification

We certify that we have read this thesis and as examination committee we examined the student ((**Laheeb Ahmed Mohammed**)) in its content and in our opinion it is adequate with standard as thesis for the Degree of Doctor of Philosophy in Physics.


Signature: 

Name: Dr. Tahseen H. Mubarak

Title: Professor

(Chairman)

Date: / / 2018


Signature: 

Name: Dr. Khalid Hellal Harbi

Title: Professor

(Member)

Date: / / 2018


Signature: 

Name: Dr. Balqees M. Dheyaa

Title: Professor

(Member)

Date: / / 2018

Signature: 

Name: Dr. Ayser. j Ibrahim

Title: Assistant professor

(Member)

Date: 30/9/ 2018

Signature: 

Name: Dr. Mohammed Abdul-Nebi

Title: Assistant professor

(Member)

Date: / / 2018


Signature: 

Name: Dr. Kareem Ali Jasim

Title: Professor

(Supervisor)

Date: 9/10/ 2018

Signature: 

Name Dr. Hasan Ahmed Hasan

Title: Assistant Professor

Address: The Dean of College of Education for Pure Science Ibn-AL-Haitham University of Baghdad.

إهداء

إلى أعلى البشر

إلى من تعجز الكلمات لتعبر عن مكنون ذاتي

إلى من علمتني لأصل إلى ما أنا فيه

إلى النور الذي ينير لي دربتي

إلى من وهبتني الحياة أمة المحببة

إلى روح والدي الغالي

إلى أخوتي وأخواتي الأعزاء

إلى فراشة قلبي مرهوفة

لهيب

Acknowledgment

First, thanks to Allah his Majesty for his uncountable blessings for helping me to complete this thesis, and I should express my thanks to my country Iraq.

Your kindness is deepest than my words and approbation, that is why I will say thanks only to :

The supervisor, Prof . Dr Kareem Ali Jassim, for invaluable assistance, the Dean of college of Education for pure science Ib Al Haitham University of Baghdad, Assistant Professor . Dr. Hasan Ahmed Hasan, ,the staff of central service laboratory special (Samir Asker & mohammed Hadi),and Ministry of Technology and science .

Also, I would like to extend my special thanks to my family for their help to overcome the distresses and difficulties that I pass through .

I would like acknowledge and express my gratitude for all people who helped me during my course of study especially my close friends .

Laheeb

Abstract

The current thesis involves the preparation of superconducting compounds both of $\text{HgBa}_2\text{Ca}_2\text{Cu}_{3-x}\text{Ni}_x\text{O}_{8+\delta}$, $\text{Hg}_{0.5}\text{Pb}_{0.5}\text{Ba}_2\text{Ca}_2\text{Cu}_{3-x}\text{Ni}_x\text{O}_{8+\delta}$, $\text{TlBa}_2\text{Ca}_2\text{Cu}_{3-x}\text{Ni}_x\text{O}_{9-\delta}$, $\text{Tl}_{0.5}\text{Pb}_{0.5}\text{Ba}_2\text{Ca}_2\text{Cu}_{3-x}\text{Ni}_x\text{O}_{9-\delta}$ and the study of the effect of partial substitution of Pb instead of Hg, Tl and Ni instead of Cu on the structural, electrical and mechanical properties of super compounds $\text{HgBa}_2\text{Ca}_2\text{Cu}_{3-x}\text{Ni}_x\text{O}_{8+\delta}$, $\text{Hg}_{0.5}\text{Pb}_{0.5}\text{Ba}_2\text{Ca}_2\text{Cu}_{3-x}\text{Ni}_x\text{O}_{8+\delta}$, $\text{TlBa}_2\text{Ca}_2\text{Cu}_{3-x}\text{Ni}_x\text{O}_{9-\delta}$, $\text{Tl}_{0.5}\text{Pb}_{0.5}\text{Ba}_2\text{Ca}_2\text{Cu}_{3-x}\text{Ni}_x\text{O}_{9-\delta}$ where $\text{Pb} = 0.5$ and the value of Ni ($x = 0.0, 0.2, 0.4, 0.6, 0.8$ and 1).

The aim of this study is to investigate the conditions and optimal replacement ratios for the formation of the high phase (Hg-1223), Tl-1223) and there stability, then try to obtain the highest critical temperature (High- T_c), as well as to know the ranges of frequency in which these specimens can be worked under normal conditions.

The specimens were synthesized by a solid state reaction method appropriate weights of high purity oxides (HgO, Tl_2O_3 , CaO, CuO, PbO, NiO), powders were mixed using a manual mortar for(40-60) minutes, hydraulic press using under pressure of 7ton / cm^2 for two minutes, in the form of tablets with a diameter of 1.5cm and a thickness of (0.2-0.3cm), specimens were sintered in normal air at 850 ° C for 24 h, (5⁰C / min) in order to obtain a bonding material and to ensure a gradual diffusion between the atoms occur. Then, the specimens were cooled to room temperature at the same heating rate.

The results of XRD showed that all specimens have a tetragonal structure and showed that they contained the large proportion of the high phase (Hg-1223), Ti-12223) with low percentages of the low phases (Hg-1212) (Hg-1201) and (H-1201) Ti-1201) with some impurities, and the highest phase

ratio (Hg-1223) was for specimens $\text{HgBa}_2\text{Ca}_2\text{Cu}_{2.4}\text{Ni}_{0.6}\text{O}_{8+\delta}$, $\text{Hg}_{0.5}\text{Pb}_{0.5}\text{Ba}_2\text{Ca}_2\text{Cu}_{2.2}\text{Ni}_{0.8}\text{O}_{8+\delta}$ which was, (82.959%), (81.737%) respectively and the highest phase ratio (Tl-1223) for specimens $\text{TlBa}_2\text{Ca}_2\text{Cu}_{2.4}\text{Ni}_{0.6}\text{O}_{9-\delta}$, $\text{Tl}_{0.5}\text{Pb}_{0.5}\text{Ba}_2\text{Ca}_2\text{Cu}_{2.6}\text{Ni}_{0.4}\text{O}_{9-\delta}$ was, (85.046%), (83.800%) respectively. The results of the lattice constants ($a = b$, c) showed an increase in the value of c . The ratio (c / a) and the unit cell density for the above specimens have the highest value of the axis c and these values are ($c = 16.2484 \text{ \AA}$), $c = (16.0635 \text{ \AA})$, $c = (16.043 \text{ \AA}^3)$, ($c = 15.8110 \text{ \AA}$) respectively .

By examining the behavior of the specimens through variation the electrical resistivity as a function of the temperature using the four-probe technique, we obtained the values of the critical transition temperatures and the energy gap values of the specimens. All specimens showed a metallic behavior and high transition temperature where the transition temperature which obtained for the specimen $\text{HgBa}_2\text{Ca}_2\text{Cu}_{2.4}\text{Ni}_{0.6}\text{O}_{8+\delta}$ was 138.5K which also had the highest value of the energy gap ($E_g = 0.0421\text{eV}$) and $\text{Hg}_{0.5}\text{Pb}_{0.5}\text{Ba}_2\text{Ca}_2\text{Cu}_{2.2}\text{Ni}_{0.8}\text{O}_{8+\delta}$ the critical transition was to ($T_c = 139\text{K}$) and the energy gap value ($E_g = 0.0419\text{eV}$), $\text{TlBa}_2\text{Ca}_2\text{Cu}_{2.4}\text{Ni}_{0.6}\text{O}_{9-\delta}$) $T_c=134.6\text{K}$ and $E_g = 0.0409\text{eV}$ and for specimen $\text{Tl}_{0.5}\text{Pb}_{0.5}\text{Ba}_2\text{Ca}_2\text{Cu}_{2.6}\text{Ni}_{0.4}\text{O}_{9-\delta}$ the value of $T_c=140\text{K}$ and $E_g = 0.0425\text{e}$.

The dielectric constant (real, imaginary), dielectric loss ($\tan\delta$) and alternating electrical conductivity) properties of the specimens were investigated as a function of frequency in the range (50 Hz-5MHz) at room temperature. It has been observed that there is a clear variation in the dielectric properties with the partial substitution of (Pb) and (Ni), and that both the dielectric (real and imaginary) and dielectric loss decreases with increasing frequency and begin to stabilize after the frequency ($\sim 10\text{KHz}$) and that the alternating electrical conductivity increases with increasing frequency. Since we conclude that the dielectric properties for all specimens depend largely on both the ratio of substitution and frequency.

The mechanical properties of the prepared specimens were calculated. It was observed that the value of the microhardness of the prepared specimens increased by increasing the percentage of partial substitution of nickel relative to the pure specimen.

To determine the surface characteristics of the specimens such as roughness, we tested the specimens by technic of AFM the atomic force microscope where the specimens showed a flaky structure with changes in homogeneity and distribution, where the specimen **Tl_{0.5}Pb_{0.5}Ba₂Ca₂Cu_{2.6}Ni_{0.4}O_{9.8}** it is best for composites prepared with a Avg. diameter equal to 73.54 nm.

It was observed that the effect of partial substitution of nickel instead of copper it was positive effective on all properties in structure as well as in critical temperatures, dielectric and mechanical properties of superconducting compounds.

List Of Contents

<i>subject</i>	<i>Page</i>
<i>Chapter One: "Introduction of Superconductor"</i>	
<i>Historical Introduction</i>	<i>1</i>
<i>Literature Survey</i>	<i>4</i>
<i>Aim of the Work</i>	<i>13</i>
<i>Chapter Two Theoretical Part</i>	
<i>Introduction</i>	<i>14</i>
<i>The superconductors Classification</i>	<i>15</i>
<i>Elementary properties of superconductors</i>	<i>15</i>
<i>Meissner-Ochsenfeld Effect</i>	<i>19</i>
<i>Josephson Effect</i>	<i>21</i>
<i>Fundamentals Parameters Of The Superconductivity</i>	<i>22</i>
<i>Types of the Superconductors materials</i>	<i>24</i>
<i>Theories of superconductivity</i>	<i>26</i>
<i>Theories Of the Superconductor At Low Temperature</i>	<i>26</i>
<i>London theory</i>	<i>26</i>
<i>Ginzburg-Landau Theory</i>	<i>29</i>
<i>BCS -Theory</i>	<i>30</i>
<i>Isotope Effect</i>	<i>31</i>

<i>High-temperature superconductivity ((Cuprate Superconductors))</i>	32
<i>Perovskite Structure</i>	33
<i>Structure of Thallium-Based Cuprate Superconductors TBCCO</i>	34
<i>Mercury Based Cuprate Superconductors HBCCO</i>	35
<i>Theories of High Tc Superconductor</i>	40
<i>Interlayer Coupling Model</i>	40
<i>Exciton Model</i>	41
<i>Isotope Model</i>	41
<i>Spin Fluctuations Model</i>	42
<i>Pairing Symmetry</i>	42
<i>Goddard's Model</i>	43
<i>Plasmon Model</i>	44
<i>Phase Transition</i>	45
<i>Phase Diagram of Cuprate Superconductors</i>	46
<i>Applications of superconductors materials</i>	48
<i>Chapter Three Experimental Works</i>	
<i>Introduction</i>	53
<i>Used Raw Materials</i>	53
<i>The weight ratios of the Powders</i>	54
<i>Specimens Synthesis</i>	58
<i>Description Techniques</i>	59

<i>Structural Study Of The Specimens</i>	<i>60</i>
<i>Measurements of Resistivity And the Critical Temperature</i>	<i>61</i>
<i>Calculation of Oxygen Content</i>	<i>64</i>
<i>Measurements of dielectric constant with different frequencies</i>	<i>65</i>
<i>The Mechanical Properties</i>	<i>66</i>
<i>Atomic Force Microscopy (AFM)</i>	<i>68</i>
Chapter Four	
<i>Introduction</i>	<i>69</i>
<i>HgBa₂Ca₂Cu_{3-x}Ni_xO_{8+δ} Compound</i>	<i>70</i>
<i>Study of Structural Properties</i>	<i>70</i>
<i>Study of Electrical Resistivity</i>	<i>76</i>
<i>Results Of Oxygen Content</i>	<i>82</i>
<i>Study of Dielectric Properties</i>	<i>85</i>
<i>Dielectric Constant (ϵ')</i>	<i>85</i>
<i>Loss Factor Of Dielectric (ϵ'')</i>	<i>88</i>
<i>Dielectric Loss Factor $\tan \delta$ </i>	<i>90</i>
<i>Alternating Electrical Conductivity (σ_{ac})</i>	<i>91</i>
<i>Result Of Mechanical Properties</i>	<i>93</i>
<i>Results of Atomic Forces Microscopic AFM</i>	<i>96</i>
<i>Hg_{0.5}Pb_{0.5}Ba₂Ca₂Cu_{3-x}Ni_xO_{8+δ} Compound</i>	<i>99</i>
<i>Study of Structural Properties</i>	<i>99</i>

<i>Study of Electrical Resistivity</i>	<i>105</i>
<i>Results Of Oxygen Content</i>	<i>109</i>
<i>Study of Dielectric Properties</i>	<i>111</i>
<i>Dielectric Constant (ϵ')</i>	<i>111</i>
<i>Loss Factor Of Dielectric (ϵ'')</i>	<i>113</i>
<i>Dielectric Loss Factor $\tan \delta$ /</i>	<i>115</i>
<i>Alternating Electrical Conductivity (σ_{ac})</i>	<i>116</i>
<i>Result Of Mechanical Properties</i>	<i>118</i>
<i>Results of Atomic Forces Microscopic AFM</i>	<i>121</i>
<i>TlBa₂Ca₂Cu_{3-x}Ni_xO_{9-δ} Compound</i>	<i>124</i>
<i>Study of Structural Properties</i>	<i>124</i>
<i>Study of Electrical Resistivity</i>	<i>130</i>
<i>Results Of Oxygen Content</i>	<i>133</i>
<i>Study of Dielectric Properties</i>	<i>135</i>
<i>Dielectric Constant (ϵ')</i>	<i>135</i>
<i>Loss Factor Of Dielectric (ϵ'')</i>	<i>137</i>
<i>Dielectric Loss Factor $\tan \delta$ /</i>	<i>139</i>
<i>Alternating Electrical Conductivity (σ_{ac})</i>	<i>141</i>
<i>Result Of Mechanical Properties</i>	<i>142</i>
<i>Results of Atomic Forces Microscopic AFM</i>	<i>145</i>
<i>Compound of Tl_{0.5}Pb_{0.5}Ba₂Ca₂Cu_{3-x}Ni_xO_{9-δ}</i>	<i>148</i>
<i>Study of Structural Properties</i>	<i>148</i>
<i>Study of Electrical Resistivity</i>	<i>154</i>

<i>Results Of Oxygen Content</i>	<i>158</i>
<i>Study of Dielectric Properties</i>	<i>159</i>
<i>Dielectric Constant (ϵ')</i>	<i>159</i>
<i>Dielectric Loss Factor (ϵ'')</i>	<i>162</i>
<i>Dielectric Loss Factor $\tan \delta$ /</i>	<i>164</i>
<i>Alternating Electrical Conductivity (σ_{ac})</i>	<i>165</i>
<i>Result Of Mechanical Properties</i>	<i>167</i>
<i>Results of Atomic Forces Microscopic AFM</i>	<i>170</i>
<i>Chapter Five Conclusion And Future Works</i>	
<i>Conclusion</i>	<i>176</i>
<i>Suggestion for Future Works</i>	<i>178</i>

List of symbols

<i>Symbol</i>	<i>Terms</i>
K	Kelvin
T_c	Critical Temperature
(HBCCO)	Hg-Ba-Ca-Cu-O
(TBCCO)	Tl-Ba-Ca-Cu-O
J_c	Critical Current Density
H_c	Critical magnetic flux density
I_c	Critical Current
$H_c(0)$	Critical magnetic flux density at $T=0K$
B_{ext}	External magnetic field
B_{in}	Magnetic field inside the superconductor
$B_{induced}$	The interior magnetic field of the superconductor
H	External magnetic field
M	Magnetization
χ_m	The magnetic susceptibility
ζ	Coherence Length

V_f	Electron velocity at Fermi surface
Δ_0	Energy gap
λ	Penetration depth
n_s	Density of superconducting electrons
m	Mass of electron
GL	Ginzburg - Landau theory
Ψ	Wave function
K_B	Boltzman constant = 1.38×10^{-23} J/k
$N(0)$	Electronic density of state at Fermi level
K	Ginzburg - landau parameter
HTSC	High Temperature Superconductor
F	Force between two like charges (Colum force)
r	Distance between charges
Hg-1223	$HgBa_2Ca_2Cu_3O_{8+\delta}$
Ti-1223	$TlBa_2Ca_2Cu_3O_{9-\delta}$
ABO_3	Formula of the family of perovskite materials
θ	angle between the diffracted and transmitted beam
RVB	Resonance Valence Bands
SSR	Solid State Reaction Method

ρ_m	The density of specimen
W_m	Molecular weight
N_A	Avocadro number = $6.022 \cdot 10^{23} \text{ mol}^{-1}$
SEM	Scanning Electron Microscopy
ϵ'	Real part of dielectric constant
ϵ''	Imaginary part of dielectric constant
$ \tan \delta $	Absolute $ \tan \delta $ loss factor of dielectric
$\sigma_{a.c}$	Alternating electric conductivity
AFM	Atomic Force Microscopy
VHN	Vickers Hardness Number
(L - peak)	Low Phase
(H - peak)	High Phase
BCS-Theory	Bardeen Cooper Schrieffer-Theory

1.1 Introduction:

In solid state physics the important properties that get attention and under very low temperature for many compounds and elements, resistivity disappeared for the material at special temperature. This temperature (critical temperature) depends on type of material, this phenomena is called superconductivity[1].

Superconductivity is an electrical resistance of exactly zero which occurs in certain materials below a characteristic temperature.

Like ferromagnetism and atomic spectral lines, superconductivity is a quantum mechanical phenomenon. It is also characterized by a phenomenon called the Meissner effect, the ejection of any sufficiently weak magnetic field from the interior of the superconductor as it transitions into the superconducting state. The occurrence of the Meissner effect indicates that superconductivity cannot be understood simply as the idealization of perfect conductivity in classical physics[2]. In superconductor, high electric current density permanently flows with absolutely without power loss [3].

The phase transition occurring at temperature called critical temperature T_c . The superconducting state can be destroyed by sufficiently strong magnetic field H_c and critical current I_c .

Onnes, first discovered superconductivity, in 1911 he started exploring the electrical properties of metal at extremely low temperature. He passed a current through a wire of pure mercury at low temperature. Mercury was chosen because it could be obtained in a very pure form [4]. There was no leveling off of the resistance, but at 4.2 K the resistance of the mercury wire suddenly vanished. In 1933, Meissner and Ochsenfeld have demonstrated that a superconductor excludes the magnetic flux and it was a perfect diamagnetic material[5] this is called a Meissner effect. In 1933 London proposed their phenomenological theory of superconductivity

to describe both infinite conductivity and diamagnetic aspects[6]. They proved that not all magnetic flux was excluded but it had a penetration depth. In 1950 Ginzburg and London introduced a quantum mechanical–phenomenological treatment based on a based complex wave function to treat the transition from the normal to the superconducting state[7]. The theory of superconductivity propose by Bardeen, Cooper and Schrieffer (BCS), in 1957, has successfully explained essentially all of the phenomena associated with the superconducting states[8]. Such phenomena included specific heat, critical field, tunneling, etc.

Bednoz . and Muller [9], began exploring a class of compounds composed of Lanthanum, Barium, Copper and Oxygen, commonly known as La-Ba-Cu-O. Chu et al [10], showed that the T_c could be raised by raising the pressure. In 1987, Wang et al.[11] found superconductivity at 90 K in a compound containing yttrium, barium, copper and oxygen. This significant it was the first time that a superconductor had broken the liquid nitrogen barrier, since it had a T_c greater than 77.2 K (the boiling point of liquid nitrogen). These compounds come to be known as high- temperature superconductors (HTS). An entire series of HTS materials have been found to exist when almost any rare earth atom is substituted for yttrium. In 1988, Meada et al. [12] announced the discovery of a compound containing Bismuth, Strontium, Calcium, Copper and Oxygen having a T_c of 110 K which showed multiple superconducting phases, and in the same year the discovery was made of a compound Tl-Ba-Ca-Cu-O with transition temperature up to 125 K by Sheng et al. [13] in 1993 Schlling et al. discovered HgBaCaCuO system has a transition temperature of about 130K [14].

Many laboratories throughout the world have reported the evidence for superconducting at room temperature for $(Tl_2Pb_2) Ba_2MgCu_{10}O_{17+\delta}$, but these however, have to be confirmed conclusively. The behavior of the resistivity as a function of temperature is shown in Figure (1-1):

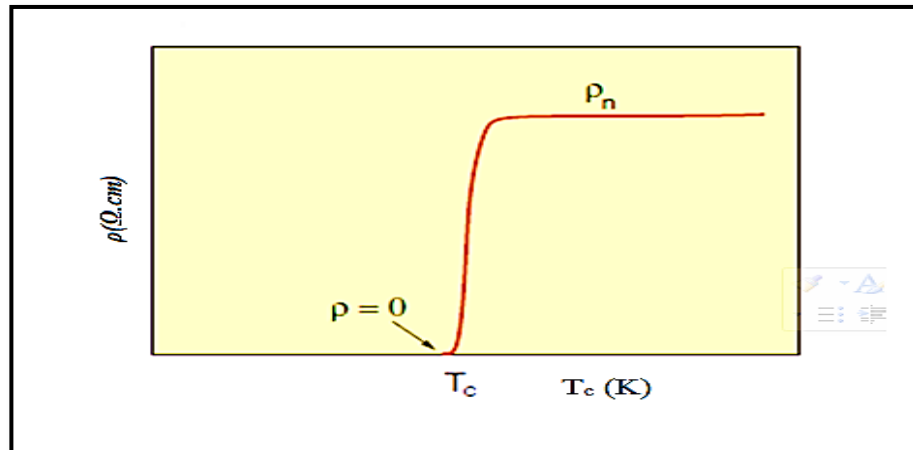


Figure (1-1): Behavior of the resistivity [15].

Finally when cooled to sufficiently low temperatures, a large number of metals and alloys can conduct electric current without resistance. Obviously, these specific materials undergo a phase transition to a new superconducting state characterized by the complete loss of d.c. resistivity below a well defined critical temperature, T_c [15].

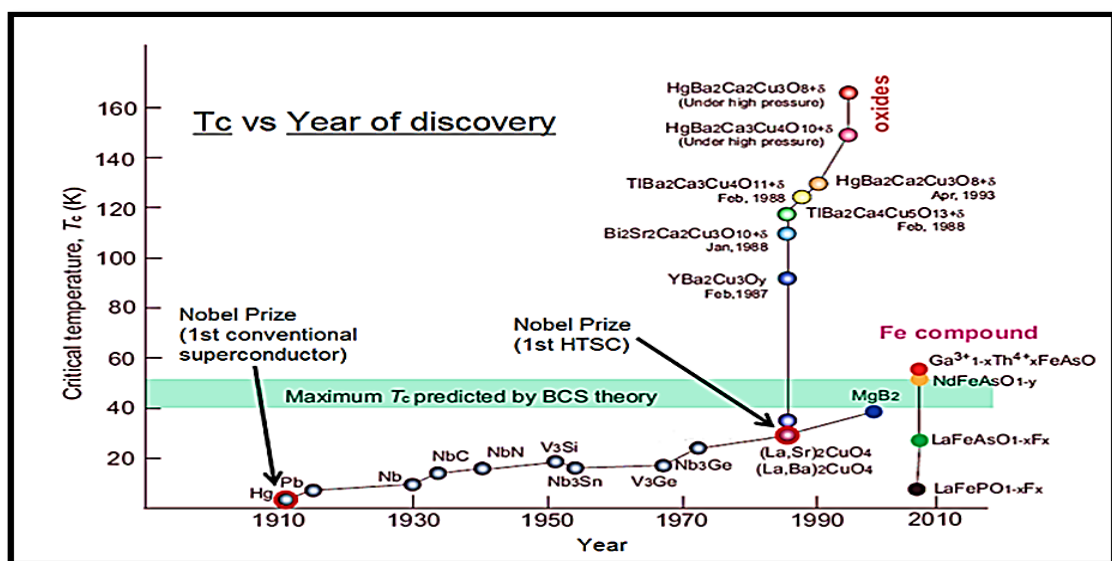


Figure.(1-2) : The Evolution of Tc with time [16].

1-2 Literature Survey:

Axnas et al.[17] (2000) measured conductivity and magnetoconductivity of polycrystalline $\text{Hg}_{1-x}\text{Tl}_x\text{Ba}_2\text{Ca}_2\text{Cu}_3\text{O}_{8+\delta}$ with $x=0$ and 0.2 . They have found that the transition temperature of Hg-1223 is 132 K and Hg-Tl-1223 is 134 K, and the resistivity ρ in zero magnetic field is much larger than for single crystal due to grain boundaries and random orientation of grains.

In the same year **Giri et al. [18]** (2001) reported investigations on the effect of substitution of Bi and Tl at the Hg sites in the oxygen deficient HgO_δ layer of $\text{HgBa}_2\text{Ca}_2\text{Cu}_3\text{O}_{8+\delta}$ cuprate superconductor. They prepared the specimens by the two-step reaction process and observed that the as-grown $\text{HgBi}_{0.2-x}\text{Tl}_x\text{Ba}_2\text{Ca}_2\text{Cu}_3\text{O}_{8+\delta}$ (with $x=0, 0.05, 0.1, 0.15,$ and 0.2) corresponds to the Hg-1223 phase. It has been found that the T_c varies with the average cationic size of the dopant cations.

The optimum T_c of ~ 131 K has been found at $x=0.05$ with a highest stability, while **Hamdan et al. [19]** (2001) prepared $\text{Hg}_{0.8}\text{Pb}_{0.2}\text{Ba}_2\text{Ca}_2\text{Cu}_3\text{O}_{y/Fx}$ (Hg, Pb)-1223 with a nominal fluorine content (weight ratio of BaF2) by a two-step solid-state reaction method and found that fluorine addition promotes the phase formation, the change carrier concentration and observed an increasing in both of T_c and J_c through controlled fluorine incorporation.

In the same year, **Altshuler et al. [20]** (2002) studied the magnetization hysteresis of $(\text{Hg}_{1-x}\text{Re}_x)\text{Ba}_2\text{Ca}_2\text{Cu}_3\text{O}_{8+\delta}$ superconductor for $x=0.1, 0.18$ and 0.25 . From this curve they found that the onset temperature T_c (onset) is close to (133.2- 131.7) K. Also, they showed that the partial substitution of Hg by Re increases the stability and pinning strength of the Hg-1223 phase, supposedly due to a decrease of the Cu–O interlayer distance, metallization of the interlayer planes, and added the structure disorder.

Han et al. [21] (2003) have measured the resistivity for polycrystalline $\text{Hg}_{1-x}\text{Tl}_x\text{Ba}_2\text{Ca}_2\text{Cu}_3\text{O}_{8+\delta}$ ($x=0.0$ and 0.2) in zero field and above the superconductor T_c . Also they analyzed the fluctuated conductivity ($\Delta\sigma$). With decreasing temperature two crossover temperatures could be identified for each specimen. The c -axis coherence length and the interlayer coupling factor were obtained.

Hase et al. [22] (2004) they reported the synthesis of $\text{HgBa}_2\text{Ca}_{n-1}\text{Cu}_n\text{O}_{2n+2+\delta}$ phases with ($n = 3, 4$) and on relationship between their structural and physical properties. They calculated Fermi velocities V_f and Fermi surface volume. From measurements of Fermi surfaces, they found (0.93-1.11) holes in Hg-1223 and (0.90 - 1.14) holes in Hg-1234 and an anisotropy defined by the ratio V_{fx}/V_{fy} is similar to that in $\text{TlBa}_2\text{Ca}_2\text{Cu}_3\text{O}_9$.

Monteverde et al. [23] (2005) have measured the pressure sensitivity of T_c in fluorinated $\text{HgBa}_2\text{Ca}_2\text{Cu}_3\text{O}_{8+\delta}$ ceramic specimen with different (F) contents, applying pressures up to 30 GPa. They obtained an increase of T_c with the increase of pressure, reaching different maximum values, depending on the F doping level, and pressures. High $T_c = (166 \pm 1)$ K was achieved by applying 23 GPa in fluorinated Hg-1223 sample near the optimum doping level.

Abbas. [24]. (2006) have prepared HTSC with a nominal composition $\text{Hg}_{1-x}(\text{Ag}, \text{In})_x \text{Ba}_{2-y} \text{Sr}_y \text{Ca}_2\text{Cu}_3\text{O}_{8+\delta}$ for ($0 \leq x \leq 0.5$) and ($0 \leq y \leq 0.5$) by a solid state reaction method. The effect of the substitution of (Ag, In) on Hg sites and Sr for Ba sites, sintering time, sintering temperature and γ -irradiation has been investigated to obtain the optimum conditions for the formation and stabilization of the high T_c -1223 phase. was found that substitution of Ag and Sr together enhances T_c to 127 K at $x=0.2$ and $y=0.1$, while for the samples substituted with In and Sr together give

$T_c=125$ K at $x=0.3$ and $y=0.1$. XRD analyses have showed a tetragonal structure and there is an increase of c -lattice parameter with increasing of Ag up to 0.3, while samples doped with In have showed a decrease in c -lattice parameter.

G. Y. Hermiz [25] [2008] studied the influence of pressure on the properties of $\text{HgBa}_2\text{Ca}_2\text{Cu}_3\text{O}_{8+\delta}$ HTSC system for different values of pressure (0.2, 0.3, 0.5, 0.6, 0.9, 1.0 & 1.1) GPa is synthesized by a solid state reaction method. It has been proved that the specimens at $P=0.2$ GPa were semiconductor, but the action of the other specimens was superconductor in the temperature rang (80-300) K. Also the $T_c =143\text{K}$ is the utmost at $P =0.5\text{GPa}$. XRD exhibits a tetragonal structure with the lowering of the lattice constant c with the raising of the pressure. Also we prove rising of the density with the pressure.

K. A. Jassim [26] (2009) studied the effect of simultaneous substitution of Tl on the Hg site in the oxygen deficient HgO_δ layer of $\text{Hg}_{1-x}\text{Tl}_x\text{Ba}_2\text{Ca}_2\text{Cu}_3\text{O}_{8+\delta}$ superconductor. Polycrystalline specimens are synthesized by the 2 step solid state reaction method. Electrical resistivity measured by four probe technique. The highest T_c (zero) were (108, 102, 113, 118, 125 and 121) K for $\text{Hg}_{1-x}\text{Tl}_x\text{Ba}_2\text{Ca}_2\text{Cu}_3\text{O}_{8+\delta}$ with $x = 0.0, 0.05, 0.10, 0.15, 0.20$ and 0.25 respectively. The best T_c (zero) =125 K and T_c (onset) = 136K was reported for the compound $\text{Hg}_{0.8}\text{Tl}_{0.2}\text{Ba}_2\text{Ca}_2\text{Cu}_3\text{O}_{8.293}$. All the specimens were synthesized with O_2 flow. (XRD) test gives a pseudo tetragonal structure with growing of the c -axis lattice constant for the specimens doped with Tl as compared with these that have no Tl content. It was discovered that the variety of the Tl ratio of all specimens gives a variation in the mass density ρ_m , c/a and volume fraction V_{Ph} (1223).

O. Babych et al [27] (2010) studied the synthesis and characteristic of Hg-based $\text{HgBa}_2\text{Ca}_2\text{Cu}_3\text{O}_{8+\delta}$ (Hg-1223) superconducting doped with Pb, Fe and Cd ceramics that were performed. Hg-free precursor $\text{Ba}_2\text{Ca}_2\text{Cu}_3\text{O}_{8+\delta}$ composed by the sol-gel method. The superconducting and impurity phases were calculated by using (SEM) and microprobe analysis shows that there are three main phases in the precursor material. Measurement of temperature dependences of the resistivity of doped $\text{HgBa}_2\text{Ca}_2\text{Cu}_3\text{O}_{8+\delta}$ ceramics (for the example of Fe doping) has given result that after the synthesis, the specimens are in oxygen over doped state and reach the optimum state in flowing argon. The Fe doped specimens of $\text{HgBa}_2\text{Ca}_2\text{Cu}_3\text{O}_{8+\delta}$ show lowering T_c .

K. A. Jassim et al [28] (2011) studied mercury-lead-antimony based superconductors with the formula $\text{Hg}_{0.5}\text{Pb}_{0.5-x}\text{Sb}_x\text{Ba}_2\text{Ca}_2\text{Cu}_3\text{O}_{8+\delta}$ ($x=0, 0.10$ and 0.15) have been prepared by using three step solid state reaction processes. the specimens doped with Sb as compared with these which have no Sb content. Was found that the increase of the Sb concentrations of all specimens produce an increase of the volume fraction (V_{phase}) and decrease c/a and Mass density ρ_M .

Kareem A. Jasim[29](2012) studied $\text{Hg}_{0.8}\text{Cu}_{0.15}\text{Sb}_{0.05}\text{Ba}_2\text{Ca}_2\text{Cu}_3\text{O}_{8+\delta}$ High temperature superconducting samples were prepared by using a standard solid-state reaction method with different sintering temperatures of 1073, 1093, 1113, 1133 and 1153 K. It was found that the increase of sintering temperatures from (1073–1153 K) caused an extremely high amount of decomposition of the low-phase (1212) superconductor and produced high-phase (1223) superconductors.

Shibing Wang et al., [30] (2014) studied the strain derivatives of T_c along the a and c axis have been calculated for $\text{HgBa}_2\text{CuO}_{4+\delta}$ (Hg1201), and the modest one layer of CuO_2 with the highest T_c of all one layer was ($T_c = 97$ K) at pest doping. The under doped compound with the first T_c of 65 K has been thoughtful as a function of pressure up to 20 GPa by magnetic susceptibility and (XRD). They found that linear growing in T_c with pressure is the same as already calculated for the optimum doped compound. The above results have a realization of the radix of the various T_c values of optimum doped Hg-1201 and the research about the compound $\text{La}_{2-x}\text{Sr}_x\text{CuO}_4$ (LSCO), which have a utmost T_c of 40 K.

M. M. Abbass, [31](2014) reported to Raman studies of $\text{Hg}_{1-x}\text{Cu}_x\text{Ba}_2\text{Ca}_2\text{Cu}_3\text{O}_{8+\delta}$ compounds. Solid state reaction method by 2-steps is used to prepare $\text{Hg}_{1-x}\text{Cu}_x\text{Ba}_2\text{Ca}_2\text{Cu}_3\text{O}_{8+\delta}$ specimens where $x = 0.1$ and 0.5 . Comparative Raman studies of Cu-doped $\text{Hg}_{1-x}\text{Cu}_x\text{Ba}_2\text{Ca}_2\text{Cu}_3\text{O}_{8+\delta}$ which were acquired in an effort to explain the phonemic amendments induced by Cu doping. A number of phonon peaks is presented up in the spectra assigned to different phases, usually few amounts of starting material that have not reacted. Strange phases have much larger Raman signals and present up strongly in the spectra.

N. M. Hamdan et. al. [32] (2015) studied fluorination of Pb-doped $\text{HgBa}_2\text{Ca}_2\text{Cu}_3\text{O}_{8+\delta}$ (Hg-1223) system. Structural and magnetic measurements detect that fluorine extension raised the phase formation, optimum the charge carrier concentration, and raised flux pinning. They report growing in both the (T_c) and the (J_c) out of controlled fluorine combination. Even a possible variation in the pinning mechanism in this technologically important system is suggested.

B. Loret et al., [33] (2016) studied un-classical high energy state contribution to the Cooper pairing in down doped copper-oxide superconductor $\text{HgBa}_2\text{Ca}_2\text{Cu}_3\text{O}_{8+\delta}$. They research the temperature of

dependent electronic B1g Raman restraint of a slightly under doped single crystal $\text{HgBa}_2\text{Ca}_2\text{Cu}_3\text{O}_{8+\delta}$ with a superconducting $T_c = 122$ K. They found that superconducting pair-breaking peak is related to a slope on its higher energy side vanish together at T_c . This result signs at an un-classical pairing mechanism, whereas spectral weighting missing in the slope is transported to the pair breaking peak at lower energies. This deduction is propped by cellular dynamical mean field theory on the Hubbard model, which could reproduce all of the major features of the B1g Raman response and expound the peak slope behavior in terms of a nontrivial relationship between the superconducting and the pseudo gaps.

Noor S. Abed et al, [34](2017) have studied the effect of the Ag partial substitution at Hg site in HgO_δ layer on the structure, T_c and oxygen content for Hg-1223 have been studied. High temperature superconductor composition $\text{Hg}_{1-x}\text{Ag}_x\text{Ba}_2\text{Ca}_2\text{Cu}_3\text{O}_{8+\delta}$, with $x=(0.0, 0.05, 0.1, 0.15, 0.2, 0.25$ and $0.3)$ have been prepared using solid state reaction method. Annealing temperature 850°C for (24) hours with a rate of $5^\circ\text{C}/\text{min}$ and under a pressure of $7 \text{ ton}/\text{cm}^2$.

[35]**K A Jasim & L A Mohammed**, [35] (2018) studied the effect of partial substitution of Cu by Ni for $\text{HgBa}_2\text{Ca}_2\text{Cu}_{3-x}\text{Ni}_x\text{O}_{8+\delta}$ compound when $x=0.2, 0.4, 0.6, 0.8$, have been prepared by using method solid state reaction the temperature sintering 850°C for (24) hours, the pressure of pressing equal to $7 \text{ ton}/\text{cm}^2$ they obtained the optimum critical temperature $T_c=137$ K.

Prauch et al [36](2000) studied Tl-based cuprate $\text{Tl}_{0.5}\text{Pb}_{0.5}\text{Ba}_{0.4}\text{Sr}_{0.6}\text{Ca}_2\text{Cu}_3\text{O}_x$ superconducting of $2\text{-}60\mu\text{m}$ films thickness were obtained using the screen printing technique with a two-step method, comprising deposition of a precursor film on polycrystalline, 8 mol%. Y_2O_3 doped ZrO_2 , substrate followed by Tl-vapor annealing at 910°C . The electrical resistivity measurements of thin films yielded $T_c(0)$ values in the

range 110-115K with transition widths of 2.4 K, which was due to the major Tl-1223 superconducting phase, as confirmed by the x-ray diffraction.

Badica et al[37] (2002) prepared $\text{Cu}_{0.5}\text{Tl}_x\text{Ba}_2\text{Ca}_3\text{Cu}_4\text{O}_{12+y}$ from free-oxides: Tl_2O_3 , BaO, CaO and CuO. Oxygen content has been controlled by using a certain amount of Cu_2O instead of CuO in the starting mixture or by placing in Au-tube a pellet of Ag_2O together with the specimens. Specimens sealed in the Au tubes were heated by applying a constant heating rate of $0.11^\circ\text{C}/\text{min}$ between 860°C and 880°C . They found that T_c of the specimens is in the range 119.1-111.3K. Both Tl and oxygen content is important for the transport properties of the superconducting grains. On the other hand the phase content strongly depends on Tl content.

Kayed [38](2003) studied the effect of Li doping on the properties of Tl-based superconductors by adding different amount of Li_2CO_3 to the $\text{Tl}_{1.8}\text{Ba}_2\text{Ca}_{2.2}\text{Cu}_3\text{O}_x$ compound. The highest T_c was observed after adding 1wt% of the Li_2CO_3 to the compound. The x-ray data of the specimens showed a tetragonal structure with a high ratio of Tl-2223 superconducting phase. The specimen showed a transition at 125K and zero resistance was observed at 117K.

Eu-substituted $(\text{Tl}_{0.6}\text{Pb}_{0.4})(\text{Sr}_{0.9}\text{Ba}_{0.1})_2(\text{Ca}_{1-x}\text{Eu}_x)\text{Cu}_2\text{O}_4$, for $x=0.2, 0.4$, and 0.6 compounds were prepared by **Kuzman et al.** [39](2004). They demonstrated that Eu can be substituted for Ca in separating the layer between Cu-O conducting layers, Cu atoms are in the center of the basal plane of pyramids of the conducting layers, in the spacing layer Ba atoms are shown, and oxygen atoms are situated both in the corners of the pyramids and in the insulating layer, surrounded by Tl atoms.

Przybylski et al . [40](2005) used the transmission electron microscopy (TEM) to investigate the microstructure of $(\text{Tl}_{0.5}\text{Pb}_{0.5}) (\text{Sr}_{0.8}\text{Ba}_{0.2}\text{Ca}_2\text{CuO}_y)$ thin films. TEM showed that the films contained planar defects such as stacking faults and twinning along the (100) zone axis and the numerous planar defects were accompanied by visible dislocations .One may assume that defects such as dislocations, stacking faults as well as twinning act as pinning sites for flux lines, thereby enhancing the in-field critical current densities.

R Awad et al .[41](2007) have been calculated parameters of Lattice and the volume thermal expansion coefficient, from room temperature down to 80 K for $\text{TlBa}_2\text{Ca}_2\text{Cu}_{3-x}\text{Mo}_x\text{O}_{9-\delta}$ with $x = 0.0, 0.05, 0.1$ and 0.2 using x-ray powder diffraction. The transition temperature for the samples prepared, determined from electrical resistivity measurements, is suppressed from 122 to 98 K as the Mo content increases from 0.0 to 0.2.

Kareem A. Jassim et al .[42](2009) prepared High temperature superconductors $\text{Tl}_{0.6} \text{Pb}_{0.4}\text{Ba}_{2-x}\text{Sr}_x\text{Ca}_2\text{Cu}_3\text{O}_{9-\delta}$.The substitutions for this compound were taken as $x = 0.0, 0.10, 0.20, 0.30, 0.40$ and 0.50 . The optimum calcination was at 1073 K and for sintering was within 1128–1133 K. The highest $T_c(\text{offset})$ was 113 K for $\text{Tl}_{0.6}\text{Pb}_{0.4}\text{Ba}_{1.5}\text{Sr}_{0.5}\text{Ca}_2\text{Cu}_3\text{O}_{8.76}$.

AI Abou Aly et al [43](2010) studies the Systematic on the $\text{Tl}_{1-x}\text{As}_x \text{Ba}_2\text{Ca}_2\text{Cu}_3\text{O}_{9-\delta}$ system, with $0.0 \leq x \leq 0.3$, have been carried out to investigate the effect of arsenic on the superconductivity of Tl-1223 phase. The specimens prepared were characterized identification by X-ray (XRD), (SEM), electron dispersive X-ray(EDX) and electrical resistivity measurements.

E.Erbilen et al [44](2013) have been studied the effects of the vanadium substitution for Ca sites on the Tl-2223 superconductor. The specimens with nominal composition $\text{Tl}_2\text{Ba}_2\text{Ca}_{2-x}\text{V}_x\text{Cu}_3\text{O}_y$ ($x=0.0, 0.1, 0.3, 0.5, 0.7$) have been prepared by the solid-state reaction method. the critical temperature (T_c) has increased for the first two substitution values, for the last two substitution values T_c has decreased. Higher amounts of vanadium substitution have caused non-superconductor. As a result, low vanadium substitution for Ca sites improved the Tl-2223 superconducting properties.

M.G.Ranjbar et al[45](2015) have been reported The effect of Cr substitution on the compound superconductors Tl-1223 type phase Specimens with nominal starting composition $(\text{Tl}_{1-x}\text{Cr}_x)\text{Ba}_2\text{Ca}_2\text{Cu}_3\text{O}_{9-\delta}$ (Tl-1223) for $x=0.3-0.9$ were prepared using the solid state reaction method. The $x=0.3, 0.4$ and 0.5 specimens showed a mixed Tl-2212 and Tl-1223 phase. The specimens with $x=0.6, 0.7$ and 0.8 showed a single Tl-1223 phase. The $x=0.6$ specimen showed the highest onset temperature of 124 K and zero-resistance temperature of 116 K.

M. G. Ranjbar et al [46](2016) Studied The Tl-1223 ($n=3$)phase superconductor compositions $(\text{Tl}_{1-x}\text{Cr}_x)\text{Ba}_2\text{Ca}_2\text{Cu}_3\text{O}_{9-\delta}$ with ($x = 0.4-0.8$) has been prepared by the solid-state reaction method. "The Aslamazov–Larkin (AL) theory was used to investigate the dimension of fluctuation-induced conductivity λ . The coherence length $\xi_c(0)$ Josephson coupling J , and anisotropy γ of the samples were calculated by using the Lawrence–Doniach (LD) theory. The highest T_c onset and T_c zero were observed in the $x = 0.6$ specimen. All specimens showed the Tl-1223 as the dominant phase. The Cr substitution induced 2D to 3D conductivity transition, and the highest transition temperature, T_{2D-3D} , was observed for $x = 0.5$. The LD model showed a decrease in the coherence length, $\xi_c(0)$ and interlayer coupling for $x = 0.6$ and 0.7 specimens These results showed that factors other than J and $\xi_c(0)$ are more important in optimizing the

superconducting transition temperature. Our results showed that excess conductivity occurs at a higher temperature for a higher- T_c superconductor".

1-3 Aim Of The Work:

Preparation of superconducting compounds (Hg ,Tl)-basis and study the effect of partial substitution of nickel in copper sites and Pb in (Hg,Tl), on the high- T_c phase, for the $HgBa_2 Ca_2 Cu_3 O_{\delta+8}$, $TlBa_2 Ca_2 Cu_3 O_{\delta-9}$ with Pb=0.5 and nickel variation concentration equal $x = 0, 0.2, 0.4, 0.6, 0.8$ and 1.0, by method of solid state reaction, then examine the specimens that synthesised to identify the properties of physical "structurally, electrical, mechanical".

And to find the optimum ratio of partial substitution that gives the higher value of critical temperature T_{cas} and its relation to the replacement ratio for either of Pb for Hg ,Tl and Ni for instead of Cu and comparing of these results obtained.

"Theoretical Part "

2-1 Introduction:

In physics, many phenomena result from the activity of specific mutual interactions. An important example is the relation between the uncorrelated thermal motion of the atomic building blocks of matter and the ordering forces between these building blocks. With increasing temperature, the thermal motional energy eventually becomes sufficiently large compared to some relevant ordering interaction energy that the ordered state of matter, established at low temperatures, breaks down. All phase transitions, say, from the liquid to the gaseous state, as well as the construction of the atoms themselves from the elementary constituents of matter, follow this rule. Therefore, it is not surprising that often unexpected new properties of matter, which subsequently also may become important for technology, are discovered in experiments performed under extreme conditions. Superconductivity is an example of such a discovery[47].

A perfect superconductor is a material that exhibits two characteristic properties, namely zero electrical resistance and perfect diamagnetism, when it is cooled below a particular temperature T_c , called the critical temperature. At higher temperatures it is a normal metal, and ordinarily is not a very good conductor. For example, lead, tantalum, and tin become superconductors, while copper, silver, and gold, which are much better conductors, do not super-conduct. In the normal state some super-conducting metals are weakly diamagnetic and some are paramagnetic[48].

The vanishing of the electrical resistance below a “critical temperature” or “transition temperature” T_c is not the only unusual property of superconductors. An externally applied magnetic field can be expelled from the interior of superconductors except for a thin outer layer (“ideal diamagnetism” or “Meissner- Ochsensfeld effect”), or superconductors can concentrate the magnetic field in the form of “flux tubes”[47].

2-2 The superconductors Classification:

There is not just one criterion to classify superconductors. The most common are[2]:

- **By their physical properties:** they can be Type I (if their phase transition is of first order) or Type II (if their phase transition is of second order).
- **By the theory to explain them:** they can be conventional (if they are explained by the BCS theory or its derivatives) or unconventional (if not).
- **By their critical temperature:** they can be high temperature (generally considered if they reach the superconducting state just cooling them with liquid nitrogen, that is, if $T_c > 77$ K), or low temperature (generally if they need other techniques to be cooled under their critical temperature).
- **By material:** they can be chemical elements (as mercury or lead), alloys (as niobium-titanium or germanium-niobium), ceramics (as YBCO or the magnesium diboride), or organic superconductors (as fullerenes or carbon nanotubes, which technically might be included among the chemical elements as they are made of carbon).

2-3 Elementary properties of superconductors:

Most of the physical properties of superconductors vary from material to material, such as the heat capacity and the critical temperature, critical field, and critical current density at which superconductivity is destroyed.

On the other hand, there is a class of properties that are independent of the underlying material. For instance, all superconductors have *exactly* zero resistivity to low applied currents when there is no magnetic field present or if the applied field does not exceed a critical value. The existence of these "universal" properties implies that superconductivity is a thermodynamic phase, and thus possesses certain distinguishing properties which are largely independent of microscopic details[2].

The many important factors : such as the critical temperature T_c , the critical current density J_c and the critical magnetic field H_c , is very dependent each of these factors on the other factors.

In general the higher value of H_c , the T_c value is lower and vice versa .

Figure (2-1) illustrates the superconducting critical surface parameters , J_c , T_c and H_c [15].

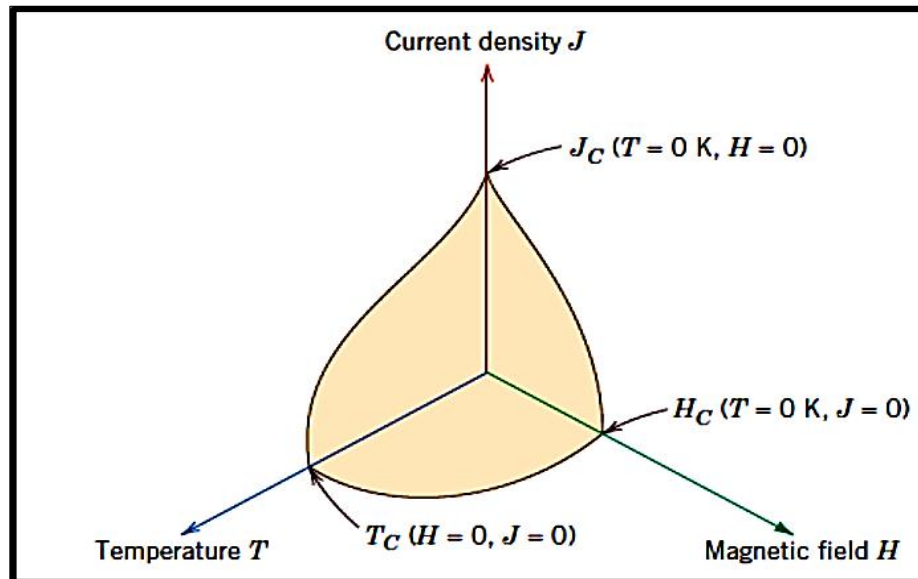


Figure:(2-1) :the Superconducting critical surface [15] .

(i) **Zero Resistivity**, i.e. Infinite Conductivity ($\rho = 0$ for all $T < T_c$): The d.c. (zero frequency) electrical resistance of a superconductor at all temperatures below a critical temperature T_c is practically zero Figure (2-2). In the first approximation, the transition is not accompanied by any change in structure of property of the crystal lattice and has been interpreted as an electronic phase transition [15,48].

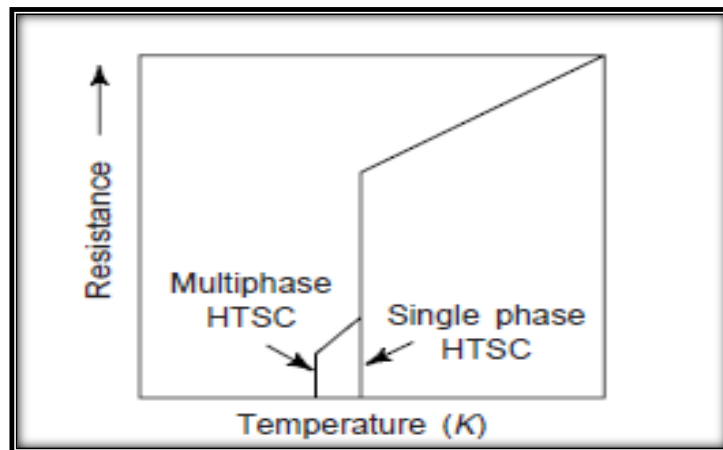


Figure (2-2):Resistance versus temperature curves of a single-and a multiphase high temperature superconductor[15].

Also T_c depends on chemical purity, and annealed quantity (time). It was found that T_c depends on the following factor [48]:

- 1- Pure material.
- 2- Pressure on material.
- 3- Material thickness.
- 4- Electrostatic charge on material.

The transition from the normal to the superconducting state occurs sharply in pure metals Figure (2-1) but not so in some impure, deformed and HTSC oxides. Bi, Tl, and Hg based cuprate superconductors are chemically complex materials, in which there may exist several superconducting phases in one specimen. A two-step transition reflects the presence of at least two superconducting phases. Figure (2-2) shows resistance versus temperature for a single and multi-phase high temperature superconductor. The transition width T_C for single-phase high temperature superconductors is typically 1 K [47].

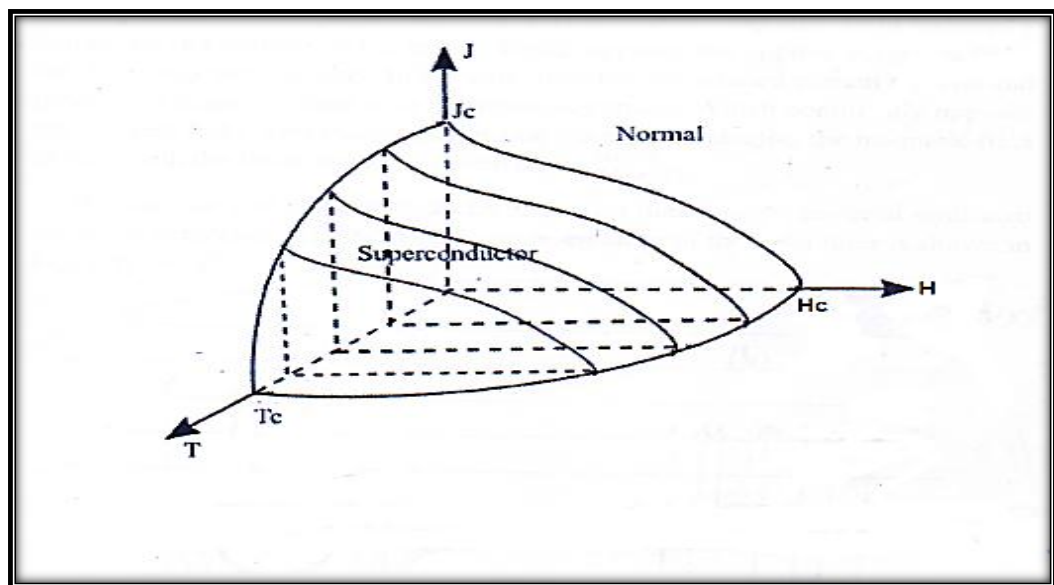
ii Critical magnetic field and critical current

The superconducting state is not determined by temperature only, but also by magnetic field applied to the sample and the magnitude of the current density flowing through it. Experimentally the critical field (H_c) with temperature given by [48]:

$$H_c = H_c(0) \left[1 - \left(\frac{T}{T_c} \right)^2 \right] \quad \dots\dots\dots(2-1)$$

Where $H_c(0)$ is the maximum value of the magnetic field that a material can tolerate and still remain superconducting at $T=0$ K, and the other factor is the critical current density which can determine the material.

These three parameters can determine whether or not the material is a superconductor. The superconductivity can thus be represented by the graph shown in Figure(2-3)

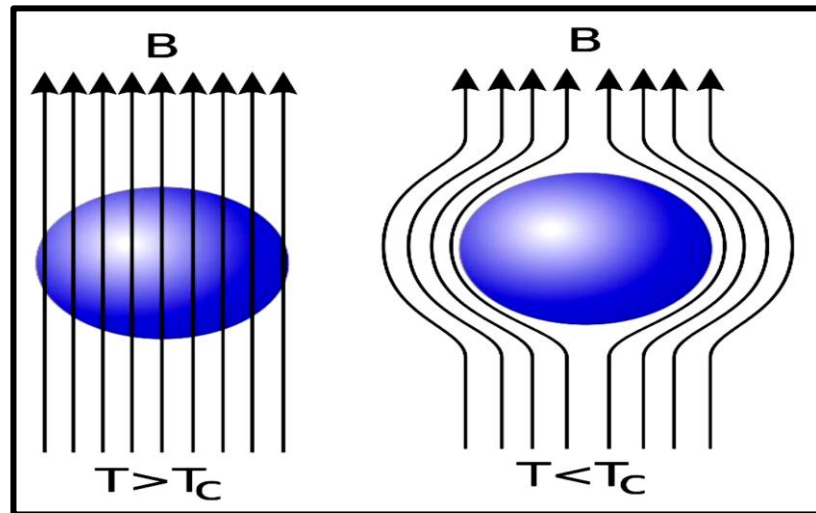


Figure(2-3) : The ability of a material to superconductor depends on three factors : the temperature (T), the magnetic field density (H) and the current density (J) [49].

In Figure (2-3), T_c represents the critical temperature in the absence of an external magnetic field and with no current flowing in the sample H_c is the critical magnetic fields strength with no current flowing at $T=0$ K with no external magnetic field. The critical surface shown in Figure(2-3) separates the superconducting and normal states.

2-4 Meissner-Ochsenfeld Effect :

($B = 0$ inside the superconductor): The magnetic inductance becomes zero inside the superconductor when it is cooled in a weak external field Figure (2-4). The effect is called the Meissner-Ochsenfeld effect. From Eq ($\frac{\partial B}{\partial t}=0$), we see that the magnetic induction in the interior of the sample has to be constant as a function of time. The final state of the sample would have been different if it were cooled under an applied external field or if the field were applied after the sample has been cooled below T_c . In the former case the field would have remained within the sample, while in the latter it would have been zero. For the specimen to be in the same thermodynamic state, independent of the precise sequence that one uses in cooling or in applying the field, the superconducting metal always expels the field from its interior, and has $\vec{B}=0$



Figure(2-4): Expulsion of a weak external magnetic field from the interior of the superconducting material[51].

$$B_{in} = B_{ext} + \mu_0 M \quad \dots\dots\dots(2-2)$$

$$B_{in} = \mu_0 H + \mu_0 \chi H \quad \dots\dots\dots(2-3)$$

$$B_{in} = \mu_0 (H + M) = \mu_0 (1 + \chi) H \quad \dots\dots\dots(2-4)$$

Where H is the external intensity of the magnetic field, M is the magnetization in medium, χ is the magnetic susceptibility and μ_0 is the permeability of free space, since $B_{in}=0$ in the superconducting state, it follows that:

$$\mathbf{M}=-\mathbf{H} \quad \dots\dots\dots(2-5)$$

$$\mathbf{X}=-1 \quad \dots\dots\dots(2-6)$$

This constraint to zero magnetic field inside a superconductor is distinct from the perfect diamagnetism which would arise from its zero electrical resistance[49]. Zero resistance would imply that if you tried to magnetize a superconductor, current loops would be generated to exactly cancel the imposed field (Lenz's law). But if the material already had a steady magnetic field through it when it was cooled through the superconducting transition, the magnetic field would be expected to remain. If there were no change in the applied magnetic field, there would be no generated voltage (Faraday's law) to drive currents, even in a perfect conductor. Hence the active exclusion of magnetic field must be considered to be an effect distinct from just zero resistance[51].

One of the theoretical explanations of the Meissner effect comes from the London equation. It shows that the magnetic field decays exponentially inside the superconductor over a distance of 20-40 nm. It is described in terms of a parameter called the London penetration depth..The Meissner effect is one of the defining features of superconductivity, and its discovery served to establish that the onset of superconductivity is a phase transition[51,92].

2-5 Josephson Effect:

Josephson observed some remarkable effects associated with the tunnelling of superconducting electrons through a very thin insulator (1-5 nm) sandwiched between two superconductors. Such an insulating layer forms a weak link between the superconductors which is referred to as the Josephson junction.

(i) The dc Josephson Effect: A dc current flows across the junction without any application of voltage.

(ii) The ac Josephson Effect: An application of rf voltage along with the dc voltage can result in the flow of direct current through the junction. Hence this effect has been utilized to measure e/h very precisely and may be used as a means of establishing a voltage standard [51,92].

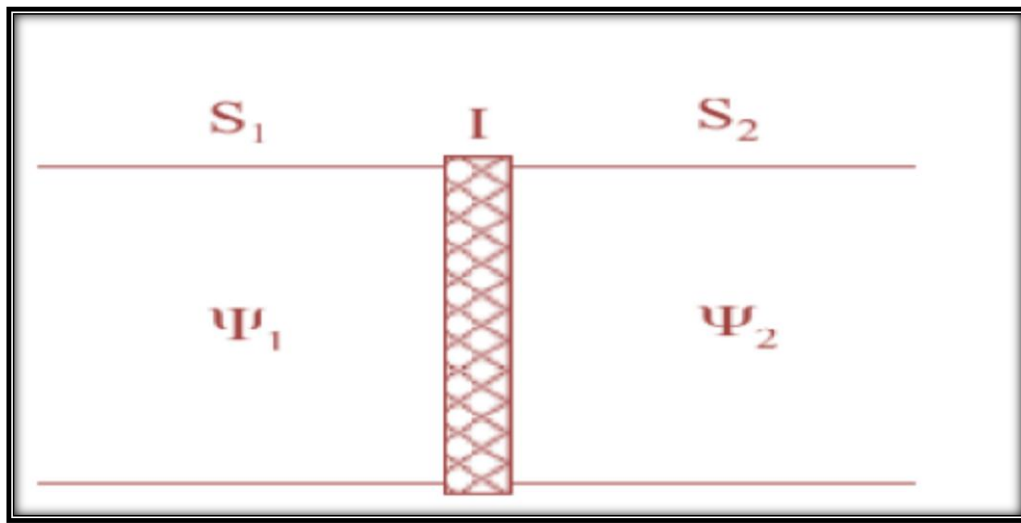


Figure (2-5): Geometry of Josephson junction (here, S_1 and S_2 two kind of superconductor, I is thin insulating[51].

2-6 Fundamentals Parameters Of The Superconductivity:**(a) The Cooper Pairs**

When A superconductor material is cooled below the critical temperature , transforms the free electron gas from the normal state to a quantum fluid of coherent electron pairs in the reciprocal space . Each individual pair is formed when one electron with momentum combine with another electron of exactly the opposite momentum and spin , giving a net momentum of zero . These charge carriers are called the Cooper pairs [55,56] .

(b) Penetration Depth (λ) While studying Meissner effect, we mentioned that the superconductor expels a (weak) magnetic field B from its interior, i.e. $\vec{B} = \mathbf{0}$ in the interior of a superconductor. The finer experiments reveal that the field B penetrates into the superconductor within a very thin surface layer. Consider the boundary of a semi-infinite slab. When the external field is applied parallel to the boundary, the applied field does not suddently drop to zero at the surface of the superconductor, but decays exponentially according to the relation

$$H(x) = H_{(0)} \exp\left(-\frac{x}{\lambda}\right) \dots\dots\dots(2-7)$$

where $H(0)$ is the value of the magnetic field at the surface and λ is a characteristic length known as the penetration depth; x is the distance for H to fall from $H(0)$ to $H(0)/e$. In most of the superconductors, λ is of the order of 500 Å. λ depends on the material and on the temperature, the latter variation being given approximately by

$$\lambda = \lambda_0 \left[1 - \left(\frac{T}{T_c}\right)^4 \right]^{-1/2} \dots\dots\dots(2-8)$$

Where λ_0 is the penetration depth at zero temperature for the particular material and is typically of order 500 Å[53,54].

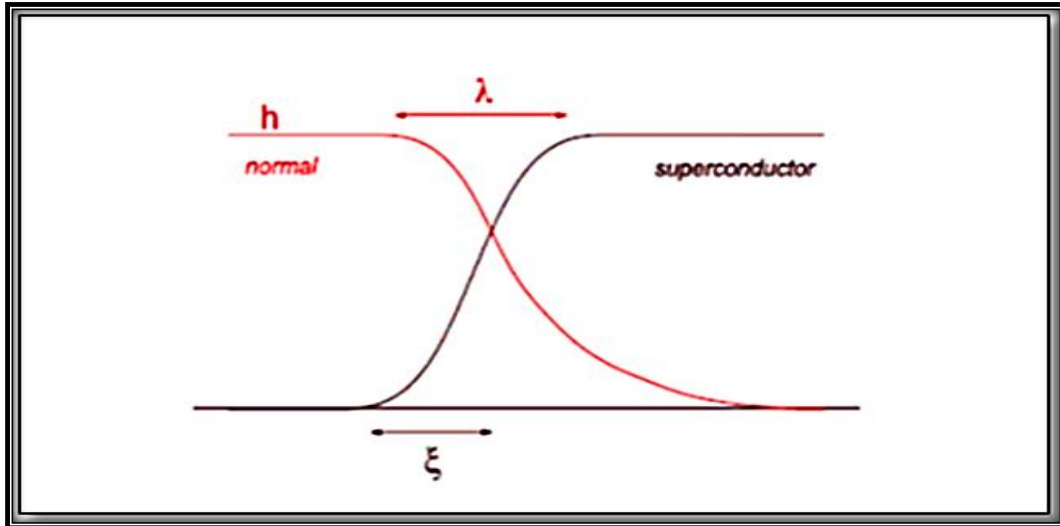


Figure (2-6) :The Coherence Length (ξ) and Penetration Depth (λ) at superconducting / normal surface boundary[52].

(c) **The Coherence Length (ξ)** It is a measure of the distance over which the gap parameter (Δ), can vary, for instance in a spatially varying magnetic field or near a superconductor-normal metal boundary. It is also referred as the distance between two electrons of the cooper pair within the highly coherent superconducting state. The intrinsic or BCS coherence length ξ_0 is defined as :

$$\xi_0 = \frac{\hbar v_F}{\pi \Delta} \dots \dots \dots (2 - 9)$$

where v_F is the Fermi velocity and Δ is the energy gap. Using order of magnitude values for v_F and Δ , one obtains $\xi = 16000 \text{ \AA}$ in pure Al, $\xi = 380 \text{ \AA}$ in pure Nb, but only about 10 \AA in the new HTSC oxides.

(D) **Ginzburg-Landau Parameter (K)** The ratio of two characteristic lengths, λ and ξ is called the Ginzburg-Landau ratio.

The GL parameter defines The ratio of the characteristic lengths $K = \lambda / \xi \dots \dots \dots (2-10)$

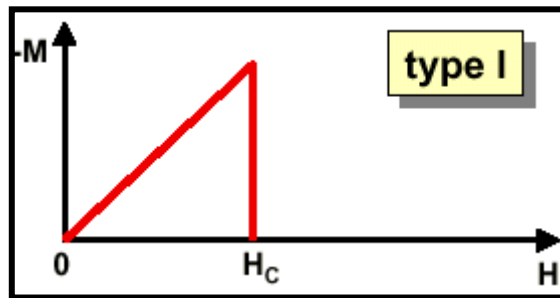
If $K < 1 / \sqrt{2}$ then is type-I of the superconductor

If $K > 1 / \sqrt{2}$ is of type-II for the material [53,54] .

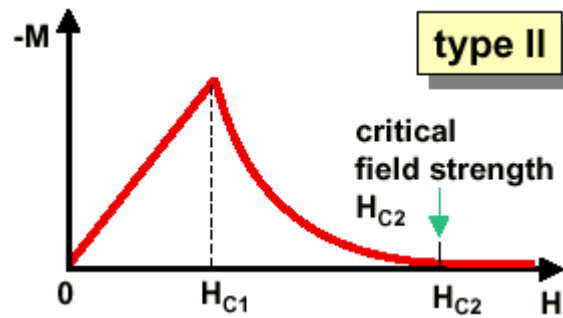
2-7 Types of the Superconductors materials:

On the basis of magnetic response, superconducting materials may be divided into two classes designated as type-I and type-II.

-Type-I materials, while in the superconducting state, are completely diamagnetic; i.e., all of an applied magnetic field will be excluded from the body of material (Meissner effect). The first type, referred to as type-I superconductors or superconductors of the first kind, expels the magnetic field up to a maximum value H_c , the critical field. Several metallic elements including aluminium, lead, tin, and mercury belong to type-I group.



-Type-II superconductors :The second type, referred to as type-II superconductors or superconductors of the second kind, shows ideal diamagnetism for magnetic fields smaller than the “lower critical magnetic field” H_{c1} . Superconductivity completely vanishes for magnetic fields larger than the “upper critical magnetic field” H_{c2} , are completely diamagnetic at low applied fields, and field exclusion is total. However, the transition from the superconducting state to the normal state is gradual and occurs between lower critical and upper critical fields, designated H_{c1} and H_{c2} , respectively Figure (2-7)[47,57].



The magnetic flux lines begin to penetrate into the body of the material at H_{c1} , and with increasing applied magnetic field, this penetration continues; at H_{c2} , field penetration is complete. For fields between H_{c1} and H_{c2} , the material exists in what is termed a mixed state-both normal and superconducting regions are present.

Type-II superconductors are preferred over type-I for most practical applications by virtue of their higher critical temperatures and critical magnetic fields[47,57].

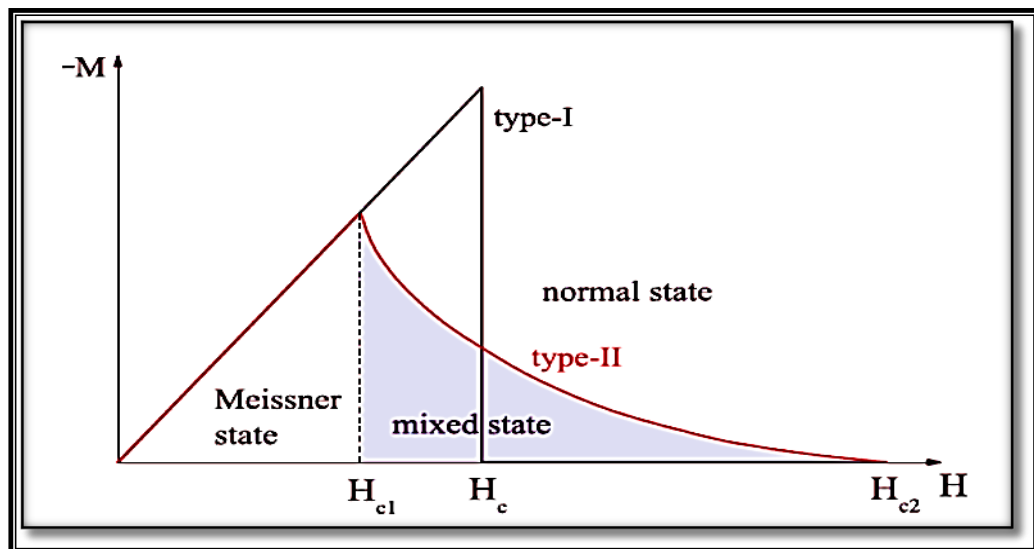


Figure (2- 7):The magnetization curve for type I and type II superconductor[57].

2-8 Theories of superconductivity:

Since the discovery of superconductivity, great efforts have been devoted to finding out how and why it works. During the 1950s, theoretical condensed matter physicists arrived at a solid understanding of "conventional" superconductivity, through a pair of remarkable and important theories: the phenomenological Ginzburg-Landau theory (1950) and the microscopic BCS theory (1957). Generalizations of these theories form the basis for understanding the closely related phenomenon of superfluidity, because they fall into the Lambda transition universality class, but the extent to which similar generalizations can be applied to unconventional superconductors as well is still controversial. The four dimensional extension of the Ginzburg-Landau theory, the Coleman-Weinberg model, is important in quantum field theory and cosmology[2].

2-9 Theories Of the Superconductor At Low Temperature:**1-London theory:**

According to the Gorter and Casimir two-fluid model (London, 1954), in a superconductor at a temperature $T = T_c$ a fraction $n_s(T)/n$ of the total number of conduction electrons are capable of flowing as a supercurrent[59,60]. The density of superconducting electrons $n_s(T)$ drops to zero as T approaches T_c , and approaches n as T falls well below T_c . Since the supercurrent flows with no resistance, it carries the entire current induced by any applied electric field, so the normal electron fluid can be ignored in the following discussion.

If an electric field \mathbf{E} appears in the superconductor, the superconducting electrons are accelerated without dissipation, so

$$\mathbf{J}_s = -[n_s e^2/m] \hat{\mathbf{A}} \quad \dots\dots\dots (2-11)$$

Where:

J_s : is supercurrent density.

n_s :is the density of superconducting electrons.

m :is the mass of electron .and $\hat{\mathbf{A}}$ is the magnetic vector potential.

By using Maxwell equations:

$$\nabla \times \mathbf{B} = \mu_0 \mathbf{J}_s \quad \dots\dots\dots (2-12)$$

$$\nabla^2 \mathbf{B} = [n_s e^2 \mu_0 / m] \mathbf{B} \quad \dots\dots\dots (2-13)$$

This is known as the London equation. It explains Meissner effect and provides description of the electromagnetic behavior of superconductor.

If the field is applied in Y-direction and surface specimen laying in the YZ plane then equation(2-12), reduces to :

$$\nabla_x \mathbf{B}_y = [n_s e^2 \mu_0 / m] \mathbf{B}_y \quad \dots\dots\dots (2-14)$$

The solution to the simple differential equation is :

$$\mathbf{B}_y(\mathbf{x}) = \mathbf{B}_y(0) e^{-\mathbf{x}/\lambda} \quad \dots\dots\dots (2-15)$$

Where:

$$\lambda = (m / n_s \mu_0 e^2)^{1/2} \quad \dots\dots\dots (2-16)$$

λ : is the London penetration depth

The London equation can be shown to require that the magnetic field exponentially decays to zero inside a superconductor in accordance with Meissner effect[61]. The nature of the decay depends upon the superconducting electron density n_s :

Another conclusion of London theory is its prediction of the variation of λ with temperature[51,61] ;

$$\lambda = \lambda_{(0)} \left[1 - \left(\frac{T}{T_c} \right)^4 \right]^{-1/2} \quad \dots\dots\dots (2-17)$$

Where $\lambda_{(0)}$ is the penetration depth at $T=0$ K. From equation (2-15) , λ increases, it becomes infinite at $T=T_c$ as shown in figure(2-8).

The third conclusion from London theory is the existence of an electric current flowing near the surface, these currents decay exponentially as one move into the superconductor; it is essentially a surface current.

$$\mathbf{J}_z(\mathbf{x}) = -\mathbf{J}_s(\mathbf{0}) e^{-x/\lambda} \quad \dots\dots\dots(2-18)$$

There are many limitations in London theory[50] : it is classical theory treats the electron as a classical particles and the penetration depth is independent of the strength of the applied magnetic field and the dimensions of the specimen. Because of these limitation London theory is therefore a weak field theory.

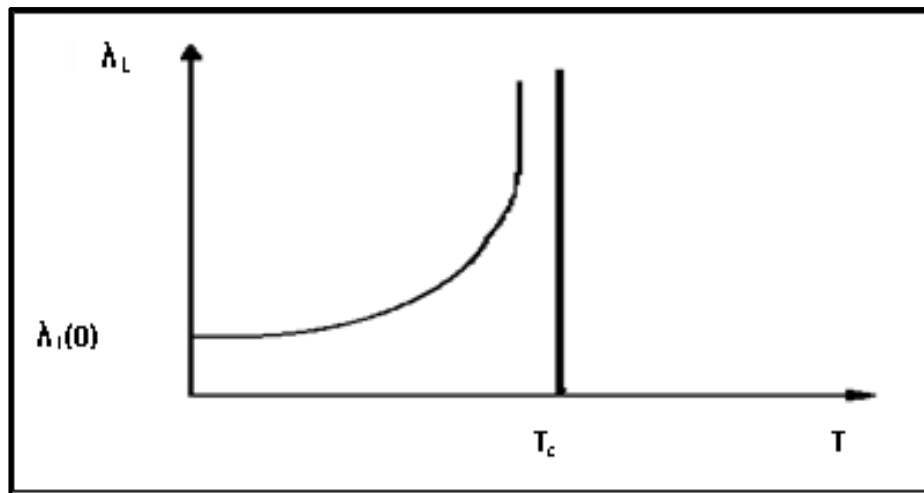


Figure (2-8): Penetration depth λ with temperature[51].

2- Ginzburg-Landau Theory:

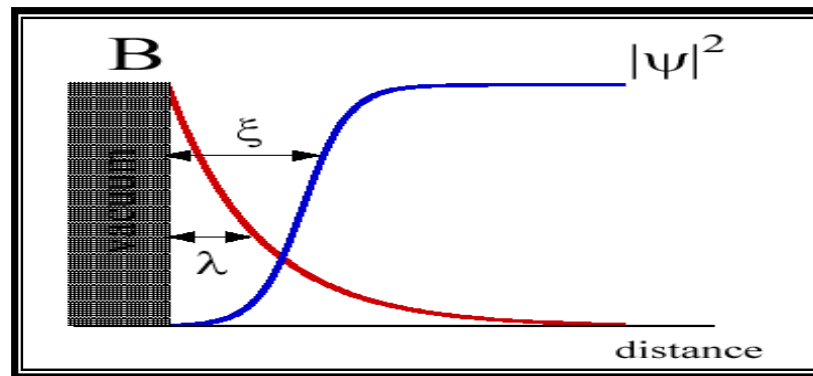
Ginzburg-Landau theory is a mathematical theory used to model superconductivity. It does not purport to explain the microscopic mechanisms giving rise to superconductivity. Instead, it examines the macroscopic properties of a superconductor with the aid of general thermodynamic arguments[62].

The major advantage of the Ginzburg-Landau (GL) theory is that it allows to study of spatially inhomogeneous system. It is most extensively used for analyzing the behavior of superconductors in an external magnetic field. When an external field is applied, the order parameter varies within the surface layer leading to a surface energy with two components, one arises from the conventional penetration magnetic field and the other from the variation of order parameter.

They expressed a significant parameter which is called Ginzburg-Landau parameter $\mathbf{K} = 0.96 \lambda_L / \zeta$ where λ_L is the Landau penetration depth and ζ is the coherence length (representing the distance over which superconductivity can be established or destroyed in a material, this is

typically on the order of 1000\AA , although it can be as 30\AA in the copper oxides)[63].

The form of the solution of GL equations and the behavior of superconductors depend on the value of this parameter as shown in Figure(2-9).



Figure(2-9): Interface between superconducting and normal domains in the intermediate state[64].

3 - BCS -Theory:

In 1957, Bardeen, Cooper and Schrieffer (BCS)[65,66] constructed a microscopic theory of superconductivity, which gave a satisfactory explanation of this phenomenon. This theory is known as the BCS theory. A central feature of BCS theory is the formation of a bound state called Cooper pair, consisting of two electrons with equal and opposite momenta and spins.

According to the theory as one negatively charged electron passes near positive charged ions in the lattice of the superconductor, the lattice distorts. This in turn causes phonons to be emitted which forms a cloud of positive charges around the electron.

Before the electron passes by and before the lattice springs back to its normal position, a second electron is drawn into the cloud. It is through this process such two electrons, which should repel one another, link up. The

forces exerted by the phonons overcome the electron repulsion. When one of the electrons that make up Cooper pair and passes close to an ion in the crystal lattice, the attraction between the negative electron and the positive ion cause a vibration to pass from ion to ion until the other electron of the pair absorbs the vibration. The net effect is that one electron emits phonons which are very quickly absorbed by the other as shown in Figure (2-10).

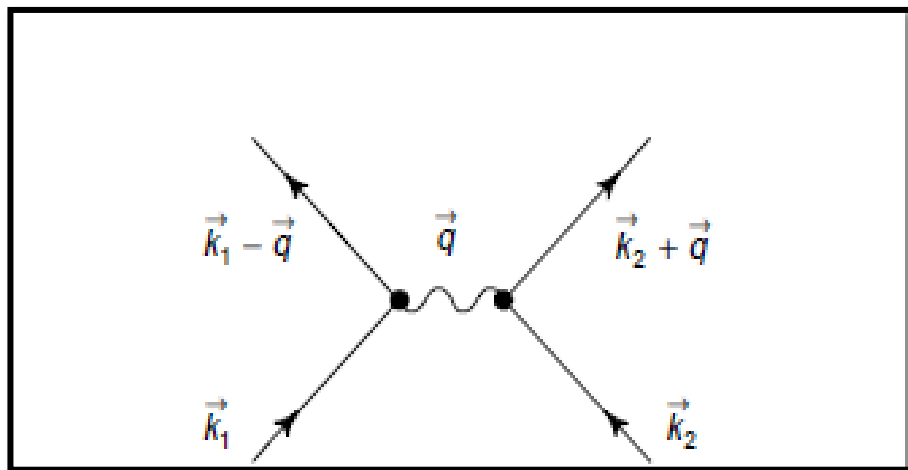


Figure (2-10):Electron-phonon interaction. An electron of wave vector \vec{k}_1 emits a virtual phonon \vec{q} which is absorbed by electron \vec{k}_2 . \vec{k}_1 is thus scattered as $\vec{k}_1 + \vec{q}$ and \vec{k}_2 as $\vec{k}_2 + \vec{q}$. If this phonon energy is negative, the electron-phonon interaction is attractive[47].

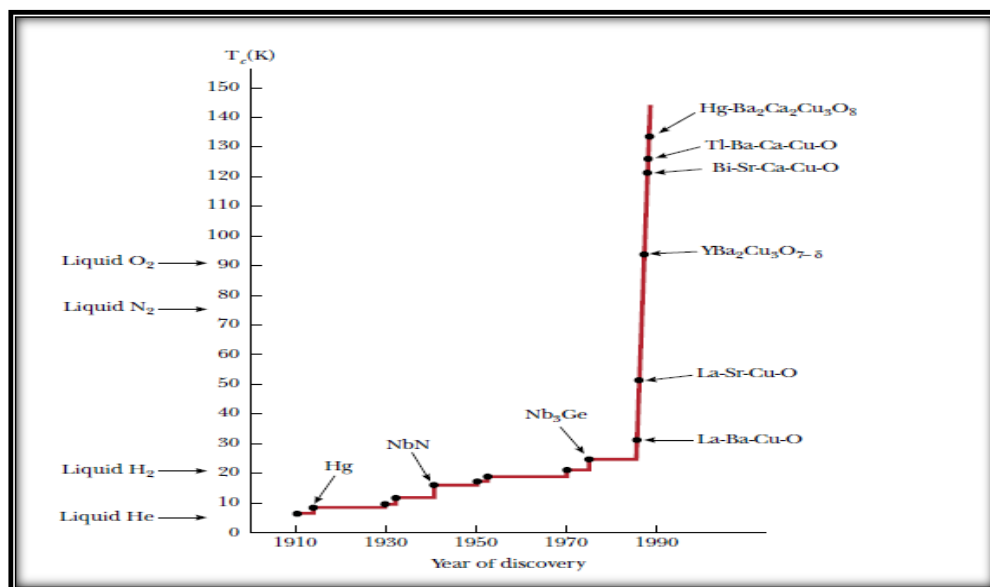
4- Isotope Effect:

The isotope effect was discovered several years before the BCS theory. Because of the dependence of phonon frequencies on isotopic mass M , the critical temperature, T_c , of these superconductors is expected to be proportional to $M^{-1/2}$ [67].

For many simple metals it has been found that $T_c \approx M^{-\alpha}$ with α is close to 0.5 [67], while for transition metal superconductors α is often smaller. The isotope effect is a strong experimental evidence for the BCS model.

2-10 High-temperature superconductivity ((Cuprate Superconductors)):

In more than 24 years of time a go from the discovery of high T_c superconductivity in copper oxides, a huge number of experimental and theoretical investigations of the physical properties of these materials have been done. The high temperature superconductivity of cuprates was discovered in 1986, when the highest superconducting transition temperature (i.e., critical temperature) characteristic of conventional superconductors ($T_c = 23.2$ K in Nb_3Ge) was substantially exceeded and a superconducting transition temperature $T_c = 30$ K was achieved in the ceramic $La_{2-x}Ba_xCuO_{4-\delta}$. The situation including the high T_c cuprate superconductors is illustrated in Figure (2-11). Within a year after this discovery, the record value of T_c exceeded 90 K ($YBa_2Cu_3O_{7-\delta}$ ceramic)[69].



Figure(2-11): Evolution of the superconducting critical temperature since the discovery of the phenomenon[70].

Since 1986, several complex metallic oxides in the form of ceramics have been investigated, and critical temperatures above 100 K (triple-digit superconductivity) have been observed. Early in 1988 researchers reported superconductivity at 120 K in a Bi-Sr-Ca-Cu-O compound and at 125 K in a Tl-Ba-Ca-Cu-O compound. As of early 1995, the record high critical temperature was 134 K, in the compound $\text{HgBa}_2\text{Ca}_2\text{Cu}_3\text{O}_8$. The increase in T_c since 1986 is dramatized in Figure (2-11). As you can see from this graph, the new high- T_c materials are all copper oxides of one form or another. The various superconducting compounds that have been extensively studied to date can be classified in terms of what are called perovskite crystal structures[70].

2-11 Perovskite Structure:

Perovskites are ceramics (solid materials combining metallic elements with non-metals, usually oxygen) that have a particular atomic arrangement. In their ideal form, described by generalised formula ABX_3 , they consist of cubes made up of three distinct chemical elements (A, B and X) that are present in a ratio 1:1:3. The A and B atoms are metallic cations (positive) and X atoms are non-metallic anions (negative). An A cation – the largest of the two kinds of metals – lies at the centre of each cube, the B cations occupy all the eight corners and the X anions lie at the mid-points of cube's twelve edges (Figure. 2-12)[71].

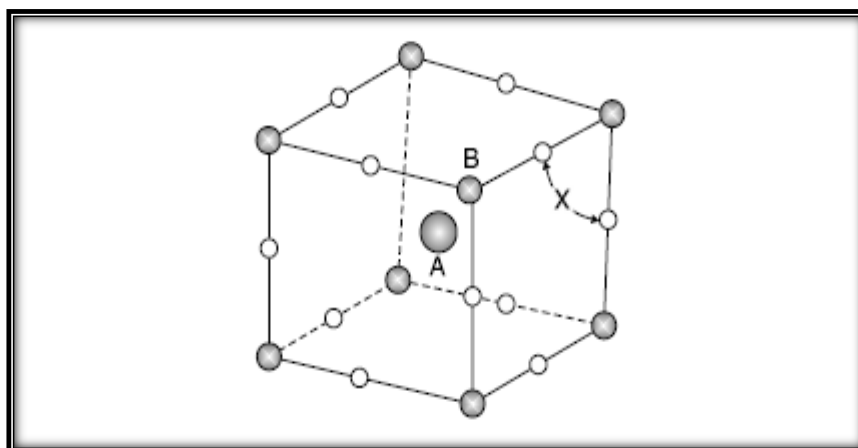


Figure (2-12): The perovskite structure ABX_3 [71].

2-12 Structure of Thallium-Based Cuprate Superconductors *TBCCO:*

Tl-Ba-Ca-Cu-O superconductors have been discovered in 1988 by Sheng and Hermann is the best among all other cuprates due to their high transition temperature, transport critical current densities and low microwave surface resistances. There are two Tl-based superconducting families, TBCCO and TSCCO. TBCCO materials have perovskite like $Ba_2Ca_{n-1}Cu_nO_{2n+1}$ layers and tetragonal crystal structures. The first series of the Tl-based superconductor containing one Tl-O layer has the general formula $TlBa_2Ca_{n-1}Cu_nO_{2n+3}$, whereas the second series containing two Tl-O layers has a formula of $Tl_2Ba_2Ca_{n-1}Cu_nO_{2n+4}$ with $n = 1, 2$ and 3 . In the structure of $Tl_2Ba_2CuO_6$ (Tl-2201), there is one CuO_2 layer with the stacking sequence, (Tl-O) (Tl-O) (Ba-O) (Cu-O) (Ba-O) (Tl-O) (Tl-O).

In $Tl_2Ba_2CaCu_2O_8$ (Tl-2212), there are two Cu-O layers with a Ca layer in between. Similar to the $Tl_2Ba_2CuO_6$ structure, Tl-O layers are present outside the Ba-O layers. One of the high temperature superconducting cuprates (HTSC) which have an inherent potential for practical application, especially at temperatures close to 120 K, is the Tl bilayer phase $Tl_2Ba_2Ca_2Cu_3O_{10}$ (TBCCO) in the form Tl-2223. In bulk form, this superconducting cuprate has a transition temperature (T_c) as high as 125K

and in thin film form, it has been found to be superconducting up to 122K in $\text{Tl}_2\text{Ba}_2\text{Ca}_2\text{Cu}_3\text{O}_{10}$ (Tl-2223), there are three CuO_2 layers enclosing Ca layers between each of these. In Tl-based superconductors, T_c is found to increase with the increase in CuO_2 layers. However, the value of T_c decreases after four CuO_2 layers in $\text{TlBa}_2\text{Ca}_{n-1}\text{Cu}_n\text{O}_{2n+3}$, and in the $\text{Tl}_2\text{Ba}_2\text{Ca}_{n-1}\text{Cu}_n\text{O}_{2n+4}$ compounds, it decreases after three CuO_2 layers[59,64,65]. The structure of Tl-2201, Tl-2223 and Tl-2212 are shown in Figure(2-13)[69,71].

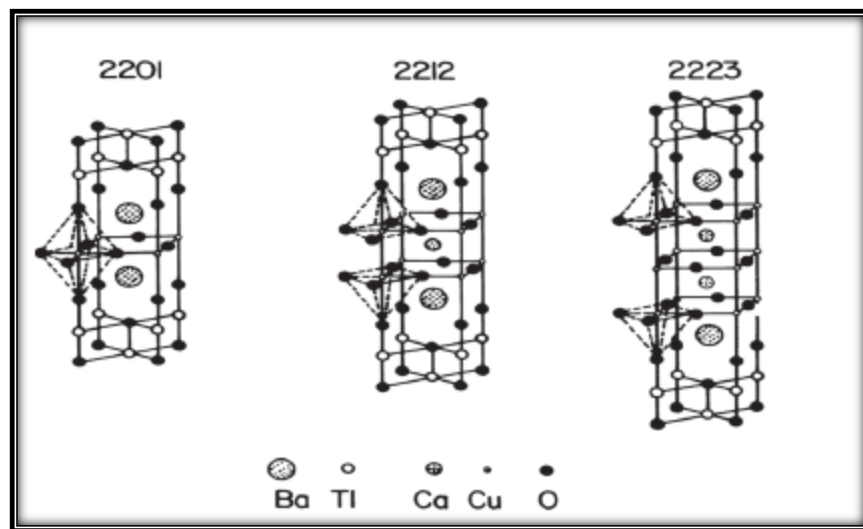


Figure (2-13): Crystal structure of the layered Tl-Ba-Ca-Cu-O compounds[69].

2-13 Mercury Based Cuprate Superconductors HBCCO:

Mercury bearing compound $\text{HgBa}_2\text{RCu}_2\text{O}_{6+x}$ (Hg: 1212), where R is a rare-earth element, was synthesized by Putilin et al. It has a structure similar to the thallium bearing superconductor $\text{TlBa}_2\text{CaCu}_2\text{O}_7$ (Tl-1212), which has one TlO layer and two CuO_2 layers per unit cell and T_c is 85K60. But inspite of the resemblance to Tl: 1212, Hg: 1212 was found to be non-superconducting. In 1993, Putilin et al. Reported the synthesis of the compound $\text{HgBa}_2\text{CuO}_{4+x}$ (Hg: 1201) with only one CuO_2 layer per unit cell. It was found to be superconducting below 94 K. Its structure is similar to that of Tl: 1201 ($T_c \leq 10\text{K}$), but its T_c is considerably higher. The

availability of such a material with high T_c and a single metal-oxide (HgO) layer may be important for technological applications, because a smaller spacing between CuO_2 planes leads to better superconducting properties in a magnetic field.

The structural arrangement of $\text{HgBa}_2\text{CuO}_{4+x}$ is similar to that of $\text{TlBa}_2\text{CuO}_5$, except for the oxygen stoichiometry of the HgO_x and TlO_{1-x} layers, respectively. For the former, x is very small and for the latter, the TlO_{1-x} layer is only slightly oxygen depleted. These different requirements for attaining the optimal concentration of holes (carriers) are due to the different preferred coordination geometries of the Tl^{3+} and Hg^{+2} cations. The rare-earth based Hg: 1212 compounds were not found to be superconducting because the hole concentration in these phases might not be high enough for inducing superconductivity. Putilin et al. Replaced the trivalent rare-earth cation by divalent Ca^{+2} and obtained a superconductive transition temperature of above 120K in $\text{HgBa}_2\text{CaCu}_2\text{O}_{6+x}$. In 1993, Schilling et al. reported their discovery of superconductivity above 130K in a material containing $\text{HgBa}_2\text{Ca}_2\text{Cu}_3\text{O}_{8+x}$ (with three CuO_2 layers per unit cell) and $\text{HgBa}_2\text{CaCu}_3\text{O}_{6+x}$ (with two CuO_2 layers per unit cell) and an ordered superstructure comprising a defined sequence of the unit cells of these phases (Figure 2-14).

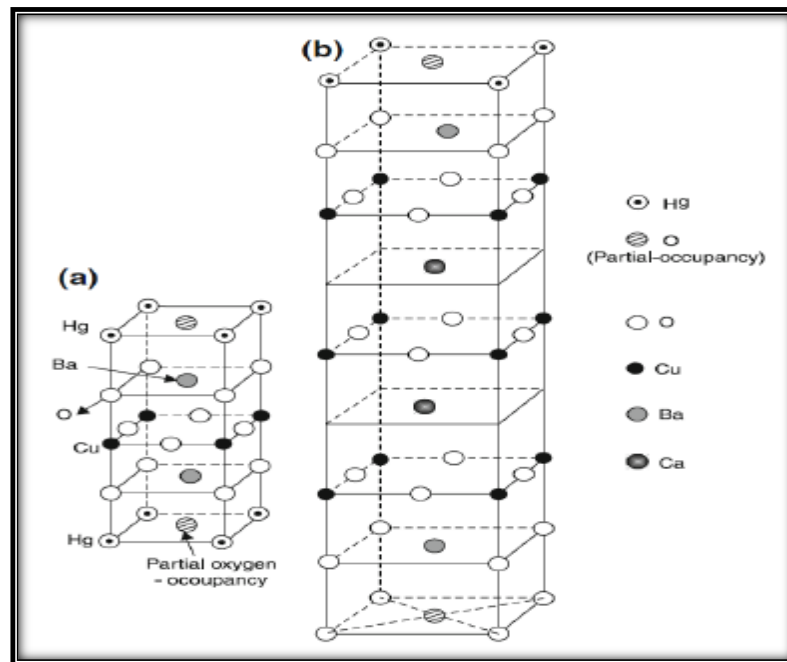


Figure (2-14): Atom cluster model for central cell of (a) Hg-1201 and (b) Hg-1223 Superconductors [69].

A maximum transition temperature of 133K had been obtained which was distinctly higher than the previously established value of 125–127K observed in $Tl_2Ba_2Ca_2Cu_3O_{10}$. In September 1993, a record T_c of 150K in $HgBa_2Ca_2Cu_3O_{8+x}$ at quasihydrostatic pressure of 150 K-bar was obtained by Chu (Texas Centre for Superconductivity, U.S.A.).

Such pressure effect on T_c might also be duplicated by chemical means, i.e. “chemical pressure” imposed by other “element” substituted on Hg-site (published in Nature) (Previous record of T_c of 135K in Hg: 1223 was at ambient pressure). Table (2-1) gives lattice parameters of Hg superconductors [69,71,72].

Table(2-1) : Lattice parameters of Hg based superconductors[69].

Cuprate	T_c^a (k)	Lattice Parameters
Hg - 1201	94	$a = b = 3.85 \text{ \AA}, c = 9.5 \text{ \AA}$
Hg - 1212	120	$a = b = 3.85 \text{ \AA}, c = 12.6 \text{ \AA}$
Hg - 1223	133	$a = b = 3.85 \text{ \AA}, c = 15.7 \text{ \AA}$

There exist four different types of layers. First of all, there are (CuO_2) layers, varying in number from 1 to n per unit cell. These (CuO_2) layers may be separated from each by (Ca) layers; evidently $(n-1)$ such layers per unit cell in general. According to current physical theory, the (CuO_2) layers are responsible for the superconductivity of these compounds. Thus, n (CuO_2) layers and $(n-1)$ (Ca) layers together form a so-called "conducting block" or "active block", which has a perovskite-type crystal structure with an approximate thickness of $[4.0 + 3.16 (n-1)] \text{ \AA}$. [69,71,73].

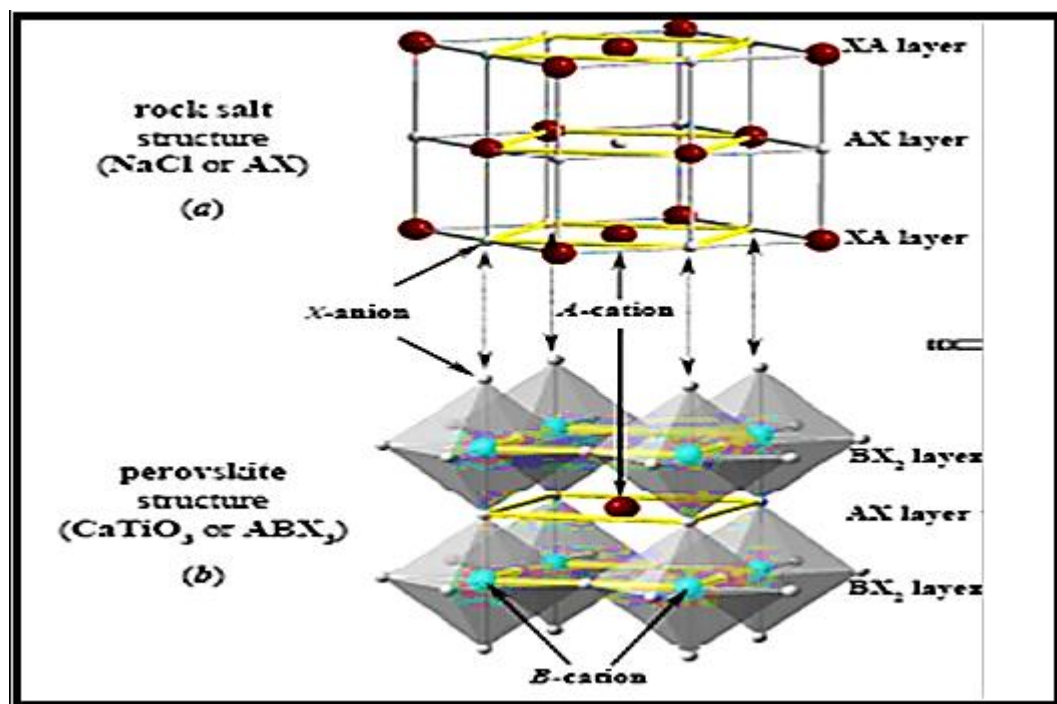
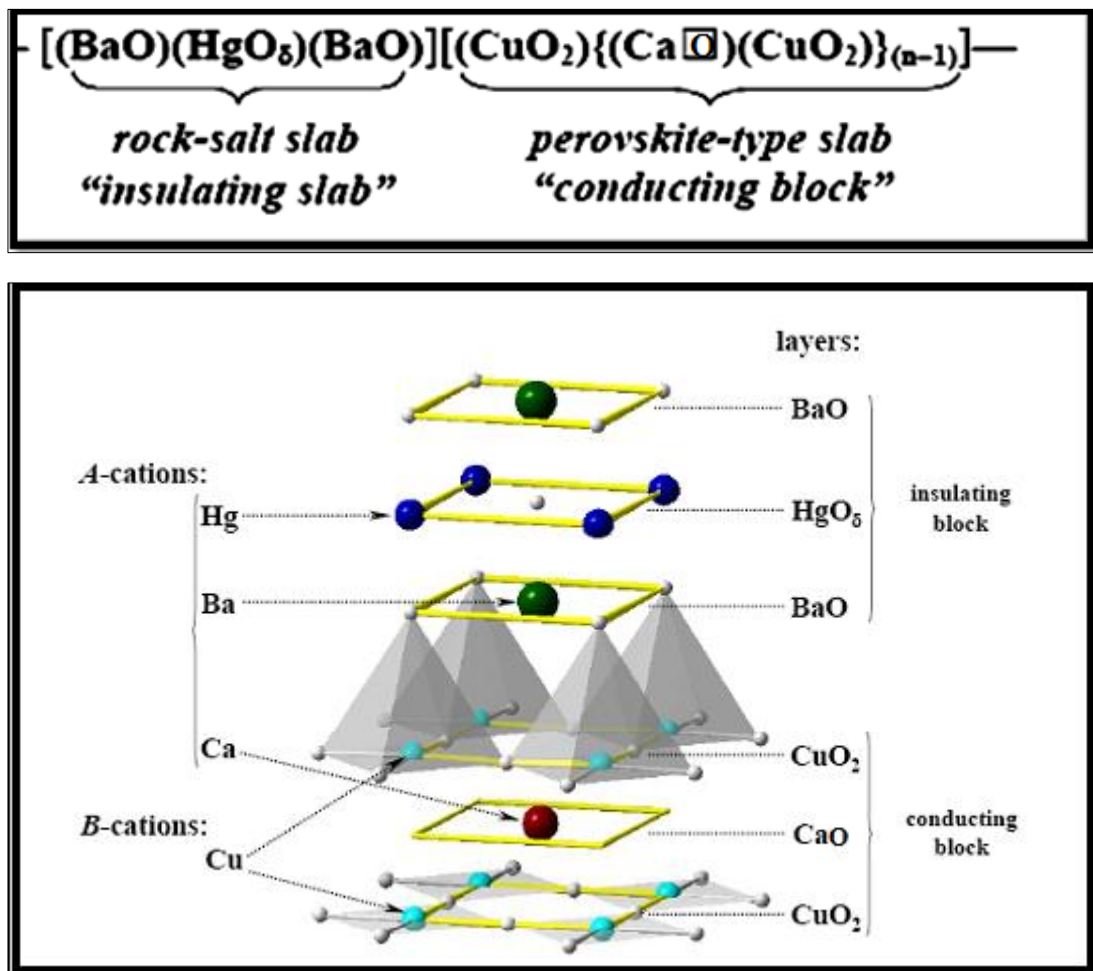


Figure (2-15): (a) Rock salt – type (AX) and (b) Perovskite – type slab (ABX_3) [74].

Between the conducting blocks there are **insulating slabs**. These slabs in Hg-based cuprates consist of insulating (HgO_δ) and (BaO) layers with a stacking sequence that results structures containing $(\text{BaO})(\text{HgO}_\delta)(\text{BaO})$. The blocks $(\text{BaO})(\text{HgO}_\delta)(\text{BaO})$ have the rock salt structure with a thickness of about 5.5 \AA [68], that known "charge reservoir blocks" (CRB) Figure (2-15). In Hg-base superconductors, the CRB consists of double rock salt block $\text{HgBa}_2\text{O}_{2+\delta}$ and the thickness of CRB for Hg - $12(n-1)$ n is about 9.5 \AA [75,76].

Thus, the layer stacking sequence along the c axis in the Hg-based cuprates could be represented schematically as follows [73,74,75, 77] and Figure (2-16).



Figure(2-16): Stacking sequence of layers along c axis for the crystal structure of $\text{HgBa}_2\text{Ca}_{n-1}\text{Cu}_n\text{O}_{2+2n+\delta}$ ($n = 2$) cuprate phase[74].

2-14 Theories of High T_c Superconductor:

The recent discovery of high temperature superconductor in rare earth elements compounds has generated enormous interest in the region of superconductivity in these compounds. Several theories have appeared proposing that a new mechanism may be responsible for the high critical temperature in the oxide superconductors. Most of them are based on pairing mechanism; they differ in explaining the origin of the attractive interaction that given rise to the pairing of electrons or holes and whether the pairing is weak or strong.

These theories may be classified in two groups[78] , first group suppose that weak coupling and second group suppose strong coupling , where these theories suppose that polarization of electron pairs in phonon – electron interaction lead to polarization of lattice electrons .

1- Interlayer Coupling Model:

The metallic nature of the Hg-O, Bi-O layers may be of importance in achieving high transition temperatures. Those layers in $\text{HgSr}_2\text{Ca}_2\text{Cu}_3\text{O}_8$ and $\text{Bi}_2\text{Sr}_2\text{Ca}_2\text{Cu}_3\text{O}_8$ are directly tied to the hole count in the Cu-O₂ layers, since they as a result of charge transfer from one to another. The former enhances interlayer coupling while the latter is an important parameter for the strength of electron correlation.

To emphasize the effects of interlayer coupling ($\xi = 4 \text{ \AA}$)[79] coherence length is shorter than the distance between the two Cu-O₂ planes ($d_{\text{Cu-Cu}} = 12.1 \text{ \AA}$) and ξ is comparable to the distance $d_{\text{Cu-M}}$ (4.4 \AA)[79] from Bi-O plane, so the supercurrents could then flow between Cu-O₂ layers by taking advantage of the metallic states on the intervening layers, essentially hopping from Cu-O₂ layer to Cu-O₂ layer by tunneling through the metallic interlayer.

2- Exciton Model:

This model proposed a metal into such intimate contact with a polarizable semiconductor, the electrons would be able to interact strongly with interband excitations of the semiconductor, pairing would then occur by exchange of these virtual excitations. The exciton mechanism weakens the direct Coulomb repulsion of electrons[81].

Excitons might play a role in addition to phonons, for high temperature superconductor, because the electron- phonon superconductors have $T_c < 23K$.

According to this model Varam et al.[82] suggested an idea in which superconductivity is via electronic polarization, they believe in the high T_c metal oxides the excitons and the carriers can co-exist in the same spatial region.

3- Isotope Model:

In this model most of studies have focused on the substitutions of O^{18} for O^{16} . Band structure calculation have demonstrated that the density of states at E_f are primarily due to the hybridization of $Cu(3d)-O(2p)$ states within the CuO_2 planes and many calculations of electron-phonon interaction have suggested that oxygen –related modes were the most likely candidates to provide sufficient coupling to lead to an enhanced T_c within a conventional, phonon mediated BCS theory[83]. Also oxygen provides the largest possible fractional change in mass of the constituents in these systems.

4- Spin Fluctuations Model:

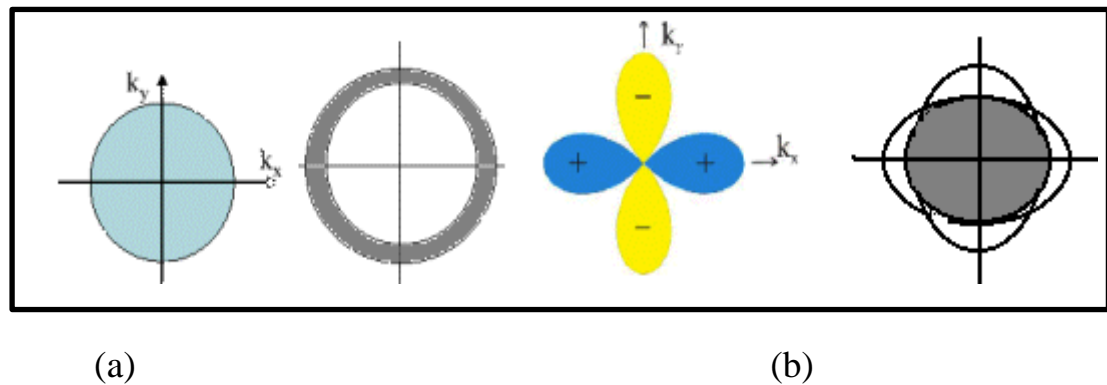
In a magnetic medium a free electron can scatter off the system, emitting a spin wave. At temperature lower than T_c superconducting, systems are magnetically ordered. In heavy fermion metal, superconductivity may be caused by exchange of antiferromagnetic spin fluctuations. The scattering of electrons from these fluctuations will alter the tendency to form pairs. This alternation assumed to be harmful, because the spin up electron will attract other electrons up spin, creating a locally ferromagnetic region and repelling the down spin electron needed for singlet cooper pairing. Antiferromagnetic spin fluctuations are more complicated situation, because it is not obvious whether an up spin electron will create or destroy local antiferromagnetic polarization, or whether this will attract or repel other electrons of opposite spin.

Schrieffer et al.[84] proposed an idea that free carriers in a material wanting commensurate antiferromagnetic will weaken the tendency to order. Thus an up-spin electron repels local spin order. Other free carriers, with either spin orientation, will be attracted to the region of depleted spin, going a net attractive interaction.

5- Pairing Symmetry:

In the BCS theory, Cooper pairs can be modeled by a single wave function. The solution to this wave function gives a spherical area of probability, indicating that a plot of the location of a second electron, with the first kept at the center, is equally likely to be in any position within a spherical area surrounding the first electron. This is called s-wave symmetry figure(2-17 a), and any BCS theory that involved cooper pair would by necessity display it. The other kind of symmetry commonly invoked is called d-wave symmetry, and essentially states that the electron can only move along 450 diagonals to the plane figure(2-17b). This would

allow the two electrons of the pair to be further away from each other, weakening the repulsion between the two electrons because their linear distance from each other has increased, but allowing them to remain paired[85].



Figure(2-17) :The energy gap for two possible pairing symmetries: s-wave(a) and d-wave (b)[85] . the s-wave symmetry has an isotropic gap value of 2Δ , while for d-wave symmetry the gap vanishes and changes at $k_x = \pm k_y$

6- Goddard's Model:

In 1988, William A. Goddard et al. [86] suggested a new model of superconductivity based on the movement of electron through copper-oxide components of the new compounds. According to this model, when a material becomes superconductive a few electrons are displaced from the oxygen atoms, which causes the atoms to become magnetic. Adjacent copper atoms are pulled into line by the magnetism and lose electrons into the quantum pockets, or holes created by the displaced oxygen atoms. This process creates new holes, and electrons will continue to flow through the material indefinitely as long as the transition temperature is maintained.

The model, which has so far proved accurate, predicts a transition temperature limit of about 200K (-73°C) for the copper oxide group of superconductors. A material could be cooled to this temperature by dry ice (frozen carbon dioxide), and commercial applications would follow.

Especially in the electronics industry where the superconductors are already use in a wide variety of scientific and medical instruments.

However, unless material that superconductor at room temperatures can be found, the use of superconductors in magnetically levitated trains, power lines, and power storage facilities will be costly.

7- Plasmon Model:

Plasmons are not a new concept in solid state physics, they are similar to phonons. Both describe collective vibrational motion, but phonon represents vibrational motion of the lattice, whereas plasmons correspond to collective vibrational motion of the carriers relative to the lattice. This motion represents charge fluctuations and is due to Coulomb correlation in the metal[87].

When there are overlapping energy bands, there is an additional plasmon branch, called demons (the word demon was associated with the distinct electron motion) (DEM). If there are two bands and two groups of carries (heavy and light electrons), then these groups will oscillate with respect to each other, interestingly, this branch has acoustic character, that is, there is no gap in the plasmon spectrum. In this case, the light carriers came from pairs by exchanging demons, in full analogy to the usual phonon exchange. The total electron – electron interaction is made up of the attraction mediated by the acoustic plasmons and of the usual repulsion, screened by the other “light” electrons [87,88].

2-15 Phase Transition:

Phase transformation a change in the structure of material, which may occur due to temperature , electric field , irradiation ,mechanical pressure , etc.

The transformation happens when the initial state of the system is unstable relative to the final state, the chemical driving force occupies a key position in the classical thermodynamics of first order diffusionless phase transformation , where the chemical composition doesnt change through phase transformation, the parent and product phases have the same homogeneous chemical composition and hence they are treated as a single component system . For those phase transformations whose structural change is easily described by a displacement parameter[88].

The Gibbs energy of a system(G) is defined in terms of its enthalpy (H) , entropy (S) and temperature (T) [90] :-

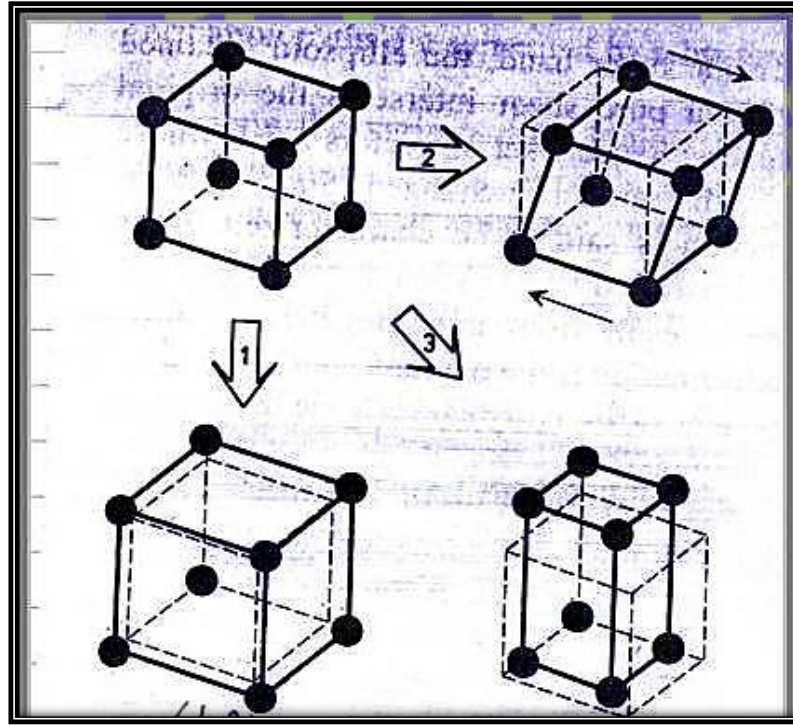
$$G = H - T\Delta S \quad \dots\dots\dots (2-19)$$

A system at constant temperature and pressure will approach an equilibrium state that minimizes G .

Transformations are usually classified into two groups "displacive" and "martensitic" transformations. The first occurs by coordinated shifts of individual atoms or groups of atoms in organized ways relative to their neighbors, a lattice-distortive deformation is a homogenous strain that transforms one lattice into another , examples are shown in Figure (2-18).

The second occurs by a complete change in the crystal structure, because of the volume change and the strain energy involved with the transformation, martensitic transformation requires heterogeneous nucleation and passes through a two-phase mixture of parent and product, it is a first order diffusion less phase transformation. consequently, the

forward and reverse transformations are accompanied by an exothermic and endothermic heat effect , respectively and forward and reverse transformation paths are separated by a hysteresis [89].



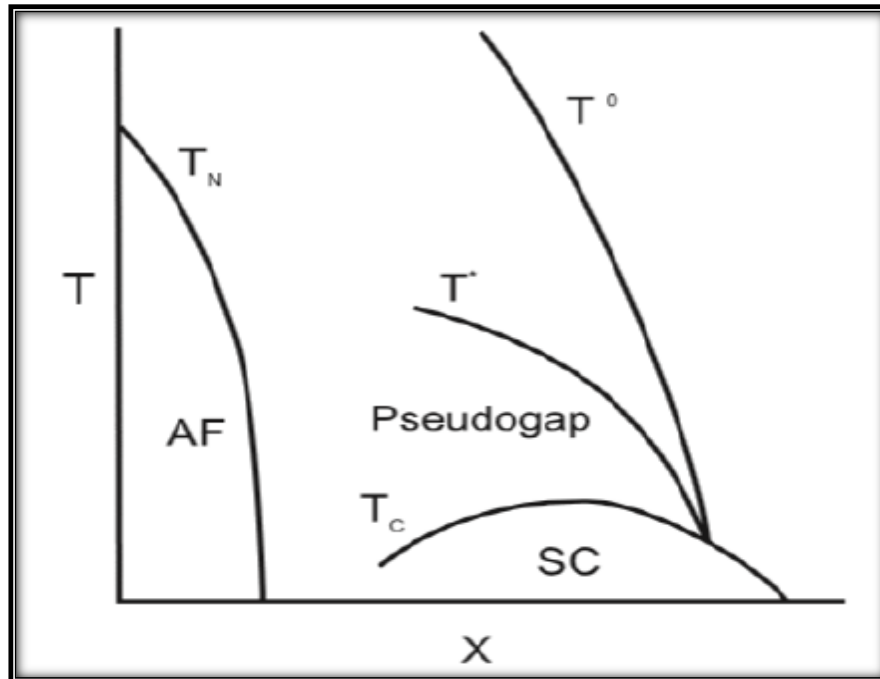
Figure(2-18) :Examples of the lattice-distortive deformations of a cubic lattice(1) a dilation in the three principle directions transforms the lattice into an other cubic with larger lattice parameters;(2) a shear along the (001) plane leads to monoclinic lattice ,and (3) an extension long the [001] axis combined with a contraction along the [100] and [010] axis results in an orthorhombic lattice[89] .

2-16 Phase Diagram of Cuprate Superconductors:

All electron properties of high temperature superconductors depend strongly on the doping. High temperature superconductors without doping are dielectrics and antiferromagnetics. As the concentration x increases, these materials become metals. Superconductivity arises at large x , behind the limits of the magnetically ordered phase. The experiments showed that the charge carriers have the hole character for all classes of high-temperature superconductors. It becomes clear recently that the high-temperature superconductivity is related to peculiarities of the behavior of

these compounds in the normal phase. As seen from phase diagram (Figure 2-19), the superconducting states arise near the antiferromagnetic phase. In yttrium containing systems, the antiferromagnetic and superconducting regions adjoin one another. The experiments on the inelastic magnetic scattering of neutrons indicate the existence of strong magnetic fluctuations in the doped region, even beyond the limits of the antiferromagnetic phase. This points out the important role of antiferromagnetic fluctuations in the compounds with high-temperature superconductivity. In high temperature superconductors, the gap is present in the absence of the phase coherence, i.e., in nonsuperconducting specimens. This gap is called a pseudogap. A pseudogap is shown in (Figure 2-19). It appears at temperatures less than some characteristic temperature T which depends on the doping. Its nature is not completely explained else. The study of a pseudogap in the electron spectrum of high-temperature superconductors was carried out in many works.¹³ Metals become superconductors, if their free electrons are bound in Cooper's pairs. Moreover, the pairs are formed in such a way that their wave functions have the same phase. The phase coherence is responsible for the change of the resistance on the cooling below the critical temperature T_c . The presence of coupled pairs in a superconductor causes the appearance of a gap in the spectrum of excitations. In the standard superconductors, the phase coherence of pairs appears simultaneously with the appearance of pairs. From one viewpoint, a pseudogap is related to the appearance of coupled pairs, which is not related to the phase coherence. Another viewpoint consists in the following. The pseudogap arises in HTSC in connection with the formation of magnetic states which compete with superconducting states. The efforts of experimenters aimed at the solution of this dilemma are complicated by a strong anisotropy of the superconductor gap. Some physicists believe that the most probable situation is related to the creation of the superconducting state with paired

electrons at a certain doping which coexists with antiferromagnetism. It is possible that just it is the “new state of matter” which has been widely discussed for the last years in connection with HTSC[91].



Figure(2-19) :Phase diagram of cuprate superconductors in the temperature-doping variables, T_N -the Néel temperature, T_c -the critical temperature of the superconducting transition, T^* -the characteristic temperature of a pseudogap, T_0 -upper crossover temperature[91].

2-17 Applications of superconductors materials:

Knowing the superconducting properties of superconductors explains their technological applications. Getting to near absolute zero is not easy and expensive. And overcoming many obstacles in this direction is still ongoing. For example, the overhead of the cooling process is not great. The real and most serious obstacles hide in the complexity of the device . The construction, installation and maintenance of the equipment requires very high professional skills, as well as advanced techniques. Operation of superconductors requires complete isolation as well as isolation from the outside, also the helium element is an expensive element and is one of the rare element, for this reason extra cooling and external liquid nitrogen is

used to reduce the cost and loss. This is the process of double-cooling makes the procedures more complex. The wrenches of these magnetic fields related to these devices are not large, In addition, it can change with time under external influences. For this reason, for several years, magnetic fields have been obtained using electric magnets. The superconducting wires are radically different from those used in conventional electrical applications. Superconductors of the latter type are used for resistance to high magnetic fields. It is important to note that the flow of electricity in the superconducting wire allows us to extinguish the power supply, because the wires can form rings and the current continues to flow indefinitely as long as the temperature is below critical transfer temperature. Also applications thin films superconductors (HTSC) are increasingly being used in the manufacture of various microwave ovens used in mobile phones and satellite communications [59,62,93].

Modern applications of superconductors will increase as their critical transmission temperature increases. Superconductors based on liquid nitrogen give factories more flexibility to use superconductivity compared to superconductors based on liquid helium. The possible discoveries of superconductors at room temperature will give us great hope to bring superconducting media to meet our energy needs[94].

Modern superconducting magnets can be made much smaller than resistive magnets, because the coils carry a greater current without loss of energy [88,95] whereas the superconductors will generate the same amount of electricity using smaller devices and less power. Once the electricity is generated, it will spread through the superconducting wires. Moreover, the energy can be stored in superconducting files for a longer period of time without significant loss [48].

The current applications of high temperature superconductors include magnetic protective media, medical imaging systems, Superconducting Quantum Interference Devices (SQUIDS), infrared sensors, symmetric signal processing media and microwave instrument[96,97], The use of films -modern superconducting can produce more compact chips that transmit information more quickly several times [88,95].

Since superconductivity has not been found at room temperature so far, applications in superconductivity are determined at temperatures close to liquid nitrogen temperature. As cooling systems have recently developed significantly, these applications will contribute significantly to society. Superconductors are used to make some of the most powerful magnetic magnets, including magnetic resonance imaging (MRI), which is one of the most powerful magnets used, which help create the necessary areas to help doctors see the body without surgical interference and without exposure to radiation risk [97]. It can also be used for magnetic isolation where the weak magnetism is extracted from a background with less magnetized or non-magnetized particles as in the pigment factories [99].

One of the most productive applications of superconductors is in the water purification system using the effect of magnetic insulation. This system is 100 times more efficient than the magnetic isolation filtering systems currently available[100].

Superconductors have also been used in digital circuitry and microwave filters for mobile phone stations.

Superconductors are used to build the Josephson junction, which are the construction units of SQUIDS, which is one of the most well-known magnetometers. Based on the special method of operation, the Josephson junction can be used as a photon oscillator.

The great change in resistivity when moving from normal to superconducting state is used to build thermometers and photon detectors for the exact high-cooling calorimeter. Early markets arose when the efficiency, quality, size and weight of the high-temperature superconductors overcame the additional cost.

As well as promising future applications include high performance transformers, such as power storage devices, power transmission, electric motors and magnetic buoys. However, superconductivity is sensitive to magnetic fields, and AC applications as transformers will be more difficult to evolve than those that rely direct current direct current Prominent future [101].

HTSC is known to be a brittle material, so there are technical difficulties in producing wires, tapes and films for use, However, research and development in this field suggests that many solutions will be obtained so that HTSC and its media will become commercially available in the future. The use of superconducting wires in high voltage transmission lines is one of the important applications of high temperature superconductors. The performance of the HTSC wires depends on the quality of the tapes. The tapes used in the power transmission cables should be long enough to accommodate the required length of the wire content to be constructed. The most important applications and applications of superconductivity are:

1-Transport wires that carry electricity from the power plants to the substations. Since these wires are made of superconducting material, this means that there is no electrical resistance to the electric current, so there is no loss or loss of energy. As these wires are electric conductors of loss when used together and be on a multi-branched wire, strong, flexible and durable and able to carry an electric current greater by (3-5) times more than those made of copper [102].

2-Generators made of superconducting wires are more efficient than copper wire generators. In fact, there are 99% efficient generators and about half the size of conventional generators. These facts make them very profitable challenges for power use[103].

3-The superconductors, such as trains, can be made to float over superconducting superconductors, and are practically explained by removing friction between the train and the rail. Not only do conventional electromagnets lose a lot of electrical energy such as heat, Physically, they are much more than superconducting magnets[104].

4-In the electronic industry, very high-performance filters are now built from superconducting wire with near-zero electrical resistance in high oscillations, stages of translation into desired frequency section and unwanted frequency closure in radio frequency (RF) applications) As well as in cellular telephone systems.

5-Among the emerging techniques with well-stabilized momentum are Gyroscope, for Earth-orbiting satellites that use superconducting friction conduction properties to close to zero, and X-ray detectors are being developed for superconductivity, Due to its ability to detect a very low amount of energy, scientists developed a camera called (S-Camera), a high-sensitivity optical camera, and superconductors can play an important role in Internet communications soon[105,106].

"Experimental Part"**3.1 Introduction:**

This chapter contain the preparation methods preparation of the compositions $\text{HgBa}_2\text{Ca}_2\text{Cu}_{3-x}\text{Ni}_x\text{O}_{8+\delta}$, $\text{TlBa}_2\text{Ca}_2\text{Cu}_{3-x}\text{Ni}_x\text{O}_{9-\delta}$, $\text{HgPbBa}_2\text{Ca}_2\text{Cu}_{3-x}\text{Ni}_x\text{O}_{8+\delta}$, $\text{TlPbBa}_2\text{Ca}_2\text{Cu}_{3-x}\text{Ni}_x\text{O}_{9-\delta}$,where $\text{Pb}=0.5$, $x=(0.0,0.2,0.4,0.6,0.8\text{ and }1)$ and the techniques that was used for studying properties and characterization of prepared specimens , such as X-ray diffraction (XRD), the electrical resistivity, dielectric properties, determination of oxygen content, the hardness and atomic force microscopy (AFM).

Also it includes of the compound , and the fractional weightings of the prepared specimens.

3.2 Used Raw Materials:

In order to prepare the specimens the following raw materials was used as showed in the table(3-1).

Table (3-1) show specifications of raw materials used in the preparation of the compounds.

Materials	Chemical formula	Molar mass g/mole	purity	Country company
NICKEL Oxide	NiO	74.69	99%	England/GCC
Mercury oxide	HgO	216.59	99%	England/GCC
Barium oxide	BaO	261.35	99%	Swizzes/ Floka
Calcium oxide	CaO	56.08	99%	England /BDH
Copper oxide	CuO	79.45	99%	Germany/ Merck
Thallium(III)Oxide	Tl ₂ O ₃	474.75	99%	England/GCC
Lead (I)Oxide	PbO	223.20	99%	Germany/ Merck

3.3 The weight ratios of the Powders:

The weight ratios of the materials involved in the compounds formation accounts in proportion to their molecular weights as shown in tables (3-2),(3-3),(3-4)and (3-5):

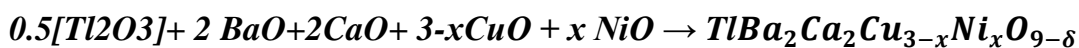
Table (3-2) Quantities of materials used in the preparation of compound($\text{HgBa}_2\text{Ca}_2\text{Cu}_{3-x}\text{Ni}_x\text{O}_{8+\delta}$)



Powder name	Ratio Atomic Weight
HgO	(15.999+200.59)
BaO	(2)*(15.999+137.327)
CaO	(2)*(15.999+40.078)
CuO	(3-X)*(63.546+15.999-
NiO	(X)*(74.69)

X concentration	HgO (g)	NiO (g)	BaO (g)	CaO (g)	CuO (g)
0	0.9912	0	1.4033	0.5132	1.0921
0.2	0.9923	0.0684	1.4049	0.5138	1.0204
0.4	0.9934	0.1370	1.4065	0.5144	0.9486
0.6	0.9945	0.2057	1.4080	0.5149	0.8766
0.8	0.9956	0.2746	1.4096	0.5155	0.8044
1.0	0.9967	0.3437	1.4112	0.5161	0.7321

Table(3-3): Quantities of materials used in the preparation of compound $TlBa_2Ca_2Cu_{3-x}Ni_xO_{9-\delta}$



Powder name	Ratio Atomic Weight
Tl ₂ O ₃	0.5[(204.3833*2)+(3*15.999)]
BaO	(2)*(15.999+137.327)
CaO	(2)*(15.999+40.078)
CuO	(3-X)*(63.546+15.999-
NiO	(X)*(74.69)

X concentration	Tl ₂ O ₃ (g)	NiO (g)	BaO (g)	CaO (g)	CuO (g)
0	1.6397	0	1.1008	0.4026	0.8567
0.2	1.6412	0.0536	1.1018	0.4029	0.8002
0.4	1.6426	0.1074	1.1028	0.4033	0.7437
0.6	1.6440	0.1613	1.1037	0.4036	0.6871
0.8	1.6455	0.2152	1.1047	0.4040	0.6304
1.0	1.6469	0.2693	1.1056	0.4043	0.5736

Table (3-4): Quantities of materials used in the preparation of compound $\text{Hg}_{0.5}\text{Pb}_{0.5}\text{Ba}_2\text{Ca}_2\text{Cu}_{3-x}\text{Ni}_x\text{O}_{8+\delta}$



Powder name	Ratio Atomic Weight
HgO	$0.5(15.999+200.59)$
PbO	$0.5*(223.2)$
BaO	$(2)*(15.999+137.327)$
CaO	$(2)*(15.999+40.078)$
CuO	$(3-X)*(63.546+15.999-$
NiO	$(X)*(74.69)$

X concentration	HgO (g)	PbO (g)	NiO (g)	BaO (g)	CaO (g)	CuO (g)
0	0.4937	0.5088	0	1.3981	0.5113	1.0879
0.2	0.4942	0.5093	0.0681	1.3996	0.5119	1.0165
0.4	0.4948	0.5099	0.1365	1.4012	0.5124	0.9450
0.6	0.4953	0.5105	0.2049	1.4027	0.5130	0.8732
0.8	0.4959	0.5110	0.2736	1.4043	0.5136	0.8014
1.0	0.4964	0.5116	0.3424	1.4058	0.5141	0.7293

Table (4-5): Quantities of materials used in the preparation of compound $Tl_{0.5}Pb_{0.5}Ba_2Ca_2Cu_{3-x}Ni_xO_{9-\delta}$



Powder name	Ratio Atomic Weight
Tl_2O_3	$0.25 * [(204.3833 * 2) + (3 * 15.999)]$
PbO	$0.5 * (223.2)$
BaO	$(2) * (15.999 + 137.327)$
CaO	$(2) * (15.999 + 40.078)$
CuO	$(3 - X) * (63.546 + 15.999 -$
NiO	$(X) * (74.69)$

X concentration	Tl_2O_3 (g)	PbO (g)	NiO (g)	BaO (g)	CaO (g)	CuO (g)
0	0.9158	0.4475	0	1.2297	0.4497	0.9570
0.2	0.9167	0.4479	0.0599	1.2309	0.4502	0.8940
0.4	0.9176	0.4484	0.1200	1.2321	0.4506	0.8310
0.6	0.9185	0.4488	0.1802	1.2333	0.4510	0.7678
0.8	0.9194	0.4493	0.2405	1.2345	0.4515	0.7045
1.0	0.9203	0.4497	0.3009	1.2357	0.4519	0.6411

3.4 Specimens Synthesis

3.4-1 Method of Solid State Reaction:

Solid state reaction method is the most used method for the preparation of superconducting compounds [107,108], including mixture of oxides, carbonates or nitrites, it was used to prepare the specimens of superconducting compound depending on the following steps below:

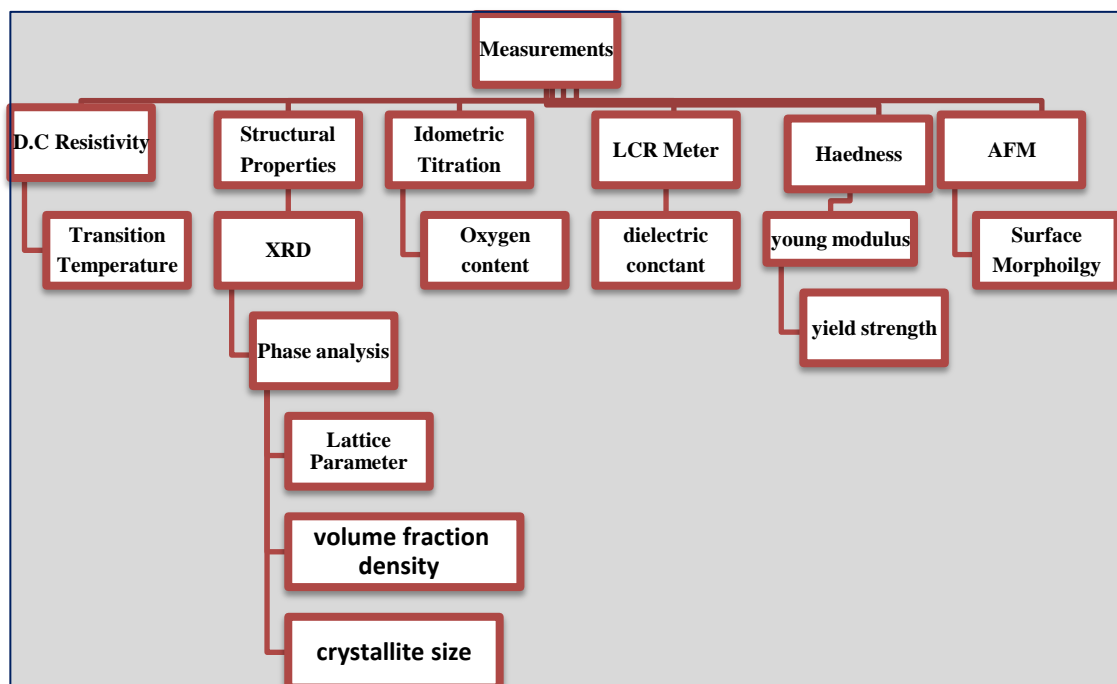
- Measure suitable weights, were selected as the starting materials for the formation of the compounds using sensitive balance (4-digit)
- The constituent compounds were mixed in suitable ratios according to the formula of compounds using a quartz mortar and pestle. With the addition of iso-propanol solution to prevent the powder from volatilization and loss and to form slurry during the process of grinding for about (40-60) minutes.
- Drying the mixed in oven at 120 C° for 1 hour to remove of the added iso-propanol solution.
- The mixed powders were pressed into pellets (1.5 cm diameter and (0.2-0.3) cm thickness) by a hydraulic press for 2 minutes under 7(ton/cm²) pressure.
- The blended powders put then sintered under atmospheric condition in a silica boat at 850C° in a electric furnace(carbolite) for 24 hours with heating rate 5C°/min after that refrigeration at 400C° for annealing and then refrigeration to room temperature at the same rate of heating. Then the pellets were taken out from the boat and carry out the necessary experimental tests.
- The structure of the prepared specimen was studied by using XRD analysis to identification the structure properties, density and the volume fraction (V_{phase}).

3.5 Description Techniques:

In order to study the superconducting structure and electric properties of the specimens following description techniques were used.

- X-ray diffraction
- Resistivity measurements
- Idometric titration
- LCR meter
- Hardness Measurement
- AFM (Atomic Force Microscopic)

Below is a diagram illustrating the measured properties and what we get through these measurements:



3.5.1 Study the Structural Of The Specimens:

The Crystalline structures of the specimens prepared for the compounds were obtained by using of technology X-ray diffraction to examine all the powders prepared specimens and was a user of the device type (SHIMADZU) company which has the following features :

The target of the type (CuK α) wavelength ($\lambda = 1.54 \text{ \AA}$), voltage (40 kV), and current (30 mA), the screening process was conducted for each specimen within the range of angular ($2\theta = 10^\circ - 80^\circ$) helped us this examination to provide the data necessary to identify the crystal structure of output and phase information, also it provided us with this test group by which to calculate other structural parameters such as the lattice constants (a,b) and (c) which calculated from the relation[109].

$$\frac{1}{d^2} = \frac{h^2+k^2}{a^2} + \frac{l^2}{c^2} \dots\dots\dots (3-1)$$

Where:

h, k, l is Miller indices

d (hkl) is the inter planer distance for different planes which estimated from Bragg's law:

$$2d \sin \theta = n \lambda \dots\dots\dots (3-2)$$

Where **n** is the reflection order.

Was studied phase transformation for many composition by using XRD to get the properties of structure [110,111,112,113]. The volume fraction of different phase were found on the relation [114].

$$V_{ph} = \frac{\sum I^o}{\sum I^o + \sum I_1 + \sum I_2} * 100\% \dots\dots\dots (3-3)$$

Where I^o is the XRD peak intensity of the phase which were determined, I_1, I_2, \dots are the peaks intensity of all XRD.

The density of Specimens Synthesis (d_m) We can calculate the density of the specimens using the results of (XRD) Through the following relationship [115].

$$\rho_{x\text{-ray}}(d_m) = Mwt/N_A V \dots\dots\dots (3-4)$$

Where:

$\rho_{x\text{-ray}}(d_m)$ is density calculated from (XRD) in units (gm/cm³).

N_A is Avogadro number (6.022*10²³ mol⁻¹).

Mwt is molecular weight .

V is volume of unit cell which equal (a^2*c) for tetragonal system.

3.5-2 The Resistivity And the Critical Temperature

Measurements:

The more common method for determining the T_c of a superconductor is the measurement of resistivity by using the four-point probe technic in a cryostat with presence of liquid nitrogen. Shows figure (3-1) the circuit diagram of the resistivity measurement . The cryostat system joined to a rotary pump to get a pressure of ($\sim 10^{-2}$ mbar) inside the cryostat , and then joined also to a sensor of a digital thermometer , and thermocouple near the specimen position . Four wires have been connected to the cryostat , the resistance measurement requires connecting of specimens with four leads , the two most outer leads are for current and the two inner leads are for voltage . The outer connections were used for supplying the sample with current from D.C power supply type (phywe) and nanoameter type (kethly model 614) , while the inner connections were used for measuring the voltage drop by a digital nonovoltmeter type (Array M3500A) with sensitivity of about (± 5 nanovolt) .

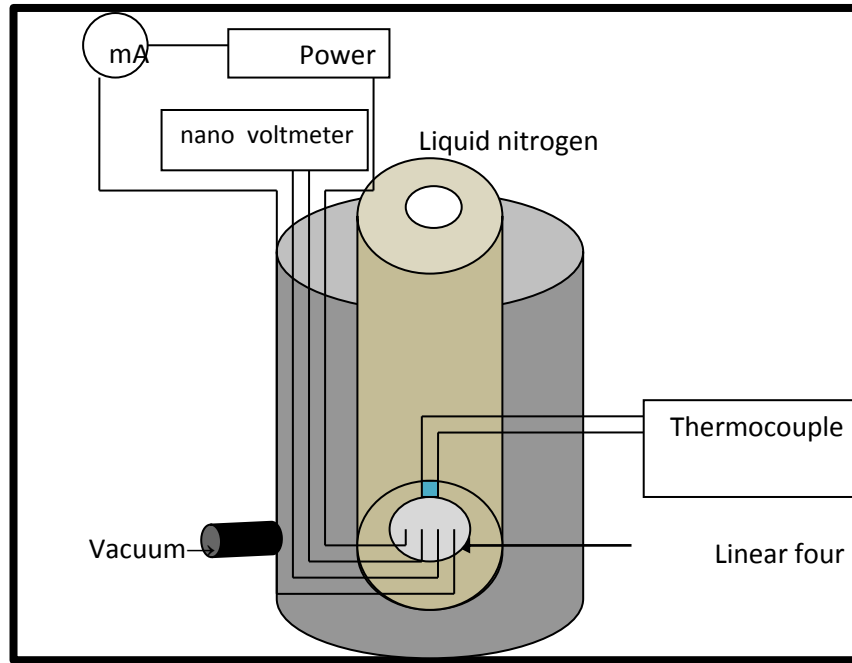


Figure (3-1): Diagram Of Circuit for four - point probe technic [115].

If (I)current passes through the specimen and the voltage drop V is across the electrodes then the resistivity of the specimen ρ also could be found from relation[116] :

$$\rho = \frac{V}{I} \frac{Wt}{L} \quad \text{(four points probe) } \dots\dots\dots(3-5)$$

- where I: is the current passing through the specimen
- V: is the voltage drop across the electrodes
- t: is the thickness of the specimen
- L: : is the effective length between the electrodes

w: is the width of the specimen

or found from equation :

$$\rho = 4.5324 V/I \quad \dots\dots\dots(3-6)$$

if the specimen as a thin film the resistivity for this method :

$$\rho = t * \frac{V}{I} \quad \dots\dots\dots(3-7)$$

where :

The critical temperature could be found from the curve of resistivity versus temperature as shown in the Figure (3-2) . In this curve it can be found three kinds of transition temperature at onset temperature (T_{c1}) , at offset temperature (T_{c2}) and the temperature at midpoint between T_{c1} and T_{c2} which is given by the relation:

$$T_{c(mid)} = \frac{T_{c1} + T_{c2}}{2} \dots\dots\dots(3-8)$$

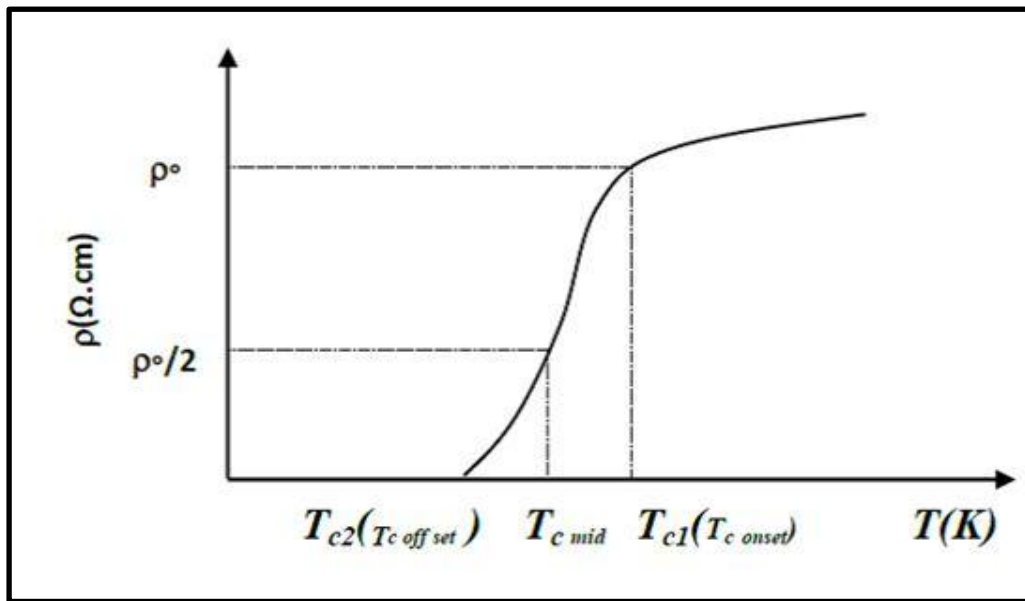


Figure (3-2): Calculate the critical temperature from the curve resistivity [115].

Then we calculated the energy gap of the superconducting samples through the following relationship[61]:

$$E_g = 3.53 K_B T_c \dots\dots\dots(3 - 9)$$

3-5-3 Calculation of oxygen content:

The Oxygen content in the Specimens ($\text{HgBa}_2\text{Ca}_2\text{Cu}_{3-x}\text{Ni}_x\text{O}_{8+\delta}$, $\text{TlBa}_2\text{Ca}_2\text{Cu}_{3-x}\text{Ni}_x\text{O}_{9-\delta}$, $\text{HgPbBa}_2\text{Ca}_2\text{Cu}_{3-x}\text{Ni}_x\text{O}_{8+\delta}$, $\text{TlPbBa}_2\text{Ca}_2\text{Cu}_{3-x}\text{Ni}_x\text{O}_{9-\delta}$) where $\text{Pb}=0.5$ and $x=(0.0,0.2,0.4,0.6,0.8,1.0)$ the value is very important factor of the critical temperature superconductor , therefore ; the Iodometric Titration method used to calculate this factor , it's a simple chemical method can be shown in the following steps [117] :

1. Grinding and weighting (40-45) mg of specimen and placed inside a conical flask on the magnetic stirrer .
2. Adding 2.5 ml of saturated KI solution (3.175g of KI with 2.5 ml of H_2O) , and 1.25ml (10%) of HCl solution are added together to the specimen's powder . The liquid in the flask turns dark brown as I_2 is produced .
3. The solution of the sodium thiosulfate $\text{Na}_2\text{S}_2\text{O}_3$ (0.3 gm of $\text{Na}_2\text{S}_2\text{O}_3 \cdot 5\text{H}_2\text{O}$ in 20 ml of H_2O to get concentration of about (0.015 gm/ml) is added to the liquid from a burette , when the liquid becomes pale brown a few drops of starch were added . The liquid turns dark blue .
4. Adding of the $\text{Na}_2\text{S}_2\text{O}_3$ solution but more slowly , the liquid turns yellow. This means the reaction is completed .
5. Stopping the titration and measuring the volume of titrated $\text{Na}_2\text{S}_2\text{O}_3$ solution that has been used , and the oxygen content (δ) could be found by the equation:

$$\delta = \frac{\left[\frac{M_A}{M_B} \right] - \left[\frac{3m_A}{CV} \right]}{\left[\frac{2m_A}{CV} \right] - \left[\frac{M_o}{M_B} \right]} \dots\dots\dots(3-10)$$

Where M_A : is the molar mass of the specimens.

M_B : is the molar mass of $\text{Na}_2\text{S}_2\text{O}_3 \cdot 5\text{H}_2\text{O} = 248.18$

M_o : is the atomic of weight of oxygen= 15.9994.

m_A : is the weight of the specimen = (40-45)mg

C : is the concentration of the $\text{Na}_2\text{S}_2\text{O}_3$ $x=0.015\text{gm/ml}$

V : is the volume of $\text{Na}_2\text{S}_2\text{O}_3$ used in titration.

3-5-4 Measurements Of Dielectric Properties At DifferentFrequencies:

A material is classified as “dielectric” if it has the ability to store energy when an external electric field is applied. If a DC voltage source is placed across a parallel plate capacitor, more charge is stored when a dielectric material is between the plates than if no material (a vacuum) is between the plates. The dielectric material increases the storage capacity of the capacitor by neutralizing charges at the electrodes, which ordinarily would contribute to the external field[118].

The dielectric constant was measured for all specimens at different frequencies ranging from (50Hz-5MHz) at room temperature (25°C) by using the (HF LCR METER) model (6500P Series, Issue A1, Wayne Kerr Electronics ,UK, frequency range (20Hz-120MHz). The real part of dielectric constant (ϵ') , dielectric loss factor and absolute $|\tan \delta|$ and alternating electric conductivity ($\sigma_{a.c}$) , were calculated by measuring the capacitance (c) using LCR meter impedance analyzer , the value of the real part dielectric constant (ϵ') is calculated from the equation[119,120,121] :

$$\epsilon' = \frac{cd}{A \epsilon_0} \dots\dots\dots (3.11)$$

and

$$|\tan \delta| = \frac{\epsilon''}{\epsilon'} \dots\dots\dots(3.12)$$

$$\sigma_{a.c} = 2\pi f \epsilon'' \dots\dots\dots(3-13)$$

Where:

ϵ'' dielectric loss factor , **d** is the thickness of the specimen , **A** is the area of the electrode , ϵ_0 is the permittivity of free space = 8.85×10^{-12} F/m , f Frequency.

The complex dielectric constant(k) consists of a real part(ϵ') which represents the storage and an imaginary part (ϵ'') which represents the loss. Permittivity describes the interaction of a material with an electric field E and is a complex quantity.

$$k = \frac{\epsilon}{\epsilon_0} \dots\dots\dots(3-14)$$

Dielectric constant (k) is equivalent to relative permittivity (ϵ_r) or the absolute permittivity (ϵ) relative to the permittivity of free space (ϵ_0). The real part of permittivity (ϵ') is a measure of how much energy from an external electric field is stored in a material. The imaginary part of permittivity(ϵ'') is called the loss factor and is a measure of how dissipative or lossy a material is to an external electric field. The imaginary part of permittivity(ϵ'') is always greater than zero and is usually much smaller than (ϵ'). The loss factor includes the effects of both dielectric loss and conductivity[118].

3-5-5 The Mechanical Properties:

The most common mechanical properties which are used in order to classify and identify materials are hardness (H_v) , yield strength (Y) and Young modulus (E) . These properties involve a reaction to applied loads . One reason for the variation in properties of a material due to the microstructure of the directivity formed during the material manufacturing process [122] .

3-5-5-1 The Hardness Measurement:

Hardness measurements of the specimens were performed on the polished surface of the examined specimens with using a digital micro hardness tester at room temperature. The applied load (F) varied in the value (2.94 N)and applied for 15 seconds. The indenter was pressed on the polished different surfaces of the specimens making sure that the indentations do not overlap.

The load dependent (Vickers) microhardness values of the specimens are calculated using the relation[123]:

$$H_v = 1.8544 (F/ d^2).....(3-15)$$

Where : **F** : the amount of inflicted force

d : arithmetic mean of the two diagonals in mm

3-5-5-2 Young's modulus(E):

The ratio between tensile stress to tensile strain in the linear elastic range is called modulus of elasticity and is a characteristic of the metal. Therefore the Young modulus describes the resistance of the body to mechanical action . The elastic modulus of crystal depends only on the type of atom and their relative position and it is a measure of the atomic binding forces in the lattice of crystal [124] .

The Young modulus E of superconductors is related to the Vickers microhardness by the relation[123]:

$$E = 81.96 H_v \quad(3-16)$$

3-5-5-3 Yield Strength (Y):

Yield strength , is one of the material property, particularly in ductile materials . It not only represents the change from a recoverable , the yield strength may be an even more important mechanical property than the modulus for certain applications[125].

The yield strength Y is related to the hardness by the relation[123]:

$$Y = H_v / 3 \quad \dots\dots\dots(3-17)$$

3-6 Atomic Force Microscopy (AFM):

Atomic force microscopy (AFM) is one of the most versatile imaging techniques to investigate surface science at the nanoscale[126].

In recent years, as the most reliable technology for experimental determination of the surface roughness of material has been used Atomic Force Microscopy (AFM). AFM was developed by Binnig and Quate in 1986, as the first technology for high-precision measurement and displaying images in real-time. Its application until today is largely present in all scientific fields, including and aesthetic dentistry. AFM enables 3D scanning topography of the contact surfaces of different materials at micro and nano level, in the form of 3D images with high-resolutions. Due to the sharper tip and small loading force, the lateral resolution in AFM is extremely improved in comparison with the conventional profilometer. However, the maximum measuring range of AFM is limited to the surface of 100 x 100 μm [127].

All experimental measurements of 3D surface topography and roughness parameters were obtained using the Atomic Force Microscopy (AFM)[127]. The tip interacts with the surface , causing the cantilever to bend. A laser spot is reflected from the cantilever onto a position - sensitive photodiode detector . As the cantilever bends , the position of the laser spot changes. The resulting signal from the detector is the deflection, in volts [128,129].

"Results and Discussion "**4.1 Introduction:**

In this part of the research we provide a systematic study and discussion the practical results obtained from the tests and measurements on the effect of the partial substitution of Ni on Cu, Pb (=0.5) on (Hg,Tl) for superconductivity behavior of $\text{HgBa}_2\text{Ca}_2\text{Cu}_{3-x}\text{Ni}_x\text{O}_{8+\delta}$, $\text{TlBa}_2\text{Ca}_2\text{Cu}_{3-x}\text{Ni}_x\text{O}_{9-\delta}$, $\text{Hg}_{0.5}\text{Pb}_{0.5}\text{Ba}_2\text{Ca}_2\text{Cu}_{3-x}\text{Ni}_x\text{O}_{8+\delta}$, $\text{Tl}_{0.5}\text{Pb}_{0.5}\text{Ba}_2\text{Ca}_2\text{Cu}_{3-x}\text{Ni}_x\text{O}_{9-\delta}$, where $x = (0.0, 0.2, 0.4, 0.6, 0.8 \text{ and } 1)$ and the conditions of preparation.

We investigated the, x-ray diffraction analysis, resistivity measurements, oxygen content determination, dielectric properties, hardness and atomic force microscopy (AFM) for all specimens.

For specimens were prepared under pressure 7 ton/cm^2 for two minutes with pallets 1.5 cm diameter and (2-3) mm thickness. It should be pointed out that pressure equal and higher than 7 ton/cm^2 is more efficient, yields brittle pellets and specimens success.

All specimen were sintered at 850°C . High sintering temperature (850°C and for a long period of time (24) hours)[130], are necessary to produce an active powder fin diffusion between the element to produce the compound with higher density, r porosity closes and the distance between the grains decreases.

We are using optimum preparation condition to get a high $-T_c$ of Hg-1223 and Tl-1223 superconductors. The optimum preparation condition are:

- 1-The forming pressure of pellets is 7 tons/cm^2 .
- 2-The sintering temperature is 850°C .
- 3-The time sintering 24 hours.
- 4-controlling furnace at 5°C for hours.
- 5- annealing temperature at 400°C , 4 hours
- 6-The partial substitution of (Hg,Tl) by Pb and Cu by Ni.

4-2 HgBa₂Ca₂Cu_{3-x}Ni_xO_{8+δ} Compound:

The compound were prepared and the molecular weights were calculated according to the following formula:



As follows the results of the tests of the physical properties (structural, electrical and mechanical) test for all compounds:

4-2-1 Study of Structural Properties:

The crystal structure of the specimens prepared by a solid state reaction method were studied by x-ray diffraction (XRD) . The XRD data collected from various specimens (specimens having various Ni concentration) . All the specimens are shown a polycrystalline and they have tetragonal structure. Results of XRD patterns are shown in Figure (4-1).

Figure (4-1) shows the X-ray diffraction analysis with miller indices of the specimen with and without Ni (x=0,0.2,0.4,0.6,0.8 and 1) .Partial substitution by nickel observed increasing intensity with increasing of nickel concentration. From this figure , it can be observed that all the specimens were consist of a major 1223 high-T_c phase (H-peaks), minor phase 1212 (M-peaks), , minor low-T_c phase 1201 (L-peaks) and a very small amounts of impurity phases with vanishingly small concentrations could be related to the stacking faults along the c-axis which are agreement with reference[25].

The appears of different phases in the pure specimen and the other specimens in general is due to the displacement of defects of the atomic or reduction of oxygen or irregularity of positive ions, which lead to the accumulation of defects in the stack along the axis (c), which ultimately lead to distort the crystalline structure[131,132].

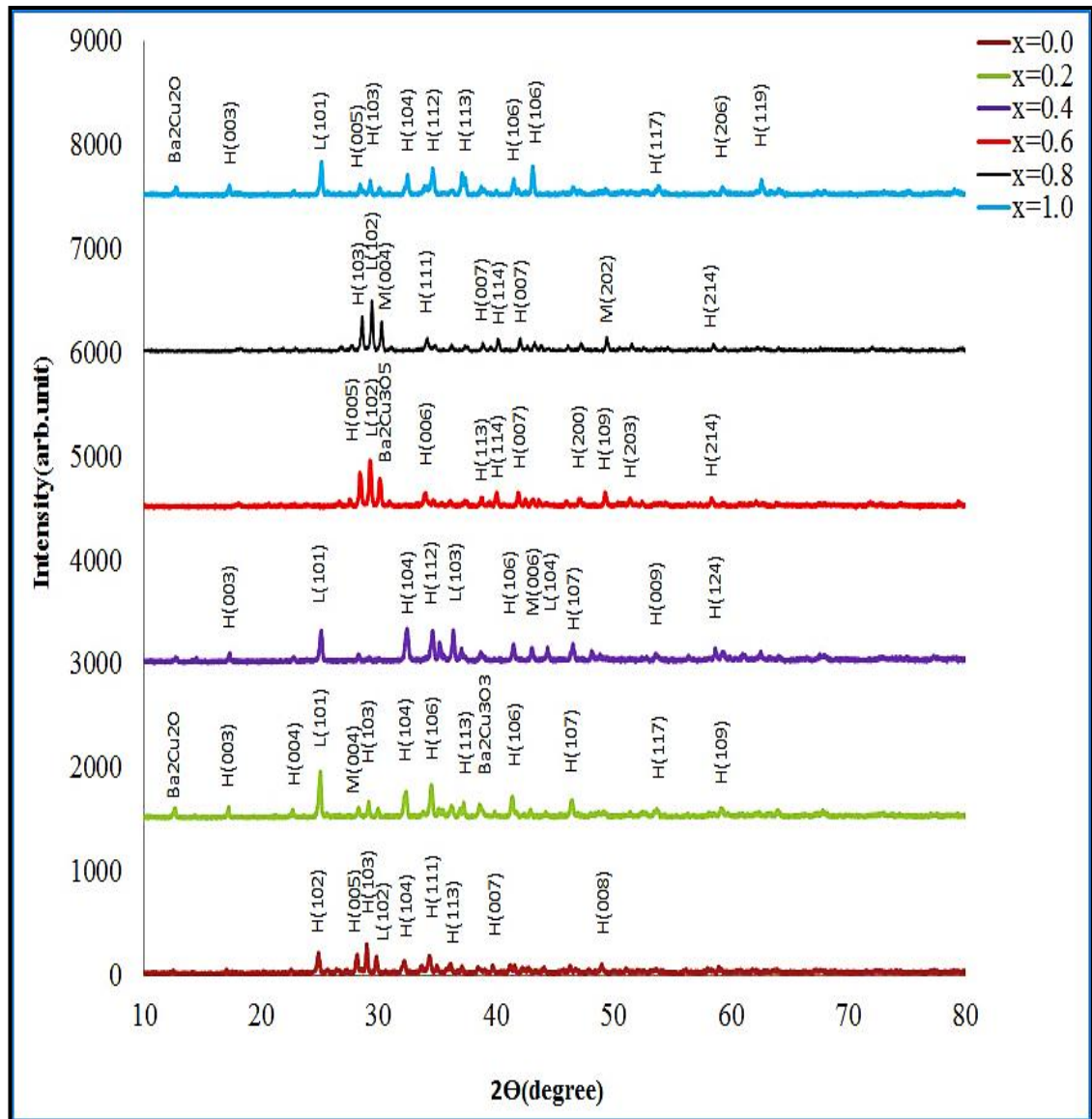


Figure (4-1): XRD pattern of $\text{HgBa}_2\text{Ca}_2\text{Cu}_{3-x}\text{Ni}_x\text{O}_{8+\delta}$

After determination the peaks and intensity compared then with the stander schemes and according to equation (3-3) and calculated the parameters a, b, c and c/a . The calculation of the value by using computer program, which showed different values, The reason for the results shown in table (4-1) due to the temperature and time of the sintering when increasing both the temperature and the time of the sintering gives more energy du to the material molecules overlap and thus reduce the large surface area of the molecules at the expense of their volume, As well as the time of sintering is necessary and required to obtain thermodynamically balanced stages where the long time of sintering is necessary to insertion

additional CuO and CaO layers in the structures of low phases 1201,1212 and this gave positive results in terms of the composition of the 1223 high phase in the specimen[133,134].

From this figure (4-1) we can easily notice the difference between all specimens, the high- T_c phase reflections of pure specimen have lower intensity than specimens which have Ni additions, besides that there is appearance of clear and sharp peaks especially when $\Theta = 31.28^\circ = 39^\circ$, and shifting of peak position in comparison with pure specimen. This may be attributed to the substitution of Ni in Cu sites that means peaked tops are overlapped and this indicates that (CuO) layers are formed which are thought to have a significant role in the superconducting process. Thus the compound is reached at its best of regularity and stability, which helps to provide safety tracks for current carriers. The peaks were in agreement with ASTM Card number (046-0439,045-0305,045-0615,048-0144) [2012 international center for Diffraction Data].

Furthermore substitution of Ni^{+2} for Cu^{+2} ions yields further holes, thus, they will modulate the structure by influencing the charge balance, oxygen distribution, and relevant interaction process between the neighboring layers, and enhance the hole concentration in Cu-O layers.

The lattice parameters have been estimated using d-values and (hkl) reflections of the observed x-ray diffraction pattern through the software program based on Cohen's least square method[134], this table shows the parameters $a=b, c$, V volume, density d_m and volume fraction V_{ph} variation of c/a for Hg(1223) phase specimens comparable with the free specimen. The values are shown in table (4-1). The result as shown from table it was found increasing of c-axis lattice constant with the increase of Ni concentration up to $x=0.6$ results in agreement with Noor S. Abed et al research[34], while then it decreases above 0.6 ($x=0.8, 1.0$). The reason is

due to the substitution of Ni for Cu where the ionic radii of Ni^{+2} (83 pm) is shorter than of Cu^{+2} (87 pm) which render c-axis to be longer or caused deformed in c-axis, another reason may be can explained the increase of the oxygen content in the unit cell. It was speculated that the excess of oxygen goes into the mercury oxide layer causing an increase in **c** the lattice parameter.

Table(4-1) : Lattice parameters and volume fraction of $\text{HgBa}_2\text{Ca}_2\text{Cu}_{3-x}\text{Ni}_x\text{O}_{8+\delta}$ compounds

X	a=b(A ^o)	c(A ^o)	c/a ratio	v(A ^o) ³	d _m (gm/cm ³)	V _{ph} (1223)%	V _{ph} (1212)%	V _{ph} (1201)%	V _{ph} impurities%
0	3.8038	15.7117	4.1305	227.330	6.38435	74.7270	16.100	1.2180	7.9540
0.2	3.8813	15.8075	4.0727	238.131	6.08800	75.7370	4.5570	13.9410	5.7640
0.4	3.9732	15.8753	3.9955	250.612	5.7783	78.421	7.631	8.421	5.526
0.6	4.0798	16.2484	3.9826	270.450	5.3485	82.959	8.247	7.701	1.091
0.8	3.9064	16.0123	4.0989	244.347	5.91335	78.8173	6.5868	14.5958	3.5179
1	3.8405	15.8451	4.1257	233.706	6.17569	78.0279	4.1149	17.8571	9.8602

The relative intensities of XRD patterns of $\text{HgBa}_2\text{Ca}_2\text{Cu}_{3-x}\text{Ni}_x\text{O}_8$ specimens we can noticed that the Ni addition increase, producing of High-phase and decrease of Medium and Low-phase by increasing Cu-O layer due to increasing hole in the structures. The presence of Ni concentration in Hg(1223) phase has been a direct influence on the increasing of high phase ,its can be clearly in X-ray diffraction analysis (XRD).

As demonstrate in Figures (4-2),(4-3),(4-4). From this figures we can found that the V_{ph} ,c/a and the density (*d_m*) which have been calculated from equations (3-3,3-4) variation with increase value Ni, due to existence

of porous in $\text{HgBa}_2\text{Ca}_2\text{Cu}_{3-x}\text{Ni}_x\text{O}_{8+\delta}$ which would leads to increase Critical temperature T_c .

In all specimen of $\text{HgBa}_2\text{Ca}_2\text{Cu}_{3-x}\text{Ni}_x\text{O}_{8+\delta}$ increase high- T_c phase and decreased low- T_c phase is promoted by Ni substitution in compound. We observed many satellite reflection that are due to ordering of the cations and or displacement of an ion or oxygen defects (the oxygen deficiency increase when Ni is substitution by Cu).

Figure (4-2) shown the ratio of volume fraction V_{ph} as function of Ni concentration.

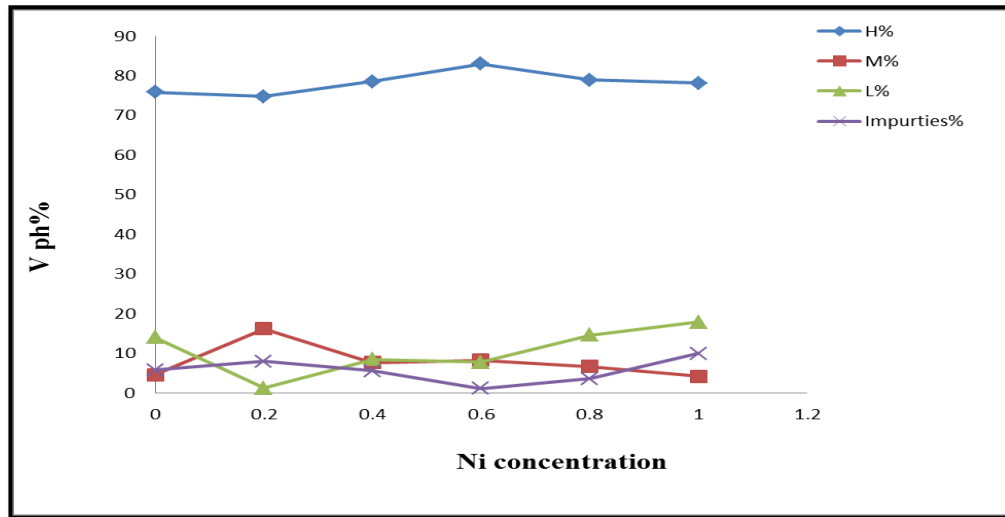


Figure (4-2) :The ratio of volume fraction V_{ph} as function of Ni concentration for the $\text{HgBa}_2\text{Ca}_2\text{Cu}_{3-x}\text{Ni}_x\text{O}_{8+\delta}$ specimens

The ratio c/a explain in figure (4-3) shown that c/a variation with Ni because the change in lattice parameter ($a=b,c$).Figure (4-4) shown the variation of d_m with increasing Ni concentration.

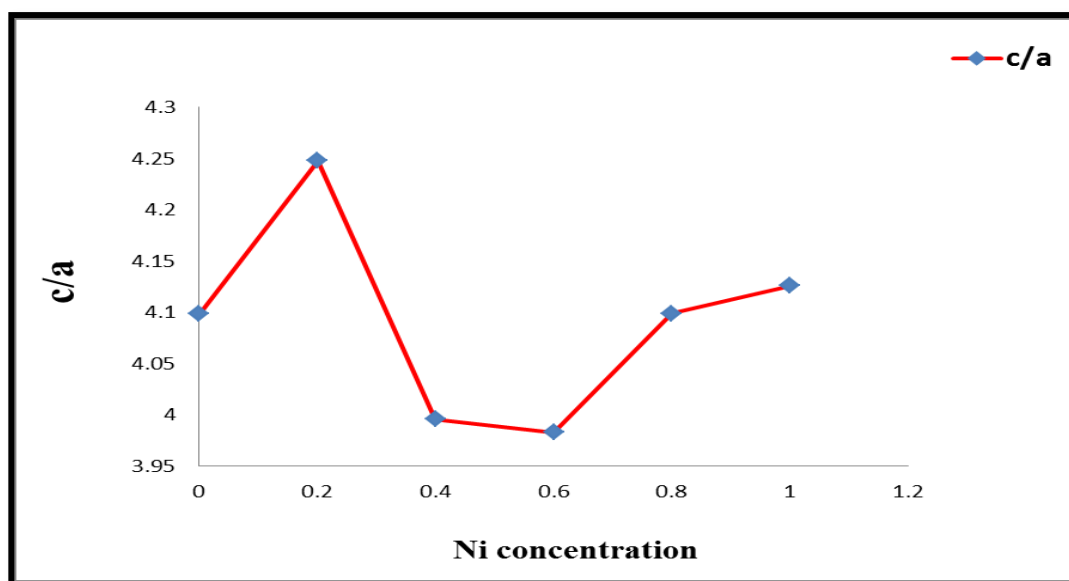


Figure (4-3) :The ratio of lattice parameters c/a as function of Ni concentration for the $\text{HgBa}_2\text{Ca}_2\text{Cu}_{3-x}\text{Ni}_x\text{O}_{8+\delta}$ specimens

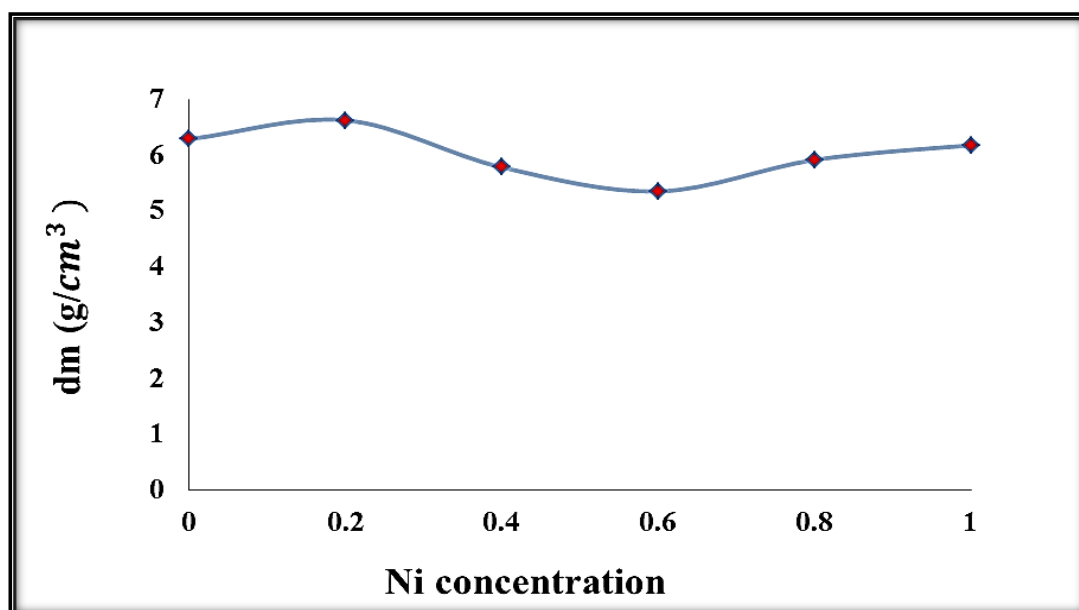


Figure (4-4): Variation density with Ni concentration for the $\text{HgBa}_2\text{Ca}_2\text{Cu}_{3-x}\text{Ni}_x\text{O}_{8+\delta}$ specimens

This is more likely to be the result of an incommensurate structure which gives rise to deformation of c-axis parameter. The structure deformation is always considered as the cause of the high conduction in the perovskite

multi layer but without the substitution of Ni occurs reversal in crystalline structure. From the above we can notes summarized:

The deformation in the c-parameter as a result of Ni partial substitution adjusts the amount of charge transfer from Hg-O layer to Cu-O layer of Hg-1223 and force the generation of hole pairing in the Cu-O layers.

The addition of Ni as partial substitution to the Hg-1223 compounds has a great effect on the enhancement of the high- T_c phase. The role of Ni is apparently to modify the structural properties and particularly the strength of the bonding between the slabs that constitute the building blocks of the compound.

4-2-2 Study of Electrical Resistivity:

The electrical resistivity as a function of temperature is one of the most important characteristics for superconductor compounds to find the critical temperature(T_c). In order to examined this property for of **HgBa₂Ca₂Cu_{3-x}Ni_xO_{8+δ}**, **TlBa₂Ca₂Cu_{3-x}Ni_xO_{9-δ}**, **HgPbBa₂Ca₂Cu_{3-x}Ni_xO_{8+δ}** and **TlPbBa₂Ca₂Cu_{3-x}Ni_xO_{9-δ}**, where Pb=0.5 and **x=(0.0,0.2,0.4,0.6,0.8and 1)** Compounds .

It was testing the voltage, current as function of temperature by using a four-point probe technique. The superconducting properties can be controlled by using the partial substitution of an cations with different ionic radius and bonding characters. The enhancements of the superconducting properties depend on the properties of the dopant.

In the figure (4-5) shown the electrical resistivity as a function of temperature for the system **HgBa₂Ca₂Cu_{3-x}Ni_xO_{8+δ}** ,all specimens displayed a metallic character above onset temperature ,which is defined as the temperature where resistance – temperature plot deviates from linearity.

Figure (4-5) and Table (4-2) shown the effect of Ni on Cu in the $\text{HgBa}_2\text{Ca}_2\text{Cu}_{3-x}\text{Ni}_x\text{O}_{8+\delta}$ with $x = (0.0, 0.2, 0.4, 0.6, 0.8 \text{ and } 1)$. It is found from figure (4-5) that the resistivity for all specimen decrease with decrease temperature to the zero resistivity. It was found the critical temperature for specimen has no Ni content ($x=0$) is equal to 119K .while specimen with ($x=0.6$) has a higher critical temperature equal 138.5K, and the resistivity went down nearly sharp , the reason may be attributed to the existence of the high T_c -phase as referred in x-ray analysis which can be due to the great increment in Hg-1223 and decrement in other phases (Hg-1212 and Hg-1201) when comparison with the pure specimen because it increasing Cu-O layer in 1201 ,1212 product 1223 and this can may be due to (Ni) substitution which tends to do disorder in (CuO) lattice and strengthen the superconducting, while the specimen when ($x=0.2, 0.4$) T_c equal at 123, 130 K respectively. Increase Ni to 0.8, 1.0 decrease the critical temperature to 129, 125 K. The decrease in T_c are further evidence that the presence of increase amount of Ni content in Hg-1223 phase stabilizes and promotes the growth of Hg-1212 and Hg-1201 phase at the expense of Hg-1223 phase.

Also increased or decreased (O_2) concentration in the mixture can be belonged to deformity in the mercury oxide layers which expected to be opposed by increment in holes concentration in (Cu-O) layers ,hence there will be a rearrangement in holes concentration between (CuO and HgO) layers which can cause the change in lattice parameters and in holes concentration in (CuO) layer leading to a great increment in the critical temperature, thus the superconductor depends on the number of (CuO) layers and the (O_2) content in the specimen, so the specimens of high (T_c) contain high (O_2) content.

Table(4-2): Lattice parameters and transition temperature of $\text{HgBa}_2\text{Ca}_2\text{Cu}_{3-x}\text{Ni}_x\text{O}_{8+\delta}$ compounds

X	V _{ph} (1223)%	V _{ph} (1212)%	V _{ph} (1201)%	V _p impurities%	T _{C(0%)} (K)	T _{C(0%)} (K)	?T _C (K)	T _{C(min)} (K)	E _g (eV)	δ
0	74.7270	16.100	1.2180	7.9540	116.5	121.5	5	119	0.0381	0.0676
0.2	75.7370	4.5570	13.9410	5.7640	121.3	124.7	3.4	123	0.0374	0.0774
0.4	78.421	7.631	8.421	5.526	9	9	3	130	0.0395	0.0862
0.6	82.959	8.247	7.701	1.091	139	143.8	4.8	138.5	0.0421	0.1058
0.8	78.8173	6.5868	14.5958	3.5179	129	130	1	129	0.0392	0.0786
1	78.0279	4.1149	17.8571	9.8602	117	133	16	125	0.03802	0.0785

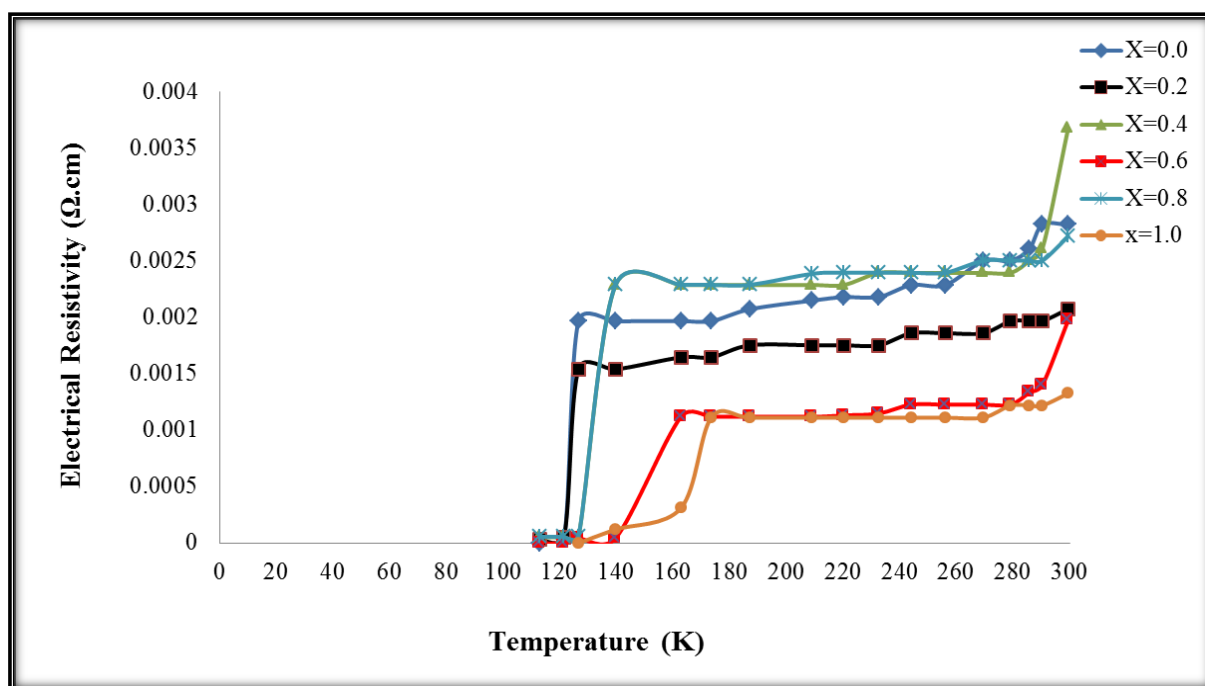


Figure (4-5): The resistivity as function of temperature for $\text{HgBa}_2\text{Ca}_2\text{Cu}_{3-x}\text{Ni}_x\text{O}_{8+\delta}$ specimens for $x=0.0, 0.2, 0.4, 0.6, 0.8$ and 1.0

Copper is present in the mixed valence state involving a partial oxidation of Cu^{2+} to Cu^{3+} [74].

The increasing value of resistivity and then decreasing trend in the value of zero-resistance critical temperature (T_{c0}) indicates that the connectivity between grains decreases gradually with the addition of Ni similar to [136]. All these effects are due to increased in homogeneities in the intergranular regions. The point defects and chemical dopants may occupy various positions in a real crystal forming substituent or interstitial impurities. Because of the grain boundary is a structurally distorted region in crystals, an extra energy form in the grain boundary region due to the distortion. As a result of the existence of grain boundary energy as well as the Coulomb interaction between the impurity and the boundaries atoms, they tend to attract impurity atoms in order to decrease the grain boundary energy.

The transition width (ΔT_c) decreases with substitution concentration. this may be due to homogeneity of specimen during preparation, then the transition width (ΔT_c) increases with substitution concentration ($x=1.0$) this may be due to the gradual occurrence of non-superconducting additional phases (over doping) and the effect of microscopic inhomogeneity.

Suggests that increase Ni the cationic substituting for Cu tend to inflict deformed in Cu-O layers which at a higher dopant level may show superconducting-like resistance behavior but don't reach to $\rho=0$. The reason of that may be ascribed to effects the changes of the carrier concentration and microstructure induced by the replacement and the decrease of T_c should be mainly attribute to the magnetic scattering induced by Ni ions.

The partial substitution of Ni in Cu site should have effect on the cooper pairs in the Cu-O plane so the increase in T_c mean that it increases the charge carriers to move easier in the Cu-O plane leading to the higher T_c .

We noticed that the specimen $x=0.6$ has optimum doping regime while decrease of T_c beyond this concentration ($x=0.8, x=1.0$) seems to be due to the shift of this specimen towards the over-doped region, the reason of that due to more addition of Ni (0.8 and 1.0) decreases T_c , due to decreasing c-lattice parameter which leads to decreasing the cooper pairs in the Cu-O plane, and the existence of high amounts of the secondary phase.

"The superconducting gap can be defined as the energy difference between the ground state of the superconductor and the energy of the lowest quasiparticle excitation"[137].

Figures (4-6),(4-7) respectively shown the relationship between(Transition temperature and Energy gap) as a concentration of Ni and it be shown that exhibit behavior similar to both T_c, E_g with Ni increase for pure specimen $x=0$ up to $x= 0.6$ and then decrease.

The nature of the gap of the high temperature superconductors came from several hints that the gap remained in the normal state at temperatures above the superconducting transition temperature. The first evidence from this came from NMR experiments which found a gap like depression of the density of state at the Fermi surface below a temperature T^* which was larger than T_c at lower doping levels but approached T_c near optimal doping[137].

A gap at the Fermi level is a signature property of the conventional BCS superconductors. High temperature superconductors have a gap with nodes but in addition, at low doping levels, there is a normal state gap called a pseudogap. Whether this gap is a result of a precursor state to superconductivity or a completely separate order that competes with superconductivity is an open question[137].

The gap was highly anisotropic in momentum space ,going to zero for electrons travelling in certain directions, and yielding a gap magnitude that varied as $(k_x^2 - k_y^2)$ around the Fermi surface[137].

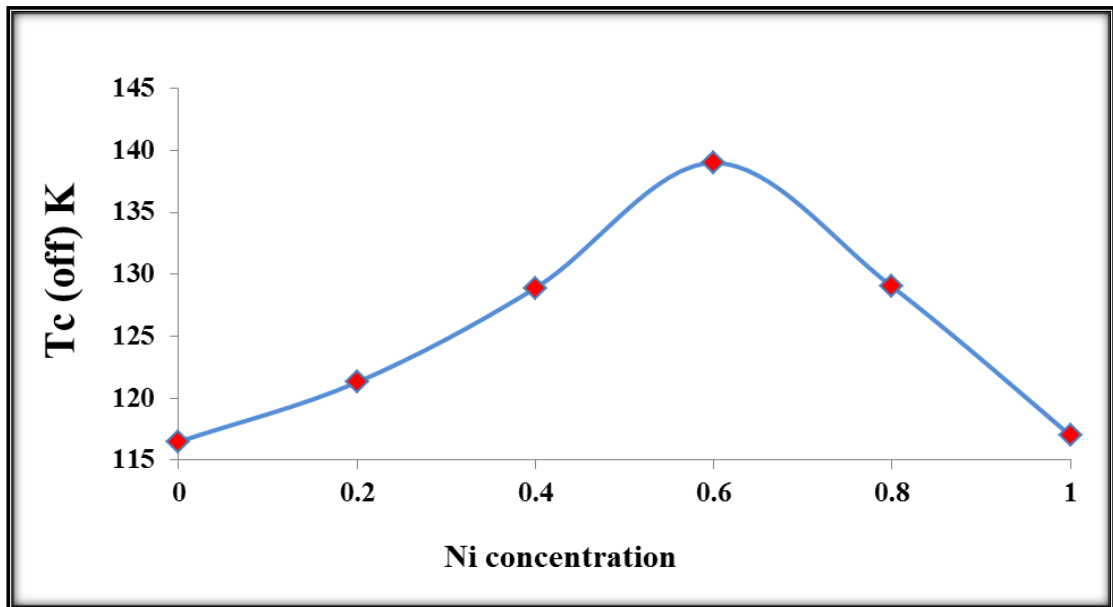


Figure (4-6) : The T_c (offset) a function of concentration Ni of $\text{HgBa}_2\text{Ca}_2\text{Cu}_{3-x}\text{Ni}_x\text{O}_{8+\delta}$ specimens

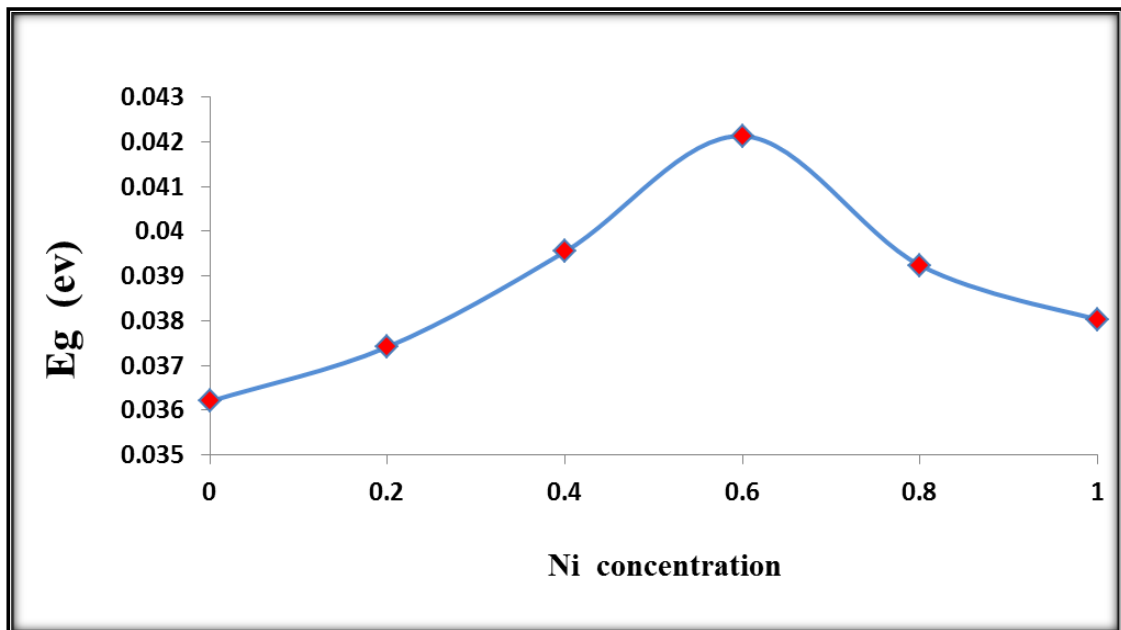


Figure (4-7): Energy gap E_g (eV) a function of concentration Ni of $\text{HgBa}_2\text{Ca}_2\text{Cu}_{3-x}\text{Ni}_x\text{O}_{8+\delta}$ specimens

4-2-3 Results Of Oxygen Content:

The values of (δ) which is the excess concentration of oxygen in the prepared specimens of $\text{HgBa}_2\text{Ca}_2\text{Cu}_{3-x}\text{Ni}_x\text{O}_{8+\delta}$ ($x=0.0,0.2,0.4,0.6,0.8,1.0$) was measured by using a chemical Iodometric titration experiment discussed in (chapter two).

Table (4-2) shows the values of critical temperature T_c related to δ for all specimens . Table (4-2) and Fig (4-9) shows the values of T_c related to δ values. It can be noticed that δ and T_c increase with the raising of the dopant concentration for $\text{HgBa}_2\text{Ca}_2\text{Cu}_{3-x}\text{Ni}_x\text{O}_{8+\delta}$ with $x=0.0,0.2,0.4,0.6,0.8,1.0$.An arise of δ has been attributed to the existence of excess oxygen atoms in the Cu-O₂ layers. This leads to create more holes in the perovskite layers and shortening in the bond length of the Cu-O and enhance the T_c .

It is observed from Table(4-2) that T_c increases as δ increases because the presence of excess oxygen atoms in the CuO₂ layers will create more holes in the perovskite layers and this creation of the holes in the CuO₂ sheet will shorten the Cu-O bond length and tend to improve the transition temperature .

Similar behavior of δ with transition temperature was found by Zhao et.al[138].

The critical temperature dependence on the oxygen amount δ of each superconducting compound is listed in table (4-2), and shown in figure (4-8).

In general this table explain clearly, the content of oxygen δ values various from (0.0676) to the value (0.1058) for the nominal compound $\text{HgBa}_2\text{Ca}_2\text{Cu}_{3-x}\text{Ni}_x\text{O}_{8+\delta}$ specimens, remaining all conditions from sintering temperature at (850°C) and time of sintering (24 hr) in air are controlled and fixed.

The oxygen content increases from 0.0676 to 0.1058 when the Ni concentration increasing from (0 to 0.6) and decreasing when the Ni increasing above 0.6 as shown in figure (4-8).

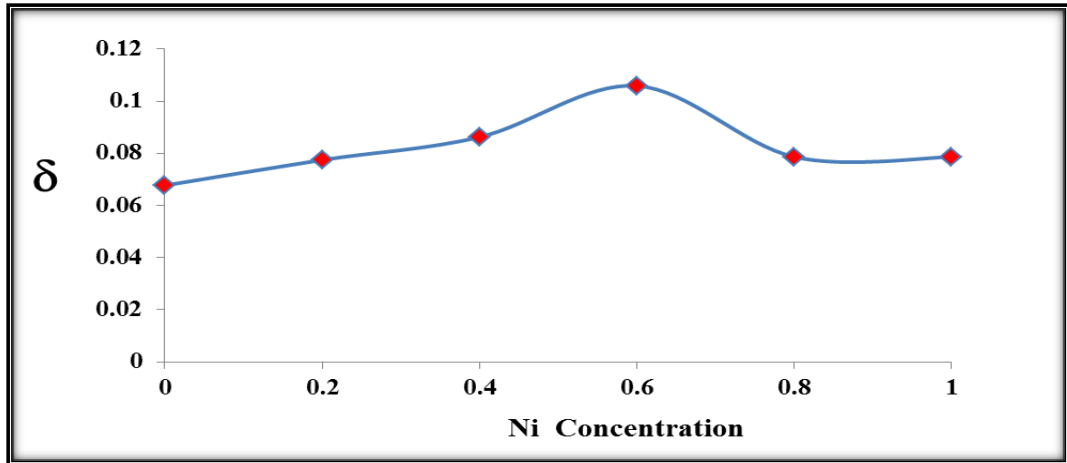


Figure (4-8): Oxygen content as a function of concentration Ni of $\text{HgBa}_2\text{Ca}_2\text{Cu}_{3-x}\text{Ni}_x\text{O}_{8+\delta}$ specimens

This reduction of δ could be explained as follows: the increases of Ni raise the acceptor levels as comparably with donor level which producer from Cu existence in CuO_2 layer.

The figure (4-9) shown variation of T_c as a function of oxygen content in $\text{HgBa}_2\text{Ca}_2\text{Cu}_{3-x}\text{Ni}_x\text{O}_{8+\delta}$ specimen. It may also affect the oxygen content in the crystals and the superconducting transition temperature they have shown to be sensitive to the oxygen content.

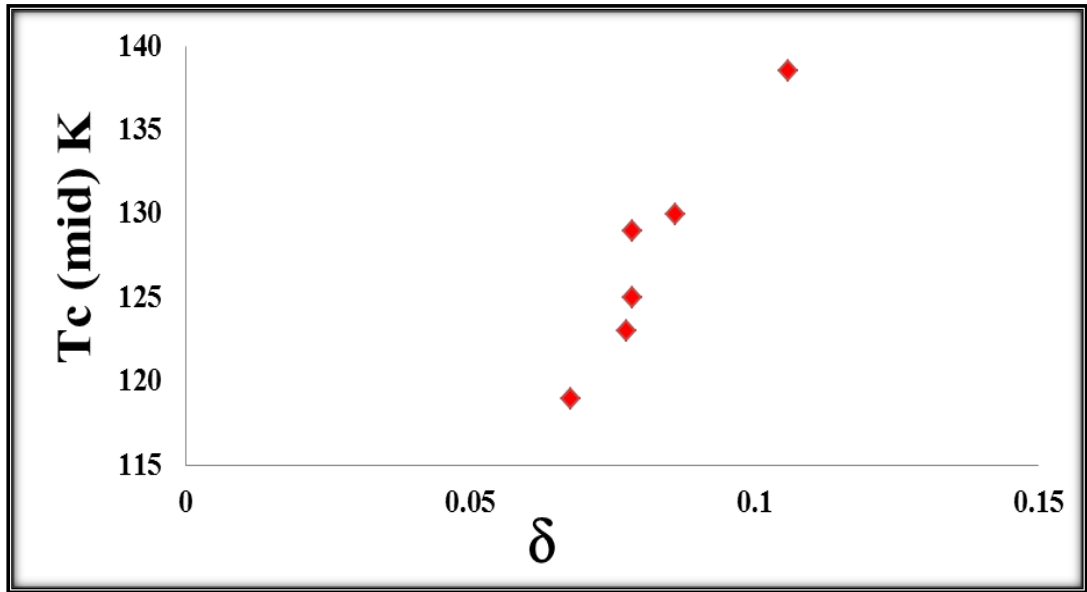


Figure (4-9) :Oxygen content as a function of T_c (mid)of $\text{HgBa}_2\text{Ca}_2\text{Cu}_{3-x}\text{Ni}_x\text{O}_{8+\delta}$ specimens

Hg-based superconductors, as well as many other high- T_c cuprates, are compounds with **hole-type** conductivity. Holes (**h**) could be formed, for instance, in the following process:



This process occurring in the charge reservoir block corresponds to δ increase or, in other words, decrease of $(\text{HgO}\delta)$ layer charge. In this situation, the charge of (CuO_2) layers should increase due to Cu increase:



Thus, charge carriers are transferred from the charge reservoir into the conducting block. It is obvious that extra-oxygen content (δ) or doping level determines the hole concentration(P). The relationship between δ and P could be different depending on the doping mechanism[74].

4-2-4 Study of Dielectric Properties:

The dielectric properties such as dielectric constant (ϵ'), dielectric loss factor (ϵ'') and alternating electric conductivity (σ_{ac}) were measured at room temperature at the frequency (from 50Hz to 5MHz) for $\text{HgBa}_2\text{Ca}_2\text{Cu}_{3-x}\text{Ni}_x\text{O}_{8+\delta}$ compounds with $x=0.0,0.2,0.4,0.6,0.8$ and 1 which are prepared by a solid state reaction. The results are discussed as a function of frequency.

4-2-4-1 Dielectric Constant (ϵ')

The behavior of the dielectric constant is measured at room temperature within the frequency (50Hz-5MHz) which was measured for $\text{HgBa}_2\text{Ca}_2\text{Cu}_{3-x}\text{Ni}_x\text{O}_{8+\delta}$ with ($x=0.0,0.2,0.4,0.6,0.8$ and 1) as shown in figure (4-10).

It was Note from the figure(4-10) the value of the dielectric constant (ϵ') decreases with the increasing of frequency this behavior was agreement with researcher[139]. Because of the space charge electric polarization and the rotated of electrical dipole inside the material which is affected by the increase of frequency. The real part of the dielectric constant awards the magnitude of the part of energy when the material is exposed to the electrical field, the energy which is stored within the material. Grains (inter sites) which act like termination ends for the crystal, are the most likely places at which this energy can be stored. The increasing of frequency of alternating electric field which applied on the material, the dipole rotated fails to keep up with the applied of the alternating field and this leads to the least value of the electric polarization, then dielectric constant decreases. Through the preview of the results listed in Table (4-3) note the change of the dielectric constant value (ϵ') with increasing the amount of material substituent of values (Ni).This could be explained as a result of the difference in volumes of the ionic and atomic size between the two

elements (Cu and Ni) .The reason is the decrease in grain size with the Ni increasing, which leads to an increase in the number of dipoles thus increasing the polarization .

When the frequency increase above 10^6 Hz (ϵ') became constant because the carriers can not follow the frequency of external applied electric ac-field at high frequencies and dielectric response becomes ineffective[140].

As a function of the changes in the applied frequencies on the specimens in the range from 50 Hz to 5 MHz, we can note the changes in the dielectric constant values (ϵ') as shown in the figure (4-10), we will discuss the behavior of superconductor specimen. The figure shows a high values in (ϵ') at low frequencies from 62.481(50 Hz) at the specimen **HgBa₂Ca₂Cu_{3-x}Ni_xO_{8+ δ}** (x= 0.0) to 66.813(50Hz) at all specimens .It was shown from this figure then the increase in Ni concentration due to increase in(ϵ') values. Also the values of dielectric constant for the specimen at 1 MHz , 2MHz ,3 MHz and 4 MHz shows in table (4-3)and from this table we notes the specimen x=0.6 **HgBa₂Ca₂Cu_{2.6}Ni_{0.6}O_{8+ δ}** showed the best behavior of dielectric constant. So in general, the dielectric constant decreased with frequency increasing because of the charge carriers at high frequencies cannot orient themselves by pursuing the frequency of the applied electric field where they need longer period of time lower frequency and dipolar polarization are dominant , when the frequency increases, the oscillation of the applied field increases and the dipolar polarization characteristic time becomes longer than the time constant of applied field was observed by many researchers [140]. The maximum results of the (ϵ') for phases 1223 at the x=0.6 content of (Ni) ions. This is may be due to the agglomeration of nickel particles in the crystal phase at higher concentration of Ni ions which occupies partial sites in the crystal lattice more than replacement sites with Cu [141].

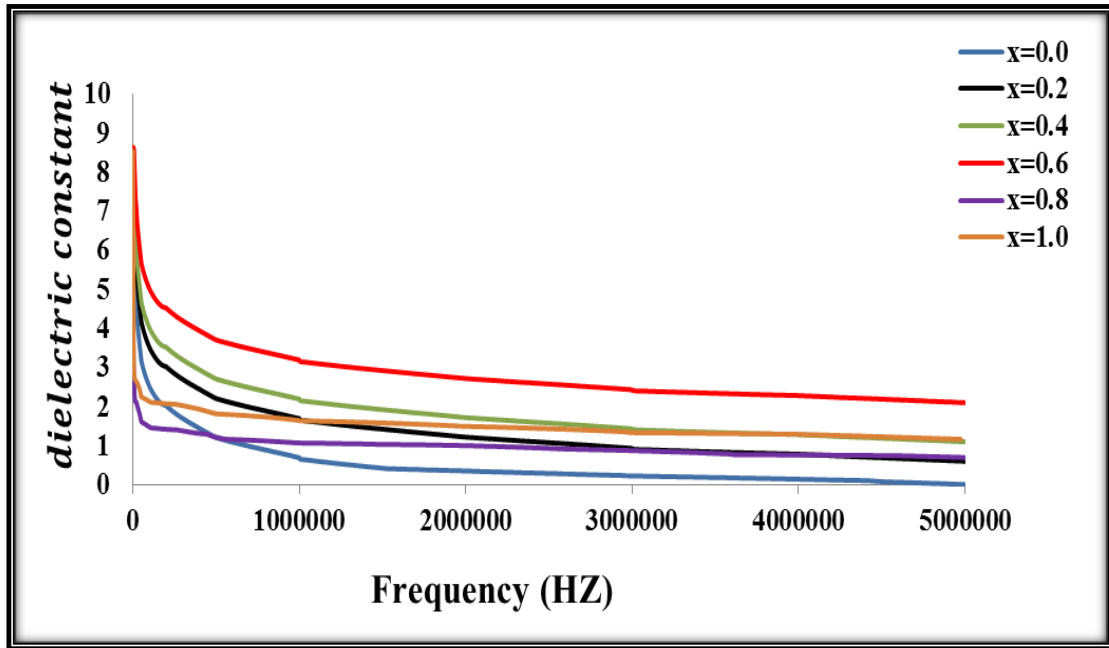


Figure (4-10): Dielectric constant(ϵ') with frequency of $HgBa_2Ca_2Cu_{3-x}Ni_xO_{8+\delta}$ specimens

Table (4-3): Dielectric constant value (ϵ') with the change of the amount of material replaced when frequency (50Hz -5MHz).

$HgBa_2Ca_2Cu_{3-x}Ni_xO_{8+\delta}$						
X	ϵ' At (50 Hz)	ϵ' At (1MHz)	ϵ' At (2MHz)	ϵ' At (3MHz)	ϵ' At (4MHz)	ϵ' At (5MHz)
0.0	8.13683	0.68809	0.34519	0.2219	0.13761	0.00076
0.2	8.13683	1.68809	1.21151	0.93104	0.77809	0.59599
0.4	8.63683	2.18809	1.7115	1.43104	1.27809	1.0959
0.6	8.63683	3.18809	2.71151	2.43104	2.2780	2.0959
0.8	4.18503	1.0647	0.9948	0.86965	0.7558	0.6933
1.0	8.53805	1.63906	1.4900	1.32699	1.28636	1.1584

4-2-4-2 Loss Factor Of Dielectric (Imaginary Part ϵ'')

The behavior of the dielectric loss factor (ϵ'') is measured at room temperature within the frequency (50Hz-5MHz) for $\text{HgBa}_2\text{Ca}_2\text{Cu}_3\text{Ni}_x\text{O}_{8+\delta}$ with $x=0.0,0.2,0.4,0.6,0.8$ and 1 .

At applied external electric field the dielectric loss factors (ϵ'') expresses, across the interfaces, the absorption and the attenuation of energy (densities of localized charge at the sites of defect, localized defects and grain boundaries). Figure (4-11) shows that the dielectric loss factors (ϵ'') decreases with increasing of frequency and this behavior was observed by many researchers[139,140] . Dipoles tend and align along the direction of applied electric field and for ac fields tend to follow the field and are in a phase with it. The friction of this dipole with other dipoles in the medium prevents this, and leads to the dielectric loss, and this loss appears as heat. The variation in frequency-dependent imaginary part of dielectric constant (ϵ'') of the specimens at room temperature is shown in Fig.(4-11)All the investigated specimen exhibit dielectric dispersion where decrease in ϵ'' is observed with the increase in frequency. The dielectric dispersion phenomenon has been explained on the basis of Maxwell–Wagner model of dielectrics [142,143].

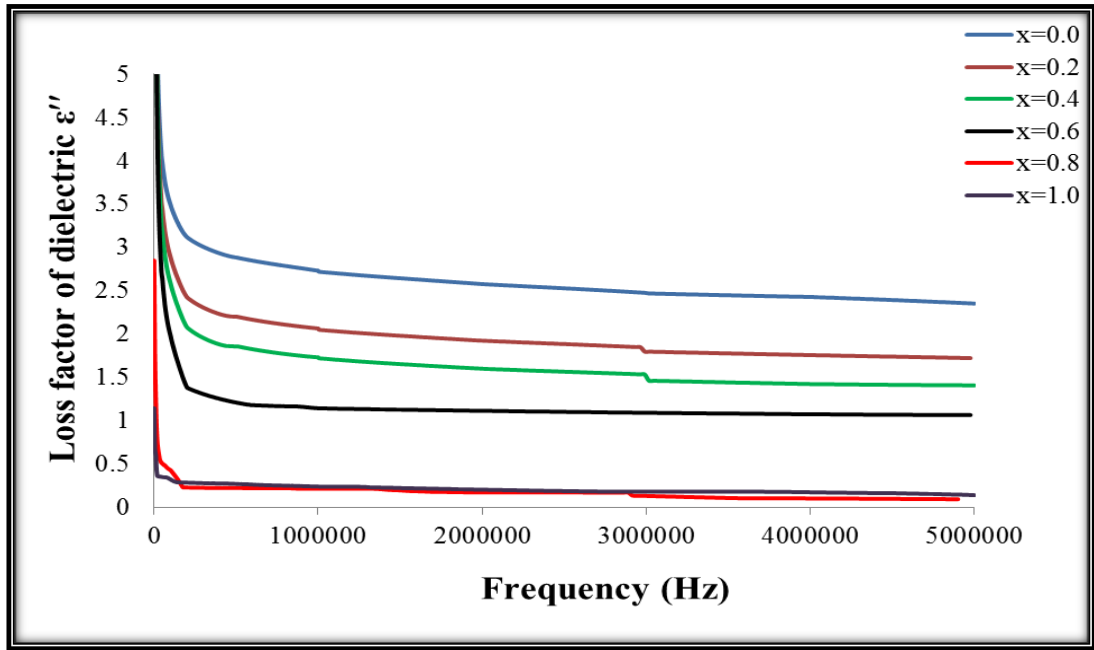


Figure (4-11) :Dielectric loss factor (ϵ'') with frequency for $HgBa_2Ca_2Cu_{3-x}Ni_xO_{8+\delta}$ specimens

Table (4-4): Dielectric loss factor value (ϵ'') with the change of the amount of material replaced when frequency (50Hz -5MHz).

$HgBa_2Ca_2Cu_{3-x}Ni_xO_{8+\delta}$						
X	" ϵ At (50 Hz)	" ϵ At (1MHz)	" ϵ At (2MHz)	" ϵ At (3MHz)	" ϵ At (4MHz)	" ϵ At (5MHz)
0.0	10.922	2.729	2.573	2.467	2.425	2.350
0.2	10.490	2.063	1.920	1.794	1.754	1.649
0.4	11.050	1.729	1.597	1.490	1.420	1.405
0.6	11.176	1.140	1.112	1.089	1.0723	1.051
0.8	2.847	0.212	0.1712	0.129	0.1004	0.088
1.0	1.142	0.238	0.201	0.179	0.1713	0.138

4-2-4-3 Dielectric Loss Factor | $\tan \delta$ |

The ratio of energy dissipated and energy stored in the specimens determines the dielectric loss factor | $\tan \delta$ |, figure (4-12) showed varied the absolute value of dielectric loss factor versus frequency (Hz) for all specimens. The variation in frequency-dependent tangent loss ($\tan \delta$) of the specimens at room temperature is shown in Fig (4-12). The peaks appeared correspond to dispersion positions indicating the relaxation process. Maximum dissipation is observed because of relaxation time of electrical dipoles, which is near the applied electric field[140].

We note the value of | $\tan \delta$ | decreases with the increase frequency for specimens shown in table (4-5) and stay approximately at same value (at high frequency) for specimens , and the value of | $\tan \delta$ | decrease with increase Ni concentration from 0 to 0.4 and increase at $x=0.6$ value then decreasing above this value because these values have high internal energy which due this specimens unstable phases. This behavior may be due to the polarization effect for specimen.

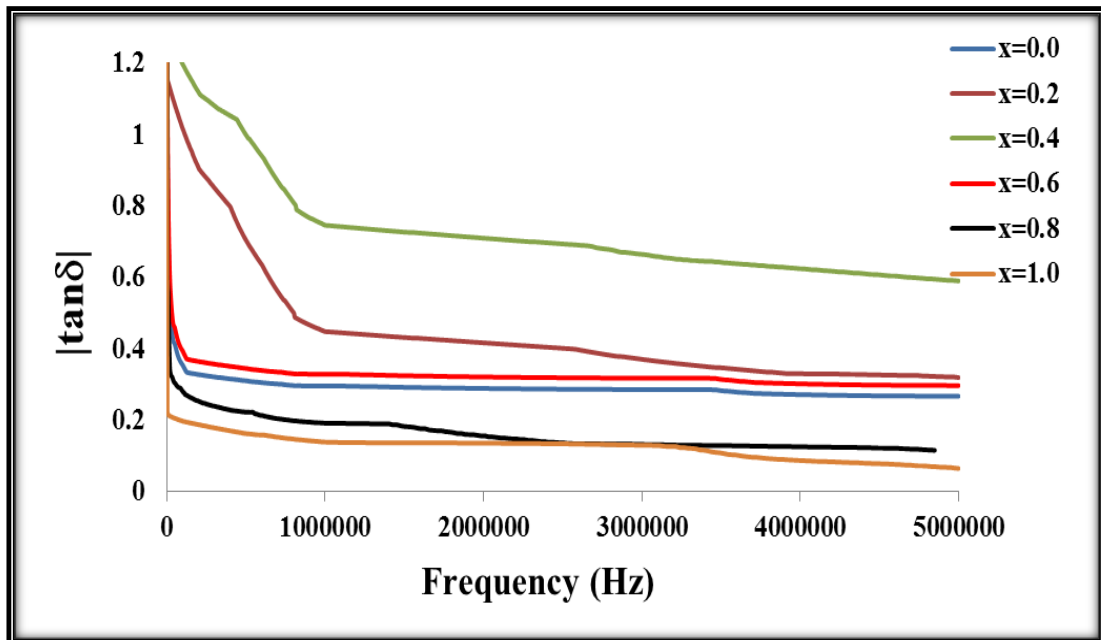


Figure (4-12): Variation of (| $\tan \delta$ |) versus frequency of $\text{HgBa}_2\text{Ca}_2\text{Cu}_{3-x}\text{Ni}_x\text{O}_{8+\delta}$

Table (4-5): Variation of ($|\tan \delta|$) versus frequency of $\text{HgBa}_2\text{Ca}_2\text{Cu}_{3-x}\text{Ni}_x\text{O}_{8+\delta}$ with frequency (50HZ-5MHZ)

$\text{HgBa}_2\text{Ca}_2\text{Cu}_{3-x}\text{Ni}_x\text{O}_{8+\delta}$						
X	$\tan\delta$ At (50 Hz)	$\tan\delta$ At (1MHz)	$\tan\delta$ At (2MHz)	$\tan\delta$ At (3MHz)	$\tan\delta$ At (4MHz)	$\tan\delta$ At (5MHz)
0.0	0.1748	0.1010	0.1089	0.1147	0.272	0.1346
0.2	3.775	0.448	0.417	0.3703	0.330	0.3202
0.4	4.433	0.746	0.710	0.664	0.624	0.5905
0.6	9.421	0.329	0.321	0.318	0.3025	0.2976
0.8	7.609	0.1922	0.156	0.1326	0.1263	0.1064
1.0	0.0435	0.0145	0.136	0.1303	0.087	0.0119

4-2-4-4 Alternating Electrical Conductivity (σ_{ac})

The Alternating electrical conductivity (σ_{ac}) is measured at room temperature within the frequency (50Hz-5MHz) for $\text{HgBa}_2\text{Ca}_2\text{Cu}_{3-x}\text{Ni}_x\text{O}_{8+\delta}$ with $x=0.0,0.2,0.4,0.6,0.8$ and 1 .

The value of σ_{ac} increases as a whole after the addition of Ni in Hg-1223 superconducting matrix. The possible reason for this increase in σ_{ac} is due to healing up of the micro-cracks, which results in the improvement of inter-grain connectivity or because at high frequencies, the amount of kinetic energy in which the electrons must have to cross the crystalline increases, so the number of electrons transmitted is more, so (σ_{ac}) increases.

The ac-conductivity (σ_{ac}) of our specimen increases at high frequencies, which happens due to bound carriers trapped in the specimens.

Note through the figure (4-13) the value of the (σ_{ac}) increases with the increase of frequency (similar reference [139]). At low frequencies, the amount of kinetic energy in which the electrons must have to cross the crystal is few, so the number of electrons which transmit is few that means (σ_{ac}) is few.

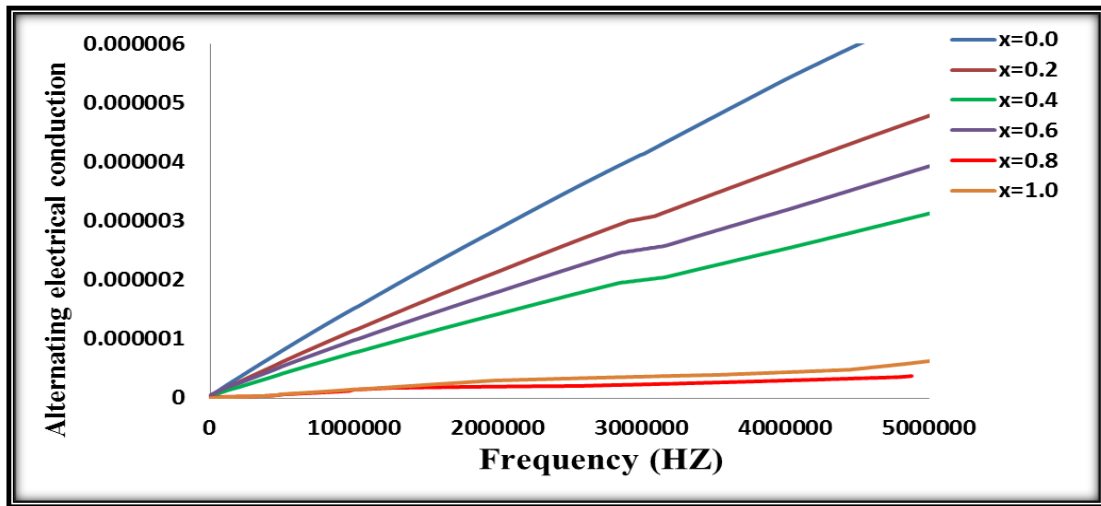


Figure (4-13) Alternating electrical conductivity(σ_{ac}) with frequency for $HgBa_2Ca_2Cu_{3-x}Ni_xO_{8+\delta}$

Table (4-6) Alternating Electrical Conductivity (σ_{ac}) with frequency (50Hz -5MHz).

$HgBa_2Ca_2Cu_{3-x}Ni_xO_{8+\delta}$						
X	$\sigma_{a.c}$ ($\Omega.cm$) ⁻¹ At (50 Hz)	$\sigma_{a.c}$ ($\Omega.cm$) ⁻¹ At (1MHz)	$\sigma_{a.c}$ ($\Omega.cm$) ⁻¹ At (2MHz)	$\sigma_{a.c}$ ($\Omega.cm$) ⁻¹ 1 At (3MHz)	$\sigma_{a.c}$ ($\Omega.cm$) ⁻¹ 1 At (4MHz)	$\sigma_{a.c}$ ($\Omega.cm$) ⁻¹ 1 At (5MHz)
0.0	2.13×10^{-5}	1.52×10^{-6}	2.88×10^{-6}	4.13×10^{-6}	5.42×10^{-6}	6.53×10^{-6}
0.2	2.15×10^{-5}	1.15×10^{-6}	2.15×10^{-6}	3.06×10^{-6}	3.92×10^{-6}	4.78×10^{-6}
0.4	1.73×10^{-5}	7.69×10^{-7}	1.41×10^{-6}	2×10^{-6}	2.54×10^{-6}	3.13×10^{-6}
0.6	4.17×10^{-5}	9.81×10^{-7}	1.81×10^{-6}	2.52×10^{-6}	3.19×10^{-6}	3.93×10^{-6}
0.8	8.85×10^{-10}	1.43×10^{-7}	1.95×10^{-7}	2.35×10^{-7}	2.97×10^{-7}	3.99×10^{-7}
1.0	4.2×10^{-10}	1.48×10^{-7}	2.99×10^{-7}	3.63×10^{-7}	4.38×10^{-7}	2.77×10^{-6}

4-2-5 Result Of Mechanical Properties:

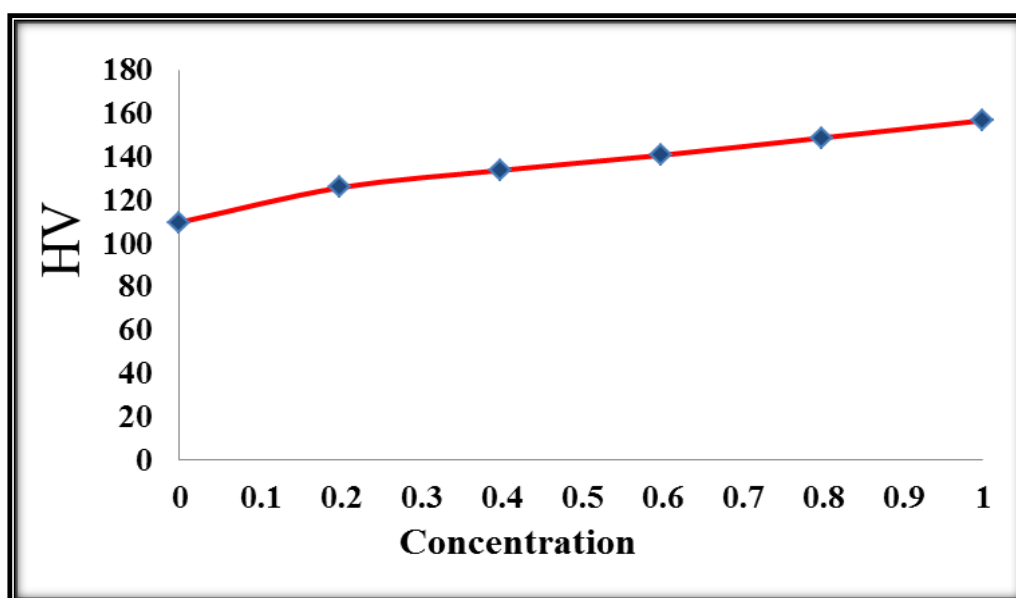
The Vicker's Hardness Number (VHN) for all specimens with nominal composition $\text{HgBa}_2\text{Ca}_2\text{Cu}_{3-x}\text{Ni}_x\text{O}_{8+\delta}$ with $x=0.0,0.2,0.4,0.6,0.8$ and 1 .

were performed with a digital microhardness at room temperature, all specimens were polished to being tested. The Vickers microhardness Number, Young's modulus (E) and Yield strength (Y) were calculated using equations (3.13) (3.14) and (3.15) respectively are summarized in table (4-7), figure (4.14) show the variation of Vickers microhardness Number with Ni concentration, from this figure it was noted the hardness increases with added Ni it clearly depended the mechanical properties of compound on Ni concentration. This behavior may be explained by the reduced porosity and good contact between the grains when added the Ni, or can be attributed to the high phases which cause reinforcement of the bond strength and addition to properties of Ni high hardness causes increase of compound hardness thus increasing in value young modulus and yield strength, Ni ferrite strengthener; increases the hardenability and impact strength of compound, Nickel is a high-density, high-strength metal and high temperature properties.

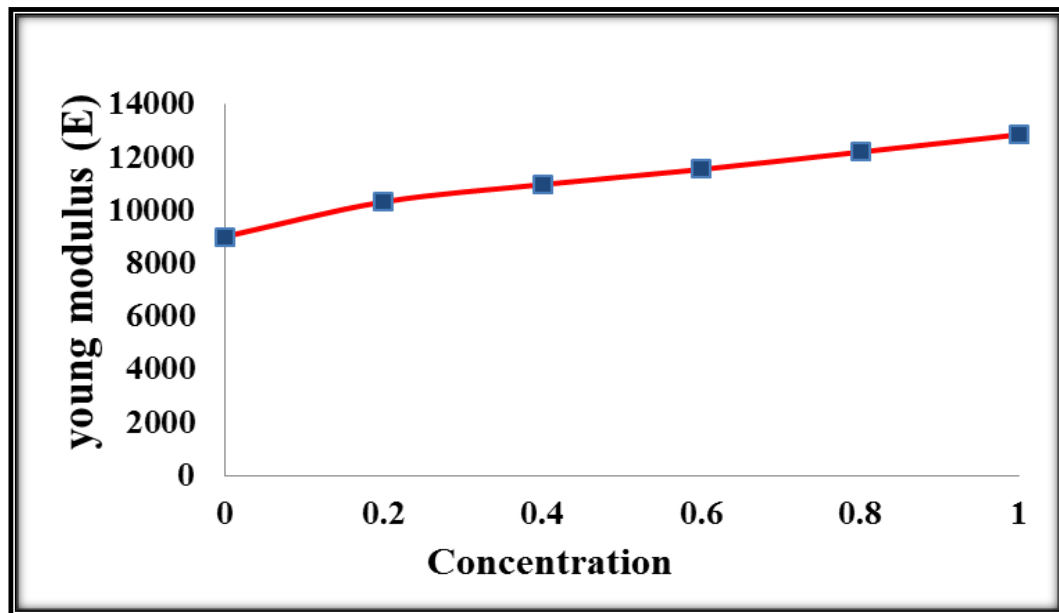
The Ni substitution filling the intergrain space causes in better grain growth and larger grains that leads to improve the (Hv,E,Y).

Table (4-7): Vicker's Hardness Number (VHN) , Young modulus (E) and Yield strength (Y) for $\text{HgBa}_2\text{Ca}_2\text{Cu}_{3-x}\text{Ni}_x\text{O}_{8+\delta}$ (for 15 sec & load=2.94N)

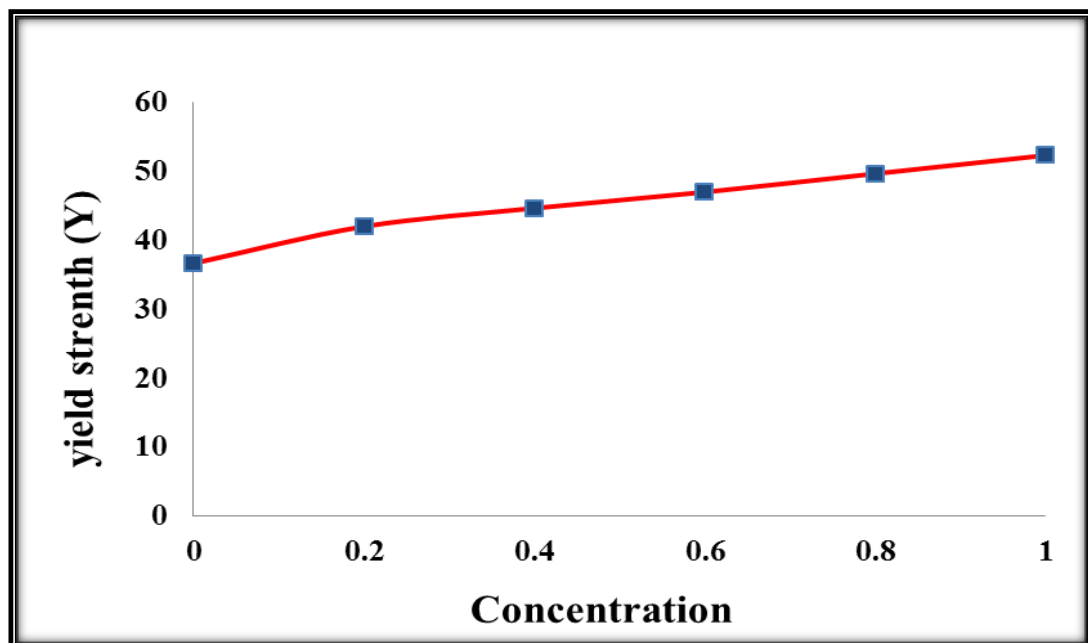
$\text{HgBa}_2\text{Ca}_2\text{Cu}_{3-x}\text{Ni}_x\text{O}_{8+\delta}$					
x	Tim/ sec	Load	Hv	E(MPa)	Y(MPa)
0.0	15	2.94	110	9015.6	36.6666
0.2	15	2.94	126	10326.96	42
0.4	15	2.94	134	10982.64	44.6666
0.6	15	2.94	141	11556.36	47
0.8	15	2.94	149	12212.04	49.6666
1.0	15	2.94	157	12867.72	52.3333



Figure(4-14): The variations of Vicker's Hardness Hv as a function Ni concentration .



Figure(4-15) The variations of young modulus E
a function Ni concentration .



Figure(4-16) The variations of yield strength Y
a function Ni concentration .

Figures (4-15),(4-16) shows the Young modulus and Yield strength increase with increasing the Ni concentration because this addition produce a high density in the specimens.

4-2-6 Results of Atomic Forces Microscopic AFM:

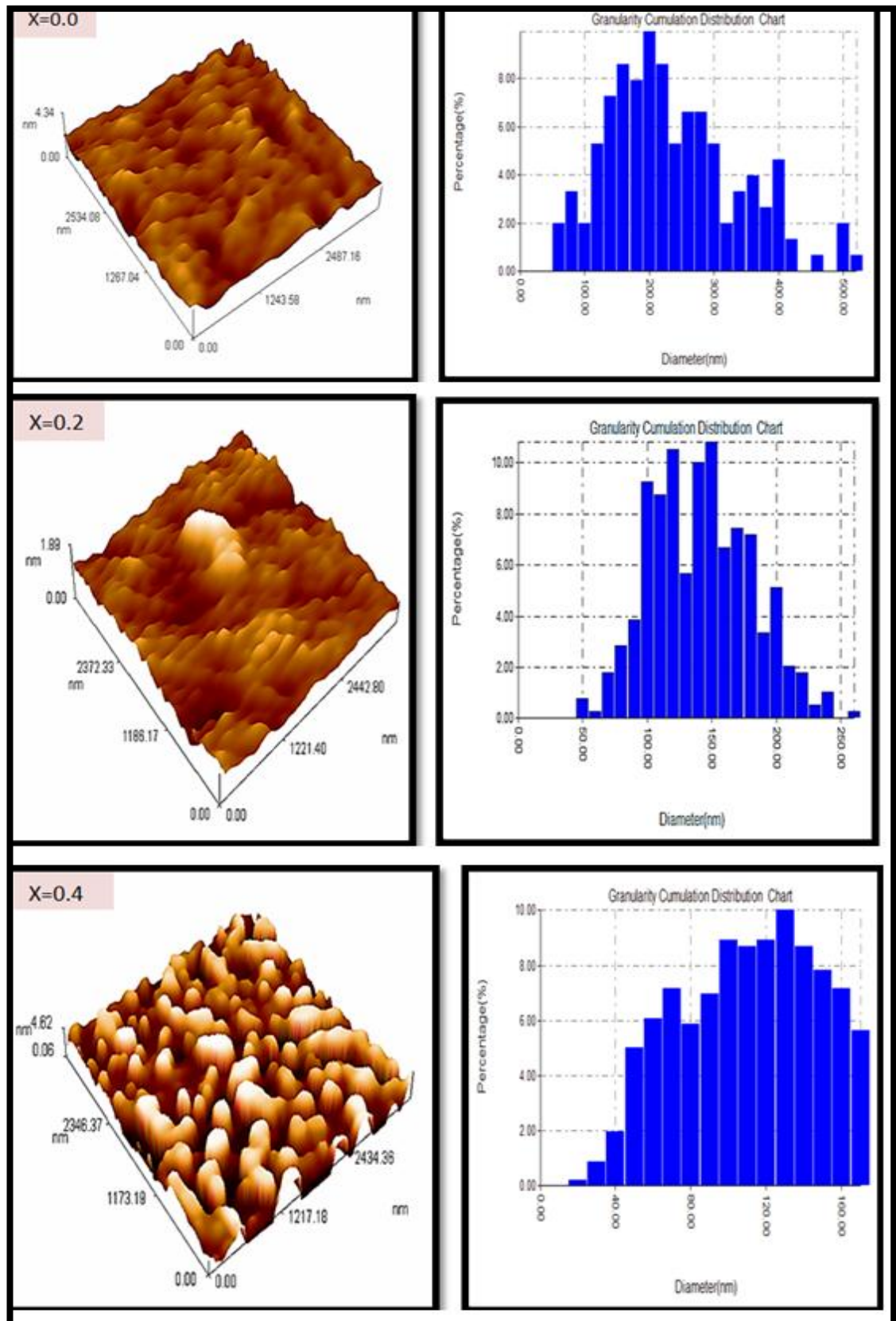
Analyzing the surface of these systems was made using atomic force microscopy (AFM)[145]. The images taken in this research of composition $\text{HgBa}_2\text{Ca}_2\text{Cu}_{3-x}\text{Ni}_x\text{O}_{8+\delta}$ with $x=0.0,0.2,0.4,0.6,0.8$ and 1 . It is found that for the various Ni concentration lead to various Roughness(nm) ,Root mean square(nm) and Avg. Diameter(nm) as shown in figure (4-17) and table (4-8) shows the values of surface roughness of the specimens which indicate that the surface of the some specimens has a good crystalline uniformity and high homogeneity. Nano- and microroughness are formed by fluctuations in the surface of short wavelengths, characterized by hills (asperities) (local maxima) and valleys (local minima) of varying amplitudes and spacing's.

Surface roughness most commonly refers to the variations in the height of the surface relative to a reference plane. It is measured either along a single line profile or along a set of parallel line profiles[146].

AFM techniques were chosen to give information about surface structure in different surface spatial wavelength regions as well as to measure surfaces of different roughness [147].

It was shows from table (4-8) that the average diameter (nm) decrease by increase Ni concentration.

Figure (4-17) reveals the (3-D) AFM images and the chart distribution of $\text{HgBa}_2\text{Ca}_2\text{Cu}_{3-x}\text{Ni}_x\text{O}_{8+\delta}$



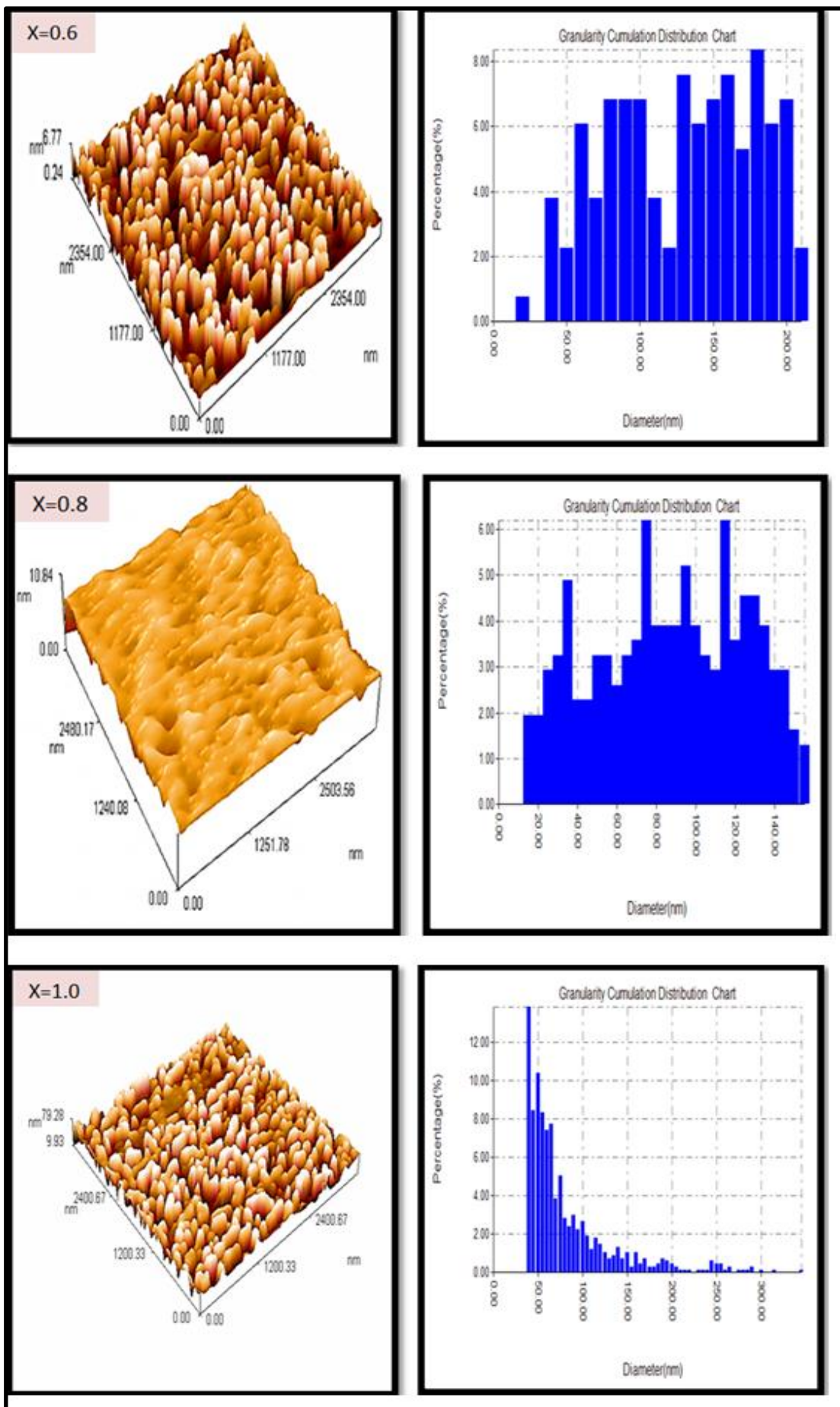


Table (4-8) Values of average surface roughness ,Crystal size and Avg. Diameter in 2D for $\text{HgBa}_2\text{Ca}_2\text{Cu}_{3-x}\text{Ni}_x\text{O}_{8+\delta}$

x	Crystallite size (nm)	Roughness (nm)	Root mean square(nm)	Avg. Diameter(nm)
0	54.52484	0.278	0.365	225.99
0.2	38.02717	18.4	22	137.40
0.4	25.42405	1.76	2.03	105.44
0.6	40.17333	0.372	0.54	124.10
0.8	44.8865	0.159	0.219	84.26
1.0	44.88948	1.18	1.36	79.99

4-3 $\text{Hg}_{0.5}\text{Pb}_{0.5}\text{Ba}_2\text{Ca}_2\text{Cu}_{3-x}\text{Ni}_x\text{O}_{8+\delta}$ Compound:

In this compound we substitution of (Pb) on(Hg) and (Ni)in (Cu) a coordinating to the following formal and studied the physical properties (structure , electrical and mechanical)and behavior of compound :



4-3-1 Study of Structural Properties:

The crystal structure of the specimens prepared by a solid state reaction method were studied by x-ray diffraction (XRD) . The XRD data collected from various specimens (specimens having **Pb=0.5** and various **Ni** concentration **x=0,0.2,0.4,0.6,0.8and 1.0**) . The results of the XRD analysis showed that all specimens present a polycrystalline phase and have tetragonal crystal structure with P4/mmm space group.

The X-ray diffraction pattern of $\text{Hg}_{0.5}\text{Pb}_{0.5}\text{Ba}_2\text{Ca}_2\text{Cu}_{3-x}\text{Ni}_x\text{O}_{8+\delta}$ specimens and these results are shown in of XRD pattern that shown in Figure (4-18) The peaks are observed due to diffraction from different planes shows mixed phases.

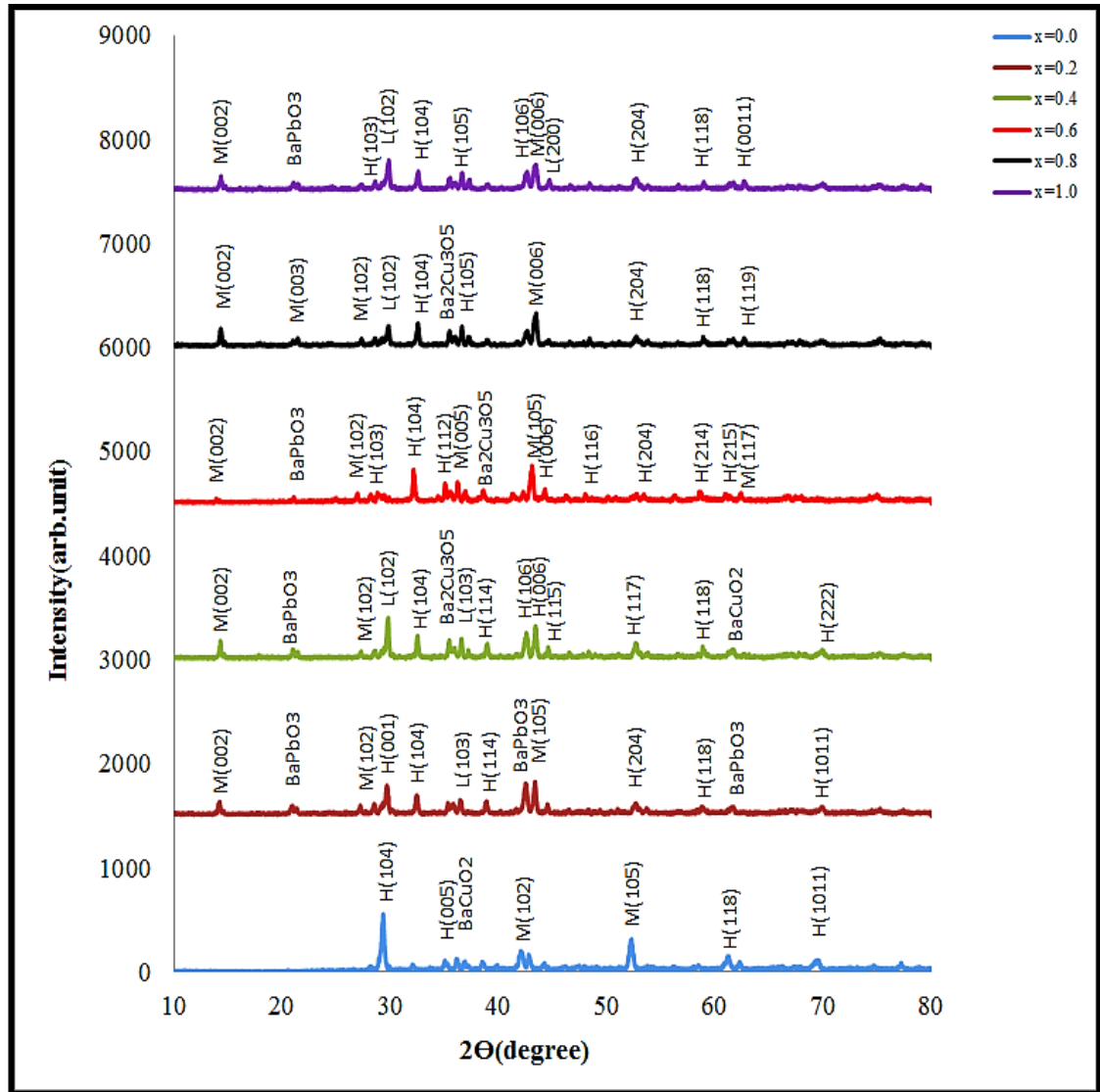


Figure (4-18): XRD pattern of $\text{Hg}_{0.5}\text{Pb}_{0.5}\text{Ba}_2\text{Ca}_2\text{Cu}_{3-x}\text{Ni}_x\text{O}_{8+\delta}$

Figure (4-18) shows the X-ray diffraction analysis of correspond to Hg(1223)the pure specimen and specimens that partial substitution by nickel observed increasing intensity with increasing of nickel concentration. XRD patterns for all the specimens (without Ni addition $x=0$ and with Ni addition $x=0,0.2,0.4,0.6,0.8$ and 1)and $\text{Pb}=0.5$ (for all

specimens), with miller indices are shown in figure (4-18) , this we can easy notice the different between the all specimens, we can be observed that all the specimens were consist of a major high- T_c phase (H-peaks) 1223 , minor phase (M-peaks) 1212,), minor low- T_c phase (L-peaks) 1201 and a very small amounts of impurity phases with vanishingly small concentrations could be related to the stacking faults along the c-axis which are agreement with references [25].

Also it can be noticed that as the Ni additions increases , the (H-peaks) increase , while the (M- peaks), (L-peaks) decrease[148], the high- T_c phase reflections of pure specimen have lower intensity than specimens which have Ni additions , beside of that there is appearance clear and sharp peaks especially when $\Theta = 29.25^\circ$, and shifting of peaks position in compression with pure specimen ,this may attributed to the substitution of Ni in Cu sites that means peaked tops are overlapped and this indicates of (CuO)layers be formed which are thought to have a significant role in superconducting process thus the compound is reach at its best of regularity and stability, which help to provides safety tracks for current carriers . The peaks were agreement with ASTM Card number (089-1645,089-6007,087-2349) [2012 international center for Diffraction Data].

The XRD data diffraction analysis collected from various specimen (specimens having various Hg, Pb, Ni, Ca, Ba and Cu concentration) were all polycrystalline and correspond to Hg-1223 phases. The representative XRD patterns are shown in figure(4-18). It could be seen from the spectra that there were three main phases in all specimens of the Hg-base systems, high- T_c phase (1223) reflections (peaks H), and Low - T_c phase reflections (peaks L)and a small amount of impurity phases.

The appearance of different phases in the pure specimen in particular and the all of the specimens in general is due to the removal of defects of the atomic or reduce of oxygen or irregularity of positive ions, which lead to

the accumulation of defects in the stacking faults along the axis (c), which ultimately lead to deformation of the crystalline structure. The comparison between the relative intensities of XRD patterns for the specimens with Ni=0, 0.2,0.4,0.6,0.8 and 1.0, with the relative intensity of the same reflections of the specimen with Ni =0 shows that all the specimens have reflection intensity of the High- T_c phase reflections and Low- T_c phase reflections the H-peaks increased and Low- T_c decreased by increasing Ni. The High- T_c phase reflections of the free specimen (Ni= 0) has lower intensity than specimens have Ni. The lattice parameters have been estimated using d-values and (hkl) reflections of the observed x-ray diffraction pattern (through the software program), the parameters a, b, c, mass density dm and volume fraction (V_{phase}) shown in table(4-9).

Table(4-9): Lattice parameters and volume fraction of $\text{Hg}_{0.5}\text{Pb}_{0.5}\text{Ba}_2\text{Ca}_2\text{Cu}_{3-x}\text{Ni}_x\text{O}_{8+\delta}$ compounds

X	a=b (Å)	c(Å)	c/a ratio	V(Å ³)	dm(gm/cm ³)	V_{ph} (1223)%	V_{ph} (1212)%	V_{ph} (1201)%	V_{ph} impurities%
0	3.9019	15.7321	4.0319	239.5184	6.0824	74.102	8.826	7.953	9.117
0.2	3.8829	15.7651	4.0601	237.689	6.1224	71.2753	14.3902	5.7435	5.0503
0.4	3.8796	15.7891	4.0697	237.6464	6.1167	74.2033	10.0957	9.6064	6.0944
0.6	3.8081	15.8953	4.1740	230.5077	6.2922	76.395	13.003	5.865	4.734
0.8	3.8524	16.0635	4.1697	238.3982	6.0907	81.7370	12.7922	8.3812	5.1461
1	3.8053	15.8806	4.1732	229.956	6.3002	78.421	7.631	8.421	5.526

The result as shown from table (4-9) it was found increasing of c-axis lattice constant with the increases of Ni concentration up to x=0.8, then it decreases with the increases for x=1.0. The reason is due to the substitution of Pb^{+2} the ionic radii (133 pm) on Hg^{+2} ionic radii (116 pm) is longer than of Hg^{+2} and Ni for Cu where the ionic radii of Ni^{+2} (83 pm) is shorter than of Cu^{+2} (87 pm) which render c-axis to be longer or caused deformed in c-

axis, another reason may be explained the increase of the oxygen content in the unit cell. It was speculated that the excess of oxygen goes into the mercury oxide layer causing an increase in c the lattice parameter. The parameters a, b, c , V volume, density d_m and volume fraction V_{ph} shown in table (4-9) show variation of c/a , density d_m and volume fraction V_{ph} for Hg 1223 specimens comparable with the free specimen.

Results in this research a significant increase of T_c . It seems that the distortion of the conducting (CuO_2) layers during this substitution is more important than the chemical compression effect.

For specimen with higher Ni content ($x = 0.8$) the c parameter is significantly higher ($c \approx 16.063 \text{ \AA}$) than for specimen with $x = 0.0$ and $0.2, 0.4, 0.6$ while the $a = b$ parameters for all specimens are close to each other ($a = b \approx 3.852 \text{ \AA}$), since the apical Cu–O distance is expected to be higher than the corresponding Hg–O distance at this position.

The relative intensities of XRD patterns of $Hg_{0.5}Pb_{0.5}Ba_2Ca_2Cu_{3-x}Ni_xO_{8+\delta}$ specimens we can notice increase of High-phase and decrease of Low-phase with increases Ni concentration reason to increasing Cu-O layer due to increasing hole in the structures that due increase the high- T_c phase that shown in figure (4-19).

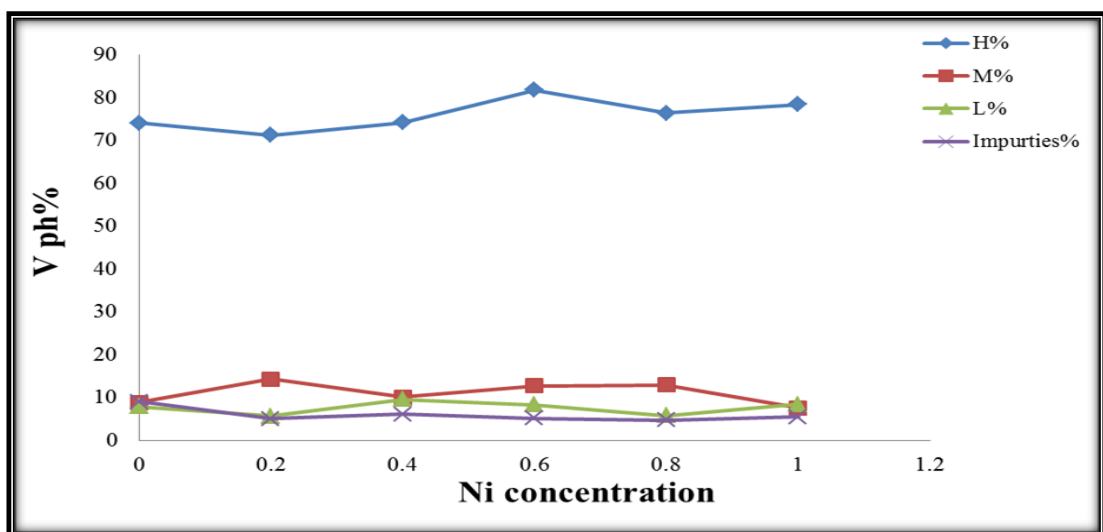


Figure (4-19) :The ratio of volume fraction V_{ph} as function of Ni concentration for the $Hg_{0.5}Pb_{0.5}Ba_2Ca_2Cu_{3-x}Ni_xO_{8+\delta}$ specimens

Figures (4-20), (4-21) show an increase of the c/a and d_m for Hg-doped specimens with increment of Ni concentration for all specimens for composition of $\text{Hg}_{0.5}\text{Pb}_{0.5}\text{Ba}_2\text{Ca}_2\text{Cu}_{3-x}\text{Ni}_x\text{O}_{8+\delta}$ as comparable with the free Ni specimen.

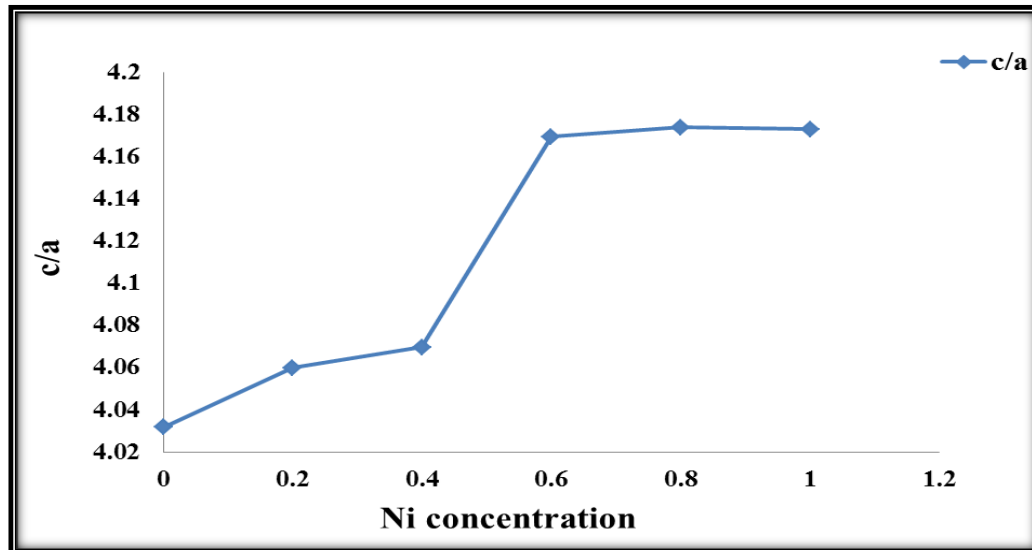


Figure (4-20): The ratio of lattice parameters c/a as function of Ni concentration for the $\text{Hg}_{0.5}\text{Pb}_{0.5}\text{Ba}_2\text{Ca}_2\text{Cu}_{3-x}\text{Ni}_x\text{O}_{8+\delta}$ specimens

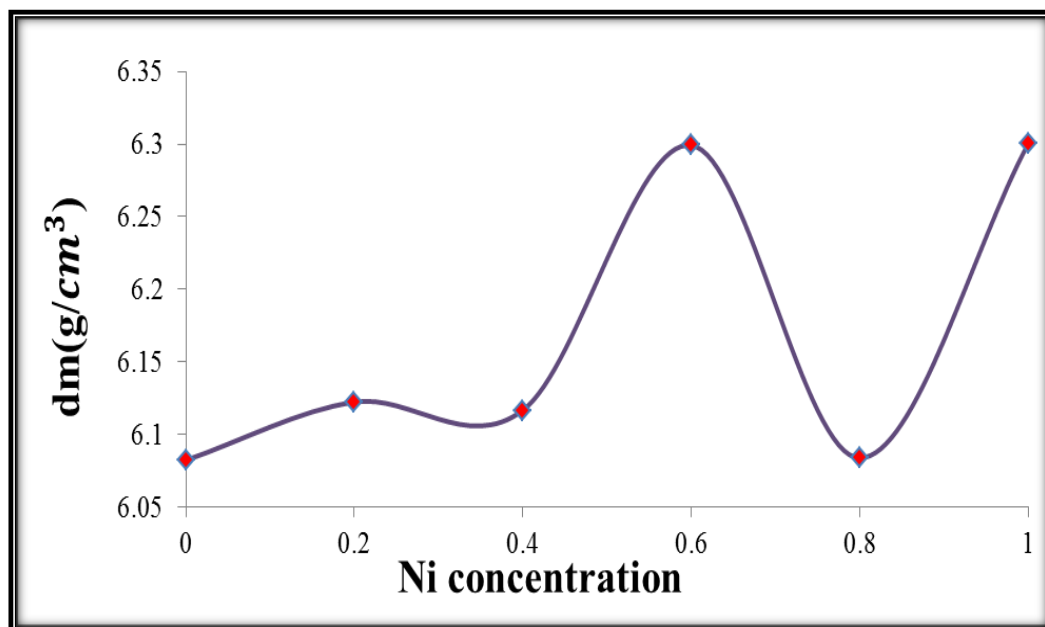


Figure (4-21) :Variation density with Ni concentration for the $\text{Hg}_{0.5}\text{Pb}_{0.5}\text{Ba}_2\text{Ca}_2\text{Cu}_{3-x}\text{Ni}_x\text{O}_{8+\delta}$ specimens

4-3-2 Study of Electrical Resistivity:

The critical transition temperature of the specimens was determined from resistivity as a function of temperature, as the specimens were cooled by liquid nitrogen. Figure (4-22) shows the variation of the resistivity of Hg-1223(Pb=0.5) specimens with temperature for specimens with substitution for copper different nickel content x .

Figure(4-22) shown the behavior of the electrical resistivity as a function of the temperature, showing all the specimens with metallic behavior in the region before $T_{c(\text{onset})}$ which the superconducting behavior appeared, the variation of the transition critical temperature with Ni (0.0,0.2,0.4,0.6,0.8,1.0) for Hg-1223 system is shown in Fig(4-22). It is clear from this figure that the transition temperature of Hg-1223 increases as Ni value is increasing up to a maximum ($x=0.8$) then it drops when ($x=1.0$).The transition temperature is directly related to the charge carrier concentration in the CuO_2 planes [149].

Each oxygen atom contributes only just over one hole into the CuO_2 planes, and therefore near one hole per nickel atom in the Cu plane will be donated to the CuO_2 planes. This result will increasing (optimizing) the hole concentration, and increase the transition temperature and Pb-doping in (Hg) causes the increase of some degrees in the transition temperature.

It is found from figure (4-22) and table (4-10) that the resistivity for all specimen decrease with decrease temperature as though is some cases a complete zero resistivity could not be found. The critical temperature for specimen has no Ni content ($x=0$) is equal to 112.5K .The specimen with ($x=0.8$) equal 139 K shows a higher critical temperature ,and the resistivity went down nearly sharp as shown in figure (4-22) the reason may be attributed to the existence of the high T_c -phase as referred in x-ray analysis and due to increasing Cu-O layer, while the specimen ($x=0.2, 0.4, 0.6$) equal at T_c 115, 126,132 K respectively. Increase Ni to 1.0 decrease the

critical temperature to 125.5 K. The decrease in T_c are further evidence that the presence of increase amount of Ni content in Hg-1223 phase stabilizes and promotes the growth of Hg-1212 and Hg-1201 phase at the expense of Hg-1223 phase.

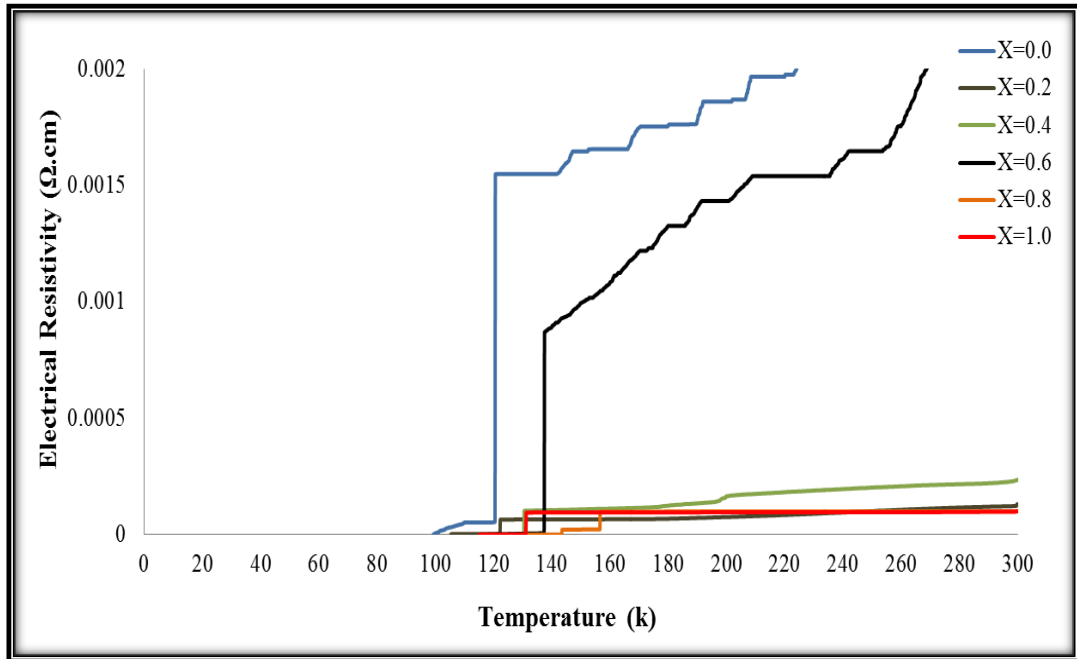


Figure (4-22) The resistivity as function of temperature for $Hg_{0.5}Pb_{0.5}Ba_2Ca_2Cu_{3-x}Ni_xO_{8+\delta}$ specimens for $x=0.0, 0.2, 0.4, 0.6, 0.8$ and 1.0

Table(4-10): Lattice parameters and transition temperature of $Hg_{0.5}Pb_{0.5}Ba_2Ca_2Cu_{3-x}Ni_xO_{8+\delta}$ compounds

X	V _{ph} (1223)%	V _{ph} (1212)%	V _{ph} (1201)%	V _{ph} impurities %	T _{C(Off)} Set (K)	T _{C(Onset)} (K)	ΔT _C (K)	T _(mid) c(K)	E _g (eV)	δ
0	74.102	8.826	7.953	9.117	105	120	15	112.5	0.0342	0.072
0.2	71.2753	14.3902	5.7435	5.0503	108	122	14	115	0.0349	0.0864
0.4	74.2033	10.0957	9.6064	6.0944	122	130	8	126	0.0383	0.1896
0.6	76.395	13.003	5.865	4.734	121	143	22	132	0.0392	0.1424
0.8	81.7370	12.7922	8.3812	5.1461	134	144	10	139	0.0418	0.1852
1	78.421	7.631	8.421	5.526	120	131	11	125.5	0.0381	0.1474

The increasing value of resistivity and then decreasing trend in the value of zero-resistance critical temperature (T_{c0}) indicates that the connectivity between grains decreases gradually with the addition of Ni similar to [136].

The transition width (ΔT_c) decreases with substitution concentration. this may be due to homogeneity of specimen during preparation. The partial substitution of Pb on Hg and Ni in Cu for (Hg-1223) compound, site should have an effect on the cooper pairs in the Cu-O plane so the increase in T_c mean that it increases the charge carriers to move easier in the Cu-O plane leading to the higher T_c .

We noticed that the specimen $x=0.8$ is in optimal doping regime while decrease of T_c beyond this concentration ($x=1.0$) seems to be due to the shift of this specimen towards the over-doped region, the reason of that due to more addition of Ni (1.0) decreases T_c , due to decreasing c-lattice parameter which leads to decreasing the cooper pairs in the Cu-O plane, and the existence of high amounts of the secondary phase.

Figures (4-23),(4-24) respectively shown the relationship between(T_c, E_g energy gap) with Ni concentration and exhibit behavior similar to both T_c, E_g with Ni increase for pure specimen $x=0$ up to $x= 0.8$ and then decrease.

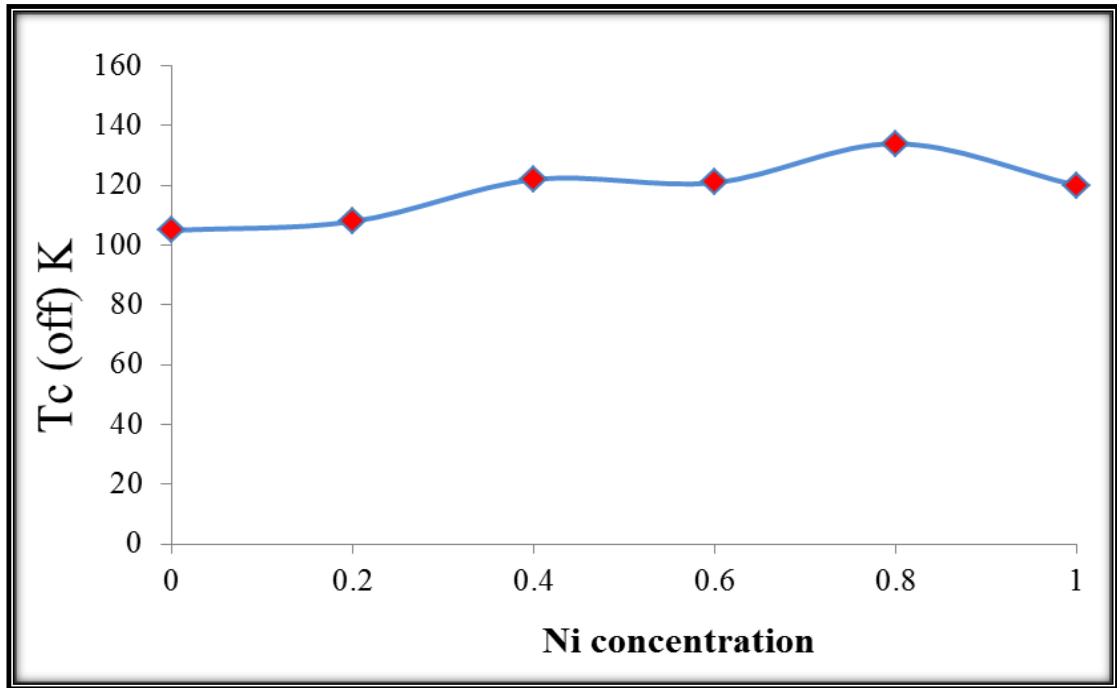


Figure (4-23) : $T_{c(\text{offset})}$ a function of concentration Ni of $\text{Hg}_{0.5}\text{Pb}_{0.5}\text{Ba}_2\text{Ca}_2\text{Cu}_{3-x}\text{Ni}_x\text{O}_{8+\delta}$ specimens

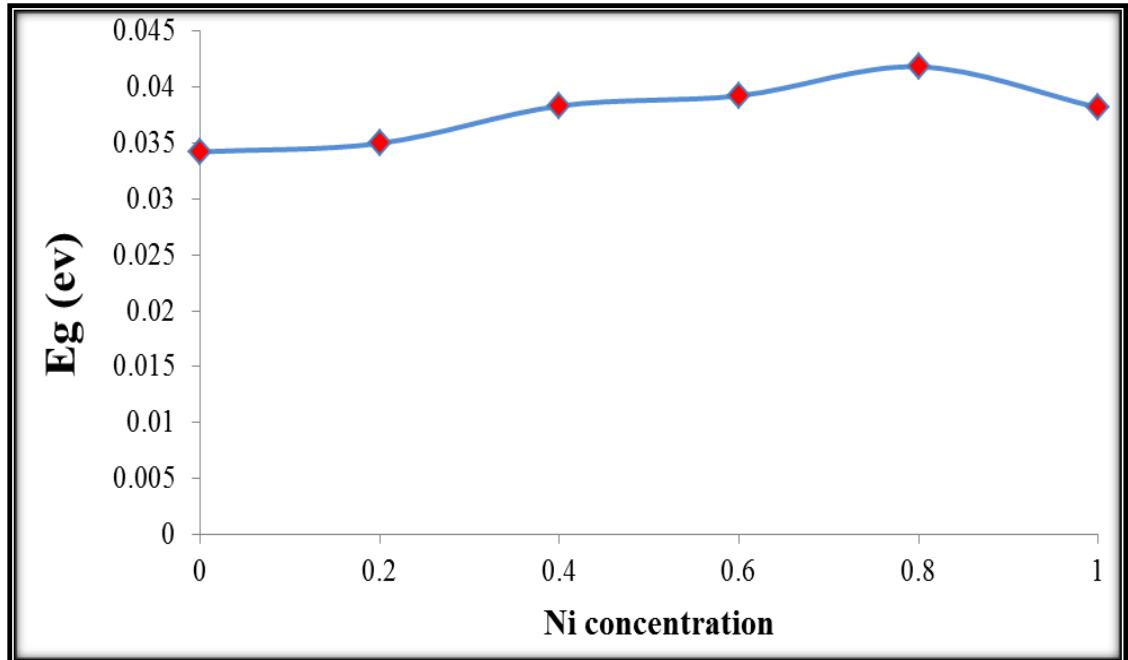


Figure (4-24) : E_g (eV) a function of concentration Ni of $\text{Hg}_{0.5}\text{Pb}_{0.5}\text{Ba}_2\text{Ca}_2\text{Cu}_{3-x}\text{Ni}_x\text{O}_{8+\delta}$ specimens

4-3-3 Results Of Oxygen Content:

The values of (δ) which is the excess concentration of oxygen in the prepared specimens of $\text{Hg}_{0.5}\text{Pb}_{0.5}\text{Ba}_2\text{Ca}_2\text{Cu}_{3-x}\text{Ni}_x\text{O}_{8+\delta}$ ($x=0.0,0.2,0.4,0.6,0.8,1.0$) was measured by using a chemical Iodometric titration experiment discussed in (part two).

Table (4-10) shows the values of critical temperature T_c related to δ for all specimens .

Table (4-10) and fig (4-25) show the values of T_c related to δ values. It can be noticed that δ and T_c increase with the raising of the dopant concentration for $\text{Hg}_{0.5}\text{Pb}_{0.5}\text{Ba}_2\text{Ca}_2\text{Cu}_{3-x}\text{Ni}_x\text{O}_{8+\delta}$ with Ni $x=0.0,0.2,0.4,0.6,0.8,1.0$. Arise of δ has been attributed to the existence of excess oxygen atoms in the Cu-O₂ layers. This leads to create more holes in the perovskite layers and shortening in the bond length of the Cu-O and enhance the T_c the agreement with research[150] .

The δ values had shown that the values ranged from 0.0720 to 0.189, remaining all conditions from sintering temperature at (850°C) and time of sintering (24 hr) at pressure (7 ton/cm²) in air are controlled and fixed.

Hence Oxygen Content increase with increase Ni concentration shown in fig (4-26) .the relation between T_c and Oxygen Content is almost parabolic for our specimens.

It is observed from Table(4-10) that T_c increases as δ increases because the presence of excess oxygen atoms in the CuO₂ layers will create more holes in the perovskite layers and this creation of the holes in the CuO₂ sheet will shorten the Cu-O bond length and tend to improve the transition temperature .

Similar behavior of δ with transition temperature was found by Zhao et.al[138].

The critical temperature dependence on the oxygen amount δ of each superconducting compound is listed in table (4-10), and shown in figure (4-25).

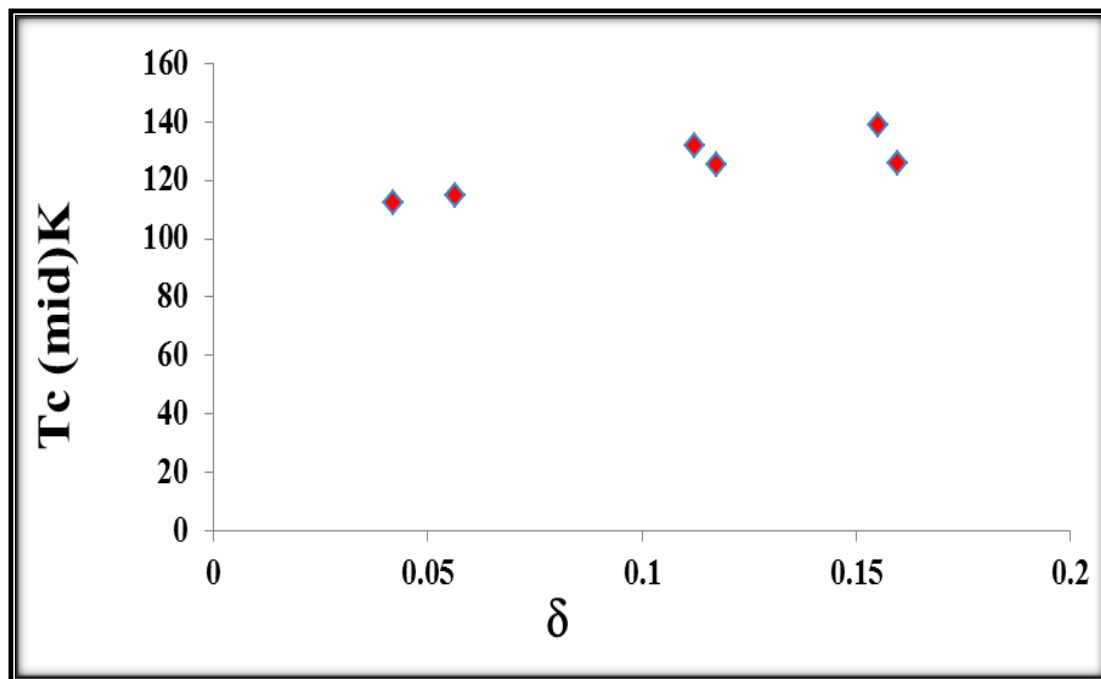


Figure (4-25) :Oxygen content as a function of T_c (mid)of $\text{Hg}_{0.5}\text{Pb}_{0.5}\text{Ba}_2\text{Ca}_2\text{Cu}_{3-x}\text{Ni}_x\text{O}_{8+\delta}$ specimens

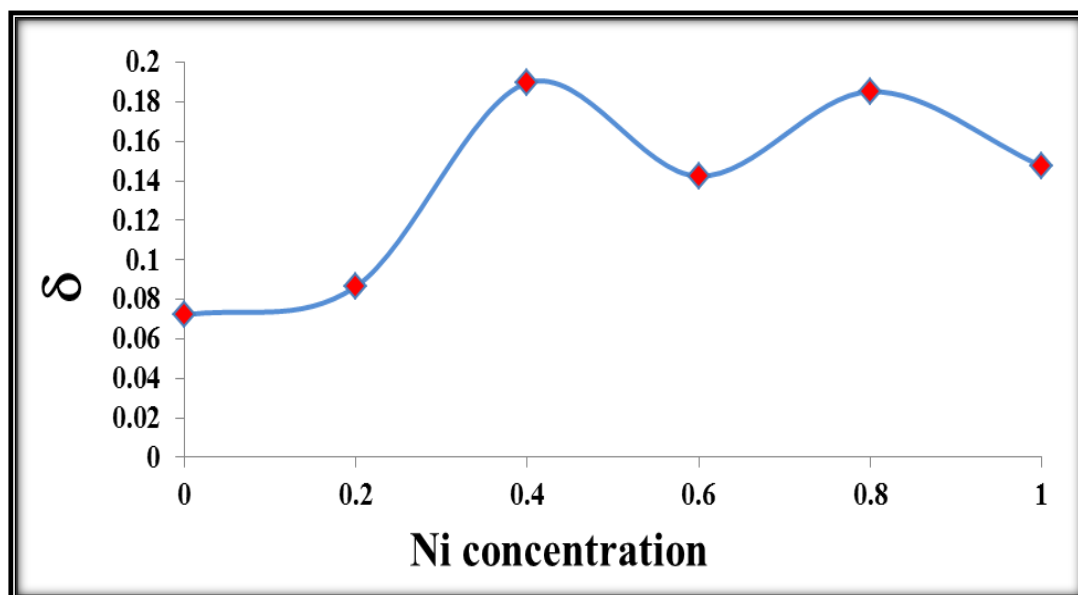


Figure (4-26) :Oxygen content as a function of concentration Ni of $\text{Hg}_{0.5}\text{Pb}_{0.5}\text{Ba}_2\text{Ca}_2\text{Cu}_{3-x}\text{Ni}_x\text{O}_{8+\delta}$ specimens

4-3-4 Study of Dielectric Properties:

The dielectric properties such as dielectric constant (ϵ'), dielectric loss factor (ϵ'') and alternating electric conductivity (σ_{ac}) were measured at room temperature at the frequency (50Hz - 5MHz) for compounds **Hg_{0.5}Pb_{0.5}Ba₂Ca₂Cu_{3-x}Ni_xO_{8+ δ}** with $x=0.0,0.2,0.4,0.6,0.8$ and 1 which are prepared by a solid state reaction. The results are discussed as a function of frequency.

4-3-4-1 Dielectric Constant (ϵ')

The behavior of the dielectric constant is measured at room temperature within the frequency (50Hz-5MHz) measured for **HgBa₂Ca₂Cu_{3-x}Ni_xO_{8+ δ}** with Pb= 0.5 and $x=0.0,0.2,0.4,0.6,0.8$ and 1.

Figure (4-27) shown the variation of (ϵ') the dielectric constant as a function of frequency(Hz) at the room temperature for the Hg-1223 specimens. We observed to decrease of (ϵ') with increasing frequency for all specimens and is almost a constant at higher frequencies was agreement with many researchers[139,151].

The carriers can not follow the frequency of external applied electric ac-field at high frequencies and dielectric response becomes ineffective [140].

This high (ϵ') of the specimen ($x=0.6$) can be mainly attributed to the polarization effect or this is may be due to the agglomeration of Pb and nickel particles in the crystal phase (Pb, Ni) which occupies partial sites in the crystal lattice more than replacement sites with Cu [141].

The contribution of polarization is most obvious at low frequency. There are four primary mechanisms of polarization in materials. Each mechanism involves a short range of motion of charge and contributes to the total polarization of the material. The polarization mechanisms include electronic polarization, ionic or atomic polarization, dipolar or orientation polarization, and interfacial polarization. The Electronic polarization occurs

at very high frequencies .At low frequencies all four type sources of polarization are occurs, whereas at higher frequencies, only the electronic polarization comes into play[151].

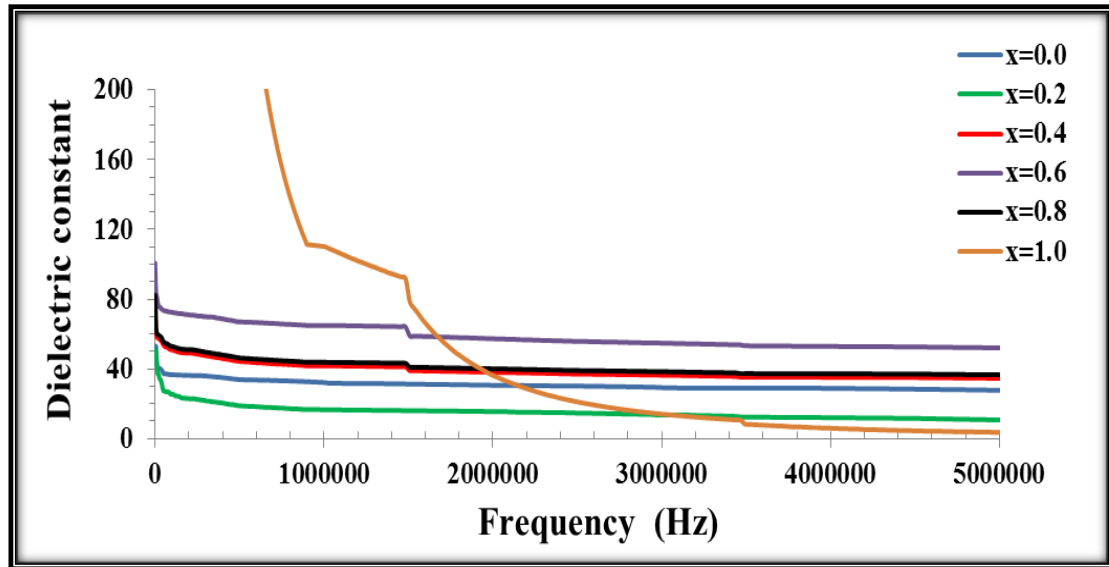


Figure (4-27): Dielectric constant(ϵ) with frequency of $Hg_{0.5}Pb_{0.5}Ba_2Ca_2Cu_{3-x}Ni_xO_{8+\delta}$ specimens

Table (4-11) Dielectric constant value (ϵ) with the change of the amount of material replaced when frequency (50Hz -5MHz).

$Hg_{0.5}Pb_{0.5}Ba_2Ca_2Cu_{3-x}Ni_xO_{8+\delta}$						
X	ϵ At (50 Hz)	ϵ At (1MHz)	ϵ At (2MHz)	ϵ At (3MHz)	ϵ At (4MHz)	ϵ At (5MHz)
0.0	53.163	32.188	30.627	29.119	28.874	27.755
0.2	50.839	16.614	15.528	13.637	11.996	10.726
0.4	80.223	41.817	38.074	36.377	35.175	34.602
0.6	100.744	64.903	57.294	54.725	52.885	52.086
0.8	82.223	43.817	40.074	38.377	37.175	36.602
1.0	69118.21	110.19	35.883	13.956	5.991	3.630

The figure shows a rise in (ϵ') values at low frequencies from 53.163(50 Hz) at the specimen $\text{Hg}_{0.5}\text{Pb}_{0.5}\text{Ba}_2\text{Ca}_2\text{Cu}_{3-x}\text{Ni}_x\text{O}_{8+\delta}$ ($x=0.0$) to 69118.21(50Hz) at the specimen $\text{HgBa}_2\text{Ca}_2\text{Cu}_{3-x}\text{Ni}_x\text{O}_{8+\delta}$ ($x=1.0$) also increasing in this values with increasing Ni addition. Moreover, the values of dielectric constant for the specimen at 1 MHz, 2MHz, 3 MHz and 4 MHz shows in table (4-11) and from this table we notes the specimen $x=0.6$ $\text{Hg}_{0.5}\text{Pb}_{0.5}\text{Ba}_2\text{Ca}_2\text{Cu}_{2.6}\text{Ni}_{0.6}\text{O}_{8+\delta}$ showed the best behavior for dielectric constant.

4-3-4-2 Loss Factor Of Dielectric (Imaginary Part ϵ''):

The behavior of the dielectric loss factor (ϵ'') is measured at room temperature within the frequency (50Hz-5MHz) that is measured for $\text{HgBa}_2\text{Ca}_2\text{Cu}_{3-x}\text{Ni}_x\text{O}_{8+\delta}$ with Pb =0.5 and $x=0.0,0.2,0.4,0.6,0.8$ and 1.

Figure (4-28) shows that the dielectric loss factors (ϵ'') decreases with increasing of frequency and this behavior was observed by many researchers[139,140]. Dipoles tend and align along the direction of applied electric field and for ac fields tend to follow the field and are in a phase with it. The friction of this dipole with other dipoles in the medium prevents this, and leads to the dielectric loss, and this loss appears as heat. The variation in frequency-dependent imaginary part of dielectric constant (ϵ'') of the specimens at room temperature is shown in Fig.(4-28) All the investigated specimen exhibit dielectric dispersion where decrease in ϵ'' is observed with the increase in frequency. The dielectric dispersion phenomenon has been explained on the basis of Maxwell–Wagner model of dielectrics [142,143].

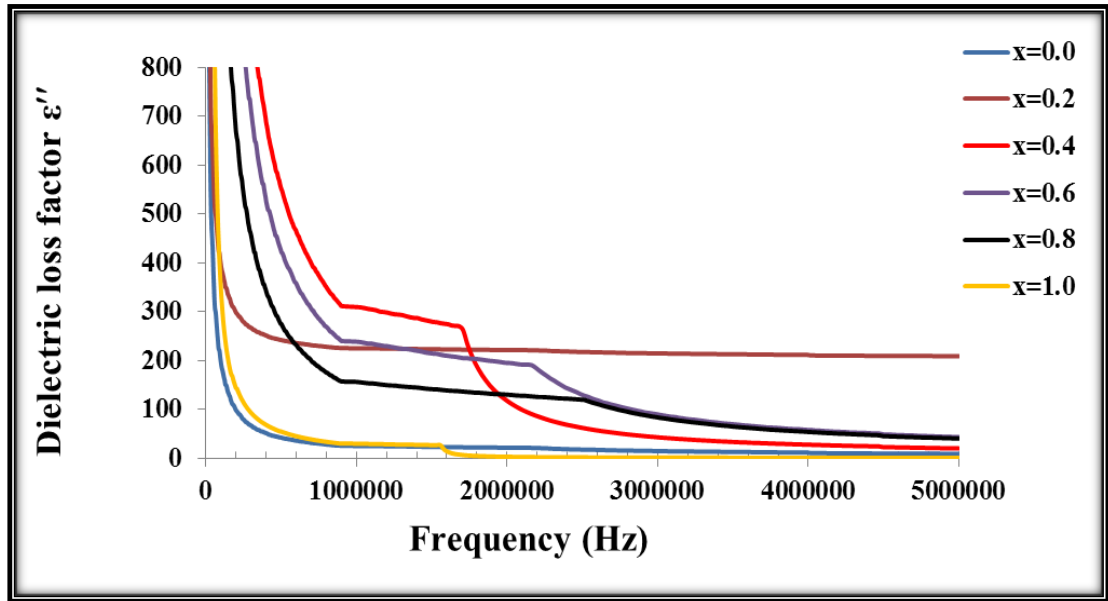


Figure (4-28): Dielectric loss factor (ϵ'') with frequency for $Hg_{0.5}Pb_{0.5}Ba_2Ca_2Cu_{3-x}Ni_xO_{8+\delta}$ specimens

Table (4-12) Dielectric loss factor value (ϵ'') with the change of the amount of material replaced when frequency (50Hz -5MHz).

$Hg_{0.5}Pb_{0.5}Ba_2Ca_2Cu_{3-x}Ni_xO_{8+\delta}$						
X	" ϵ At (50 Hz)	" ϵ At (1MHz)	" ϵ At (2MHz)	" ϵ At (3MHz)	" ϵ At (4MHz)	" ϵ At (5MHz)
0.0	274140.8	24.810	21.159	14.172	10.024	8.6141
0.2	274340.7	224.810	221.159	214.173	210.024	208.614
0.4	52456.94	309.36	115.002	42.178	27.160	19.732
0.6	37007.13	238.33	194.745	88.431	57.428	42.887
0.8	22115.13	155.962	129.603	82.434	53.191	39.987
1.0	18883.99	29.398	2.516	0.856	0.515	0.3701

4-3-4-3 Dielectric Loss Factor | $\tan \delta$ | :

The ratio of energy dissipated and energy stored in the specimens determines the dielectric loss factor | $\tan \delta$ | , figure (4-29) showed varied the absolute value of dielectric loss factor verses frequency (Hz) for all specimens . The variation in frequency-dependent tangent loss ($\tan \delta$) of the specimens at room temperature is shown in Fig (4-29). The peaks appeared correspond to dispersion positions indicating the relaxation process. Maximum dissipation is observed because of relaxation time of electrical dipoles, which is near the applied electric field.[140]

From behaviors of dielectric ($\tan \delta$), a strong dielectric dispersion is observed in system of the HBCCO superconductor. For our experiments on the HBCCO compound superconductor, it is believed that the dielectric dispersion effects are attributable to the dipolar polarizations due to hopping of carriers.

We notice the value of | $\tan \delta$ | decreases with the increase frequency for specimens shown in table (4-13) and stay approximately at comparable value (at high frequency) for specimens , and the value of | $\tan \delta$ | decrease with increase Ni concentration . This behavior may be due to the polarization effect for specimen.

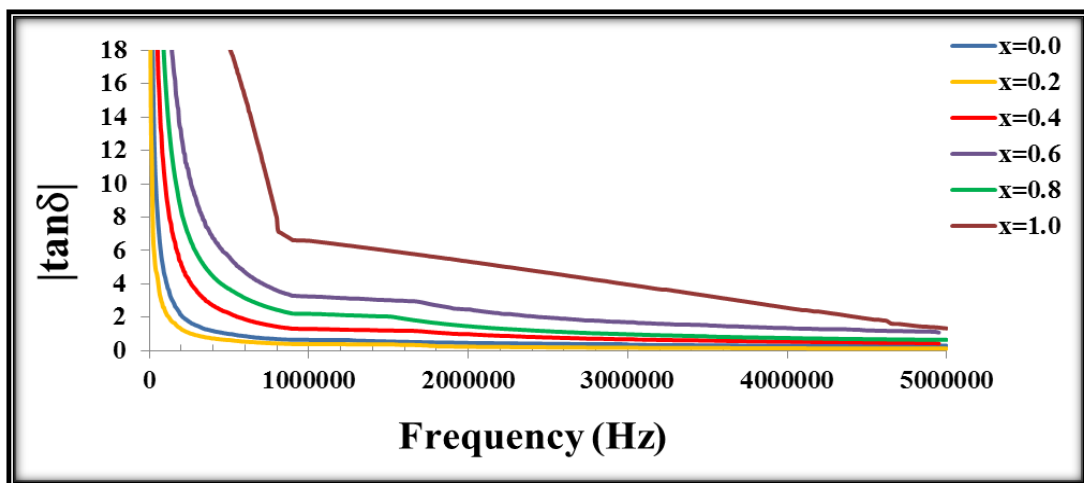


Figure (4-29) : Variation of (| $\tan \delta$ |) versus frequency of



Table (4-13): Variation of $\tan \delta$ versus frequency of $\text{Hg}_{0.5}\text{Pb}_{0.5}\text{Ba}_2\text{Ca}_2\text{Cu}_{3-x}\text{Ni}_x\text{O}_{8+\delta}$ with frequency (50HZ-5MHZ)

$\text{Hg}_{0.5}\text{Pb}_{0.5}\text{Ba}_2\text{Ca}_2\text{Cu}_{3-x}\text{Ni}_x\text{O}_{8+\delta}$						
X	$\tan \delta$ At (50 Hz)	$\tan \delta$ At (1MHz)	$\tan \delta$ At (2MHz)	$\tan \delta$ At (3MHz)	$\tan \delta$ At (4MHz)	$\tan \delta$ At (5MHz)
0.0	55.911	0.6501	0.4615	0.3447	0.3031	0.294
0.2	724.148	0.3969	0.2354	0.1716	0.141	0.125
0.4	223.904	1.3002	0.989	0.680	0.541	0.416
0.6	559.76	3.2506	2.473	1.700	1.354	1.013
0.8	22750.5	2.2135	1.461	0.979	0.756	0.649
1.0	41.45	6.594	5.334	3.947	2.536	1.337

4-2-4-4 Alternating Electrical Conductivity (σ_{ac}):

The Alternating electrical conductivity (σ_{ac}) is measured at room temperature within the frequency (50Hz-5MHz) for $\text{HgBa}_2\text{Ca}_2\text{Cu}_{3-x}\text{Ni}_x\text{O}_{8+\delta}$ with Pb= 0.5 and $x=0.0,0.2,0.4,0.6,0.8$ and **1**.

The value of σ_{ac} increases as a whole after the addition of Ni in Hg-1223 superconducting matrix. The possible reason for this increase in σ_{ac} is due to healing up of the micro-cracks, which results in the improvement of inter-grain connectivity or because at high frequencies, the amount of kinetic energy in which the electrons must have to cross the crystalline increases, so the number of electrons transmitted is more, so (σ_{ac}) increases.

The ac-conductivity (σ_{ac}) of our specimen increases at high frequencies, which happens due to bound carriers trapped in the specimens.

Note through the figures (4-30) and table (4-14) the value of the (σ_{ac}) increases with the increase of frequency (same reference [139]). At low frequencies, the amount of kinetic energy in which the electrons must have to cross the crystal is few, so the number of electrons which transmit is few that means (σ_{ac}) is few.

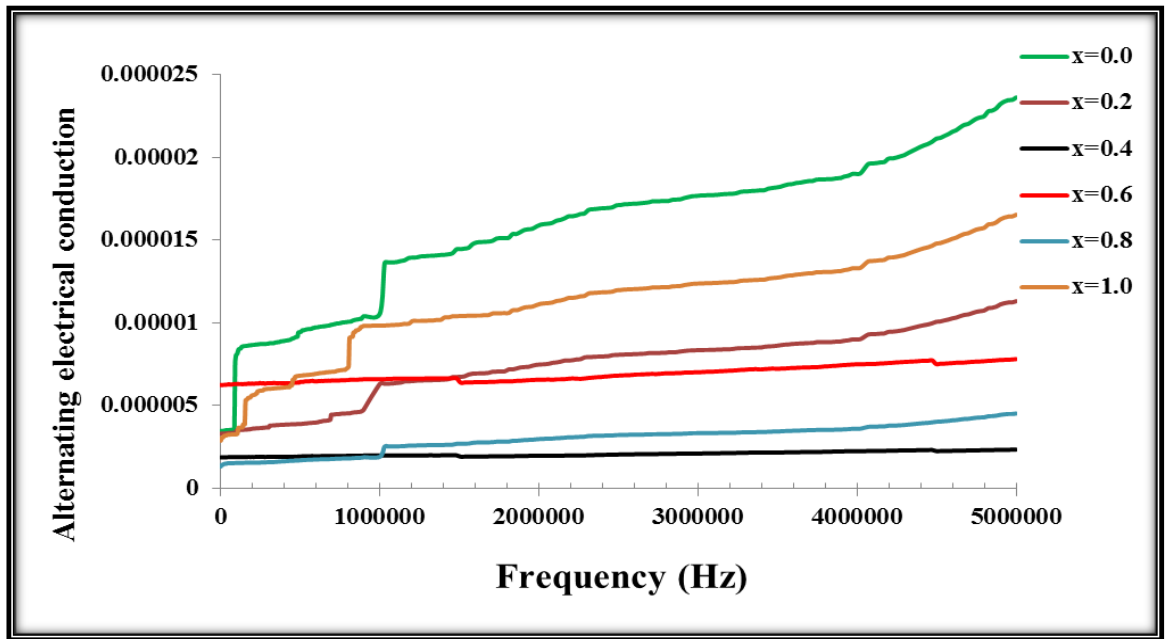


Figure (4-30) : Alternating electrical conductivity(σ_{ac}) with frequency for $Hg_{0.5}Pb_{0.5}Ba_2Ca_2Cu_{3-x}Ni_xO_{8+\delta}$

Table (4-14): Alternating Electrical Conductivity (σ_{ac}) with frequency (50Hz -5MHz).

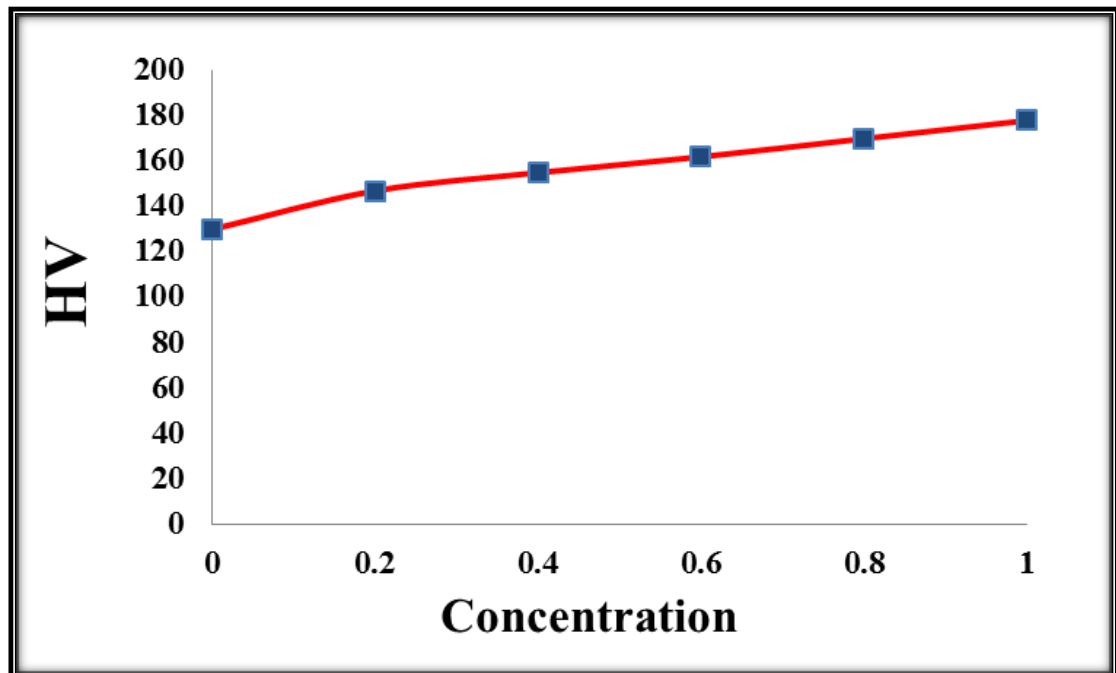
$Hg_{0.5}Pb_{0.5}Ba_2Ca_2Cu_{3-x}Ni_xO_{8+\delta}$						
X	$\sigma_{a.c}$ ($\Omega.cm$) ⁻¹ At (50 Hz)	$\sigma_{a.c}$ ($\Omega.cm$) ⁻¹ At (1MHz)	$\sigma_{a.c}$ ($\Omega.cm$) ⁻¹ At (2MHz)	$\sigma_{a.c}$ ($\Omega.cm$) ⁻¹ At (3MHz)	$\sigma_{a.c}$ ($\Omega.cm$) ⁻¹ At (4MHz)	$\sigma_{a.c}$ ($\Omega.cm$) ⁻¹ At (5MHz)
0.0	$3.47 \cdot 10^{-6}$	$1.06 \cdot 10^{-5}$	$1.59 \cdot 10^{-5}$	$1.77 \cdot 10^{-5}$	$1.90 \cdot 10^{-5}$	$2.36 \cdot 10^{-5}$
0.2	$3.31 \cdot 10^{-6}$	$6.31 \cdot 10^{-6}$	$7.49 \cdot 10^{-6}$	$8.35 \cdot 10^{-6}$	$9.02 \cdot 10^{-6}$	$1.13 \cdot 10^{-5}$
0.4	$1.88 \cdot 10^{-6}$	$1.98 \cdot 10^{-6}$	$1.97 \cdot 10^{-6}$	$2.11 \cdot 10^{-6}$	$2.25 \cdot 10^{-6}$	$2.35 \cdot 10^{-6}$
0.6	$6.25 \cdot 10^{-6}$	$6.6 \cdot 10^{-6}$	$6.57 \cdot 10^{-6}$	$7.02 \cdot 10^{-6}$	$7.5 \cdot 10^{-6}$	$7.82 \cdot 10^{-6}$
0.8	$1.32 \cdot 10^{-6}$	$1.91 \cdot 10^{-6}$	$2.99 \cdot 10^{-6}$	$3.34 \cdot 10^{-6}$	$3.61 \cdot 10^{-6}$	$4.53 \cdot 10^{-6}$
1.0	$2.88 \cdot 10^{-6}$	$9.84 \cdot 10^{-6}$	$1.12 \cdot 10^{-6}$	$1.24 \cdot 10^{-5}$	$1.33 \cdot 10^{-5}$	$1.65 \cdot 10^{-5}$

4-3-5 Result Of Mechanical Properties:

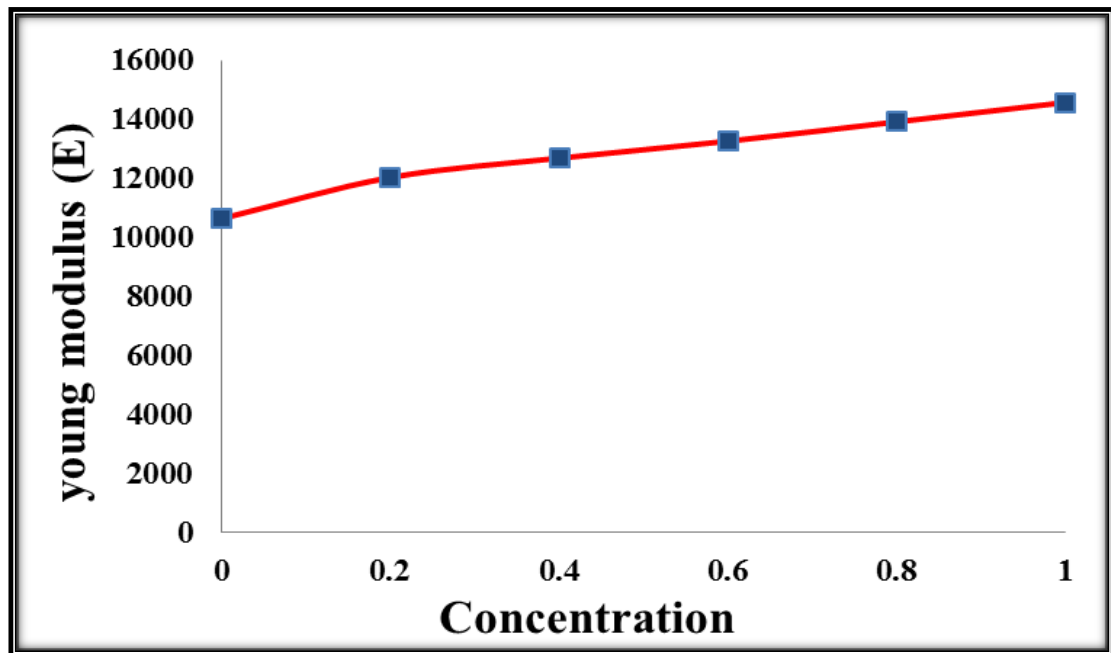
The Vicker's Hardness measurements of substitution Pb =0.5 On Hg and Ni substitution on copper in $\text{Hg}_{0.5}\text{Pb}_{0.5}\text{Ba}_2\text{Ca}_2\text{Cu}_{3-x}\text{Ni}_x\text{O}_{8+\delta}$ specimens with $x=0.0,0.2,0.4,0.6,0.8$ and **1**. were done with a digital microhardness tester at room temperature. All specimens were polished before to being tested a Vickers pyramidal indenter with loads (2.94 N), the applied time was 15 second to measure the diagonals of indentation. The Vickers microhardness (HV), Young's modulus (E) and yield strength (Y) were calculated using the equations (3.14) ,(3.15) and (3.16) respectively for applied loads are summarized in Table(4-15) . figure (4-31) shows the variation of Vickers microhardness Number with Ni concentration , from this figure it was notes the hardness increases with added Ni this not agreement changes were reported [144].This behavior may be explained by the reduced porosity and good contact between the grains when added the Ni , or can be attributed to the high phases which cause reinforcement of the bond strength and addition to properties of Ni high hardness causes increase of compound hardness thus increasing in value young modulus and yield strength, Ni ferrite strengthener; increases the hardenability and impact strength of compound, Nickel is a high-density, high-strength metal and high temperature properties.

Table (4-15): Vicker's Hardness Number (VHN) , Young modulus (E) and Yield strength (Y) for $\text{Hg}_{0.5}\text{Pb}_{0.5}\text{Ba}_2\text{Ca}_2\text{Cu}_{3-x}\text{Ni}_x\text{O}_{8+\delta}$ (for 15 sec &load=2.94N)

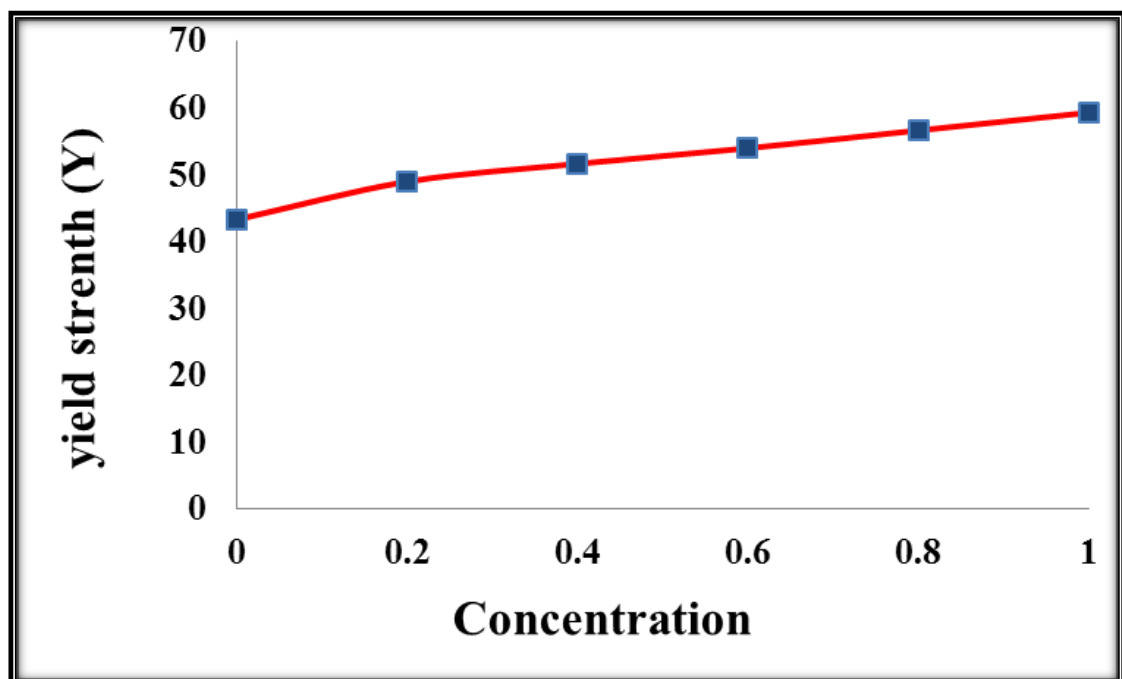
$\text{Hg}_{0.5}\text{Pb}_{0.5}\text{Ba}_2\text{Ca}_2\text{Cu}_{3-x}\text{Ni}_x\text{O}_{8+\delta}$					
x	Tim/ sec	Load N	Hv	E(MPa)	Y(MPa)
0.0	15	2.94	130	10654.8	43.33
0.2	15	2.94	147	12048.12	49
0.4	15	2.94	155	12703.8	51.66
0.6	15	2.94	162	13277.52	54
0.8	15	2.94	170	13933.2	56.66
1.0	15	2.94	178	14588.88	59.33



Figure(4-31) : The variations of Vicker's Hardness Hv as a function Ni concentration .



Figure(4-32) The variations of young modulus E
a function Ni concentration .



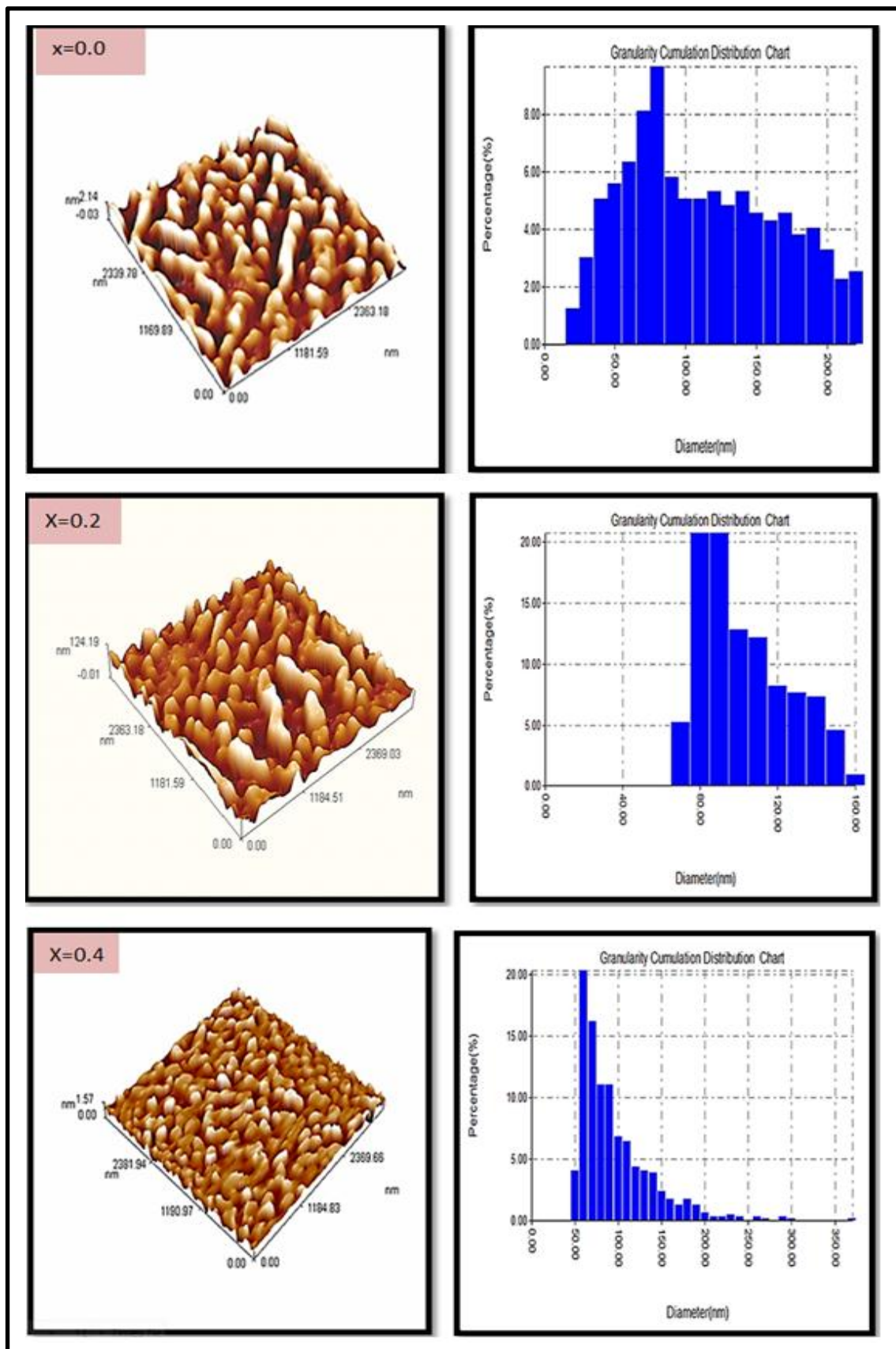
Figure(4-33) The variations of yield strength Y
a function Ni concentration .

4-3-6 Results of Atomic Forces Microscopic AFM:

After the preparation of the specimens by solid state method. Using a agate mortar, the elements were converted to small dimensions and imaged by an atomic force microscope the images taken in this research of composition $\text{Hg}_{0.5}\text{Pb}_{0.5}\text{Ba}_2\text{Ca}_2\text{Cu}_{3-x}\text{Ni}_x\text{O}_{8+\delta}$ with $\text{Pb}=0.5$ and $x=0.0,0.2,0.4,0.6,0.8,1$. It is found that for the various Ni concentration and with substitution of Pb on Hg lead to various Roughness(nm) ,Root mean square(nm) and Avg. Diameter(nm) and it is clearly seen that in figure (4-34) AFM images. Table (4-16) shows the values of surface roughness of the specimens which indicate that the surface of the some specimens has a good crystalline uniformity and high homogeneity surface give a best nano size value is 98.17 nm at $x=1.0$.

Surface roughness most commonly refers to the variations in the height of the surface relative to a reference plane. It is measured either along a single line profile or along a set of parallel line profiles[146].

Figure (4-34): Reveals the (3-D) AFM images and the chart distribution of $Hg_{0.5}Pb_{0.5}Ba_2Ca_2Cu_{3-x}Ni_xO_{8+\delta}$



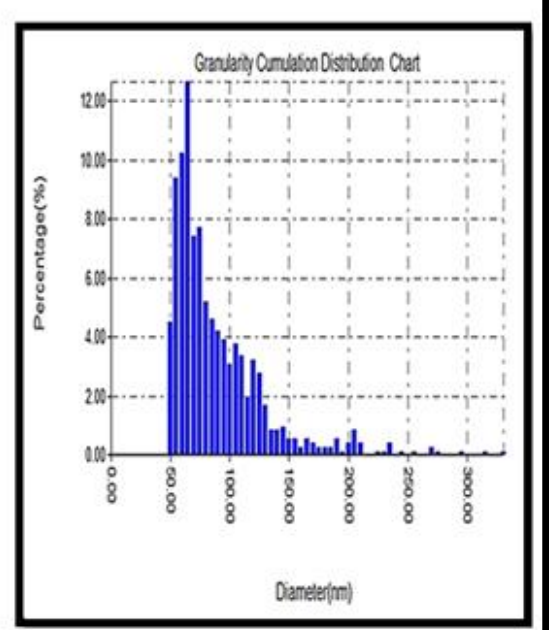
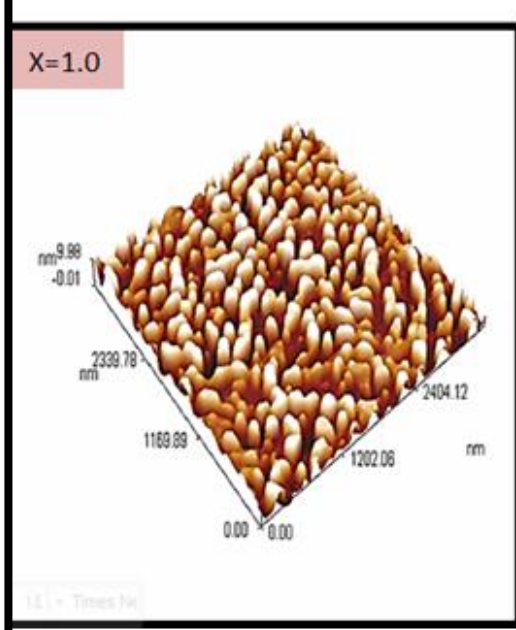
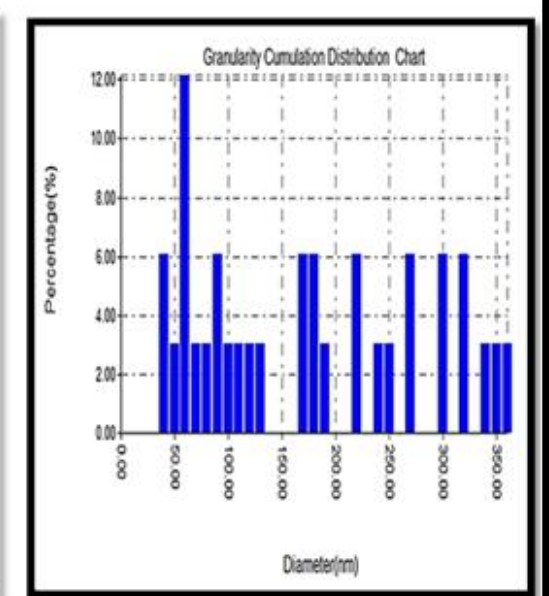
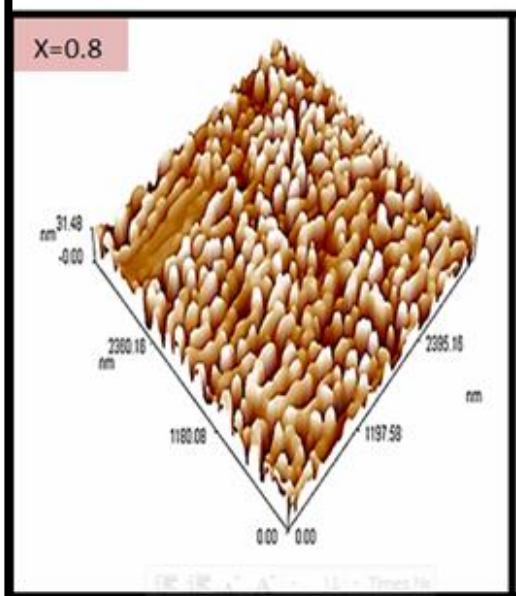
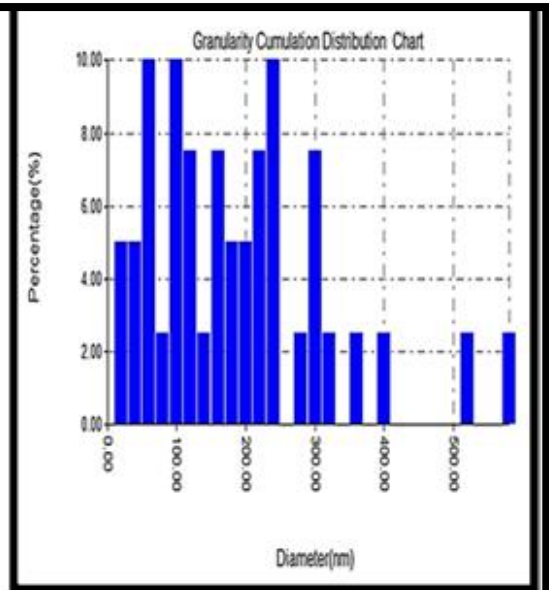
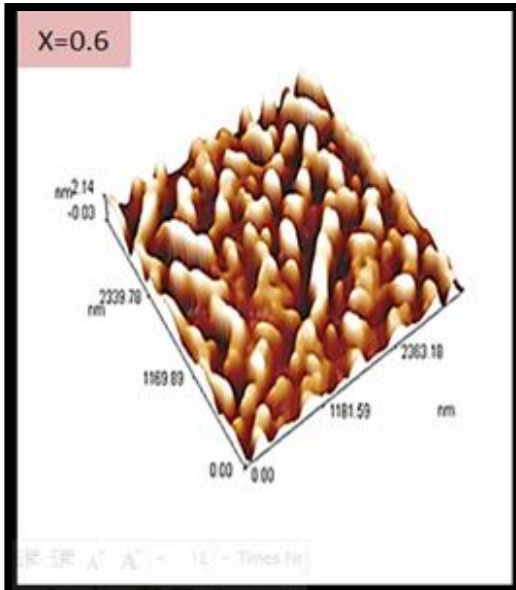
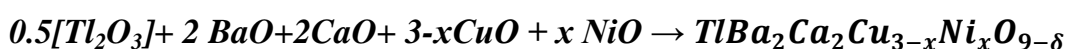


Table (4-16): Values of average surface roughness ,Crystal size and Avg. Diameter in 2D for $\text{Hg}_{0.5}\text{Pb}_{0.5}\text{Ba}_2\text{Ca}_2\text{Cu}_{3-x}\text{Ni}_x\text{O}_{8+\delta}$

x	Crystallite size(nm)	Roughness (nm)	Root mean square(nm)	Avg. Diameter(nm)
0	28.11172	0.219	0.282	91.35
0.2	32.57997	19.3	23.6	107.23
0.4	36.47015	35.8	41.3	178.84
0.6	25.21534	0.884	1.02	170.79
0.8	22.36517	0.564	0.645	87.11
1.0	29.91793	2.52	2.9	98.17

4 -4 TlBa₂Ca₂Cu_{3-x}Ni_xO_{9-δ} Compound:

The molecular weights of the compound were calculated according to the following formula and then were studied the physical properties (structure , electrical , mechanical) that will be explained later



4-4-1 Study of Structural Properties:

The structure and phase purity of compound was determined by XRD pattern analyses'. We analyzed nominal composition $\text{TlBa}_2\text{Ca}_2\text{Cu}_{3-x}\text{Ni}_x\text{O}_{9-\delta}$ ($x = (0.0, 0.2, 0.4, 0.6, 0.8 \text{ and } 1)$) high- T_c superconductor with Tl-1223 phase. These superconductor system have a tetragonal unit cell with $a = 3.1464$ and $c = 15.1171$ °A and pertain to the P4/mmm space group. This has one insulating TlO layer, two spacing BaO layers, two separating Ca layers, and three conducting CuO₂ planes forming them "1223" type.

Figure (4-35) contrast the XRD patterns of the pure specimens and those substitution by Ni measurements in a assortment of 2Θ from 10° to 80° . All the peaks are well resolved and indicate good crystallinity of the compound. It can be seen from Fig.(4-35) that the main peaks are at (1223) for the high HTSC phase and implying that the some of secondary phases Tl-1212, Tl-1201 and appears small amounts of impurities. The relative intensities of XRD patterns of $\text{TlBa}_2\text{Ca}_2\text{Cu}_{3-x}\text{Ni}_x\text{O}_{9.8}$ specimens we can notice increase of High-phase and decrease of Low-phase by increasing Cu-O layer due to increasing hole in the structures that due increase the high- T_c phase beside of that there is appearance clear and sharp peaks especially when $\Theta = 30.34^\circ$, 48° and shifting of peaks position in compression with pure specimen, this may attributed to the substitution of Ni in Cu sites that means peaked tops are overlapped and this indicates of (CuO)layers be formed which are thought to have a significant role in superconducting process thus the compound is reach at its best of regularity and stability, which help to provides safety tracks for current carriers.

The lattice parameters for the XRD patterns of the prepared specimens of Tl-1223 are reported in Table (4-17) which shows that as the sintering temperature increases the (c) lattice parameter in the same time changes (a=b) lattice parameter increases with increasing Ni indeed the behavior of the lattice constant may attributed to the incorporation of Ni ions into interstitial sites in the unit cell rather than occupation of the Cu sites or the larger Ba atoms contribute to the increase of c-parameter. Hence, the super electrons will move more freely in the Cu-O planes. Thus, we attribute that the c-parameter play influential role in the HTSC process.

Table(4-17): Lattice parameters and volume fraction of $TlBa_2Ca_2Cu_{3-x}Ni_xO_{9.8}$ compounds

X	a=b (Å)	c(Å)	c/a ratio	v(Å) ³	dm(gm/cm ³)	V _{ph(1223)} %	V _{ph(1212)} %	V _{ph(1201)} %	V _{p impurities} %
0	3.1464	15.1171	4.80457	149.6568	10.40618	71.2909	17.5337	6.2620	4.6242
0.2	3.4210	15.3458	4.485764	179.5956	8.662477	72.1082	4.6643	4.6643	12.8731
0.4	3.5357	15.5546	4.399299	194.4508	7.99241	74.6478	5.9859	14.9647	6.3380
0.6	3.5520	16.0433	4.516695	202.4136	7.670029	85.0467	15.5763	4.9532	4.6728
0.8	3.7023	15.6143	4.217459	214.0256	7.246355	60.2702	16.4864	18.6486	4.5945
1	3.9592	14.6648	3.703981	229.8746	6.739731	54.8455	28.7539	13.3120	3.5143

The substitution of Cu^{+2} by Ni^{+2} may well relax the modulation by influencing the charge balance oxygen content and structure of the relevant layers[152] . According to these, it was found from Table (4-17) increase of the c- axis lattice constant with the increases of the Ni content . The presence of Ni in the structure of the Tl-1223 compound has a direct influence on the increasing of the high T_C - phase, which can be clearly in the x-ray diffraction (XRD) pattern in Fig. (4-35). In all specimens of **$TlBa_2Ca_2Cu_{3-x}Ni_xO_{9.8}$ compounds**, the High phases increased with increasing Ni. We noted many satellite reflections that are due to arrangement of the cations and displacement of an ion or oxygen defects (the oxygen deficiency increment when Cu is substituted by Ni which has smaller ionic radius than that of Cu). This is more likely to be the result of an incommensurate structure which gives rise to deformation of the c-parameter. The deformation of the structure is always considered as the reason of the high conduction in the perovskite multi-layer.

From figures(4-36),(4-37) and (4-38) we find that the V_{ph} , c/a and the density (d_m) which have been calculated from equations (3-3) and (3-4) noted V_{ph} increase with increase value Ni, the c/a ratio and d_m decreases

with increasing Ni as compared with this pure specimen. This result may be explained by the shorter ionic radius of Ni^{+2} (83 pm) than that of Cu^{+2} (87 pm) or reason due to existence of porous in $\text{TlBa}_2\text{Ca}_2\text{Cu}_{3-x}\text{Ni}_x\text{O}_{9.8}$ which would leads to increase Critical temperature T_c .

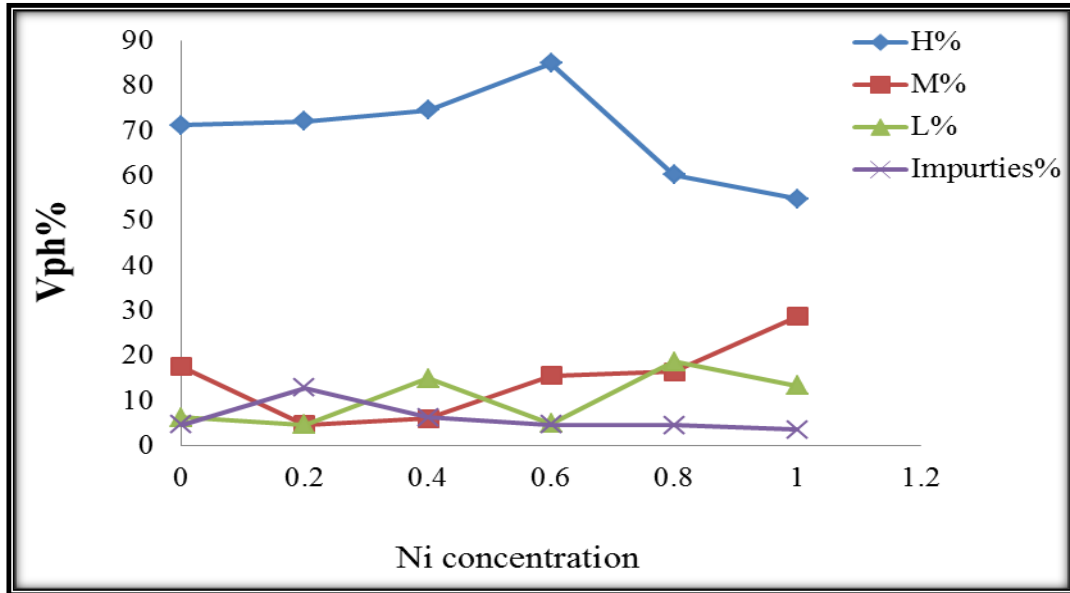


Figure (4-36): The ratio of volume fraction V_{ph} as function of Ni concentration for the $\text{TlBa}_2\text{Ca}_2\text{Cu}_{3-x}\text{Ni}_x\text{O}_{9.8}$ specimens

Figures(4-37) shows that the density (dm) is decreased with the increase of Ni, this can be explained by an increase in porosity reason to decrees in the density value. The produce a high concentration of the hole pairing, resulting to a decrease in the density (dm).

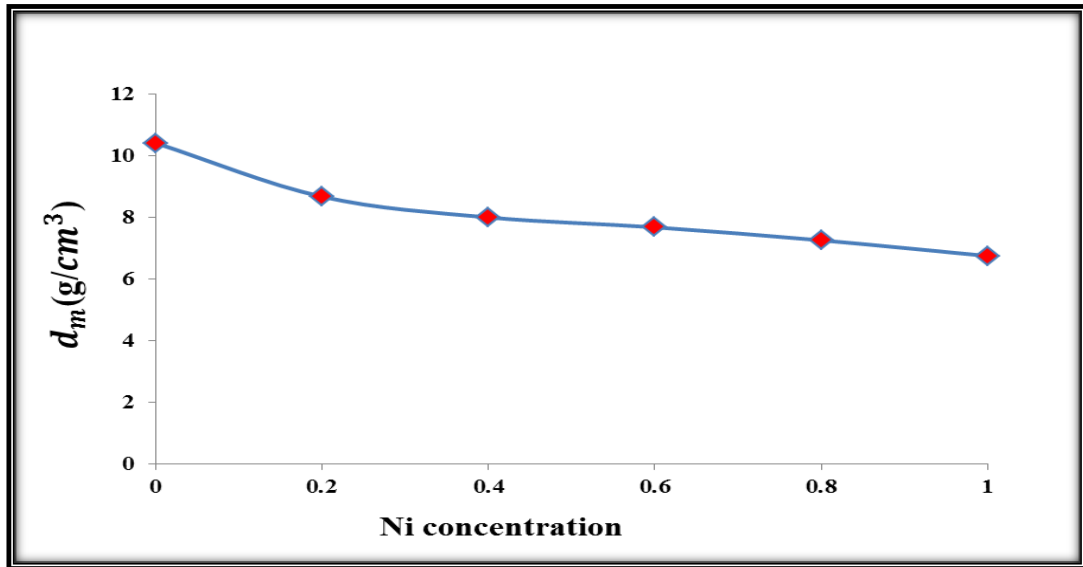


Figure (4-37): Variation density with Ni concentration for the $\text{TlBa}_2\text{Ca}_2\text{Cu}_{3-x}\text{Ni}_x\text{O}_{9.8}$ specimens

The altering in the c- lattice parameter is belong to the distribution of holes between Thallium oxides layers and CuO planes. The doped ions may change the spacing between the CuO planes and thus affect the charge transfer to the CuO layers [153].

Figure (4-48) shown the ratio of c/a changing with increment of Ni concentration due to the variation in values of (a=b,c) parameter by changing of density.

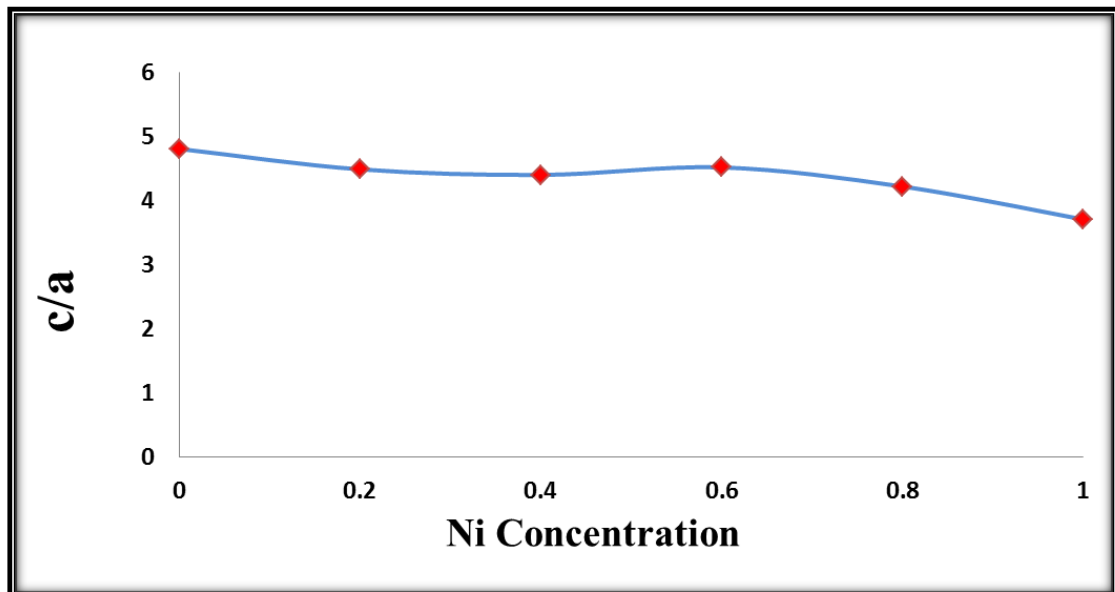


Figure (4-38): The ratio of lattice parameters c/a as function of Ni concentration for the $\text{TlBa}_2\text{Ca}_2\text{Cu}_{3-x}\text{Ni}_x\text{O}_{9.8}$ specimens

4-4-2 Study of Electrical Resistivity:

The resistivity versus temperature diagram for specimens with nominal composition $\text{TlBa}_2\text{Ca}_2\text{Cu}_{3-x}\text{Ni}_x\text{O}_{9-\delta}$ with $x=(0.0,0.2,0.4,0.6,0.8\text{ and }1)$ shown in figure(4-39) the compounds a four-point probe technique has been recommended as a good method ..

The figure(4-39) and table (4-18) shown the effect of Ni on Cu in the $\text{TlBa}_2\text{Ca}_2\text{Cu}_{3-x}\text{Ni}_x\text{O}_{9-\delta}$ with $x=(0.0,0.2,0.4,0.6,0.8\text{ and }1)$ by preparing a specimen at sintering equal $850\text{ }^\circ\text{C}$ for 24h reveals that the behavior of resistivity of this research specimens decreases with the decrease of temperature, although all specimens showed metal-like behavior with respect to temperature.

A graph of the normalized resistivity vs. temperature behavior of specimens with various Ni concentrations. It can be noticed that the value of $T_{c(\text{offset})}$ increased from 117K in the pure specimen to 123 K in the Ni-doped specimen (Ni =0.2). The values of critical transition temperature $T_{c(\text{offset})}$ for ($x= 0.4, 0.6, 0.8\text{ and }1.0$) HTSC phases are 123.5, 129,113 and 113.5 K respectively. It is found the greatest value of transition temperature T_c when Ni content ($x=0.6$) reason due to attributed to the existence of the high T_c -phase as referred in x-ray analysis and due to increasing Cu-O layer increase Ni and then decrease when $x= 0.8,1.0$ the critical temperature receptivity equal 129,125 K. The decrease in T_c are further evidence that the presence of increase amount of Ni content in Tl-1223 phase stabilizes and promotes the growth of Tl-1212 and Tl-1201 phase at the expense of Tl-1223 phase.

The transition temperature (T_c) of most specimens in $\text{TlBa}_2\text{Ca}_2\text{Cu}_{3-x}\text{Ni}_x\text{O}_{9-\delta}$ compound increases with the increase of the value of Ni content, because the increase of the Ni content is necessary to insert extra layers of Cu-O₂ and Ca planes into the layer structure of low- T_c phase (1212) to produce high phase(1223) superconductors [154].

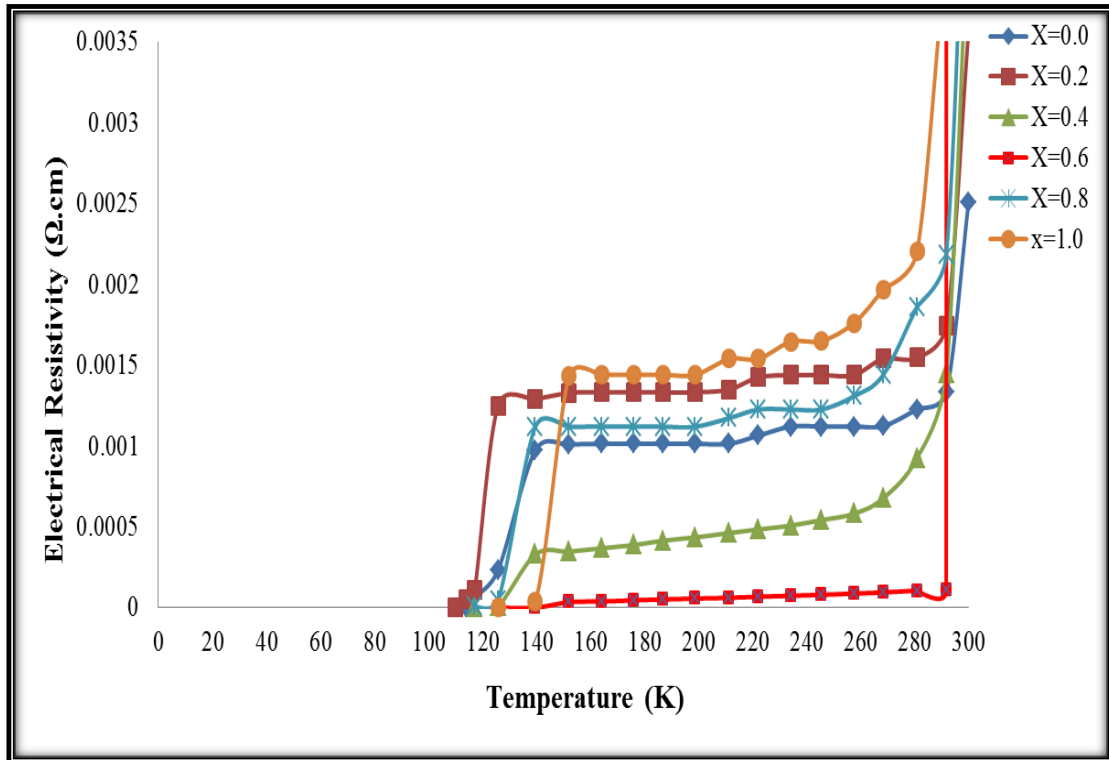


Figure (4-39) : The resistivity as function of temperature for $\text{TlBa}_2\text{Ca}_2\text{Cu}_{3-x}\text{Ni}_x\text{O}_{9-\delta}$ specimens for $x=0.0, 0.2, 0.4, 0.6, 0.8$ and 1.0

It is clear from table (4-18) that the increment of the Cu-O layers which leads to increment the holes in the structures thus reinforce the transition temperature from and reduced the transition width ΔT . The transition width (ΔT_c) decreases with substitution concentration. this may be due to homogeneity of specimen during preparation or indicates that a very small admixture of some other phases exist, then the transition width (ΔT_c) increases with substitution concentration ($x=0.6, x=0.8$) this may be due to the effect of microscopic inhomogeneity and may be due to an electronic problem in the experiment.

Table(4-18) : volume fraction , E_g , δ and transition temperature of $TlBa_2Ca_2Cu_{3-x}Ni_xO_{9-\delta}$ compounds

X	V ph (1223)%	V ph (1212)%	V ph (1201)%	Vph impurities %	$T_{c(off)}$ (K)	$T_{c(on)}$ (K)	ΔT_c (K)	$T_{c(mid)}$ (K)	E_g (eV)	δ
0	71.2909	17.5337	6.2620	4.6242	117	125.6	8.6	121.3	0.0368	0.0464
0.2	72.1082	4.6643	4.6643	12.8731	123	128	5	125.5	0.0381	0.1157
0.4	74.6478	5.9859	14.9647	6.3380	123.5	130	6.5	126.6	0.0385	0.1137
0.6	85.0467	15.5763	4.9532	4.6728	129	140.2	11.2	134.6	0.0409	0.1253
0.8	60.2702	16.4864	18.6486	4.5945	113	126.2	13.2	119.6	0.0363	0.1333
1	54.8455	28.7539	13.3120	3.5143	113.5	116.5	3	115	0.0349	0.1173

Figure(4-40) shows the variation of $T_{c(off)}$ with Ni concentration and we can observed the value of $T_{c(off)}$ increment from $x=0.0$ (pure specimen) to $x=0.6$ (129 K) and the decrease above $x=0.6$.This behavior its seem the results for E_g and we noted the optimum of E_g equal (0.0409eV) where $x=0.6$.

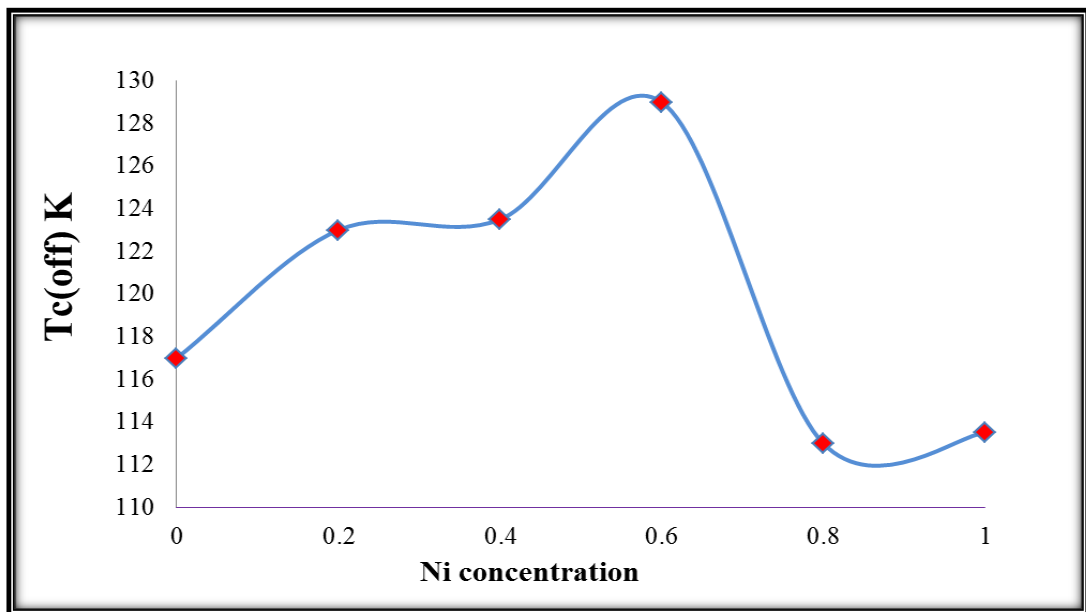


Figure (4-40): $T_{c(offset)}$ a function of concentration Ni of $TlBa_2Ca_2Cu_{3-x}Ni_xO_{9-\delta}$ specimens

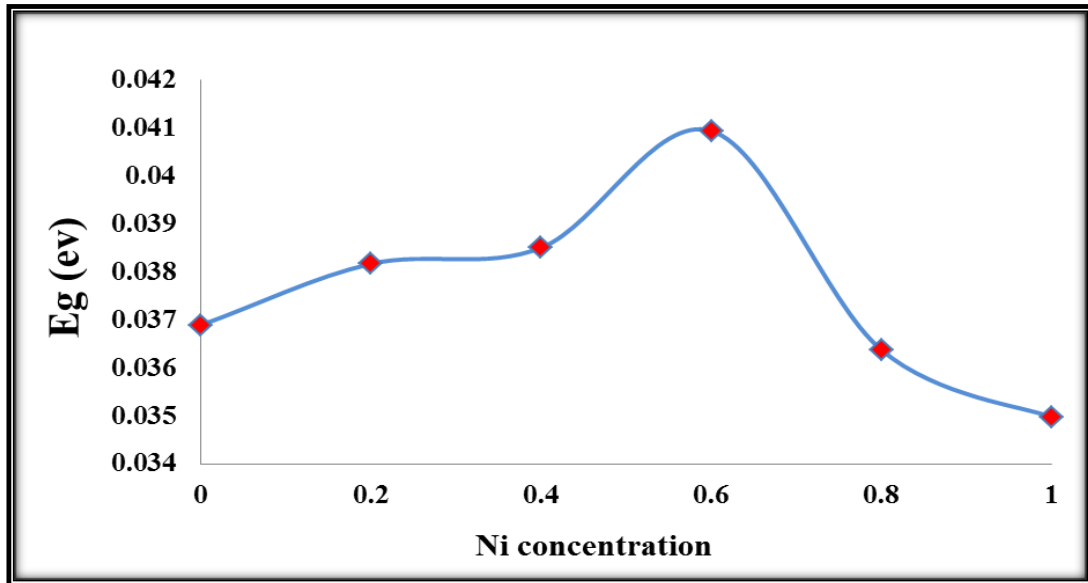


Figure (4-41): E_g (eV) a function of concentration Ni of $TlBa_2Ca_2Cu_{3-x}Ni_xO_{9.8}$ specimens

4-4-3 Results Of Oxygen Content:

The values of (δ) which is the excess concentration of oxygen in the prepared specimens of $TlBa_2Ca_2Cu_{3-x}Ni_xO_{9.8}$ ($x=0.0,0.2,0.4,0.6,0.8,1.0$) was measured by using a chemical Iodometric titration experiment discussed in (chapter two).

Table (4-18) and fig (4-42) shows the values of T_c related to δ values for all specimens. It can be noticed that δ and T_c increase with the raising of the dopant concentration and T_c increases with the increases δ for $TlBa_2Ca_2Cu_{3-x}Ni_xO_{9.8}$ with $x=0.0,0.2,0.4,0.6,0.8,1.0$.

From the table(4-18) we noted increase in oxygen content plays a very important role in increasing the critical transition temperature. This may be caused by decreasing the structure defects and also could be due to the intergrowth of a large number of Cu–O layers in the unit cell [150].

Calculation the oxygen excess play an important role to determine the value of oxygen diffusion, which is of critical importance in optimizing the fully dense polycrystalline specimens.

We noted the variability in oxygen content that may be due to change of Ni concentration add to different location of specimens inside furnace during heat treatments.

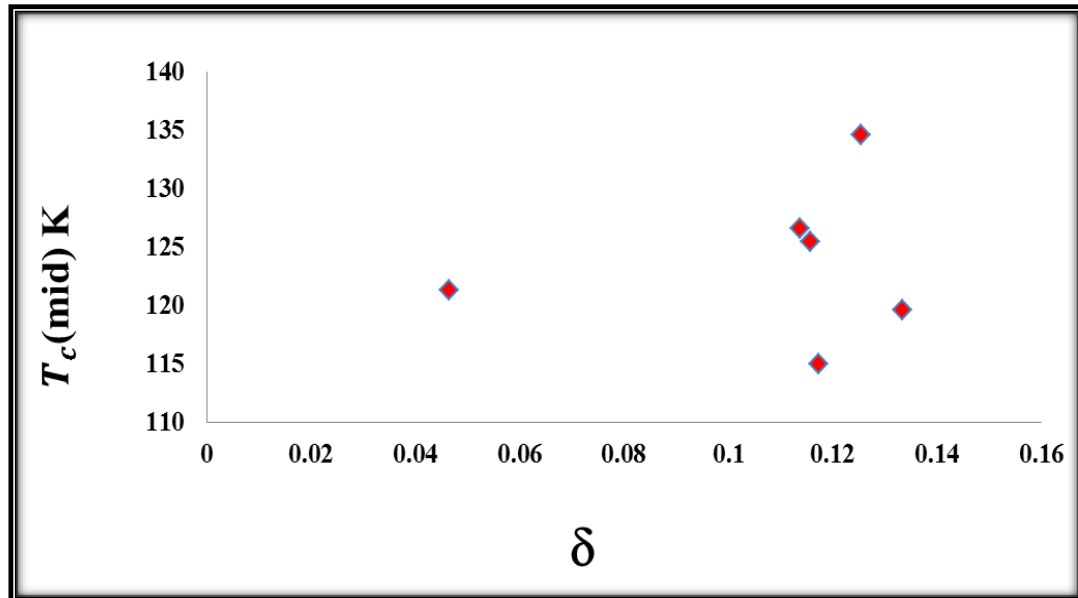


Figure (4-42): The Oxygen content as a function of T_c (mid) of $TIBa_2Ca_2Cu_{3-x}Ni_xO_{9-\delta}$ specimens

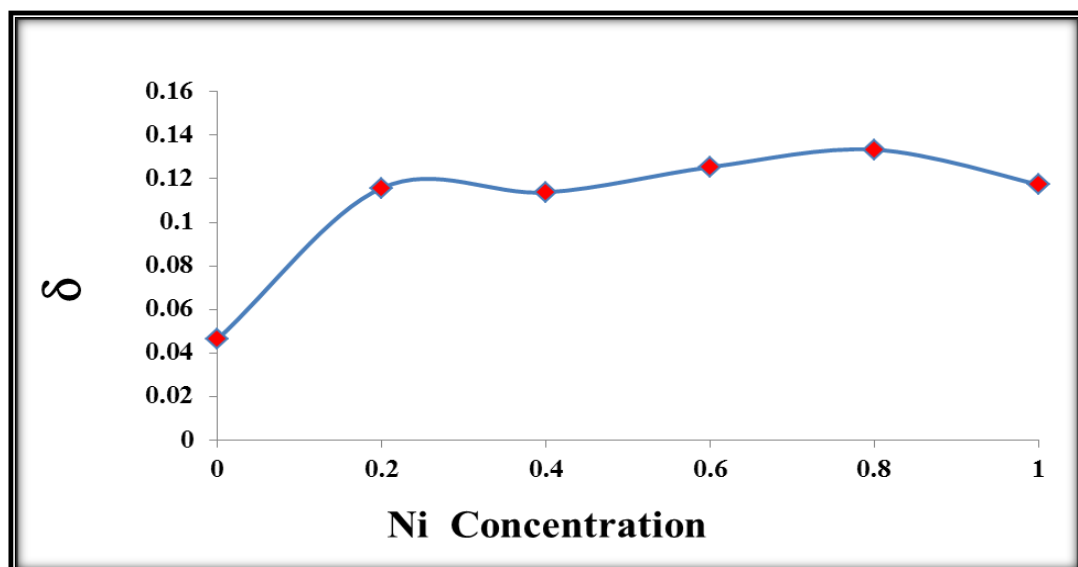


Figure (4-43) : The Oxygen content as a function of concentration Ni of $TIBa_2Ca_2Cu_{3-x}Ni_xO_{9-\delta}$ specimens

4-4-4 Study of Dielectric Properties:

The dielectric properties such as dielectric constant (ϵ'), dielectric loss factor (ϵ'') and alternating electric conductivity (σ_{ac}) were measured at room temperature at the frequency (50Hz - 5MHz) for compounds $TlBa_2Ca_2Cu_{3-x}Ni_xO_{9.8}$ with $x=0.0,0.2,0.4,0.6,0.8$ and 1 which are prepared by a solid state reaction. The results are discussed as a function of frequency .

4-4-4-1 Dielectric Constant (ϵ'):

The behavior of the dielectric constant is measured at room temperature within the frequency (50Hz-5MHz) measured for $TlBa_2Ca_2Cu_{3-x}Ni_xO_{9.8}$ with $x=0.0,0.2,0.4,0.6,0.8$ and 1.

Figure (4-44) shows the dielectric constant dependence of the frequency electrical for a $TlBa_2Ca_2Cu_{3-x}Ni_xO_{9.8}$ with $x=0.0,0.2,0.4,0.6,0.8$ and 1. This figure shows the dielectric constant values start to be stable and became approximately constant constant for many phases at frequencies ($f \geq 1 * 10^5$ Hz). We noted clarified in figure (4-44) that the dielectric constant increase with increase Ni concentration ,this could be explained as a result of the difference in volumes of the ionic and atomic size between the two elements (Cu and Ni) .The reason is the decrease in grain size with the Ni increasing, which leads to an increase in the number of dipoles thus increasing the polarization. This variation in dielectric constant behaviors refers to the polarization effects, at low frequencies ($f < 1 * 10^5$ Hz) there are four polarization mechanisms or all polarization mechanisms can follow the applied field, so the dielectric constant arrive a maximum value at lower frequencies. At higher frequencies, the space charge, cannot shift orientation direction with the applied field, polarization drops out, only ionic and electronic contributions remain, so the dielectric constant values decrease with the increases of frequencies[155]. The carriers can not follow

the frequency of external applied electric ac-field at high frequencies and dielectric response becomes ineffective[140].

The (ϵ) gives the part of energy stored in the matter(within the grains inter-granular) at electric field applied. The most likely place at which this energy could be stored is the material is within the grain acts like termination ends for the crystal.

The figure (4-44) and table (4-19) show a rise in (ϵ) values at low frequencies from 27.784(50 Hz) at the specimen $\text{TlBa}_2\text{Ca}_2\text{Cu}_{3-x}\text{Ni}_x\text{O}_{9.8}$ ($x=0.0$) to 84161.24(50Hz) at the specimen $\text{TlBa}_2\text{Ca}_2\text{Cu}_{3-x}\text{Ni}_x\text{O}_{9.8}$ ($x=1.0$) also increasing in this values at 5MHz with increasing Ni addition from 12.557 (at $x=0$) to 213.14 (at $x=0.6$). Also, the values of dielectric constant for the specimen at 1 MHz , 2MHz ,3 MHz and 4 MHz shows in table (4-19)and from this table we notes the specimen $x=0.6$ $\text{TlBa}_2\text{Ca}_2\text{Cu}_{2.6}\text{Ni}_{0.6}\text{O}_{9.8}$ showed the best behavior for dielectric constant .

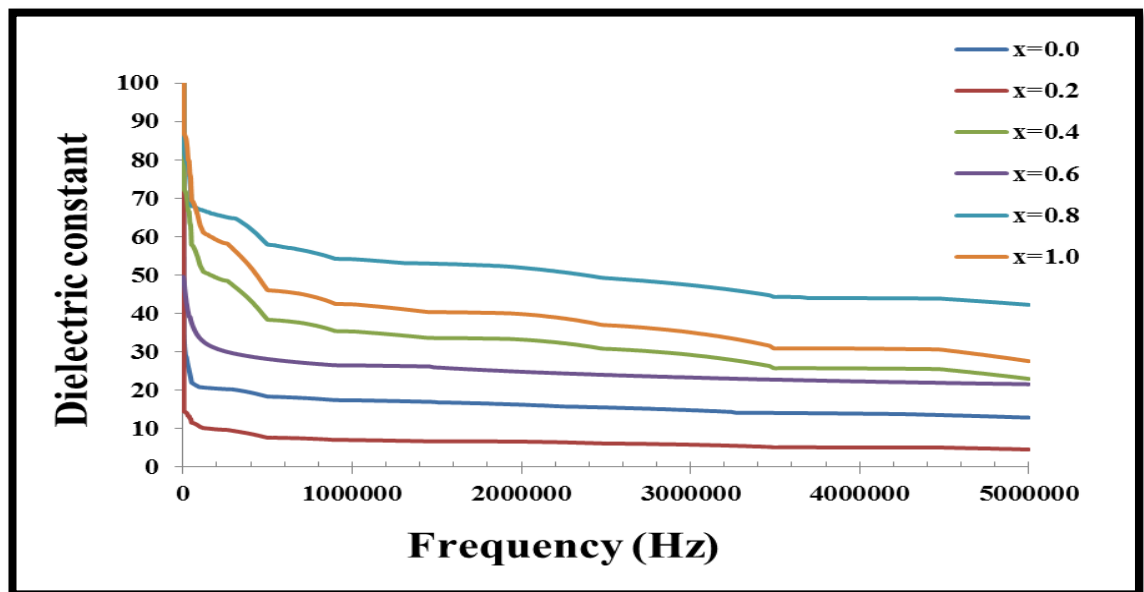


Figure (4-44) : Dielectric constant(ϵ) with frequency of $\text{TlBa}_2\text{Ca}_2\text{Cu}_{3-x}\text{Ni}_x\text{O}_{9.8}$ specimens

Table (4-19): Dielectric constant value (ϵ') with the change of the amount of material replaced when frequency (50Hz -5MHz).

<i>TlBa₂Ca₂Cu_{3-x}Ni_xO_{9-δ}</i>						
X	ϵ' At (50 Hz)	ϵ' At (1MHz)	ϵ' At (2MHz)	ϵ' At (3MHz)	ϵ' At (4MHz)	ϵ' At (5MHz)
0.0	27.784	17.051	15.790	14.178	13.831	12.557
0.2	14.436	6.667	6.168	5.125	5.089	4.022
0.4	37.559	0.1667	0.116	0.012	0.008	0.0009
0.6	4385.58	2607.88	2408.03	2282.11	2198.51	2131.14
0.8	675.565	53.136	49.281	44.313	43.854	40.563
1.0	84161.24	938.184	913.863	898.007	895.588	802.152

4-4-4-2 Loss Factor Of Dielectric (Imaginary Part ϵ''):

The behavior of the dielectric loss factor (ϵ'') is measured at room temperature within the frequency (50Hz-5MHz) that is measured for **TlBa₂Ca₂Cu_{3-x}Ni_xO_{9-δ}** with **x=0.0,0.2,0.4,0.6,0.8**and **1**.

The imaginary part of the dielectric constant (ϵ'') demonstrate the absorption and the attenuation of energy across the interfaces under an external electric field .Examples of interfaces are grain boundaries, localized defects and localized charge densities at the defect sites and at grain boundaries[135].

Figure (4-45) shows that the dielectric loss factors (ϵ'') decreases with increasing of frequency and this behavior was observed by many researchers[139,140]. Dipoles tend and align along the direction of applied electric field and for ac fields tend to follow the field and are in a phase with it. The friction of this dipole with other dipoles in the medium prevents this, and leads to the dielectric loss, and this loss appears as heat.

The variation in frequency-dependent imaginary part of dielectric constant (ϵ'') of the specimens at room temperature is shown in Fig.(4-45) and table (4-20). All the investigated specimen exhibit dielectric dispersion where decrease in ϵ'' is observed with the increase in frequency. The dielectric dispersion phenomenon has been explained on the basis of Maxwell–Wagner model of dielectrics [142,143].

We noted clarified in figure (4-45) that the dielectric loss factor increase with increase Ni concentration ,this maybe explained as a result of the difference in ionic radius between the two elements (Cu and Ni).

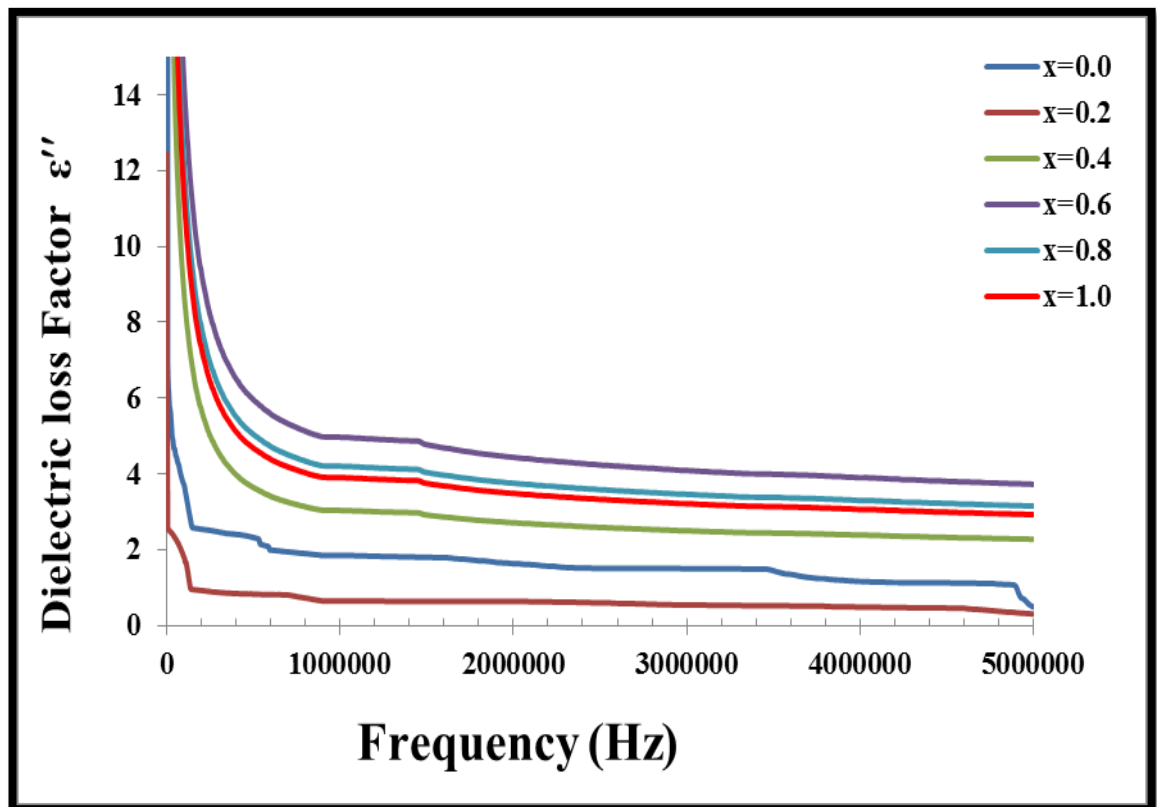


Figure (4-45): Dielectric loss factor (ϵ'') with frequency for $\text{TlBa}_2\text{Ca}_2\text{Cu}_{3-x}\text{Ni}_x\text{O}_{9-\delta}$ specimens

Table (4-20) :Dielectric loss factor value (ϵ'') with the change of the amount of material replaced when frequency (50Hz -5MHz).

$TlBa_2Ca_2Cu_{3-x}Ni_xO_{9-\delta}$						
X	" ϵ At (50 Hz)	" ϵ At (1MHz)	" ϵ At (2MHz)	" ϵ At (3MHz)	" ϵ At (4MHz)	" ϵ At (5MHz)
0.0	286.57	1.8479	1.630	1.499	1.160	0.4922
0.2	12.448	0.648	0.632	0.542	0.486	0.3029
0.4	67.409	3.036	2.709	2.498	2.383	2.277
0.6	110.309	4.968	4.433	4.088	3.899	3.727
0.8	93.336	4.204	3.751	3.459	3.299	3.153
1.0	86.669	3.904	3.483	3.212	3.063	2.928

4-4-4-3 Dielectric Loss Factor | $\tan \delta$ | :

The ratio of energy dissipated and energy stored in the specimens determines the dielectric loss factor | $\tan \delta$ | , figure (4-46) showed varied the absolute value of the loss tangent | $\tan \delta$ | verses frequency (Hz) for all specimens. The loss tangent ($\tan\delta$), which is measured at room temperature, is plotted as a function of applied frequency-range 50 Hz - 5MHz -for specimens as shown in Figure (4-46).Where the specimens are compacted to 7ton/cm² followed by heat treatment (sintering) at (850)^oC for 24 hours, we noted from the figure and teble (4-21) that, the loss tangent has a low value ($\tan\delta\leq 1$) decrease in $\tan\delta$ with the increase in Ni concentration for all specimens.

The variation in frequency-dependent tangent loss ($\tan\delta$) of the specimens at room temperature is shown in Fig (4-46). The peaks appeared

correspond to dispersion positions indicating the relaxation process. Maximum dissipation is observed because of relaxation time of electrical dipoles, which is near the applied electric field[140].

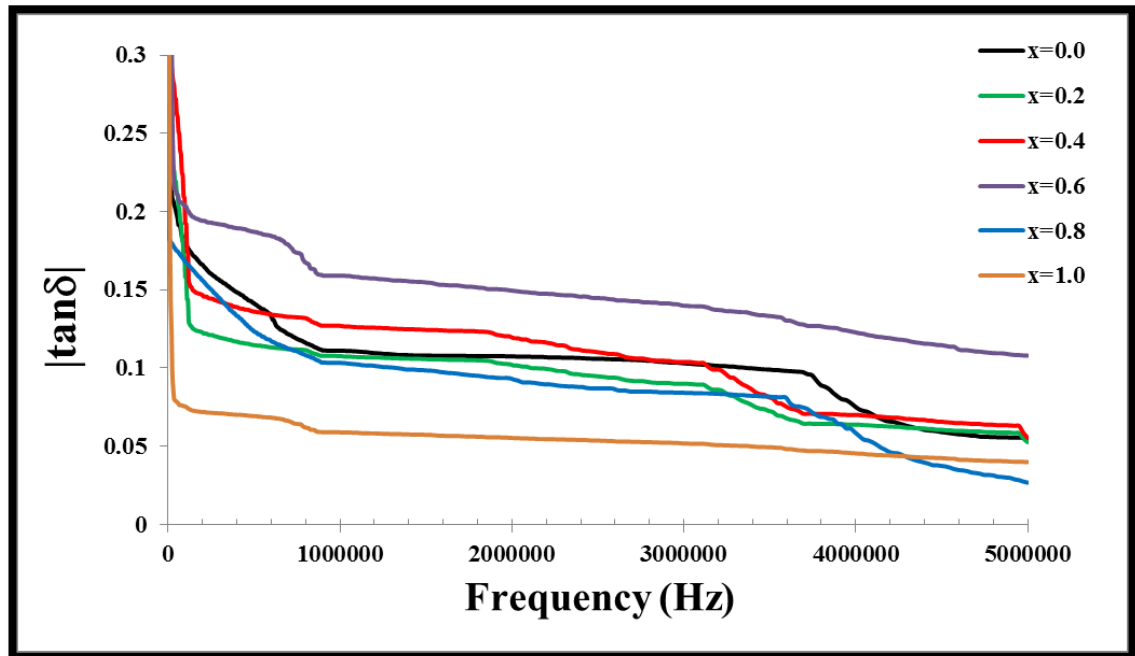


Figure (4-46) :Variation of ($|\tan \delta|$) versus frequency of $TlBa_2Ca_2Cu_{3-x}Ni_xO_{9-\delta}$

Table (4-21): Variation of ($|\tan \delta|$) versus frequency of $TlBa_2Ca_2Cu_{3-x}Ni_xO_{8+\delta}$ with frequency (50HZ-5MHZ)

$TlBa_2Ca_2Cu_{3-x}Ni_xO_{9-\delta}$						
X	$\tan \delta$ At (50 Hz)	$\tan \delta$ At (1MHz)	$\tan \delta$ At (2MHz)	$\tan \delta$ At (3MHz)	$\tan \delta$ At (4MHz)	$\tan \delta$ At (5MHz)
0.0	2.244	0.111	0.107	0.1029	0.0736	0.0540
0.2	0.2432	0.1076	0.1016	0.0899	0.0638	0.0526
0.4	0.3031	0.1269	0.1191	0.1038	0.0699	0.055
0.6	1.562	0.1591	0.1493	0.1398	0.1222	0.1079
0.8	1.177	0.1033	0.0927	0.0841	0.0566	0.0267
1.0	0.5786	0.0589	0.0553	0.0518	0.0452	0.0399

4-4-4-4 Alternating Electrical Conductivity (σ_{ac}):

The Alternating electrical conductivity (σ_{ac}) is measured at room temperature within the frequency (50Hz-5MHz) for $TlBa_2Ca_2Cu_{3-x}Ni_xO_{9.8}$ with $x=0.0,0.2,0.4,0.6,0.8$ and 1 .

The results of the alternating electrical conductivity (σ_{ac}) measurement at room temperature for specimens. Which is showed the figure (4-47) and table (4-22) that (σ_{ac}) increases as the applied frequency increases up to 5MHz.

Increasing in (σ_{ac}) with the applied frequency attributes to the direct relation between (σ_{ac}) and frequency ($\sigma_{ac} = 2\pi f \epsilon_0 \epsilon''$), and as a result of charge carriers polarization. The change in composition in grain boundaries and crystal structure which has an effect on ϵ'' and the loss tangent ($\tan\delta$), subsequently on the (σ_{ac}) values [156].

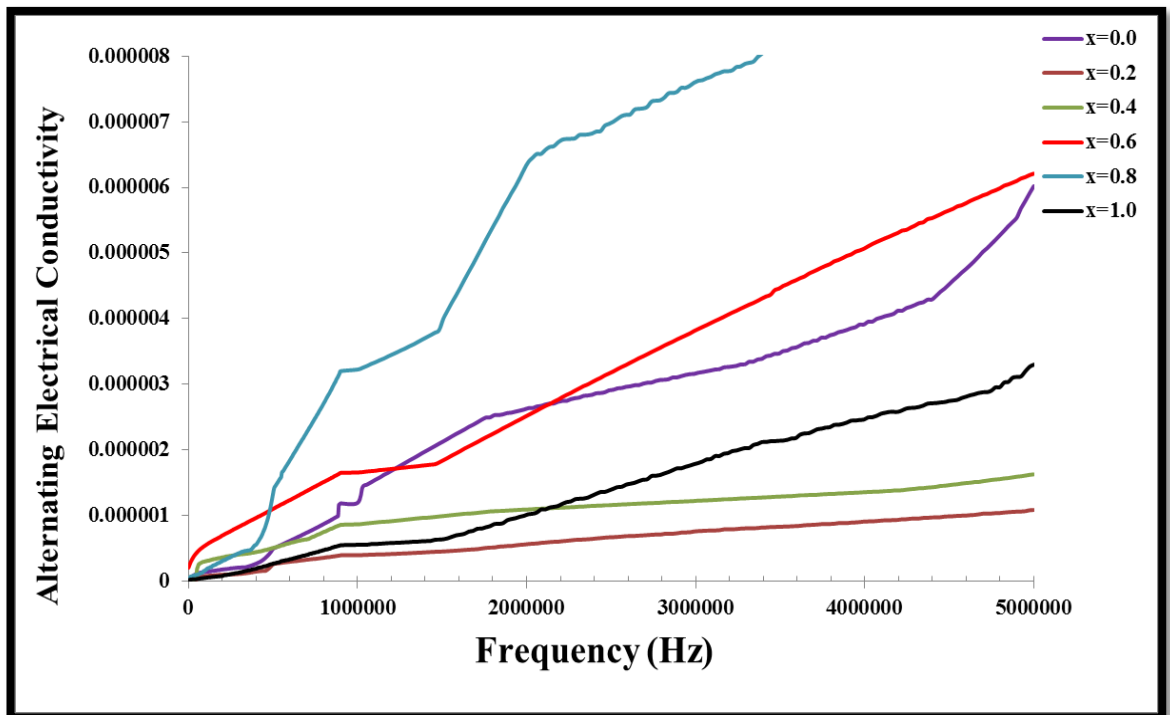


Figure (4-47): Alternating electrical conductivity(σ_{ac}) with frequency for $TlBa_2Ca_2Cu_{3-x}Ni_xO_{9.8}$

Table (4-22): Alternating Electrical Conductivity ($\sigma_{a.c}$) with frequency (50Hz -5MHz).

$TlBa_2Ca_2Cu_{3-x}Ni_xO_{9-\delta}$						
X	$\sigma_{a.c}$	$\sigma_{a.c}$	$\sigma_{a.c}$	$\sigma_{a.c}$	$\sigma_{a.c}$	$\sigma_{a.c}$
	$(\Omega.cm)^{-1}$	$(\Omega.cm)^{-1}$	$(\Omega.cm)^{-1}$	$(\Omega.cm)^{-1}$	$(\Omega.cm)^{-1}$	$(\Omega.cm)^{-1}$
	At (50 Hz)	At (1MHz)	At (2MHz)	At (3MHz)	At (4MHz)	At (5MHz)
0.0	$7.96*10^{-9}$	$1.19*10^{-6}$	$2.64*10^{-7}$	$3.18*10^{-6}$	$3.95*10^{-6}$	$6.02*10^{-6}$
0.2	$2.04*10^{-10}$	$3.98*10^{-7}$	$5.67*10^{-7}$	$7.65*10^{-7}$	$9.12*10^{-7}$	$1.09*10^{-6}$
0.4	$8.14*10^{-10}$	$8.68*10^{-7}$	$1.09*10^{-6}$	$1.23*10^{-6}$	$1.36*10^{-6}$	$1.63*10^{-6}$
0.6	$2.05*10^{-7}$	$1.66*10^{-6}$	$2.53*10^{-6}$	$3.84*10^{-6}$	$5.1*10^{-6}$	$6.21*10^{-6}$
0.8	$1.94*10^{-9}$	$3.226*10^{-6}$	$6.38*10^{-6}$	$7.62*10^{-6}$	$9.703*10^{-6}$	$1.27*10^{-5}$
1.0	$3.86*10^{-7}$	$2.77*10^{-5}$	$5.108*10^{-5}$	$9.004*10^{-5}$	0.0001248	0.00016

4-4-5 Result Of Mechanical Properties:

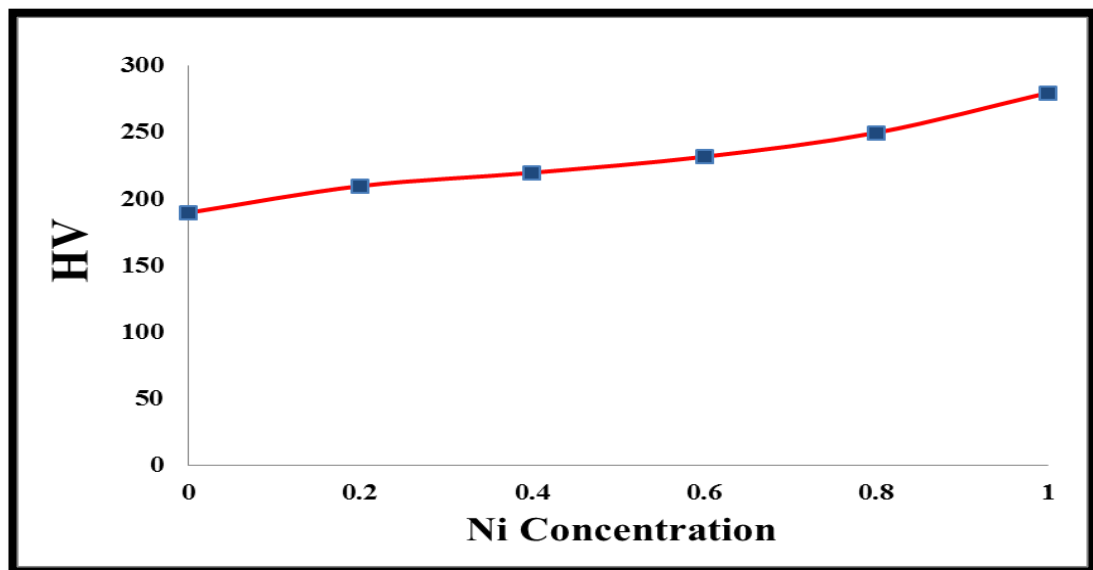
The Vicker's Hardness Number (VHN) for all specimens with nominal composition $TlBa_2Ca_2Cu_{3-x}Ni_xO_{9-\delta}$ with $x=0.0,0.2,0.4,0.6,0.8$ and 1 .

were performed with a digital microhardness at room temperature , all specimen were polished to being tested . The Vickers microhardness Number , Young's modulus (E) and Yield strength (Y) were calculated using equations (3.13) (3.14) and (3.15) respectively are summarized in table (4-23) , figure (4-48) shows the variation of Vickers microhardness Number with Ni concentration , Figure (4-48) shows the Hardness values VHN as function Ni concentration. Hardness value increases with increasing Ni concentration , this means increasing the value(Ni) lead to decreasing brittleness of the specimens. This behavior may be explained by the reduced porosity and good contact between the grains when added the

Ni, or can be attributed to the high phases which cause reinforcement of the bond strength and addition to properties of Ni high hardness causes increase of compound hardness thus increasing in value young modulus and yield strength, Ni ferrite strengthener; increases the hardenability and impact strength of compound, Nickel is a high-density, high-strength metal and high temperature properties.

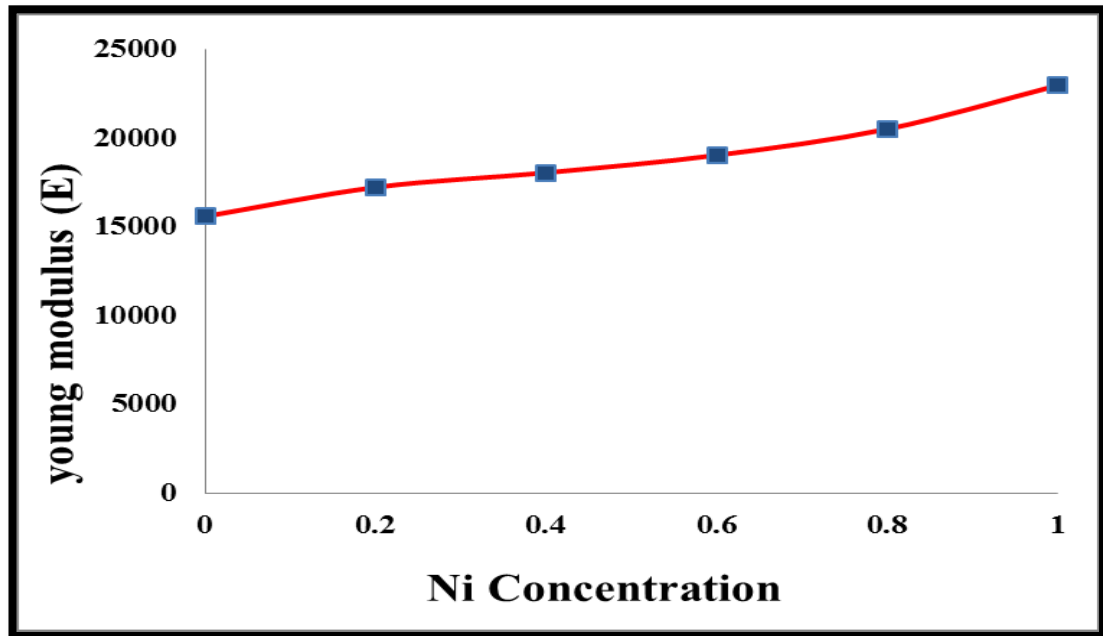
Table (4-23) :Vicker's Hardness Number (VHN) , Young modulus (E) and Yield strength (Y) for $TiBa_2Ca_2Cu_{3-x}Ni_xO_{9+\delta}$ (for 15 sec & load=2.94N)

$TiBa_2Ca_2Cu_{3-x}Ni_xO_{9+\delta}$					
x	Tim/ sec	Load N	Hv	E(MPa)	Y(MPa)
0.0	15	2.94	190	15572.4	63.33333
0.2	15	2.94	210	17211.6	70
0.4	15	2.94	220	18031.2	73.3333
0.6	15	2.94	232	19014.72	77.3333
0.8	15	2.94	250	20490	83.3333
1.0	15	2.94	280	22948.8	93.3333

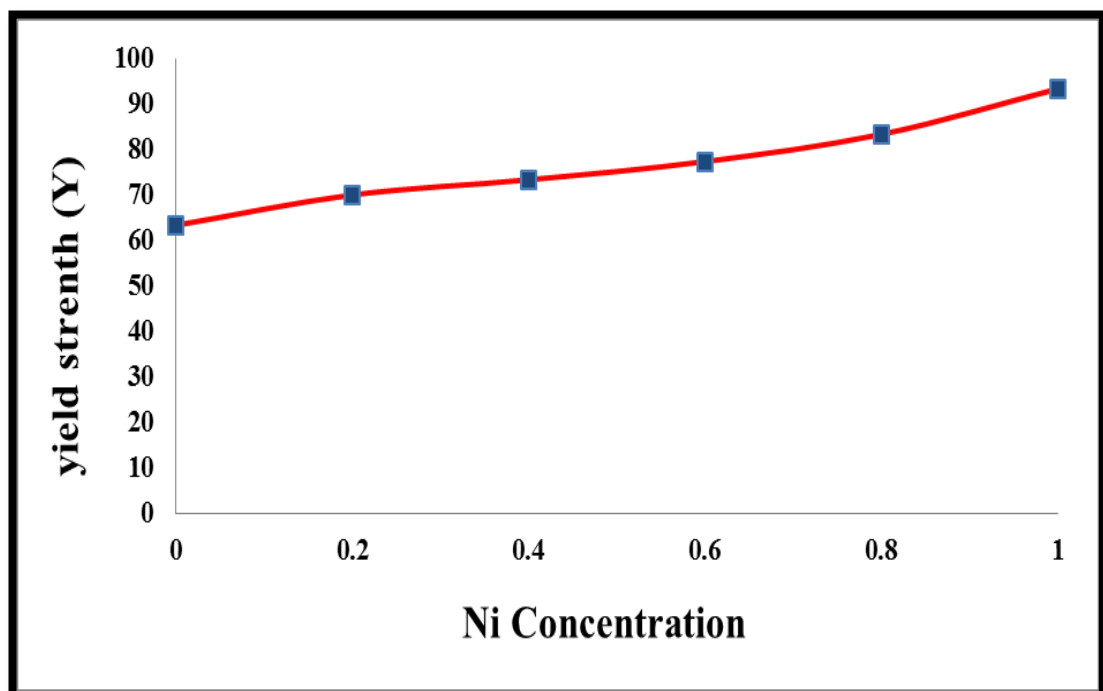


Figure(4-48) :The variations of Vicker's Hardness Hv as a function Ni concentration .

Figures of (4-49) and (4-50) shown the result obtained for Young's modulus (E) and Yield strength (Y) versus Ni concentration.



*Figure(4-49): The variations of young modulus E
a function Ni concentration .*



*Figure(4-50) :The variations of yield strength Y
a function Ni concentration .*

4-2-6 Results of Atomic Forces Microscopic AFM:

Analyzing the surface of these systems was made using atomic force microscopy (AFM) it give information about the surface [145]. The images taken in this research of composition $TlBa_2Ca_2Cu_{3-x}Ni_xO_{9.8}$ with $x=0.0,0.2,0.4,0.6,0.8$ and 1 .

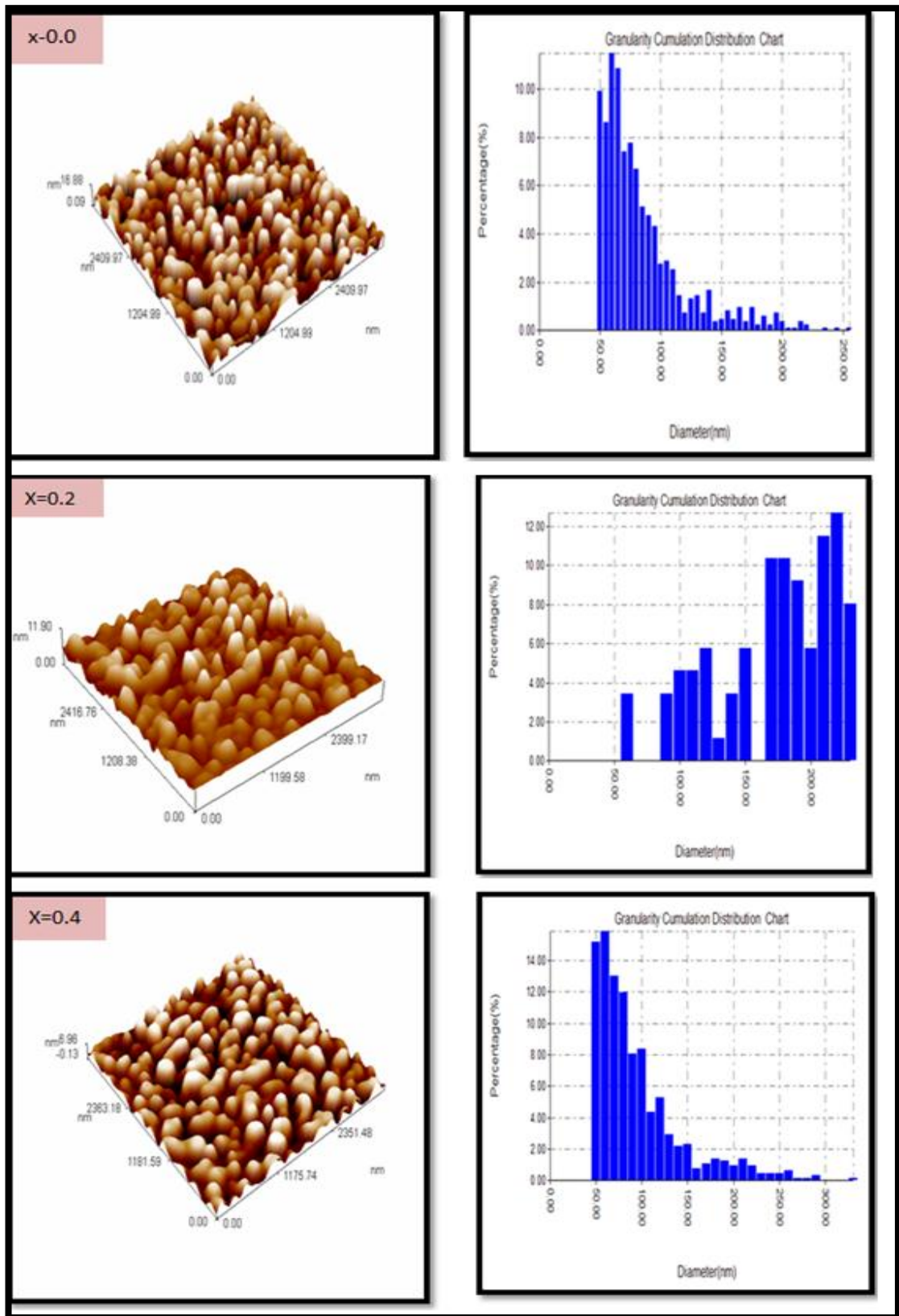
It is found that for the various Ni concentration lead to various Roughness(nm) ,Root mean square(nm) and Avg. Diameter(nm) this is agreement with researchers [34,35]shown in figure (4-51) AFM images. Table (4-24) shows the values of Average particle size, surface roughness, and square root for mean roughness of the specimens which indicate that the surface of the some specimens has a good crystalline uniformity and high homogeneity[34].

The morphology of specimens suggests that specimens grow in a columnar fashion . the roughness of these specimens was of the order (4.26-0.74) clearly seen that the specimens roughness surface decreases with increase Ni concentration.

Nano- and microroughness are formed by fluctuations in the surface of short wavelengths, characterized by hills (asperities) (local maxima) and valleys (local minima) of varying amplitudes and spacing's. Surface roughness most commonly refers to the variations in the height of the surface relative to a reference plane. It is measured either along a single line profile or along a set of parallel line profiles.[146]

AFM techniques were chosen to give information about surface structure in different surface spatial wavelength regions as well as to measure surfaces of different roughness[147].

Figure (4-51) :Reveals the (3-D) AFM images and the chart distribution of $TlBa_2Ca_2Cu_{3-x}Ni_xO_{9-\delta}$



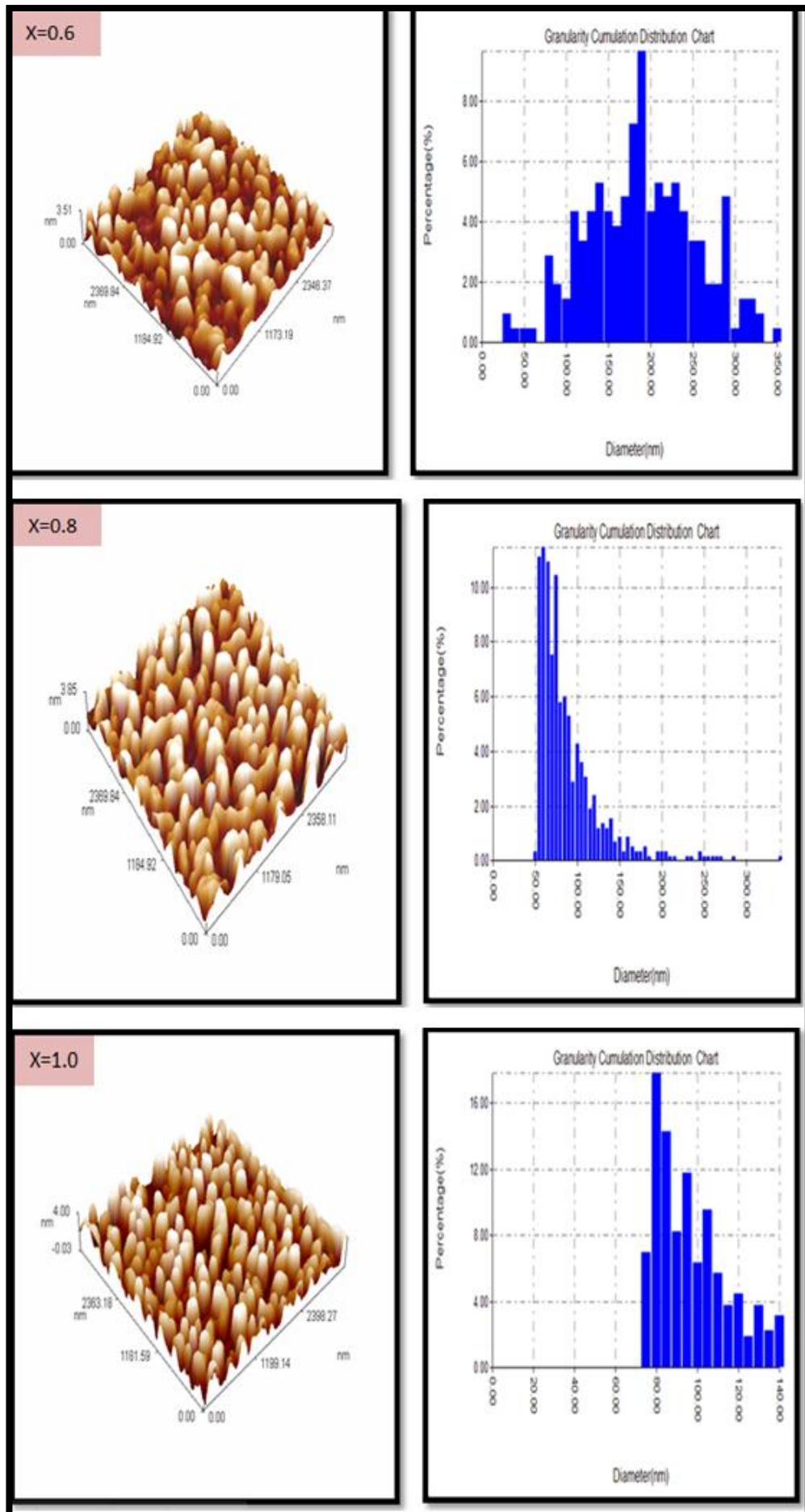


Table (4-24): Values of average surface roughness ,Crystal size and Avg. Diameter in 2D for $TlBa_2Ca_2Cu_{3-x}Ni_xO_{9-\delta}$

x	Crystallite size(nm)	Roughness (nm)	Root mean square(nm)	Avg. Diameter(nm)
0	19.87377	4.26	4.9	185.08
0.2	10.37594	1.46	1.83	89.84
0.4	15.56031	1.83	2.1	167.21
0.6	4.731678	0.743	0.868	81.86
0.8	24.44281	0.935	1.08	86.54
1.0	21.29885	0.935	1.09	94.95

4 -5 Compound of $Tl_{0.5}Pb_{0.5}Ba_2Ca_2Cu_{3-x}Ni_xO_{9-\delta}$:

High critical temperature superconducting (HTS) was synthesized by solid state reaction process, Using the required amounts of pure powders materials high purity oxides, and in Commensurate with the molecular weights, accordingly for these chemical formulas:



4-5-1 Study of Structural Properties :

The structural study performed by X-ray diffraction (XRD). We analyzed nominal composition $Tl_{0.5}Pb_{0.5}Ba_2Ca_2Cu_{3-x}Ni_xO_{9-\delta}$ ($x=(0.0,0.2,0.4,0.6,0.8, 1.0$ and $Pb=0.5$)).The XRD patterns of all the specimens confirmed the specimens are pure Tl-1223. the main phase correspond in all specimens to the Tl-1223 phase, but some minor phases

can be identified, Tl-1212 phase and Tl-1201 phase and appears small amounts of impurities. The Structural properties that studied by using X-ray powder pattern, the phase high temperature superconductor (Tl-1223) have been the tetragonal structure with space group P4/mmm didn't change with the partial substitution of Pb and Ni.

The appearance of different phases in the pure specimen in particular and the rest of the specimens in general is due to the displacement of defects of the atomic or oxygen deficiency or irregularity of positive ions, which lead to the accumulation of defects in the stack along the axis (c), which ultimately lead to deformation of crystalline structure [131,132].

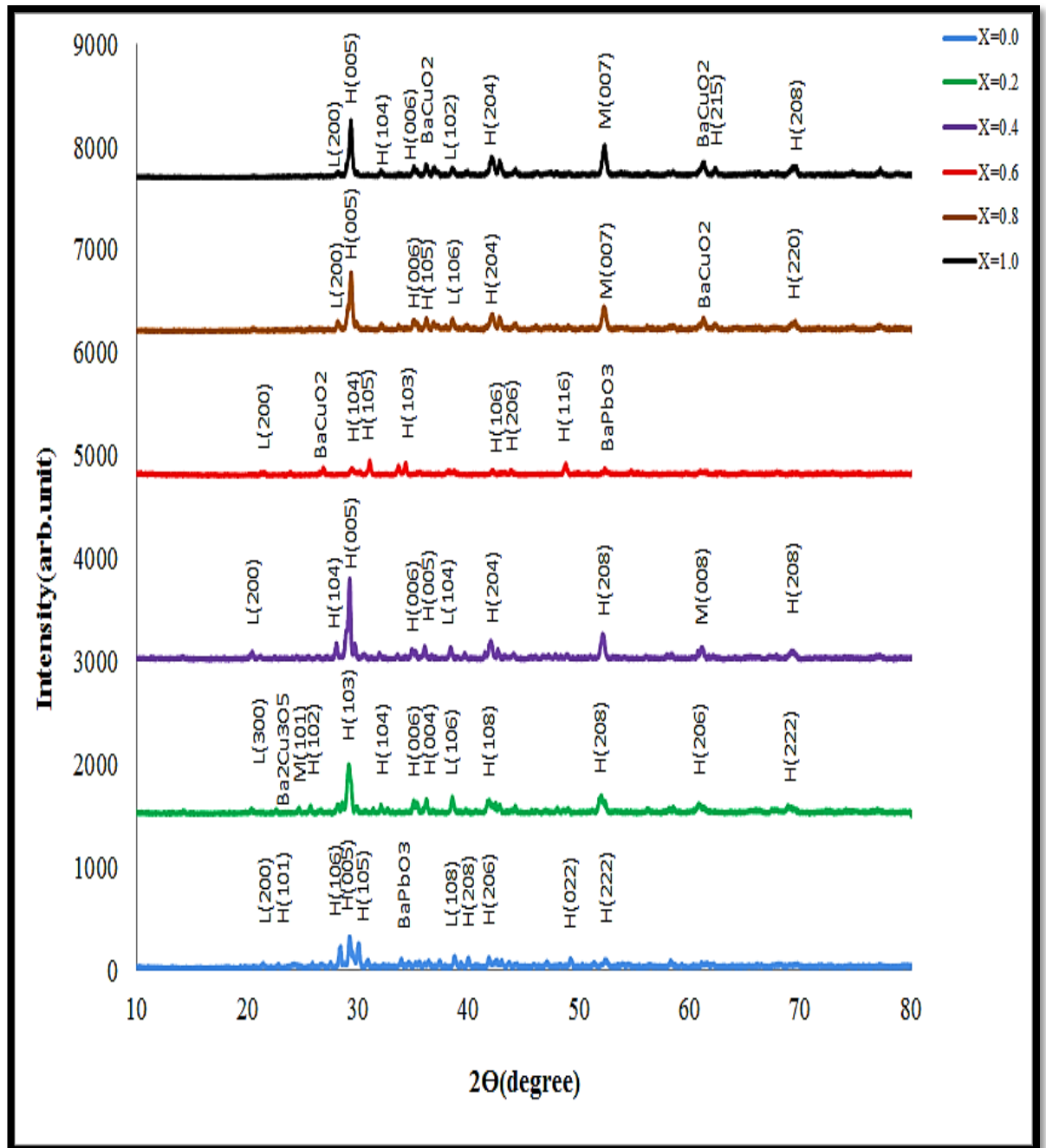


Figure (4-52) :XRD pattern of $Tl_{0.5}Pb_{0.5}Ba_2Ca_2Cu_{3-x}Ni_xO_{9.8}$

XRD data shows various crystalline phases will occur, Figure (4-52) depicts XRD pattern of all specimens indicating that lead and nickel addition promotes the growth of Tl-1223 high. It can be seen from figure(4-52) that there is a slight shift in peak positions to higher 2θ values with the increase of Ni content and the patterns of x-ray diffraction for the free specimen gave increase in the intensity and enhancement of the peaks

due to the high - T_C - phase, which is most probably due to the increase in the c-axis length of the unit cell. The overall contraction of the unit cell can be seen from the decrease of c axis with increase the Ni content. It was noted also that an increase in the peaks intensity for the doped specimen in comparison with that of the pure specimens.

Have been estimated the lattice parameters using d values and (hkl) reflections of the observed X-ray diffraction pattern through the software program based on Cohen's least square method [157,135]. The peaks were agreement with ASTM Card number (042-0351,042-0352,084-1826,079-1839). [2012 international center for Diffraction Data].

The parameters a , b , c , density d_m , and volume fraction (V_{phase}) are shown in Table (4-25).

The dimensions of unit cell were calculated from check cell. The unit cell parameters change significantly. According to the XRD measurements, Ni addition increasing the lattice c parameter from 15.2769 \AA ($x=0.0$) to 15.811 \AA ($x=0.4$).

The change in (c) axis can be due to many causes, the first was the increment in (O_2) concentration that resulted from substitution of Pb^{+2} instead on Hg^{+2} and (Ni^{+2}) replacement instead of (Cu^{+2}) and this increment will Cu layers which cause a stronger link because of the (Ni^{+2}) valence that lead to increase ion bonding forces formed in the (Tl) layers and thus increase the lattice parameter c , increase ($a=b$), the rate c/a change with (Ni) and ($Pb=0.5$) concentration as shown in table(4-25).

Table(4-25): Lattice parameters and volume fraction of $Tl_{0.5}Pb_{0.5}Ba_2Ca_2Cu_{3-x}Ni_xO_{9.8}$ compounds

X	a=b (Å)	c (Å)	c/a ratio	v(Å) ³	dm(gm/cm ³)	V _{ph(1223)} %	V _{ph(1212)} %	V _{ph(1201)} %	V _{p impurities} %
0	3.8135	15.2769	4.006005	222.1686	7.454971	74.9457	10.5206	8.7852	5.6399
0.2	3.7326	15.3323	4.107673	213.6142	7.745964	77.5539	11.8944	8.1534	8.4412
0.4	3.8379	15.811	4.119701	232.8878	7.097994	83.8009	10.1357	5.8823	9.0497
0.6	3.8299	15.5589	4.062482	228.22	7.236103	72.619	16.522	5.114	5.743
0.8	3.838	15.7034	4.091558	231.3149	7.132317	76.0471	11.0852	9.07441	10.3266
1	3.8221	15.409	4.031553	225.1016	7.322022	70.1117	8.8427	7.9448	8.7825

The change of (a=b), c lattice parameter effect on the V volume of the unit cell and then reason variation of the density. It can be seen in Figure (4-52) that the peak intensities of $Tl_{0.5}Pb_{0.5}Ba_2Ca_2Cu_{3-x}Ni_xO_{9.8}$ increase when the Ni concentration increased and increase of the a=b and c lattice parameters for Ni substitution specimens as comparable with the Ni-free specimen. The reason for that can be attributed to the decomposition of $Tl_{0.5}Pb_{0.5}Ba_2Ca_2Cu_{3-x}Ni_xO_{9.8}$ by inserting Cu-O layer in it to produce Tl-1223 phase.

Figure (4-53) show an increase of the volume fraction (V_{ph}) up x=0.4 then decrement when increase Ni and Figure (4-54) show an increase of the c/a, while Figure (4-55) shows a decrease of the mass density (dm) with incrementing Ni concentration for different compositions of $Tl_{0.5}Pb_{0.5}Ba_2Ca_2Cu_{3-x}Ni_xO_{9.8}$, the reason is the substitution of Pb^{+2} (133 pm) for Tl^{+3} (102.5 pm) where the ionic radius of Pb^{+2} is greater than that of Tl^{+3} , and Ni for Cu where the ionic radius of Ni^{+2} (83 pm) is smaller than

that of Cu^{+2} (87pm), which changes the c-parameter and produces a deformation on the structures.

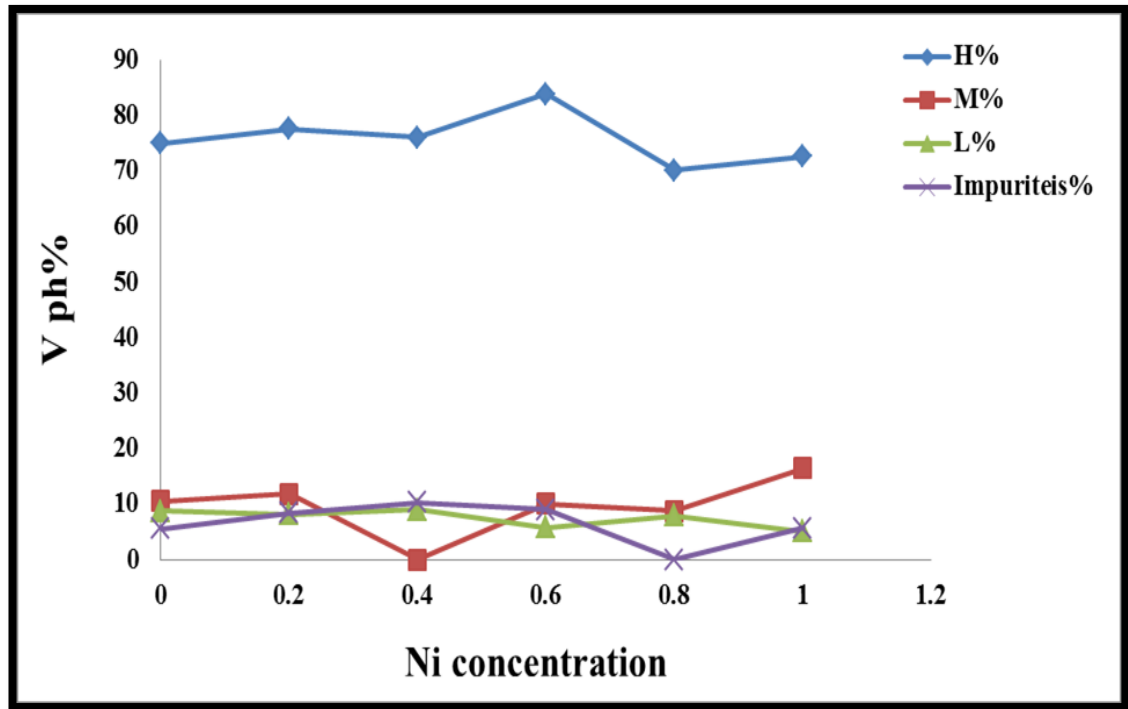


Figure (4-53) The ratio of volume fraction V_{ph} as function of Ni concentration for the $\text{Tl}_{0.5}\text{Pb}_{0.5}\text{Ba}_2\text{Ca}_2\text{Cu}_{3-x}\text{Ni}_x\text{O}_{9.8}$ specimens

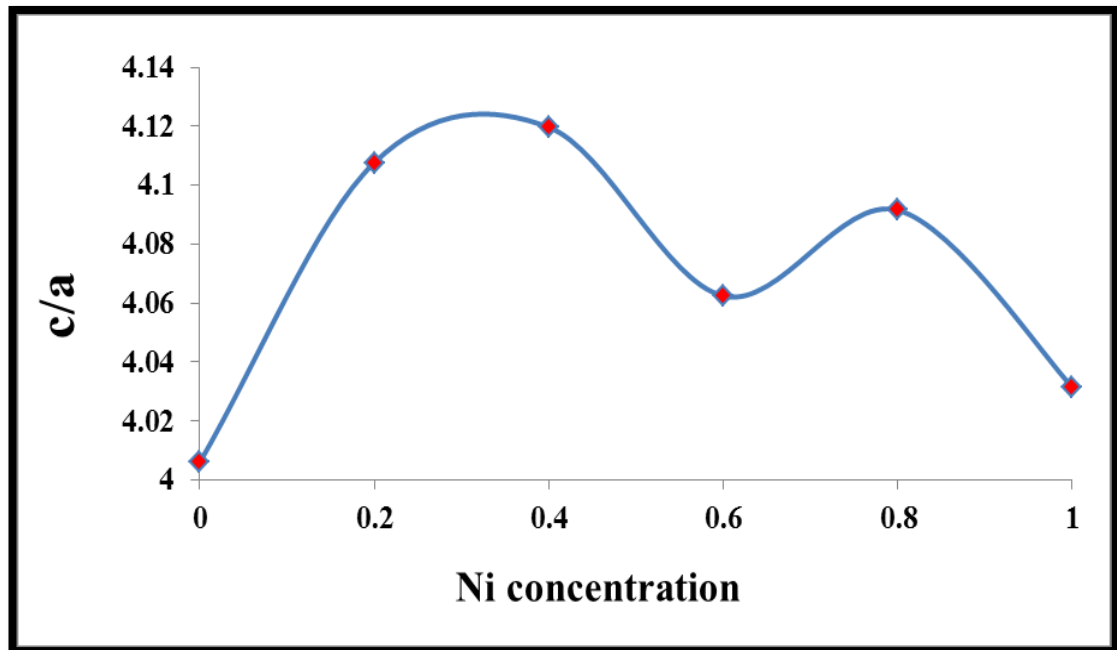


Figure (4-54) :The ratio of lattice parameters c/a as function of Ni concentration for the $\text{Tl}_{0.5}\text{Pb}_{0.5}\text{Ba}_2\text{Ca}_2\text{Cu}_{3-x}\text{Ni}_x\text{O}_{9.8}$ specimens

We observed from the table(4-25) a decrease in the values of density and this because the increase Ni concentration causes defects in the crystalline structure and therefore the occurrence of voids, which increases the porosity and thus less density this shown in figure(4-55)

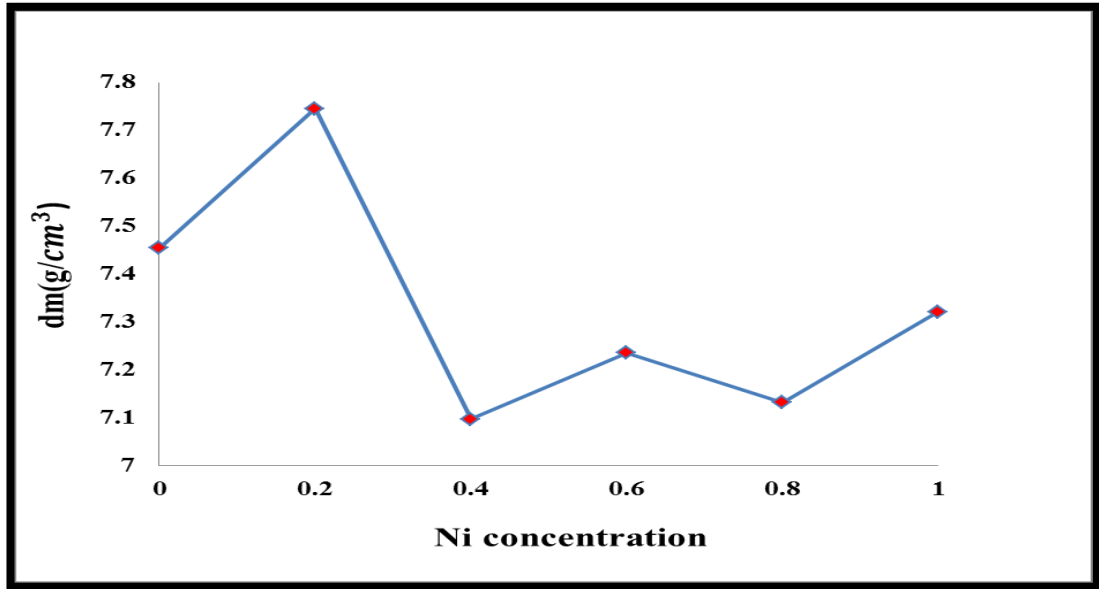


Figure (4-55) : Variation density with Ni concentration for the $\text{Tl}_{0.5}\text{Pb}_{0.5}\text{Ba}_2\text{Ca}_2\text{Cu}_{3-x}\text{Ni}_x\text{O}_{9.8}$ specimens

4-5-2 Study of Electrical Resistivity:

The variation of resistance with temperature of the as synthesized $\text{Tl}_{0.5}\text{Pb}_{0.5}\text{Ba}_2\text{Ca}_2\text{Cu}_{3-x}\text{Ni}_x\text{O}_{9.8}$ HTSC specimens was measured by the four-probe technique. All specimens are prepared without oxygen treatments. The normal state resistance of all the specimens shows metal-like behavior with respect to temperature. A plot of the normalized resistivity vs. temperature ($\rho-T$) behavior of specimens with various Ni concentrations are shown in Figure (4-56). The values of critical transition temperature T_c for the $\text{Tl}_{0.5}\text{Pb}_{0.5}\text{Ba}_2\text{Ca}_2\text{Cu}_3\text{O}_{9.8}$, $\text{Tl}_{0.5}\text{Pb}_{0.5}\text{Ba}_2\text{Ca}_2\text{Cu}_{2.8}\text{Ni}_{0.2}\text{O}_{9.8}$, $\text{Tl}_{0.5}\text{Pb}_{0.5}\text{Ba}_2\text{Ca}_2\text{Cu}_{2.6}\text{Ni}_{0.4}\text{O}_{9.8}$ phases are 118.5, 119.5 and 139 K, respectively. Transition temperature (T_c) increases with increment Ni concentration up $x=0.4$ and then decrement $\text{Tl}_{0.5}\text{Pb}_{0.5}\text{Ba}_2\text{Ca}_2\text{Cu}_{2.4}\text{Ni}_{0.6}\text{O}_{9.8}$

, $Tl_{0.5}Pb_{0.5}Ba_2Ca_2Cu_{2.2}Ni_{0.8}O_{9-\delta}$, $Tl_{0.5}Pb_{0.5}Ba_2Ca_2Cu_2Ni_{1.0}O_{9-\delta}$ phases are 128.5, 133.5 and 129 K, respectively .We noted the optimum value of transition temperature T_c is 140 K for (x=0.4) specimen the reason due to that the increase of the Cu-O plane which leads to increase the holes in the structures thus enhanced the transition temperature. A small width in the superconducting transition of this specimens indicates that mainly, the small width(ΔT_C) in the transition indicates that a very small admixture of some other phases exists. Also small differences observed in these data and this may be due to an electronic problem in the experiment. ΔT_C , T_c , E_g and δ shown in table (4-26):

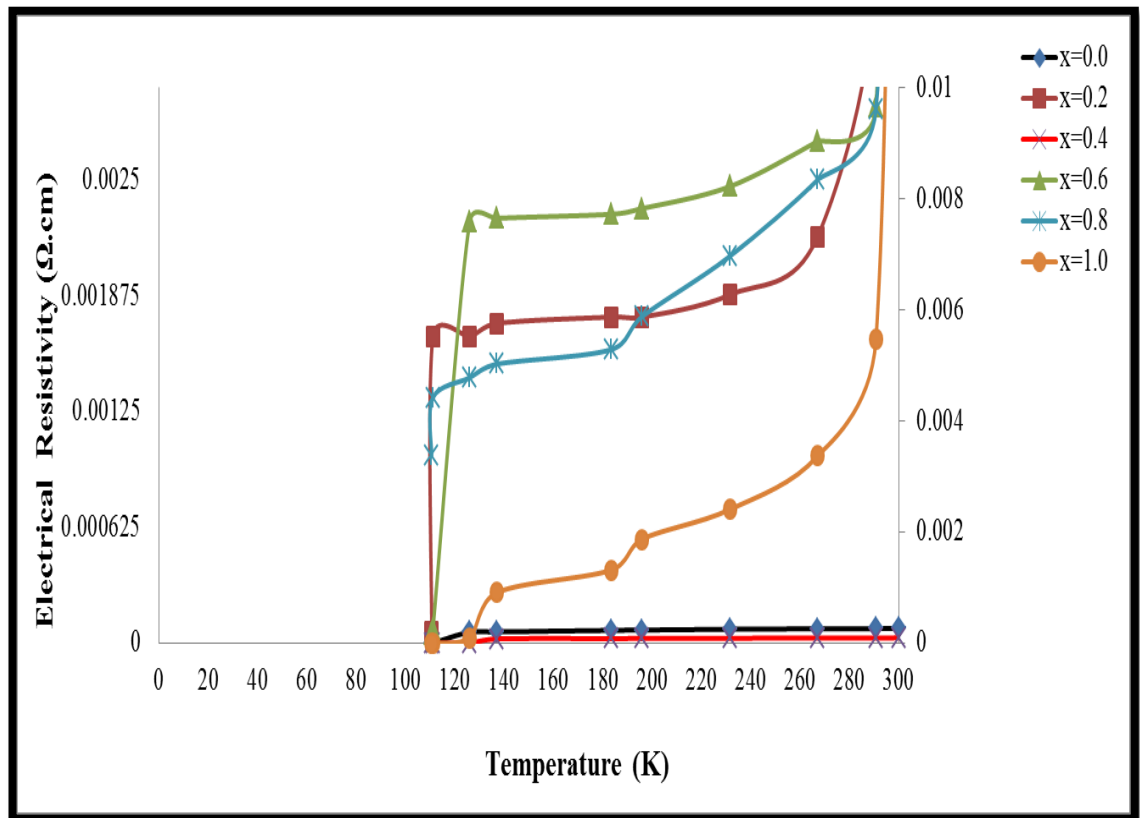


Figure (4-56) :The resistivity as function of temperature for $Tl_{0.5}Pb_{0.5}Ba_2Ca_2Cu_{3-x}Ni_xO_{9-\delta}$ specimens for $x=0.0$, $0.2,0.4,0.6,0.8$ and 1.0

Table(4-26) :volume fraction , E_g , δ and transition temperature of $Tl_{0.5}Pb_{0.5}Ba_2Ca_2Cu_{3-x}Ni_xO_{9-\delta}$ compounds

X	V ph (1223)%	V ph (1212)%	V ph (1201)%	Vph impurities %	$T_{c(off)}$ (K)	$T_{c(on)}$ (K)	ΔT_c (K)	$T_{c(mid)}$ (K)	E_g (eV)	δ
0	74.9457	10.5206	8.7852	5.6399	114	124	10	119	0.0361	0.06190
0.2	77.5539	11.8944	8.1534	8.4412	115	125	10	120	0.0365	0.0659
0.4	83.8009	10.1357	5.8823	9.0497	137	144	7	140	0.0425	0.2325
0.6	72.619	16.522	5.114	5.743	127.5	130.5	3	129	0.0392	0.0913
0.8	76.0471	11.0852	9.07441	10.3266	132	135	3	133.5	0.0406	0.1116
1	70.1117	8.8427	7.9448	8.7825	122	130	8	126	0.0383	0.1258

It was found that the hole concentration was increased with Ni concentration increment and oxygen content δ and Pb-substitution in (Hg) causes the increase of some degrees in the transition temperature T_c .

The existence of an energy gap is always related to the binding energy of the fermions pairs. In this case, the energy gap is always temperature-dependent. At $T = 0$ K, the energy gap parameter Δ has a maximum value because all Cooper pairs are in the ground state.

Figure (4-57) and (4-58) show the variation of $T_{c_{off\ set}}$ and E_g as function of Ni concentration. It noticed the values of $T_{c_{off\ set}}$ increasing with increase of Ni up $x=0.4$ then decrease. Also, fig (4-58) shown changing in E_g values with increasing Ni concentration.

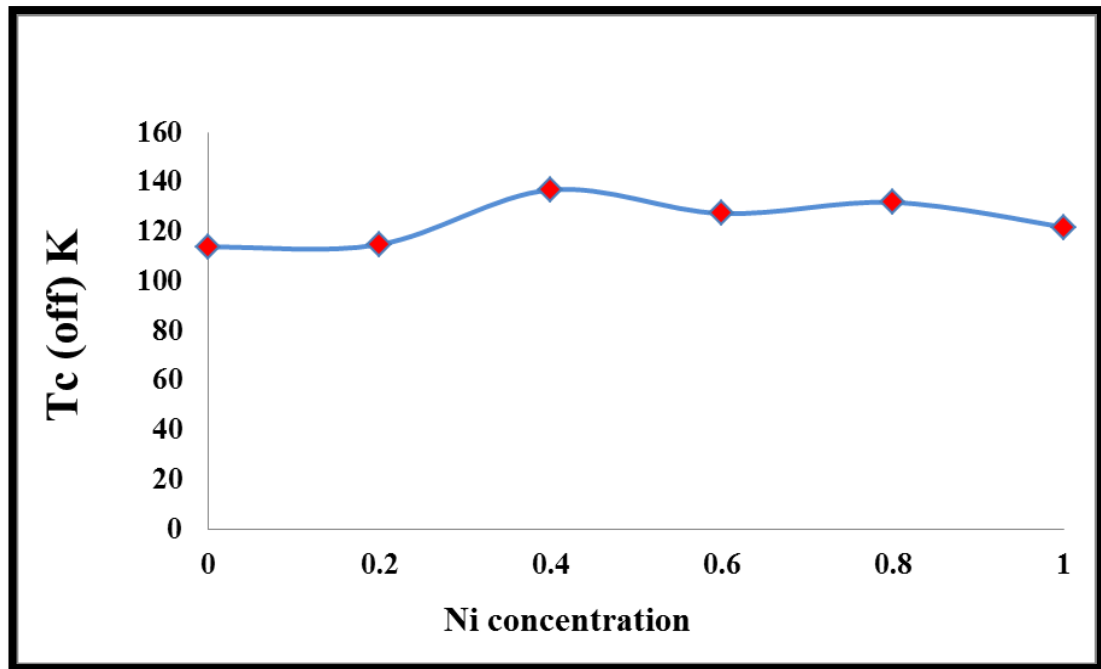


Figure (4-57): $T_{c(\text{offset})}$ a function of concentration Ni of $\text{Tl}_{0.5}\text{Pb}_{0.5}\text{Ba}_2\text{Ca}_2\text{Cu}_{3-x}\text{Ni}_x\text{O}_{9-\delta}$ specimens

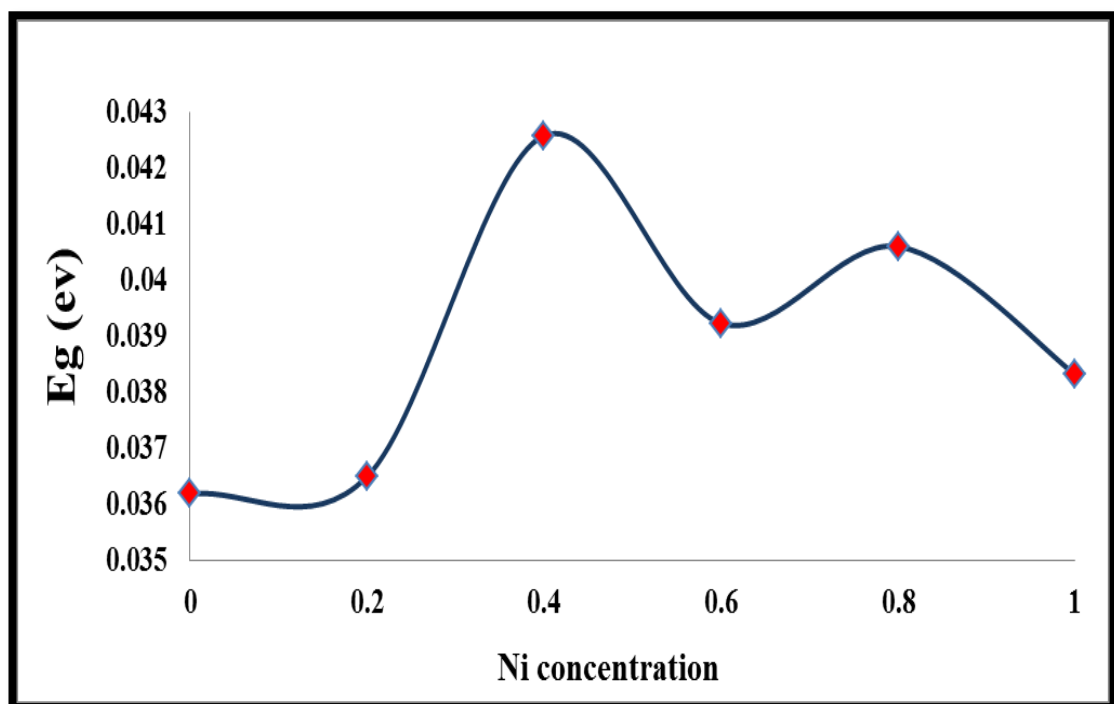


Figure (4-58) : E_g (eV) a function of concentration Ni of $\text{Tl}_{0.5}\text{Pb}_{0.5}\text{Ba}_2\text{Ca}_2\text{Cu}_{3-x}\text{Ni}_x\text{O}_{9-\delta}$ specimens

4-5-3 Results Of Oxygen Content:

The values of oxygen content (δ) which is the excess concentration of oxygen in the prepared specimens was found by the iodometric titration method .

Table (4-26) and figurer (4-59) show the values of critical temperature T_c related to δ for all specimens .

It is observed from this Table(4-26) that T_c increases as δ increases because the presence of excess oxygen atoms in the CuO_2 layers will create more holes in the perovskite layers and this creation of the holes in the CuO_2 sheet will shorten the Cu-O bond length and tend to improve the transition temperature .

Similar behavior of δ with transition temperature was found by Zhao et.al[138].

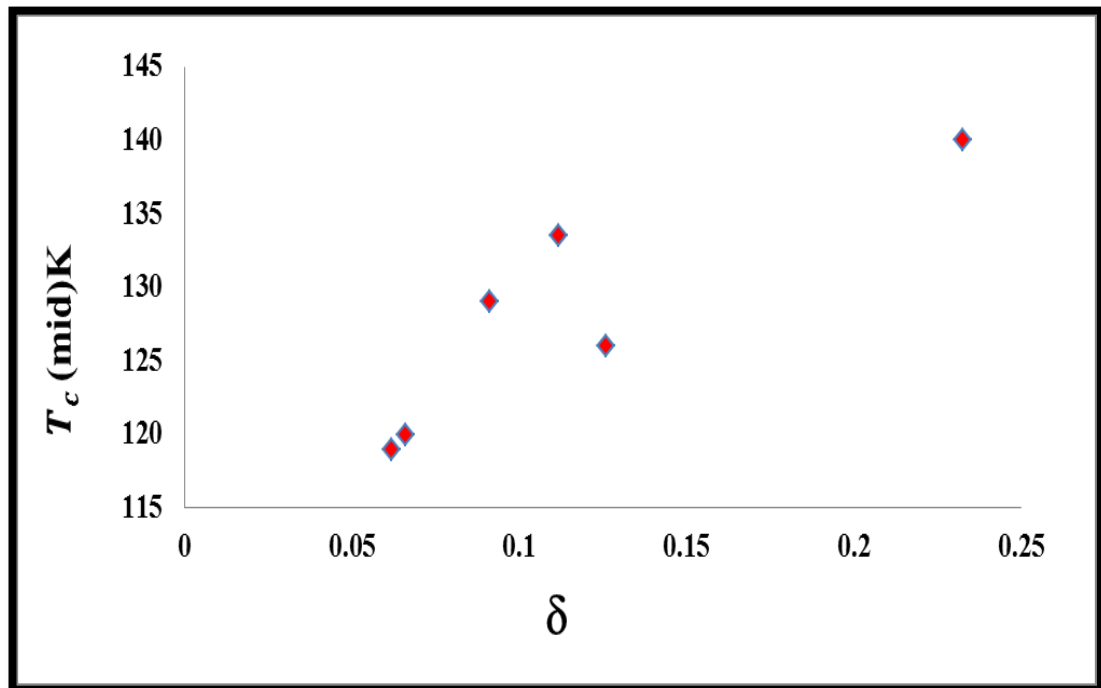


Figure (4-59): Oxygen content as a function of T_c (mid)of $\text{Tl}_{0.5}\text{Pb}_{0.5}\text{Ba}_2\text{Ca}_2\text{Cu}_{3-x}\text{Ni}_x\text{O}_{9-\delta}$ specimens

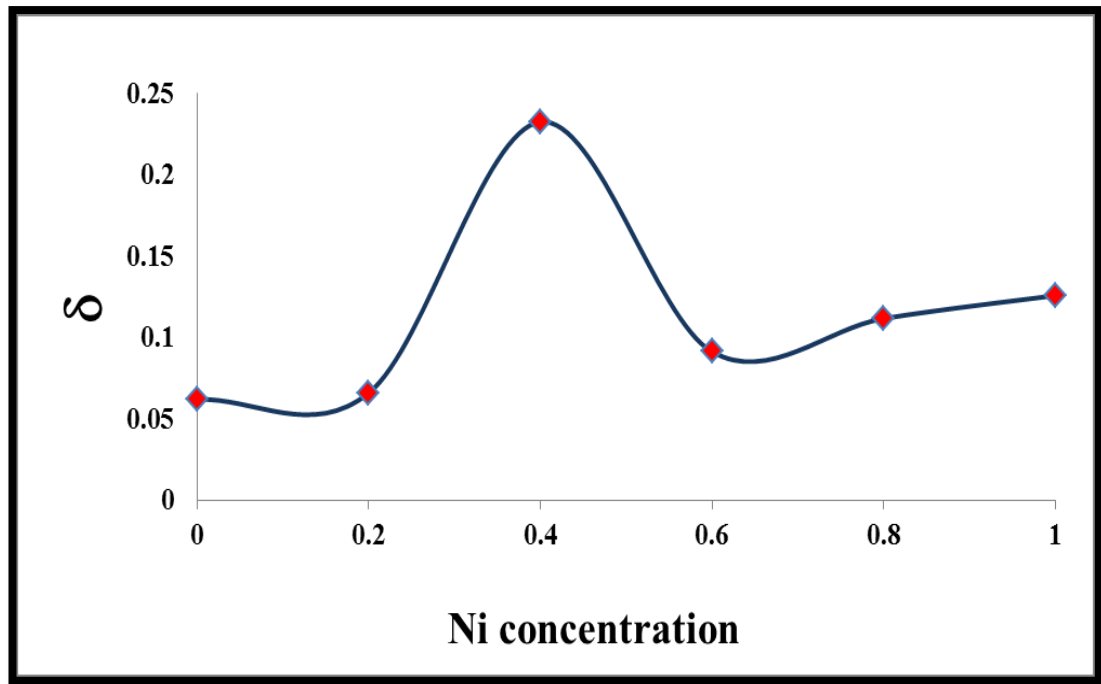
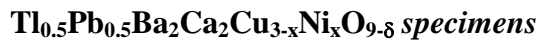


Figure (4-60): Oxygen content as a function of concentration Ni



4-5-4 Study of Dielectric Properties :

The dielectric properties such as dielectric constant (ϵ'), dielectric loss factor (ϵ'') and alternating electric conductivity (σ_{ac}) were measured at room temperature at the frequency (50Hz - 5MHz) for high superconductor compounds $\text{Tl}_{0.5}\text{Pb}_{0.5}\text{Ba}_2\text{Ca}_2\text{Cu}_{3-x}\text{Ni}_x\text{O}_{9.8}$ with $x=0.0,0.2,0.4,0.6,0.8,1.0$ and $\text{Pb}=0.5$ which are prepared by a solid state reaction. The results are discussed as a function of frequency.

4-5-4-1 Dielectric Constant (ϵ')

The behavior of the dielectric constant is measured at room temperature within the frequency (50Hz-5MHz) measured for $\text{Tl}_{0.5}\text{Pb}_{0.5}\text{Ba}_2\text{Ca}_2\text{Cu}_{3-x}\text{Ni}_x\text{O}_{9.8}$ with $x=0.0,0.2,0.4,0.6,0.8,1.0$ and $\text{Pb}=0.5$.

We observe from figure (4- 61)) and table (4-27) that the value of the dielectric constant decreases with frequency increase and starts to stabilize on the whole after frequency (10KHz). The values of the dielectric constant

become almost constant after this frequency for most models. This behavior can be explained by the frequency constant in low frequency, ($f < 10\text{kHz}$), There are four mechanics of polarization [158, 159] that is, the dielectric constant is at its highest value at low frequencies and with increasing frequency, the polarization effect from the vacuum charge (polarization interlayer) will begin to decay [160, 161] with increased frequency.

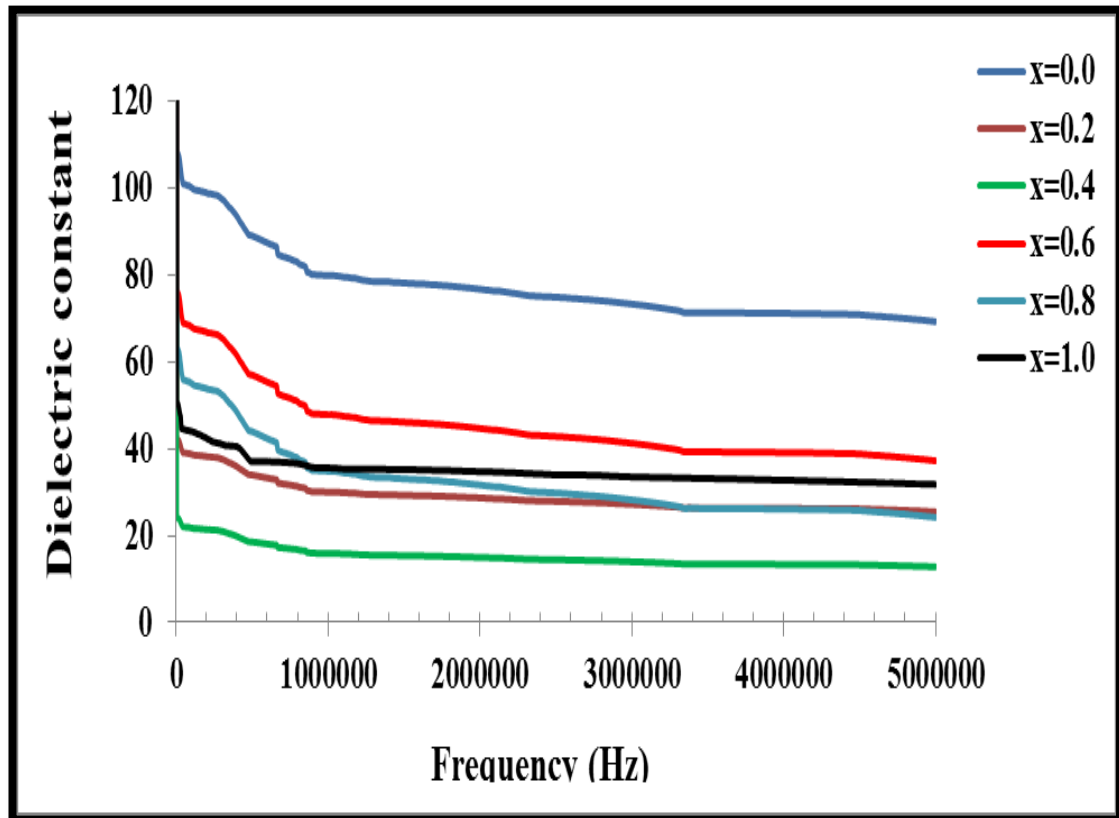


Figure (4-61): Dielectric constant(ϵ) with frequency of $\text{Tl}_{0.5}\text{Pb}_{0.5}\text{Ba}_2\text{Ca}_2\text{Cu}_{3-x}\text{Ni}_x\text{O}_{9-\delta}$ specimens

Table (4-27): Dielectric constant value (ϵ') with the change of the amount of material replaced when frequency (50Hz -5MHz).

$Tl_{0.5}Pb_{0.5}Ba_2Ca_2Cu_{3-x}Ni_xO_{9-\delta}$						
X	ϵ' At (50 Hz)	ϵ' At (1MHz)	ϵ' At (2MHz)	ϵ' At (3MHz)	ϵ' At (4MHz)	ϵ' At (5MHz)
0.0	744.177	73.979	72.607	70.935	69.860	35.380
0.2	1859.92	69.780	66.590	63.165	61.060	59.186
0.4	4318.86	14.794	14.755	14.560	13.831	9.890
0.6	506.44	37.141	36.360	35.908	35.477	35.277
0.8	618.89	82.565	81.960	81.861	81.727	81.330
1.0	301.379	7.11	6.938	6.692	6.538	6.348

In Table (4-27), which gives the values of the dielectric constant at (50Hz-5MHz) for $Tl_{0.5}Pb_{0.5}Ba_2Ca_2Cu_{3-x}Ni_xO_{9-\delta}$ specimens, we observe that the values of the dielectric constant are decrease for the compounds containing nickel. This is because the addition of Ni, Leading to increase of the vacuum charge and ion mobility. This results in an improvement in the electrical properties, such as an increase in high residual polarization and a low leakage current[162].

On the other hand the specimen when (x=0.8) showed an increase in the values of dielectric constant compared to the pure specimen at frequencies(1,2,3,4,5 MHz) this the best specimen through this examination (LCR) meter.

4-5-4-2 Dielectric Loss Factor (Imaginary Part ϵ''):

The behavior of the dielectric loss factor (ϵ'') is measured at room temperature within the frequency (50Hz-5MHz) that is measured for **Tl_{0.5}Pb_{0.5}Ba₂Ca₂Cu_{3-x}Ni_xO_{9.8}** with **x=0.0,0.2,0.4,0.6,0.8 ,1.0 and Pb=0.5**.

Explain figure (4-62) and table (4 - 28) change the dielectric Loss Factor (ϵ'') with the change of frequency and measured at room temperature. We note through these form in general that dielectric Loss Factor the of residual loss decreases with frequency crease and explains this behavior according to equation of (ϵ'') is dependent on its frequency value, ie, increasing the frequency leads to a decrease in the value of dielectric Loss Factor (ϵ'').

In this table, we observe that the values of the loss factor are generally increased with increase Ni concentration At frequencies(1,2,3,4,5 MHz), While we notice a decrease in i value of dielectric Loss Factor (ϵ'') with increasing of Ni concentration at the frequency (50Hz).

The increase and decrease in the values of (ϵ'') with the change in the values of Ni ,Pb concentration is due to the increase and decrease in the values of the alternating electrical conductivity ($\sigma_{a.c}$) have a positive relationship with alternating electrical conductivity according to equation (3-12).

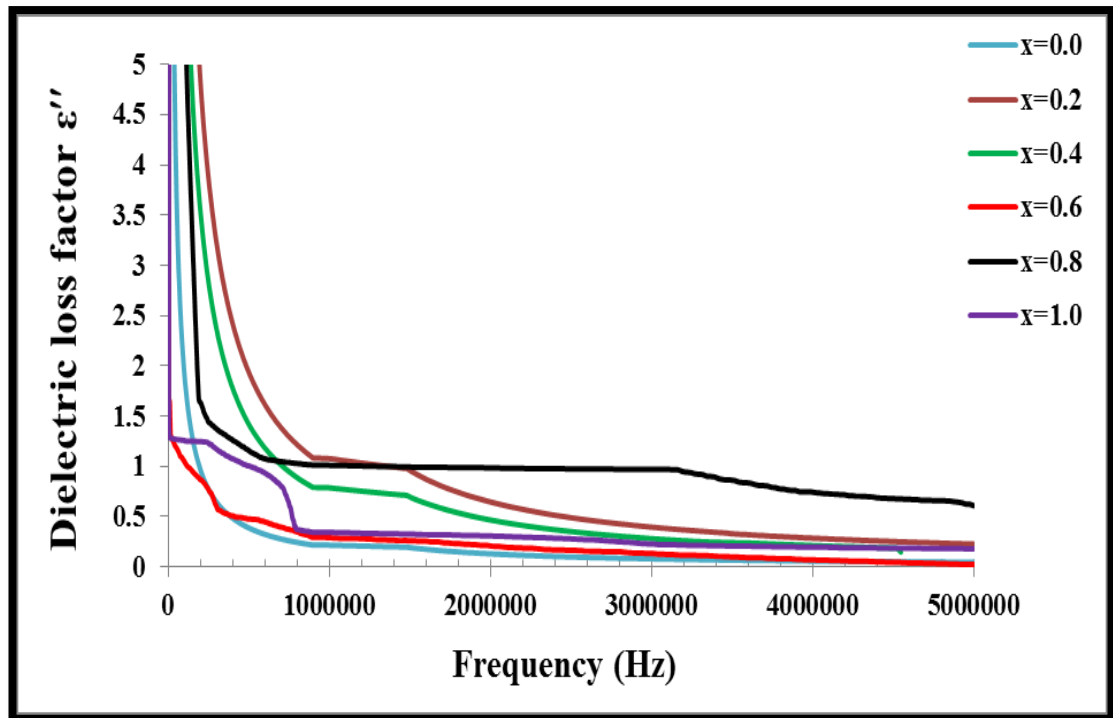


Figure (4-62): Dielectric loss factor (ϵ'') with frequency for $Tl_{0.5}Pb_{0.5}Ba_2Ca_2Cu_{3-x}Ni_xO_{9-\delta}$ specimens

Table (4-28) :Dielectric loss factor value (ϵ'') with the change of the amount of material replaced when frequency (50Hz -5MHz).

$Tl_{0.5}Pb_{0.5}Ba_2Ca_2Cu_{3-x}Ni_xO_{9-\delta}$						
X	" ϵ At (50 Hz)	" ϵ At (1MHz)	" ϵ At (2MHz)	" ϵ At (3MHz)	" ϵ At (4MHz)	" ϵ At (5MHz)
0.0	19414932	0.215	0.128	0.078	0.056	0.0452
0.2	133754.6	15.566	8.912	6.449	1.553	1.007
0.4	1378451	0.785	0.463	0.279	0.210	0.1339
0.6	450.148	0.291	0.205	0.1312	0.682	0.0232
0.8	11075.08	1.0098	0.984	0.969	0.7377	0.6075
1.0	205.622	0.343	0.3068	0.2264	0.1952	0.1788

4-5-4-3 Dielectric Loss Factor $|\tan \delta|$:

The ratio of energy dissipated and energy stored in the specimens determines the dielectric loss factor $|\tan \delta|$, figure (4-63) and table (4-29) showed varied the absolute value of the loss tangent $|\tan \delta|$ with the frequency and measured at room temperature, and note that the value of the angle of loss for all compounds is of low values, Gives an indication that the behavior of these compounds is similar to the normal behavior of ferroelectric materials where the four polarization mechanics are effective at low frequencies [163, 164]. Is plotted as a function of applied frequency-range 50 Hz -5MHz -for specimens as shown in Figure (4-63).

We noted from table (4-29) that the value of the loss tangent $|\tan \delta|$ has decreased with increased Ni concentration this agreement with the research[165].

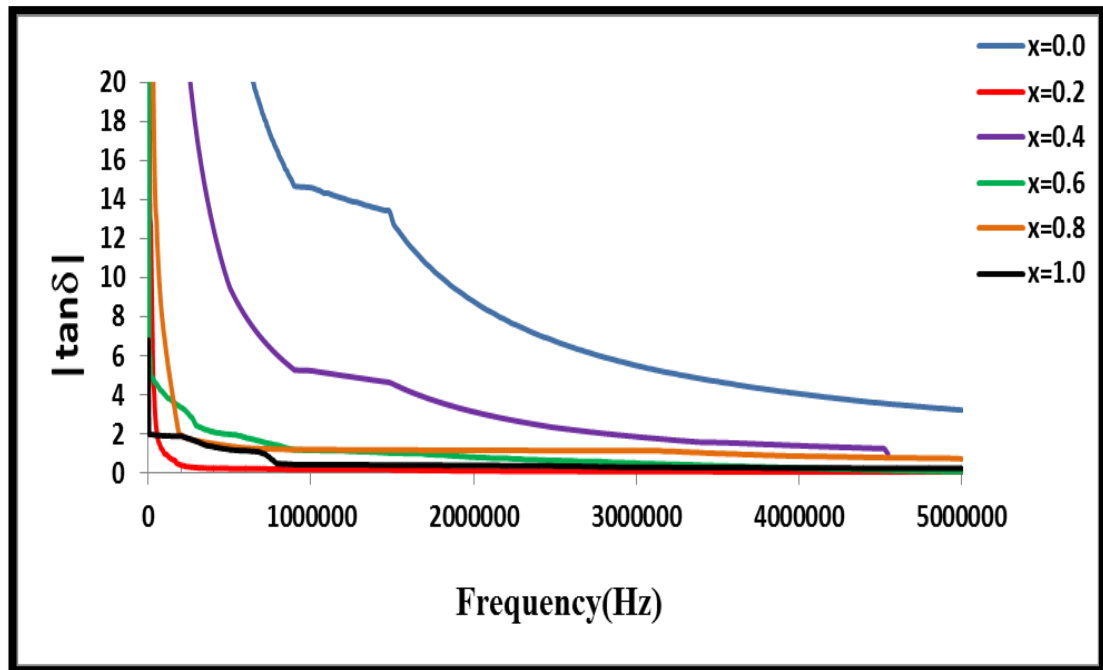


Figure (4-63): Variation of ($|\tan \delta|$) versus frequency of $Tl_{0.5}Pb_{0.5}Ba_2Ca_2Cu_{3-x}Ni_xO_{9.δ}$

Table (4-29) :Variation of ($|\tan \delta|$) versus frequency of $Tl_{0.5}Pb_{0.5}Ba_2Ca_2Cu_{3-x}Ni_xO_{8+\delta}$ with frequency (50HZ-5MHZ)

$Tl_{0.5}Pb_{0.5}Ba_2Ca_2Cu_{3-x}Ni_xO_{9-\delta}$						
X	$\tan \delta$ At (50 Hz)	$\tan \delta$ At (1MHz)	$\tan \delta$ At (2MHz)	$\tan \delta$ At (3MHz)	$\tan \delta$ At (4MHz)	$\tan \delta$ At (5MHz)
0.0	26089.1	14.61	8.739	5.490	4.055	3.244
0.2	71.914	0.215	0.137	0.102	0.026	0.0168
0.4	319.17	5.254	3.137	1.871	1.416	0.9608
0.6	133.326	1.192	0.831	0.525	0.273	0.960
0.8	1789.5	1.223	1.189	1.171	0.891	0.747
1.0	6.8227	0.459	0.415	0.323	0.286	0.2595

4-5-4-4 Alternating Electrical Conductivity (σ_{ac}):

The Alternating electrical conductivity (σ_{ac}) is measured at room temperature within the frequency (50Hz-5MHz) for $Tl_{0.5}Pb_{0.5}Ba_2Ca_2Cu_{3-x}Ni_xO_{9-\delta}$ with $x=0.0,0.2,0.4,0.6,0.8,1.0$ and $Pb=0.5$.

We noted from figure (4-64) and table (4-30) increase the alternating electrical conductivity (σ_{ac}) with frequency increased , Also note a change between increase and decrease in value of the Alternating electrical conductivity (σ_{ac}) with increased Ni concentration.

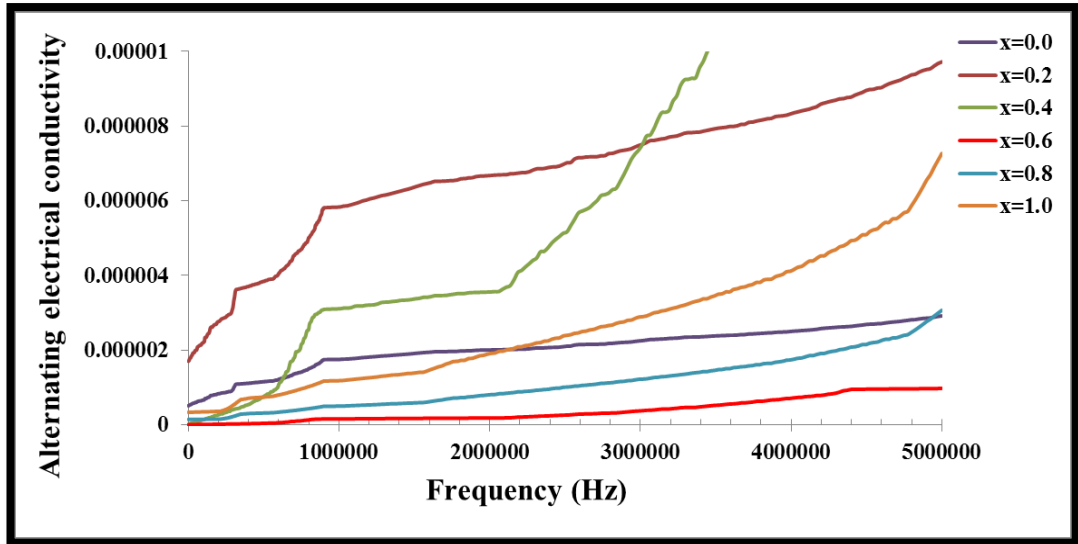


Figure (4-64) :Alternating electrical conductivity(σ_{ac}) with frequency for $Tl_{0.5}Pb_{0.5}Ba_2Ca_2Cu_{3-x}Ni_xO_{9.5}$

Table (4-30): Alternating Electrical Conductivity (σ_{ac}) with frequency (50Hz -5MHz).

$Tl_{0.5}Pb_{0.5}Ba_2Ca_2Cu_{3-x}Ni_xO_{9.5}$						
X	$\sigma_{a.c}$ ($\Omega.cm$) ⁻¹ At (50 Hz)	$\sigma_{a.c}$ ($\Omega.cm$) ⁻¹ At (1MHz)	$\sigma_{a.c}$ ($\Omega.cm$) ⁻¹ At (2MHz)	$\sigma_{a.c}$ ($\Omega.cm$) ⁻¹ At (3MHz)	$\sigma_{a.c}$ ($\Omega.cm$) ⁻¹ At (4MHz)	$\sigma_{a.c}$ ($\Omega.cm$) ⁻¹ At (5MHz)
0.0	5.1×10^{-7}	1.75×10^{-6}	2.0×10^{-6}	2.25×10^{-6}	2.51×10^{-6}	2.91×10^{-6}
0.2	1.7×10^{-6}	5.83×10^{-6}	6.68×10^{-6}	7.51×10^{-6}	8.35×10^{-6}	9.71×10^{-6}
0.4	3.15×10^{-9}	3.104×10^{-6}	3.55×10^{-6}	7.52×10^{-6}	1.44×10^{-5}	1.95×10^{-5}
0.6	1.59×10^{-10}	1.55×10^{-7}	1.78×10^{-7}	3.76×10^{-7}	7.21×10^{-7}	9.75×10^{-7}
0.8	1.41×10^{-7}	4.97×10^{-7}	8.07×10^{-7}	1.22×10^{-6}	1.76×10^{-6}	3.06×10^{-6}
1.0	3.34×10^{-7}	1.18×10^{-6}	1.91×10^{-6}	2.89×10^{-6}	4.16×10^{-6}	7.26×10^{-6}

4-5-5 Result Of Mechanical Properties:

This test includes presenting and discussing the results of the effect of the Pb=0.5 of (Tl) and Ni (0.2,0.4,0.6,0.8,1.0) concentration of copper in the compound $Tl_{0.5}Pb_{0.5}Ba_2Ca_2Cu_{3-x}Ni_xO_{9.8}$, Compound when the state of excessive conductivity on its mechanical properties as well as the relationship of these characteristics to each other.

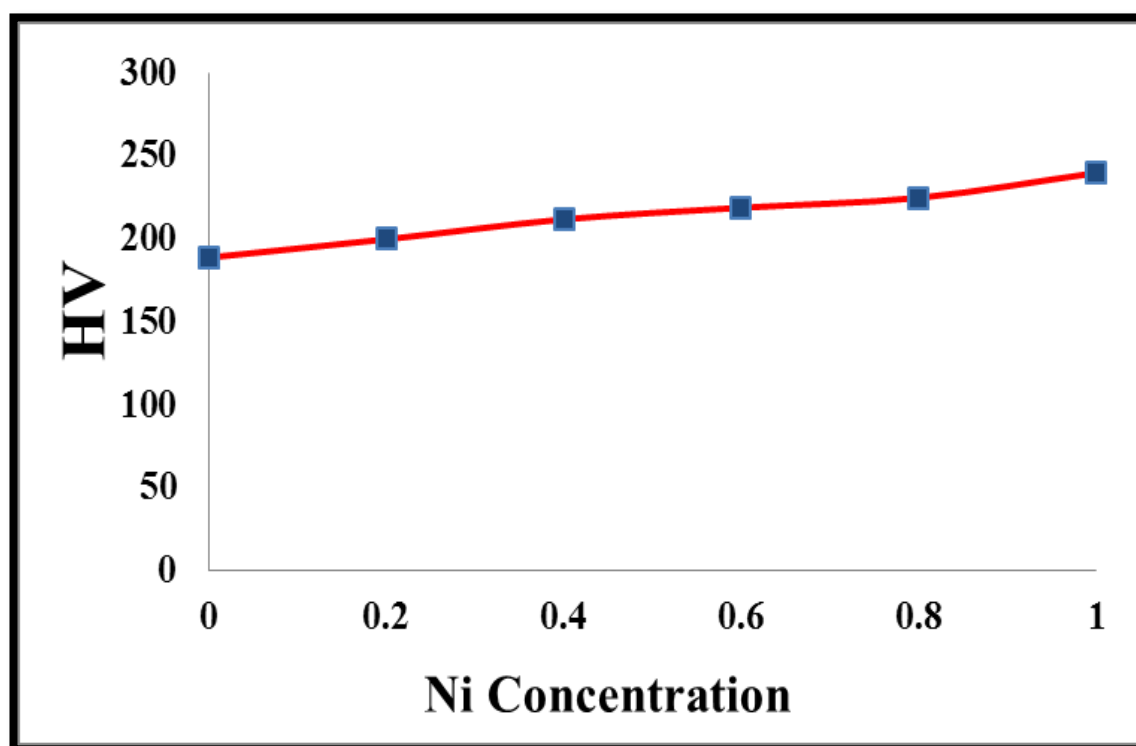
The mechanical properties, such as the Vickers micro- hardness (HV), yield strength (Y) and Young modulus (E) of superconductor specimens were calculated as referred in the previous paper [166].

The effects of nickel on the mechanical properties of $Tl_{0.5}Pb_{0.5}Ba_2Ca_2Cu_{3-x}Ni_xO_{9.8}$ specimens were studied. The specimens were pressed under $7(\text{ton}/\text{cm}^2)$. It is noticed from table (4-31) and Figure (4-65) an increases of the microhardness with increases of load for specimens with Pb-doping and increasing Ni concentration . This behavior may attribute to the presence of strong grain boundaries of the superconducting ceramics.

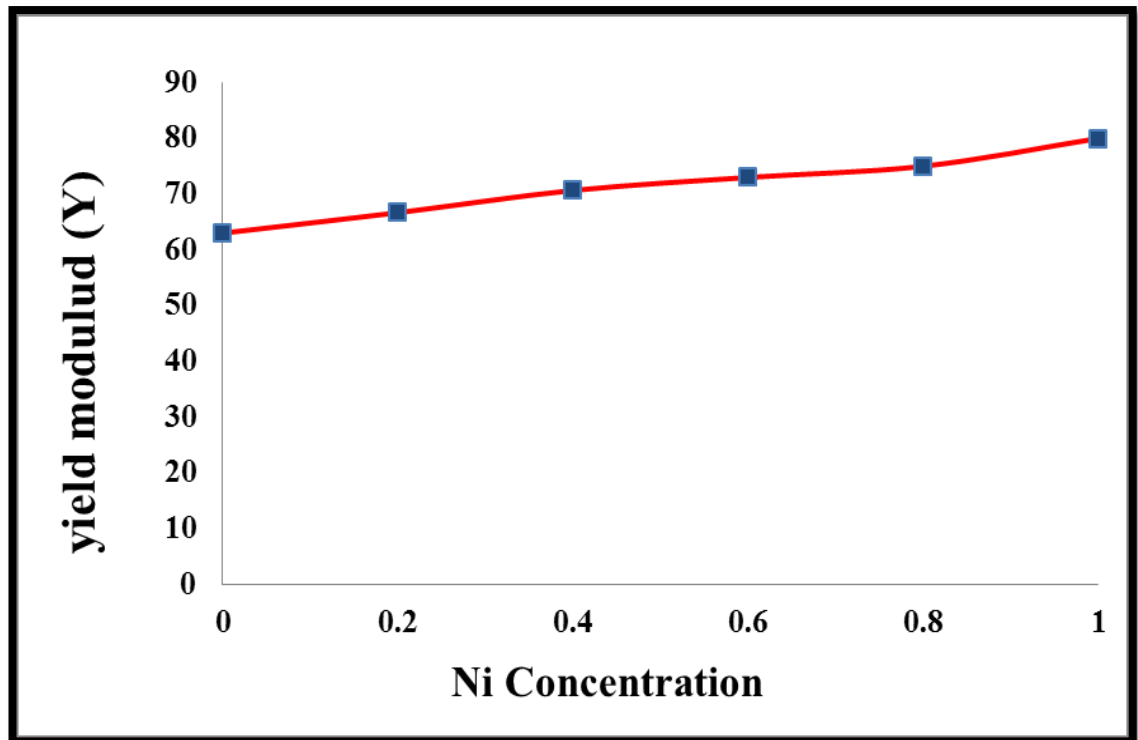
Figures(4-65),(4-66),(4-67) and Table(4-31) show the variation of Vickers microhardness, yield strength and Young modulus, as a function of Ni concentration . increase of microhardness, yield strength and Young's modulus was observed with increasing Ni concentration. This result indicates that an enhancement of the mechanical properties contacts which get rearranged to fill the voids and pores resulting in more densification of the specimen [167], which leads to a remarkable increase in the mechanical resistance of the specimens. This increase of mechanical properties is due to the increase in strength of bonding between the grains and consequently causes the strengthen compound.

Table (4-31): Vicker's Hardness Number (VHN) , Young modulus (E) and Yield strength (Y) for $Tl_{0.5}Pb_{0.5}Ba_2Ca_2Cu_{3-x}Ni_xO_{9+\delta}$ (for 15 sec &load=2.94N)

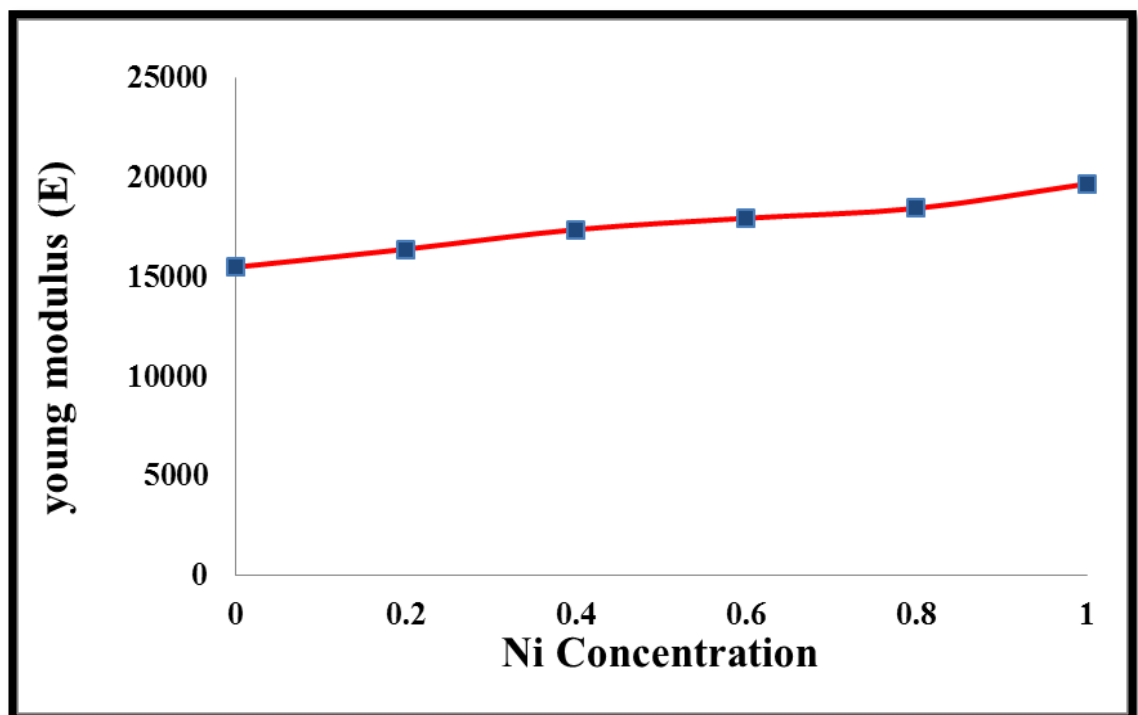
$Tl_{0.5}Pb_{0.5}Ba_2Ca_2Cu_{3-x}Ni_xO_{9+\delta}$					
x	Tim/ sec	Load N	Hv	E(MPa)	Y(MPa)
0.0	15	2.94	189	15490.44	63
0.2	15	2.94	200	16392	66.66
0.4	15	2.94	212	17375.52	70.66
0.6	15	2.94	219	17949.24	73
0.8	15	2.94	225	18441	75
1.0	15	2.94	240	19670.4	80



Figure(4-65): The variations of Vicker's Hardness Hv as a function Ni concentration .



Figure(4-66) :The variations of young modulus E a function Ni concentration .

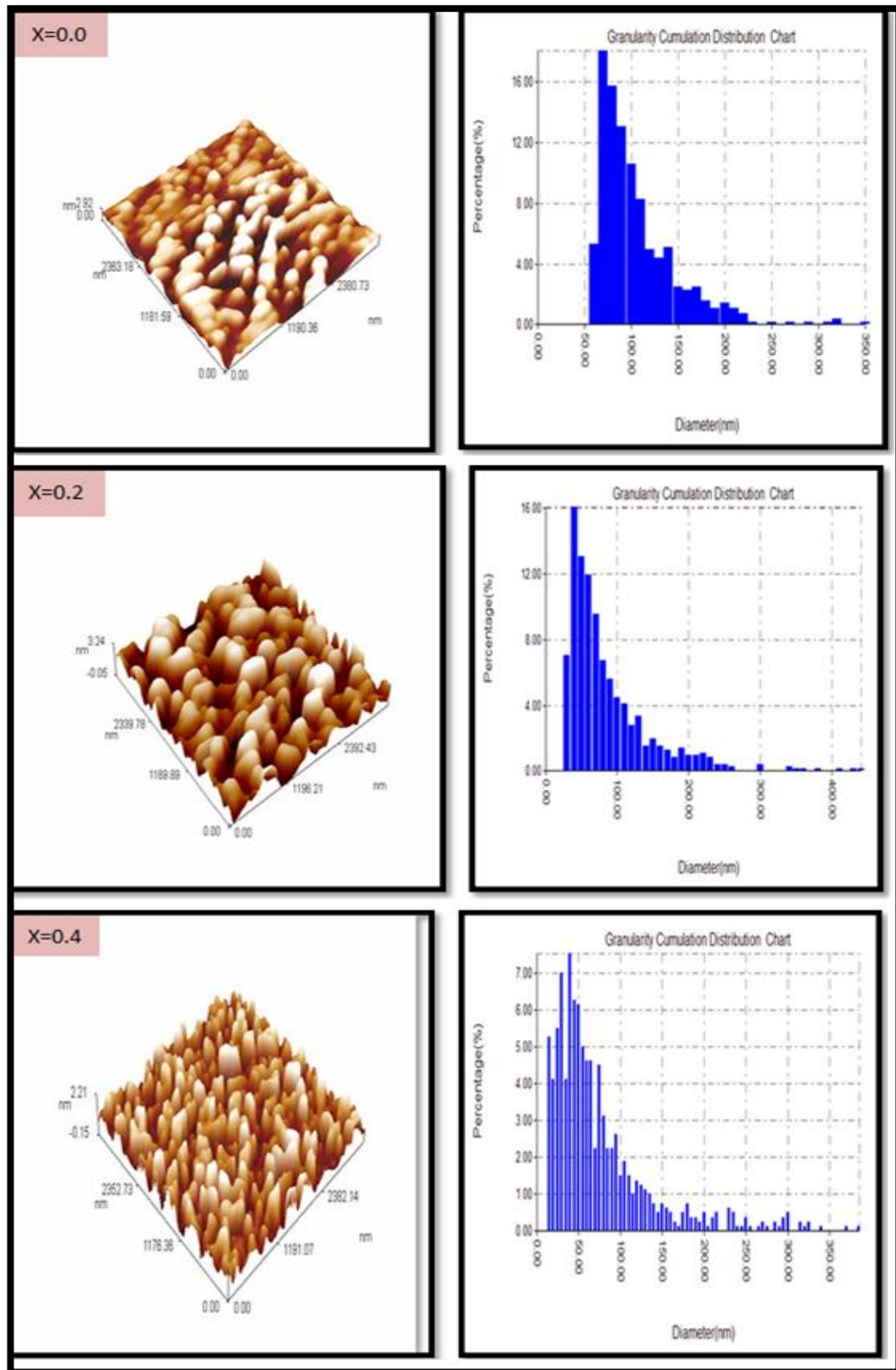


Figure(4-67): The variations of yield strength Y a function Ni concentration .

4-5-6 Results of Atomic Forces Microscopic AFM:

Analyzing the surface of these systems was made using atomic force microscopy (AFM)[141]. The images taken in this research of composition **Tl_{0.5}Pb_{0.5}Ba₂Ca₂Cu_{3-x}Ni_xO_{9-δ}** with Pb=0.5 and **x=0.0,0.2,0.4,0.6,0.8** and **1**. It is found that for the various Ni concentration with Pb-substitution lead to various Roughness(nm),Root mean square(nm) and Avg. Diameter(nm) and Crystal size shown in table (4-32) from AFM images. Figure (4-68) represent the 3-D AFM images of superconductor compounds for all specimens.

Figure (4-68): reveals the (3-D) AFM images and the chart distribution of $Tl_{0.5}Pb_{0.5}Ba_2Ca_2Cu_{3-x}Ni_xO_{9-\delta}$



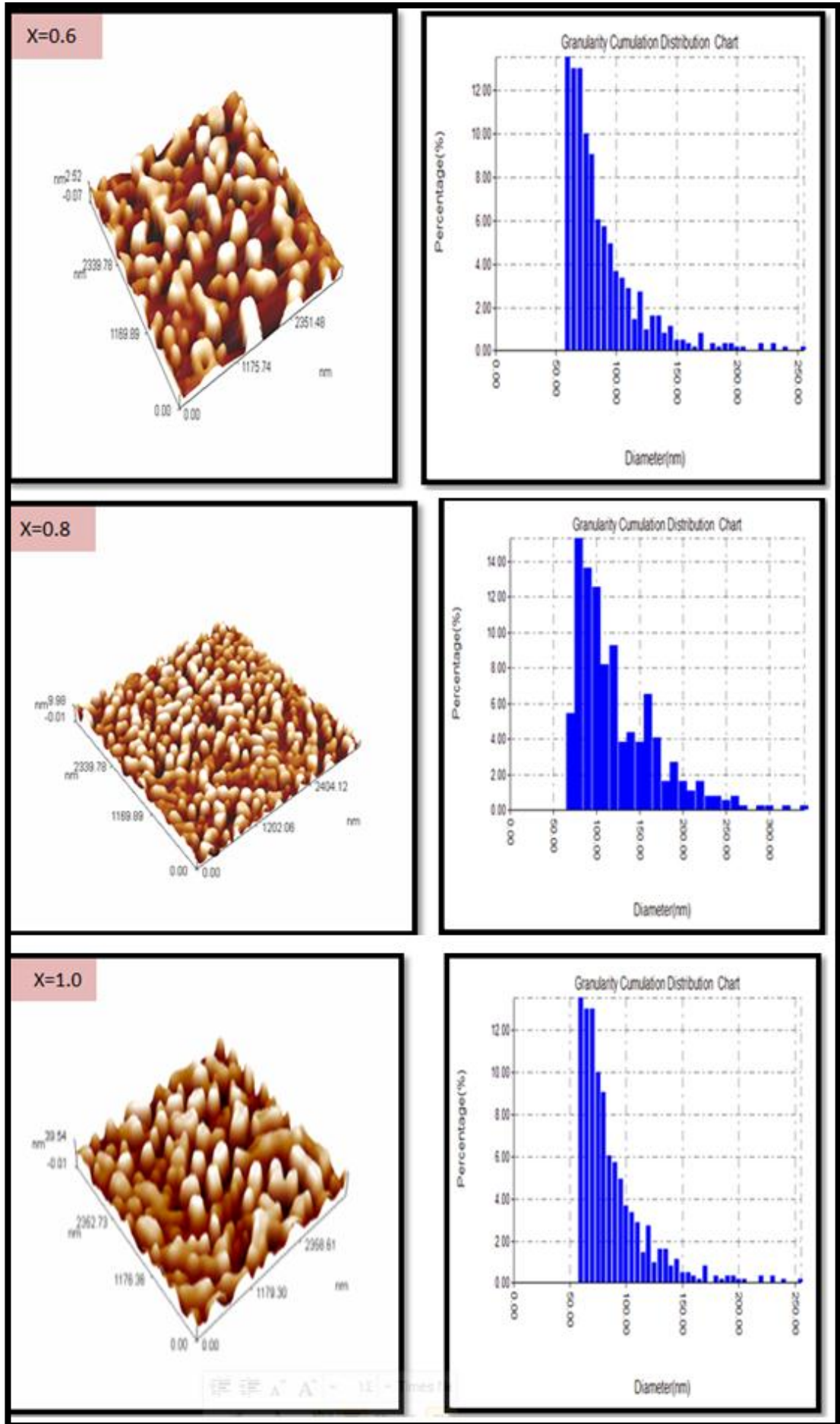


Table (4-32) : Values of average surface roughness ,Crystal size and Avg. Diameter in 2D for $Tl_{0.5}Pb_{0.5}Ba_2Ca_2Cu_{3-x}Ni_xO_{9-\delta}$

X	Crystallite size(nm)	Roughness (nm)	Root mean square(nm)	Avg. Diameter(nm)
0	32.81515	0.673	0.794	100.84
0.2	19.42573	0.769	0.892	81.88
0.4	35.70736	0.666	0.762	73.54
0.6	38.87102	0.474	0.56	84.89
0.8	27.99676	9.36	10.9	90.20
1.0	28.74334	0.259	0.348	118.85

Finally, when comparing the superconducting compounds($HgBa_2Ca_2Cu_{3-x}Ni_xO_{8+\delta}$, $TlBa_2Ca_2Cu_{3-x}Ni_xO_{9-\delta}$, $Hg_{0.5}Pb_{0.5}Ba_2Ca_2Cu_{3-x}Ni_xO_{8+\delta}$, $Tl_{0.5}Pb_{0.5}Ba_2Ca_2Cu_{3-x}Ni_xO_{9-\delta}$) for the results we obtained through the examinations: x-ray diffraction analysis, resistivity measurements, oxygen content determination and dielectric properties , , hardness and atomic force microscopy (AFM) for all specimens where Ni= (0.0,0.2,0.4,0.6,0.8and 1) .

Where we found the best specimens during the preparation shown in the table (4-33).

We have noted through the results of that partial substitution(Ni with Cu and Pb=0.5 with Hg ,Tl) has a positive effect on improving of the structural, electrical, mechanical and surface properties of superconducting compounds. We can see from result which obtained by choosing a best

specimens as shown in table (4-33), We can see from this table that there are clear differences between the four compounds , Where we noted that the best transition critical temperature was for the compound **Tl_{0.5}Pb_{0.5}Ba₂Ca₂Cu_{3-x}Ni_xO_{9-δ}** when x= 0.4 equal 140K and has volume fraction $V_{ph} 1223=83.8009$ as well as having the best size of crystalline (357.0736) and granular size (73.54) where it can be considered as an ideal specimen almost.

As for the dielectric and mechanical properties, the specimen (**TlBa₂Ca₂Cu_{3-x}Ni_xO_{9-δ} where x=0.6**) was the best at room temperature $\epsilon_{50Hz}=4385.58$, $\epsilon_{5MHz}=2131.14$, $H_v=232$.

Table (4-33): Comparison between of the best specimens of the critical transition temperature of the four compounds

Compounds	X	T_c (K)	δ	V_{ph} 1223	a=b ($^{\circ}$)
$HgBa_2Ca_2Cu_{3-x}Ni_xO_{8+\delta}$	0.6	138.5	0.0758	82.959	4.0798
$Hg_{0.5}Pb_{0.5}Ba_2Ca_2Cu_{3-x}Ni_xO_{8+\delta}$	0.8	139	0.1552	81.7370	3.8524
$TlBa_2Ca_2Cu_{3-x}Ni_xO_{9-\delta}$	0.6	134.6	0.0953	85.0467	3.5520
$Tl_{0.5}Pb_{0.5}Ba_2Ca_2Cu_{3-x}Ni_xO_{9-\delta}$	0.4	140	0.1925	83.8009	3.8379
Compounds	X	c ($^{\circ}$)	c/a ratio	d_m (gm/cm^3)	Crystallite size(nm)
$HgBa_2Ca_2Cu_{3-x}Ni_xO_{8+\delta}$	0.6	16.2484	3.9826	5.3485	40.1733
$Hg_{0.5}Pb_{0.5}Ba_2Ca_2Cu_{3-x}Ni_xO_{8+\delta}$	0.8	16.0635	4.1697	6.0907	22.36517
$TlBa_2Ca_2Cu_{3-x}Ni_xO_{9-\delta}$	0.6	16.0433	4.2174	7.2463	4.731678
$Tl_{0.5}Pb_{0.5}Ba_2Ca_2Cu_{3-x}Ni_xO_{9-\delta}$	0.4	15.811	4.1197	7.0979	35.70736
Compounds	X	ϵ 50Hz	ϵ'' 50Hz	$\tan\delta$ 50Hz	$\sigma_{a.c}$ 50Hz
$HgBa_2Ca_2Cu_{3-x}Ni_xO_{8+\delta}$	0.6	8.63683	11.922	9.421	$4.17*10^{-8}$
$Hg_{0.5}Pb_{0.5}Ba_2Ca_2Cu_{3-x}Ni_xO_{8+\delta}$	0.8	82.223	22115.13	22750.5	$1.32*10^{-6}$
$TlBa_2Ca_2Cu_{3-x}Ni_xO_{9-\delta}$	0.6	4385.58	110.309	1.562	$2.05*10^{-7}$
$Tl_{0.5}Pb_{0.5}Ba_2Ca_2Cu_{3-x}Ni_xO_{9-\delta}$	0.4	4318.86	1378541	319.17	$3.15*10^{-9}$
Compounds	X	ϵ 5MHz	ϵ'' 5MHz	$\tan\delta$ 5MHz	$\sigma_{a.c}$ 5MHz
$HgBa_2Ca_2Cu_{3-x}Ni_xO_{8+\delta}$	0.6	2.0959	1.051	0.2976	$3.93*10^{-6}$
$Hg_{0.5}Pb_{0.5}Ba_2Ca_2Cu_{3-x}Ni_xO_{8+\delta}$	0.8	36.602	39.987	0.649	$4.53*10^{-6}$
$TlBa_2Ca_2Cu_{3-x}Ni_xO_{9-\delta}$	0.6	2131.14	3.727	0.1079	$6.21*10^{-6}$
$Tl_{0.5}Pb_{0.5}Ba_2Ca_2Cu_{3-x}Ni_xO_{9-\delta}$	0.4	9.890	0.1339	0.9608	$1.95*10^{-5}$
Compounds	X	Hv	E	Y	Avg. Diameter (nm)
$HgBa_2Ca_2Cu_{3-x}Ni_xO_{8+\delta}$	0.6	141	11556.36	47	124.10
$Hg_{0.5}Pb_{0.5}Ba_2Ca_2Cu_{3-x}Ni_xO_{8+\delta}$	0.8	170	13933.2	56.66	87.11
$TlBa_2Ca_2Cu_{3-x}Ni_xO_{9-\delta}$	0.6	232	19014.72	77.33	81.86
$Tl_{0.5}Pb_{0.5}Ba_2Ca_2Cu_{3-x}Ni_xO_{9-\delta}$	0.4	212	17375.52	70.66	73.54

Conclusion

In our experimental work, we investigated the effect of partial substitution of both Pb and Ni on the superconducting compound ($\text{HgBa}_2\text{Ca}_2\text{Cu}_{3-x}\text{Ni}_x\text{O}_{8+\delta}$, $\text{TlBa}_2\text{Ca}_2\text{Cu}_{3-x}\text{Ni}_x\text{O}_{9-\delta}$, $\text{Hg}_{0.5}\text{Pb}_{0.5}\text{Ba}_2\text{Ca}_2\text{Cu}_{3-x}\text{Ni}_x\text{O}_{8+\delta}$, $\text{Tl}_{0.5}\text{Pb}_{0.5}\text{Ba}_2\text{Ca}_2\text{Cu}_{3-x}\text{Ni}_x\text{O}_{9-\delta}$), where we were able to successfully obtain superconducting specimens and within the preparatory conditions we adopted, To obtain the results and reflect on her study, we were able to obtain from these conclusions:

- ❖ The method of preparation has a very important role in the production of superconducting specimens Especially in the production of the higher phase (Hg-1223), (Tl-1223) .
- ❖ From (XRD) analysis , it was found that all of the specimens had tetragonal structure , and that the replacement with both Pb and Ni instead of (Hg ,Tl ,Cu) did not change of the crystalline structure for the pure specimen. The crystalline structure remains the same for all specimens. The specimens contain the phases (Hg-1223), (Hg-1212, Hg-1201) ,(Tl-1223), (Tl-1212, Tl-1201), with a few impurities
- ❖ The results of the XRD analysis showed that the high phase ratios (Hg-1223,Tl-1223) and the other phases, as well as the parameters of unit cell (a, b, c) and there is an increase of value for parameter c-axis value with the incrementing of Ni concentration , and the ratio of c / a and unit cell density were changed randomly compared to the pure specimen , Replacement for both Pb and Ni , Most of the specimens had a metallic behavior in terms of changing their electrical resistance by lowering the temperature before transition it into a superconducting state.

- ❖ The highest critical temperature for specimens sintered at 850 °C in air for 24h is 138.5 K for $\text{HgBa}_2\text{Ca}_2\text{Cu}_{2.4}\text{Ni}_{0.6}\text{O}_{8+\delta}$ under 7(ton/cm^2), 139 K for $\text{Hg}_{0.5}\text{Pb}_{0.5}\text{Ba}_2\text{Ca}_2\text{Cu}_{2.2}\text{Ni}_{0.8}\text{O}_{8+\delta}$, 134.6 K for $\text{TlBa}_2\text{Ca}_2\text{Cu}_{2.4}\text{Ni}_{0.6}\text{O}_{9-\delta}$, 140 K for $\text{Tl}_{0.5}\text{Pb}_{0.5}\text{Ba}_2\text{Ca}_2\text{Cu}_{2.6}\text{Ni}_{0.4}\text{O}_{9-\delta}$
- ❖ The results of Iodometric titration for high superconductor compounds ($\text{HgBa}_2\text{Ca}_2\text{Cu}_{3-x}\text{Ni}_x\text{O}_{8+\delta}$, $\text{TlBa}_2\text{Ca}_2\text{Cu}_{3-x}\text{Ni}_x\text{O}_{9-\delta}$, $\text{HgPbBa}_2\text{Ca}_2\text{Cu}_{3-x}\text{Ni}_x\text{O}_{8+\delta}$, $\text{TlPbBa}_2\text{Ca}_2\text{Cu}_{3-x}\text{Ni}_x\text{O}_{9-\delta}$) show an enhancement of (δ)value with the increase of Ni concentration.
- ❖ In our present research, shown the positive effect nickel concentration on superconducting compounds Hg-based cuprate and Tl-based cuprate in the improvement of structure ,electrical, and mechanical properties.
- ❖ In the hardness test, we observed an increase in the value of The Vickers microhardness (HV), Young's modulus (E) and yield strength (Y) with increasing Ni concentration and also the partial substitution of lead . The results showed that the effect of lead and nickel substitution has a positive effect on the mechanical properties measurement.
- ❖ The measurement of dielectric constant ,dielectric loss factor and $|\tan \delta|$ decrease with the increase of frequency (50 Hz -5MHz) for the all specimens .
- ❖ The surface morphology ,average grain size and surface roughness for all prepared specimens showed an improvement in homogeneous and uniformity.

Suggestion For Future Works

- ❖ Study the effect of pressure on critical temperature of high superconductor compounds ($\text{HgBa}_2\text{Ca}_2\text{Cu}_{3-x}\text{Ni}_x\text{O}_{8+\delta}$, $\text{TlBa}_2\text{Ca}_2\text{Cu}_{3-x}\text{Ni}_x\text{O}_{9-\delta}$, $\text{HgPbBa}_2\text{Ca}_2\text{Cu}_{3-x}\text{Ni}_x\text{O}_{8+\delta}$, $\text{TlPbBa}_2\text{Ca}_2\text{Cu}_{3-x}\text{Ni}_x\text{O}_{9-\delta}$).
- ❖ Preparation of high superconductor compounds ($\text{Bi}_2\text{Ba}_2\text{Ca}_2\text{Cu}_{3-x}\text{Ni}_x\text{O}_{10+\delta}$ and $\text{Bi}_{2-x}\text{Pb}_x\text{Ba}_2\text{Ca}_2\text{Cu}_{3-y}\text{Ni}_y\text{O}_{10+\delta}$ where $x=0.5$ and $y=0.2,0.4,0.6,0.8,1.0$ and $\text{Bi}_{2-x}\text{Pb}_x\text{Ba}_2\text{Ca}_2\text{Cu}_{3-y}\text{Ni}_y\text{O}_{10+\delta}$ ($x=0.5, y=0.5$) for balanced values and study all physical properties of compounds and preparation of high superconductor compounds ($\text{HgBa}_2\text{Ca}_2\text{Cu}_{3-x}\text{Ni}_x\text{O}_{8+\delta}$, $\text{TlBa}_2\text{Ca}_2\text{Cu}_{3-x}\text{Ni}_x\text{O}_{9-\delta}$, $\text{Hg}_{0.5}\text{Pb}_{0.5}\text{Ba}_2\text{Ca}_2\text{Cu}_{3-x}\text{Ni}_x\text{O}_{8+\delta}$, $\text{Tl}_{0.5}\text{Pb}_{0.5}\text{Ba}_2\text{Ca}_2\text{Cu}_{3-x}\text{Ni}_x\text{O}_{9-\delta}$) where $x=0.5, 0.55, 0.65, 0.7$ ($0.5 \geq x \geq 0.7$).
- ❖ Preparation of high superconductor compounds ($\text{HgBa}_2\text{Ca}_2\text{Cu}_{3-x}\text{Ni}_x\text{O}_{8+\delta}$, $\text{TlBa}_2\text{Ca}_2\text{Cu}_{3-x}\text{Ni}_x\text{O}_{9-\delta}$, $\text{Hg}_{0.5}\text{Pb}_{0.5}\text{Ba}_2\text{Ca}_2\text{Cu}_{3-x}\text{Ni}_x\text{O}_{8+\delta}$, $\text{Tl}_{0.5}\text{Pb}_{0.5}\text{Ba}_2\text{Ca}_2\text{Cu}_{3-x}\text{Ni}_x\text{O}_{9-\delta}$) by sol-gel method and thin film by pulse laser deposition method and studying all the measurements (electrical resistivity and XRD).
- ❖ Choosing the best specimens obtained at high temperature and carry out a partial replacement of silver(nano size) with copper.
- ❖ Measuring the dielectric properties Under cooling for compound prepared ($\text{HgBa}_2\text{Ca}_2\text{Cu}_{3-x}\text{Ni}_x\text{O}_{8+\delta}$, $\text{TlBa}_2\text{Ca}_2\text{Cu}_{3-x}\text{Ni}_x\text{O}_{9-\delta}$, $\text{Hg}_{0.5}\text{Pb}_{0.5}\text{Ba}_2\text{Ca}_2\text{Cu}_{3-x}\text{Ni}_x\text{O}_{8+\delta}$, $\text{Tl}_{0.5}\text{Pb}_{0.5}\text{Ba}_2\text{Ca}_2\text{Cu}_{3-x}\text{Ni}_x\text{O}_{9-\delta}$).
- ❖ studying the characterization of high superconductor compounds ($\text{HgBa}_2\text{Ca}_2\text{Cu}_{3-x}\text{Ni}_x\text{O}_{8+\delta}$, $\text{TlBa}_2\text{Ca}_2\text{Cu}_{3-x}\text{Ni}_x\text{O}_{9-\delta}$, $\text{HgPbBa}_2\text{Ca}_2\text{Cu}_{3-x}\text{Ni}_x\text{O}_{8+\delta}$, $\text{TlPbBa}_2\text{Ca}_2\text{Cu}_{3-x}\text{Ni}_x\text{O}_{9-\delta}$) for all the measurements (SEM, DTA, TG and magnetic properties).

References

References

- [1] M.A. Omar, "Elementary solid state physics", 5th ed., Addison – Wesley, (1993).
- [2] Mollie Reichert ,Leila Humes , "Superconductivity and superconductors " (2016).
- [3] B.John.Fredrich.Muller , "The development of SQUID-based gradiometers" MSC thesis, Stellenbosch University, (2010).
- [4] K. Onnes, A .V. w. chppen 14 818. (1911).
- [5] W. Meissner and R . Ochsenfeld ; Naturwissenschaften , 21, 787 (1993).
- [6] F. London and H. London " super fluids 1" , 152 (1950).
- [7] M.M. Abbass" effect of the electron beam and laser radiation on Tc of $Y_{1-x}(Gd,Br)_x Ba_{2-y}Sr_y Cu_{3.7-s}$ compound ,(2003).
- [8]] B . Batlogg , "Physical Properties of High – Tc Superconductors" , phys V.44, P.44, (1991).
- [9] J . G . Bednoz and K.A. Muller, phys. B64,189, (1986).
- [10] C.W. Chu , P. H. Hor , R.L.Meng , L .GaO and Z. J. Huang, Science 58 567. (1987).
- [11] G.C.KIM,D. Ahmed ,Y. C .Kim. J of superconductivity and Novel Magnetism . V 25, pp 67-70, (2012).
- [12] H. Maeda ,Y.Tanaka ,Fukatomi ,T.Asano, Jap.J. Appl.Phys.27(1988)L209.
- [13] I.Verma ,R. Rawat , D.M.Phase ,B. Dasj of superconductivity and Novel Magnetism. V25,pp 85-90, (2012).
- [14] A. Schilling, M.Gantoni, H.V. Niessen and H.R. Otl: Phys.V215N1

References

- P11(1993).
- [15] William D. Callister , Jr . " Materials Science and Engineering " 7th ed (2007).
- [16] Junjing . Zhao , PhD. thesis Dept. Physics , Graduate College , University of Illinois at Chicago, (2012).
- [17] J. Axnas, I. Bryntse, I. Safanova and O. Rapp: Phys B, V.284-288, P. 1010 (2000).
- [18] R. Giri, H. K. Singh, R. S. Tiwari & O. N. Srivastova : Bull. Mater . Sci , V 24, No. 5, PP. 523 – 528 (2001).
- [19] N.H. Hamdan , P.V.P.S.S. Sarstry , and J.Schwartz: Phys C., V. 356, No. 254, P. 1-4 (2001).
- [20] E. Altshuler, C.W.Chu, M. T. Orland, A. Sin, A. J. Batista-Leyva, V. Buntar, and H. W. Weber, Phys C: superconductivity, V.371, Issue. 3, PP.224 , (2002).
- [21] S. H. Han, I. Bryntse, J. Axnas, B. R . Zhao, and O . Rapp : Phys C: Superconductivity , V.388-389, PP.349-350 (2003).
- [22] I. Hase , N. Hamada & Y. Tanaka : Phys , superconductivity C V.412 – 414 , No. 1, P. 246 (2004).
- [23] M. Monteverde , C. Acha , M. Nunez – Regueiro , D. A. Pavlov, K. A. Lokshin , S. N. Putilin and E. Antipor : Euro phys Lett , V. 72 , No. 3 P.458 , (2005).
- [24] L . K . Abbas "Effect of Ag and In substitutions and superconducting properties of the Hg $1-x$ (Ag , In) x Ba $2-y$ Sry Ca 2 Cu 3 O $8+\delta$ " Ph.D. Thesis, Baghdad University , (2006).
- [25] G. Y. Hermiz "Effect of Pressure on the Properties of HgBa 2 Ca 2 Cu 3 O $8+\delta$ HTSC System" Iraqi Journal of Physics, Vol. 5, No.1, (2008).
- [26] K. A. Jassim "Influence of Simultaneous Doping of Tl on the Transition Temperature Tc and the Lattice Parameters of HgBa 2 Ca 2 Cu 3 O $8+\delta$

References

- Superconductors" *Ibn Al-Haitham Jour. for Pure & Appl. Sci.* ,Vol. 22 No . 3, (2009) .
- [27] O. Babych , Ya. Boyko, I. Gabriel, R. Luticiv, M. Matviyiv and M. Vasyuk "Preparation and Properties of Doped Hg-Based Superconducting Copper Oxides" *Acta Physica Polonica* , Vol. 117, No. 1, (2010).
- [28] K . A. Jasim , M . Abdul - Nebi , M . M. Ali ," Synthesis and Study Structural and Electrical Properties of $\text{Hg}_{0.5}\text{Pb}_{0.5-x}\text{Sb}_x\text{Ba}_2\text{Ca}_2\text{Cu}_3\text{O}_{8+\delta}$ Superconductors", *Ibn Al-Haitham Jour. for Pure & Appl. Sci*, VOL.24 (2), (2011).
- [29] Kareem A. Jasim ," Superconducting Properties of $\text{Hg}_{0.8}\text{Cu}_{0.15}\text{Sb}_{0.05}\text{Ba}_2\text{Ca}_2\text{Cu}_3\text{O}_{8+\delta}$ Ceramic with Controlling Sintering Conditions", *Journal of Superconductivity and Novel Magnetism*, VOL.19 (1), (2012).
- [30] Shibing Wang , Jianbo Zhang, Jinyuan Yan , Xiao-Jia Chen , Viktor Struzhkin , Wojciech Tabis, Neven Barisic, Mun K. Chan, Chelsey Dorow, Xudong Zhao, Martin Greven, Wendy L. Mao and Ted Geballe "Strain derivatives of T_c in $\text{HgBa}_2\text{CuO}_{4+\delta}$: The CuO_2 plane alone is not enough" *physical review B* ,Vol 89, (2014).
- [31] Muna . Moussa . Abbass "Raman Studies of $\text{Hg}_{1-x}\text{Ca}_x\text{Ba}_2\text{Ca}_2\text{Cu}_3\text{O}_{8+\delta}$ Compounds" *Eng. &Tech. Journal*, Vol. 32, No.2, (2014) .
- [32] N. M. Hamdan , P.V.P.S.S. Sastry and J. Schwartz "Magnetic Properties of Fluorinated Pb-doped Hg-1223 High T_c Superconductors" *Journal of Physics, Conference Series* 289, (2015) .
- [33] B. Loret, S. Sakai, Y. Gallais , M. Cazayous, M. A. Measson , A. Forget, D. Colson, M. Civelli and A. Sacuto "Unconventional high-energy-state contribution to the cooper pairing in under-doped copper-oxide superconductor $\text{HgBa}_2\text{Ca}_2\text{Cu}_3\text{O}_{8+\delta}$ " *cond - mat .supr -con* ,(2016).

References

- [34] Noor S. Abed, Sabah J. Fathi , Kareem A. Jassim," Effect of Partial Substitution of Ag on the Structural and Electrical Properties of High Temperature $\text{HgBa}_2\text{Ca}_2\text{Cu}_3\text{O}_{8+\delta}$ Superconductor", International Journal of Recent Research and Applied Studies, Volume 4, Issue 6 (18) June (2017).
- [35]K A Jasim and L A Mohammed," The partial substitution of copper with nickel oxide on the Structural and electrical properties of $\text{HgBa}_2\text{Ca}_2\text{Cu}_3\text{Ni}_x\text{O}_{8+\delta}$ superconducting compound", Journal of Physics: Conference Series ,volume 1003, (2018).
- [36] J. Prauch, T. Konig, G. Gritzner and K. Prybylski , Physica C, V.331, p.227, (2000).
- [37] P. Badica, A. Crrisonn and H. Ihara , Physica C , V.378, p.683, (2002).
- [38] T. S. Kayed , Cryst. Res. Technal , V.38 , No.11, p.946 , (2003).
- [39] K. Kuzman, Z. Klencsar ,A. Sasvari , Z. Homonnay , M. Mair and A. Vertes , Physica C , V.420, p.17, (2004).
- [40] K. Przybylski , O. Heiml and G. Gritzner , Physica C , V. 423, p.63,(2005)
- [41] R Awad , A I Abou-Aly , S A Mahmoud and M ME Barakat ," Thermal expansion measurements using x-ray powder diffraction of Tl-1223 substituted by molybdenum",Superconductor Science and Technology, Volume 20, Number 4 ,(2007).
- [42] Kareem A. Jassim,Tariq J.Alwan,"The Effect of Simultaneous Substitution of Strontium at the Barium site of $\text{Tl}_{0.6}\text{Pb}_{0.4}\text{Ba}_{2-x}\text{Sr}_x\text{Ca}_2\text{Cu}_3\text{O}_{9-\delta}$ Superconductors", J Supercond Nov Magn 861–865:22, (2009).
- [43] AI Abou Aly, IH Ibrahim, R Awad, A El-Harizy, A Khalaf," Stabilization of Tl-1223 phase by arsenic substitution", Journal of superconductivity and novel magnetism, Volume23,Issue 7,p.p 1325-1332,(2010).
- [44] E .ErbilenŞ, ÇavdarH ,Koralay A. Günen ,"Effect of vanadium substitution on the microstructural and superconducting properties of $\text{Tl}_2\text{Ba}_2\text{Ca}_{2-x}\text{V}_x\text{Cu}_3\text{O}_y$ superconductors", Physica B: Condensed Matter

References

- V 413, Pages 36-39, 15 March (2013).
- [45] M.G.Ranjbar,R.Abd-Shukor," Formation of Tl-1223 phase in Cr substituted $(Tl_{1-x}Cr_x)Ba_2Ca_2Cu_3O_{9-\delta}$ ($x=0.3$ to 0.9) superconductor" Ceramics International, Volume 40, Issue 9, Part A, , Pages 13869-13872 (2014).
- [46] M. G. Ranjbar, R. Abd-Shukor , " Excess Conductivity and Superconducting Fluctuation Analysis of Cr-Substituted Tl-1223 Type Phase and $(Tl_{1-x}Cr_x)Ba_2Ca_2Cu_3O_{9-\delta}$ ($x = 0.4-0.8$), Journal of Superconductivity Novel Magnetism, Volume 29, pp 2235-2240,(2016).
- [47] S.L.Kakani ,Amit Kakani," Material Science ", 2004.
- [48] A. Magsood and M. Magsood, " Proceeding of the international workshop held at Rajshahi university" Bangladesh edited by AKMA Islam, 28, (1996).
- [49] W. Meissner,and R.Ochsenfeld ; Naturwissenschaften , 21, 787 (1993).
- [50] J. C. Phillips "Physics of High-Tc Superconductors" Printed in the U.S.A.(1992).
- [51] M. A. Omar, „Elementary solid state physics principles and applications,, Ch 10, Addison-Wesley, (1975).
- [52] Ginzburg V . L and Andry shin E . A ., " Superconductivity ", world publishing , p 63 ,(2004) .
- [53] A.C.Rose-Innes and E.H. Rhoderick, "Introduction to superconductivity" Pergamon Press, (1978).
- [54] Ginzburg and Andryushin , Superconductivity ,p 63,(1998).
- [55] Bardeen J , Cooper L. N and Schrieffer J. R , Theory of Superconductivity Phys. Rev.volume 108 , number 5, p1175 , (1957) .
- [56] Waing C.S , " Electronic structure , Lattice Dynamics and magnetic Interations in High temperature Superconductivity ,W. Lynn ,springer (1990) .

References

- [57] Werner Buckel , and Reinhold Kleiner " Superconductivity fundamentals and Applications " , Second Edition , Wiley , p 160 , (2004).
- [58] د. يحيى نوري الجمال، "فيزياء الحالة الصلبة"، ط2، جامعة الموصل، (2000).
- [59] Charles P. Poole, Jr, Horacio A. Farach ,Richard J. Creswick," Superconductivity " , Elsevier Ltd ,Second Edition ,p.p23,(2007).
- [60] J. W. Halley"Theories of High Temperature Superconductivity" Addison-Wesley, (1988).
- [61]Charles Kittel "Introduction to solid state physics " six addition, Copyright by John Wiley and Sons in (1986).
- [62] V.L. Ginzburg and L.D. Landau, Zh. Eksp. Teor. Fiz. 20, 1064 (1950) .
- [63] A. Mourachkine , " Room-Temperature Superconductivity " , Cambridge International Science Publishing (2004).
- [64] A. C. Rose-Innes and E. H. Rhoderick , " Introduction to Superconductivity", M. C. Grawhill, New York (1978).
- [65] Z . M . Galasiewicz , " Superconductivity and Quantum Fluids " Vol.29 Pergamon Press Warszawa (1970).
- [66] J.R.Gavaler:Appl.phys.Lett.V.23, P.480, (1973).
- [67] E . Maxwell , Phys.Rev.V.78, P.477, (1950)
- [68] J .W. Garland, Phys.Rev.Lett.V.11, P.114, (1963).
- [69] Md. Atikur Rahman , Md . Zahidur Rahaman , Md . Nurush Samsuddoha "A Review on Cuprate Based Superconducting Materials Including Characteristics and Applications" ,American Journal of Physics and Applications , Vol. 3, No. 2, pp. 41-51, (2015).
- [70] Paul A .Tipler and Ralph A . Liewellyn , " Modern physics " fourth Edition , freeman New York , pp 487 - 495 , (2002).
- [71] Ajay Kumar Saxena," High-Temperature Superconductors" , 2nd Edition (2012).

References

- [72] A. Schilling et al , "Superconductivity above 130 K in the Hg–Ba–Ca–Cu–O system" , Nature 363, 56 (1993).
- [73] Z. Z. Sheng and A. M. Hermann., Nature (London), V.332, P. 55, (1998).
- [74] D. Pavlov " Synthesis and Properties of Substituted Hg-based Superconductors : Ph . D . University of Stockholm, Department of Inorganic Chemistry (2004).
- [75] E. V. Antipov, J. J. Capponi , Chaillout, O. Chaissem, O. M. Loureiro, M. Marezie , S. N. Putin, Santoro and O. L. Tholence : Phys C. Superconductivity, V. 218, Issuer 3 -4, P . 348 , (1993).
- [76] M-S. Kim, K-T. Kim, H-J. Kim, K-H. Kim, J-J. Kio, J-D. Kim, S-I. Lee and A. Lyo: Solid state communications: V. 133, P. 459 (2005).
- [77] O. Chmaissem, L. Wessels, and Z. Z. Sheng: Phys C, V. 230, P. 231-238 (1994).
- [78] F. Herman R . .Kasowski and W .Y.Hsu :phys. Rev . B,V.38,No .1,P. 204. (1988).
- [79] B. Batlog, T. T. M. Palstra , L .F .Schneemeyer , R. B. Van Dover and R. J Cava : Physica C , V.(153-155), P. 1062, (1988).
- [80] S. A. Sunshine , T. Siegrist , L. F. Schneemeyer , D. W. Murphy , R. J. Cava: Phys. Rev. B, V.38, P.893, (1988).
- [81] D. Allender, J. Bray and J. Bardeen: Phys. Rev., B, V.7, P.1020, (1973).
- [82] C .M. Varma, S. Schnitt -Rink and E. Abrahams: Solid State Commun., V.6 No.10, P.681, (1987).
- [83] W. Weber : Phys. Rev. Lett. V.58, No.13, P.1371, (1987)
- [84] J. R. Schrieffer, X .G. Wen and S. C. Zhang: Phys. Rev. Lett , V.60, P .944 (1988)
- [85] V. L. Ginzburg , Sov.:Phys.-Usp.13, 335, (1970)
- [86] <http://www.ort.edu.uy/Redos/Supercon.html>.
- [87] J. W. Lynn, "High Temperature Superconductivity" Springer-Verlag (1990)

References

- [88] V.Z. Kresin and S.A.Wolf, "Fundamentals of Superconductivity" Plenum Presses, New York, (1990).
- [89] T . Kirschner, J . Bankuti , M . Gal and K .Torkos : phys . Rev ., B,P.2313 (1987).
- [90] D . A . Porter, K . E . Easter ling , " phase transformation in Materials and allays ", Ch . 1, (1992).
- [91] S. P. Kruchinin;"Physics of High-Tc Superconductors" American Scientific Publishers, Vol. 2, pp. 1–22, (2014)
- [92] Shreelekha Mishra," SYNTHESIS AND CHARACTERIZATION OF Superconductors composite $\text{Bi}_2\text{Sr}_2\text{Ca}_1\text{Cu}_2\text{O}_8/\text{La}_{0.85}\text{Sr}_{0.15}\text{MnO}_3$ ",Ph.D National Institute of Technology, Rourkela, India, (2012) .
- [93] P. A . Tipler , R. A. Llewlyly " Modren physics " fourth edition , freeman New York , pp 487 - 495 , (2003).
- [94] A.Mourachkine "Room-Temperature Superconductivity", Cambridge International Science Publisher First Published (2004) .
- [95] ISTE 1998 International Workshop on Superconducting Materials and Technology Issues for HTS Wires and Bulk Applications", Hotlin Applied Superconductivity- July, (1998).
- [96] P. Komarck , Supercond.Sci Technol.V.13, P.456. (2000) .
- [97] K.K. Likharev, Dynamics of Josephson Junctions and Circuits", Gordon and Breach Science Publishers, P.30, (1986).
- [98] J.P. Jones "Materials science for electrical and electronic engineers" Ch 11, University of Birmingham Oxford University press, Inc .New York, P287,(2001) .
- [99] L. Solyner and D.Walsh "Electrical properties of materials" ,Oxford, York Tokyo, Oxford University, press , p.365 (1998).
- [100] Shoji . Tanaita "High-temperature superconductivity: History and out look" SAP international ,V.10-13, No. 4 (2001).

References

- [101] P.J Ford and G.A.Saunders " high temperature superconductors Eten years on " contemporary .Phys ,J ,V.38, No.1 ,P63, (1997) .
- [102] G.Y.Hermiz, B.A.Aljurani, H.A.Thabit, Journal of superconductivity and Novel Magnetism Vol. 25, No .6 ,1629-1634, (2012) .
- [103] K.Aka, M. Saito,M.Ito, K. Nakan and Heromiunoki “ Advances in superconductivity” Kitazawa, Ishigguro {EDS},p225 -227, Aug. (1988).
- [104] M. R. Beasley “ Advances in superconductivity” Kitazawa, Ishiguro (EDS) 3- 15 (1988).
- [105] Oka-Ridge ,National Laboratory.Oran Facilities and Equipment for use in High-Temperature Superconductivity Research and Development (2004)
- [106] S. A. Sunshine, T. Siegrist, L.F. Schneemeyer, D. W. Murphy, R.J. Cava: Phys. Rev. B, V.38, P 893,(1988) .
- [107] Kareem Ali Jassim , " The Effect of Cadmium Substitution on The Superconducting properties of $Tl_{1-x}Cd_xBa_2Ca_2Cu_3O_{9-\delta}$ Compound" Journal of superconductivity and novel magnetism , vol 26 , pp 549 – 552 , (2013) .
- [108] Barsoum M . W, " Fundamentals of Ceramics " , university of Oxford UK Iop publishing Ltd , pp 304 - 306 ,(2003) .
- [109] C. W. Chu, L. Gao, F. Chen, Z. J. Huang, R. L. Meng, Y. Y. Xue, Nature vol 365, p 323(1993) .
- [110] A. Simon, P.S.Mukherjee , M.S.Sarma and A.D.Damodaram : J.Mater. Sci., V.29. P.5059, (1994).
- [111] G.C.Che, Y.K.Du, F.Wu, Y.Yang, C.dong and Z.X.Zhao Solid state Commun., V.89, No.11, P.903,(1994).
- [112] Brian S .Mitchell"An Introduction to materials Engineering And Science" wiley , inc , p p 45 - 60 , (2004) .
- [113] Vijaya Kumar K and Sreekanth T "Solid State Physics"Chand &company Ltd , New Delhi ,(2005).

References

- [114] BIJU. A; "structure and transport properties of pure earth modified (Bi,Pb)superconductors" ,thesis university of kerala ,p52,(2007).
- [115] Ebtisam Khalil Alwan Al-beyaty ; "Effect of n variation on Tc of (Hg_{0.8}Tl_{0.2})Ba₂Can-1CunO_{2n+2+δ} compounds" , MS. Thesis ,Baghdad university , college of science ,pp 38-39, (2007).
- [116] Kareem Ali Jassim " Comparison Study of Transition Temperature Between the Superconducting Compounds Tl_{0.9} Pb_{0.1}Ba₂Ca₂Cu₃O_{9-δ} Tl_{0.9}Sb_{0.1}Ba₂Ca₂Cu₃O_{9-δ} and Tl_{0.9}Cr_{0.1}Ba₂Ca₂Cu₃O_{9-δ} " acceptor in Eight International Conference on Material Sciences CSM8 - ISMS UNE SCO palace , Beirut - Lebanon , May 28-30 , (2012) .
- [117] Witold Ciesielski and Robert Zakr Zewski " Iodimetric Tiration of Sulfur Compounds in Alkaline Medium " chem . Anal . Vol 51 , p 653 , (2006).
- [118] Agilent Basics of Measuring the Dielectric Properties of Materials - Application Note , (2005).
- [119] Raghavan V ," Materials Science and Engineering " ,fifth Edition , A soke k . Ghosh Limited , New Delhi , pp 412 - 414 , (2010).(
- [120] Kwan Chi Kao"Dielectric phenomena in solids " ,Elsevier Academic press p p 54 - 60 , (2009).
- [121] Ali M .Omer," Elementary Solid State physics" fifth Impression , Dorling Kindersley Ltd , pp 372 - 380 , (2009).
- [122] Bhat , M , Kaur, B , Kumar, R , Bamzai , K.K , Kotru , P.N ,and Wanklyn B . M . V.234 , P 494 , (2005).
- [123] M. Musa Abbas ," Mechanical Properties of Bi_{2-x}CdxPb_{0.3}Sr₂Ca₂ Cu₃O_{10+δ} superconductors",International Journal of Current Engineering and Technology, Vol.5, No.3,June (2015.(
- [124] BoltonW,"Engineering Materials Technology" ,3'ed,Butterworth-Heinemann , Oxford , p 293 ,(1998) .
- [125] BrianS.Mitchell "An Introduction To Materials Engineering and Science"

References

- John Wiley & Sons, (2004).
- [126] Jinho Yang, Ilkyu Yang, Yun Won Kim, Dongwoo Shin, " Construction of a ^3He magnetic force microscope with a vector magnet", 19 January (2016).
- [127] M. Pantić a, S. Mitrović a, M. Babić a, D. Jevremović b," AFM Surface Roughness and Topography Analysis of Lithium Disilicate Glass Ceramic " Tribology in Industry, Vol. 37, No. 4,P.P 391-399,(2015).
- [128] Valentina Roxana Vlad " Growth And Characterization of Chemical Solution " thesis , university of Barcelona , P 37 ,(2011) .
- [129] Bharat Bhushan " Handbook of Nanotechnology " ,springer,P 331 (2004)
- [130] G.Xing, M.Wang, X.Fan and X.Tang, : Appl.Phys. A56, P.99 ,(1993).
- [131] B.Solunke, P.U. Sharma, M. P. Pandya , V. K. Lakhani, K.B. Modi, P. Venugopl Reddy and S. S. Shah .Indian Academy of Sciences, | joul of physics, V.12, N.32, P. 1,(2005).
- [132] S. Koyama, U. Endo and T. Kawai :Jap.J. Appl. Phys , 27, 10, L1861 (1988).
- [133] A. Ohta, A. Kirihigashi , Y.Sasaki and K. Ohba:Jap.J.Appl.Phys, V.27, No.12, P.L2289,(1988) .
- [134] Y. Mizauno , A. Sawa, H. Obara, M. Umeda , and H. Yamasaki, Physica C2255, pp 282-287, (1997).
- [135] V. Manivannan et al, Synthesis of Cuprates of Perovskite Structure in the Ba-Pb-Cu-O, Ba-Bi-Cu-O, and Ba-Pb-Tl-Cu-O Systems: Possible High T_c Superconductivity in a Perovskite -like Phase in the Ba- Pb –Tl -Cu-O System, Journal of Solid State Chemistry 109, p.p 205-209,(1994).
- [136] M . M. Abbas " Influences of the Cu Substitution at Hg Site in $\text{Hg}_{1-x}\text{Cu}_x\text{Ba}_2\text{Ca}_2\text{Cu}_3\text{O}_{8+\delta}$ Superconductors " Iraqi Journal of Physics, Vol. 5, No. 1, (2008).
- [137] Tom Timusk , LA physIQUE AU CANADA ,vol.67,No.2 ,(2011).

References

- [138] J . Zhao , M . Wu , W . Abdul – Razzaq and M . S . Seehra : *physica C* V . 165 , P . 135, (1990).
- [139] Noor Q. Fadhel " study the effect of (Y₂O₃,SbO₂) additives on the dielectrically properties of [Hg-1223] compound” *International Journal for Sciences and Technology* ,Vol.11, No.1,(2016)
- [140] Mumtaza M , Liaqat A,Shoaib A, Saad U, Hssaina G, Rabbania M,Abdul Jabbar,Nadeem K "Dielectric properties of (Zn)_x/CuTi-1223 Nanoparticle – superconductor composites", *Journal of Advanced Ceramics*, vol.5, \ No.2, (2016).
- [141] Salma M. Shaban,Bushra M, Matti N and Raad M. S, "Substitution Effect on Dielectric Permittivity and AC Conductivity of Bi_{2-x}(CuPb)_xSr₂Ca₂Cu₃O_{10+δ} Compound”, *International Journal of Application or Innovation in Engineering & Management (IJAIEM)*, Vol.2 No. 3, (2013).
- [142]Wagner KW. Zur Theorie der unvollkommenen Dielektrika. *Annalen der Physik* , 345: 817–855, (1913).
- [143] Tselev A,Brooks CM,Anlage SM,et al.Evidence for power-law frequency dependence of intrinsic dielectric response in the CaCu₃Ti₄O₁₂. *Phys Rev B* , 70: 144101, (2004).
- [144] Intisar Abbas Hamad," Synthesis of High Temperature Superconductor HgBa_{2-x}Y_xCa_{n-1}Cu_nO_{2n+2+δ}Substituted with Yttrium for n=1 and n=2" *International Journal of Science and Research (IJSR)* , Volume . 6 Issue 3 March (2017).
- [145]G. Binnig, C. F. Quate, and C. Gerber. Atomic Force Microscope. *Phys. Rev. Lett.* 56, 930(1986).
- [146] Bharat Bhushan," Surface Roughness Analysis and Measurement Techniques", (2001).
- [147] Angela Duparre´, Josep Ferre-Borrull, Stefan Gliech," Surface characterization techniques for determining the root-mean-square roughness and

References

- power spectral densities of optical components", APPLIED OPTICS
Vol. 41, No. 1 ,p.p 155, (2002).
- [148] Kareem. A . Jasim , Muhammed Abdul- Nebi and Mostafa M Ali
"Synthesis and study Structural and Electrical properties of $\text{Hg}_{0.5}\text{Pb}_{0.5-x}\text{Sb}_x\text{Ba}_2\text{Ca}_2\text{Cu}_3\text{O}_{8+\delta}$ superconductors", Vol.24(2), (2011).
- [149] N. M. Hamdan, Kh. A. Ziq A. S. Al-Harhi, Physica C, vol. 314 ,P.P 125-132,(1999).
- [150] Kareem A. Jasim," Superconducting Properties of $\text{Hg}_{0.8}\text{Cu}_{0.15}\text{Sb}_{0.05}\text{Ba}_2\text{Ca}_2\text{Cu}_3\text{O}_{8+\delta}$ Ceramic with Controlling Sintering Conditions", J Supercond Nov Magn , volume 19, No 1,(2006).
- [151] Sukru Cavdar , Haluk Koralay, Nihat tuğluoğlu , " Frequency-dependent dielectric characteristics of Tl-Ba-Ca-Cu-O bulk superconductor"
Supercond. Sci. Technol. 18,p.p1204–1209, (2005).
- [152] Y . Ikeda , M . Takano , Z . Hiroi , K . Oda , H . Kitaguchi , J . Takada , O . Yamamoto and H . Mazaki : Jpn . J . Appl . phys., V . 27, No . 3, P . L372,(1988) .
- [153] G. A. AL-Dahash; (Effect of Deformation on Electronic Structure and Magnetic properties of Some High Temperature Superconductors) Ph.D Thesis, Baghdad University, College of Science (1998).
- [154] Jasim , K .A . : Comparison study of T_c between the superconducting Compounds $\text{Bi}_{2-x}(\text{Hg,Pb})_x\text{Sr}_{2-y}\text{Ba}_y\text{Ca}_2\text{Cu}_3\text{O}_{10+\delta}$ and $\text{Hg}_{1-x}\text{Pb}_x\text{Sr}_{2-y}\text{Ba}_y\text{Ca}_2\text{Cu}_3\text{O}_{8+\delta}$. Ph.D. thesis, University of Baghdad, College of Science, Physics Dep., Iraq ,(2005).
- [155] W. Shaohong, Z. Heping, and L. Linghong, Materials Research Bulletin, 1367-1374, 38(8), (2003).
- [156] W. Ryan, "Clay sand ceramic raw material", Applied Science publishers LTD ,London, (1979)
- [157] Jassim, K.A., Alwan, T.J.: J. Supercond. 22, 861 ,(2009)

References

- [158] W.B. Michel, "Fundamentals of ceramics", 1st edition, Mc. Grow-Hill Book, Inc. New York. (1997).
- [159] C.K. Saman, K. Parasad., N.P. Choudhary, "Bull.Mater. Sci." Vol.27, No.6 (2004).
- [160] W.D. Kinger , H.K. Bowden, D.R. Uhlmann , "Introduction to ceramic" Second ed., John Wiley and Sons. (1976).
- [161] X.Du, I.W. Chen , "J.Am. Ceram. Soc." Vol.81 , P 3253,(1998).
- [162] K.S .Jin , "J. Kore. Phy. Soc. "Vol.43, No.6 , PP. 1081-1086,(2003).
- [163]C.K. Saman, K. Parasad., N.P. Choudhary,"Bull.Mater. Sci." Vol.27, No.6 (2004).
- [164] C.K. Suman, K. Prasad, R.N. Choudhary, "Mater. Sci. Lett." Vol.11, P 788,(2003).
- [165] P.Jha, Ashok, A. Ganguli, "Proc. Indian Acad.Soc.(Chem. Sci.)", Vol.115 No.5 and 6 , PP. 431-438, (2003).
- [166]G. Y. Hermiz, B. A. Aljurani and H. A. Thabit, "Mechanical Properties of $\text{Bi}_{1.6}\text{Pb}_{0.4}\text{Sr}_{1.8}\text{Ba}_{0.2}\text{Ca}_2\text{Cu}_{3-x}\text{Ni}_x\text{O}_{10+\delta}$ Superconducting System " Journal of Superconductivity and Novel Magnetism, Vol. 25, No. 6, pp. 1629- 1634, doi:10.1007/s10948-012-1584-3 , (2012).
- [167] V. M . Anandakumar and M. A. Khadar , " Microhardness Studies of Nanocrystalline Calcium Tungstate " Crystal Research and Technology Vol. 43, No. 2, pp. 193- 199. doi:10.1002/crat. 20071098 , (2008).

الملخص

يتضمن البحث الحالي تحضير المركبات الفائقة التوصيل كل من $\text{HgBa}_2\text{Ca}_2\text{Cu}_3$.



و $\text{Tl}_{0.5}\text{Pb}_{0.5}\text{Ba}_2\text{Ca}_2\text{Cu}_{3-x}\text{Ni}_x\text{O}_{9-\delta}$ ودراسة تأثير الاستبدال الجزئي لكل من (Pb) بدلا من (Hg,Tl) و (Ni) بدلا من (Cu) على الخواص التركيبية، والخواص الكهربائية والخواص الميكانيكية للمركبات اعلاه حيث أن $\text{Pb}=0.5$ وقيمة Ni ($x=0.0,0.2,0.4,0.6,0.8$ and 1). وهدفت الدراسة الى التحري عن الظروف ونسب الاستبدال المثلى لتشكيل الطور العالي (Hg-) (1223)، (TI-1223) واستقراره ومحاولة الحصول على اعلى درجة حرارة انتقال حرجة (High-T_c)، وكذلك لمعرفة المديات الترددية التي من الممكن ان تعمل بها هذه العينات في الظروف الاعتيادية.

حضرت العينات بطريقة تفاعل الحالة الصلبة، وذلك باستخدام أوزان مناسبة من مساحيق اكاسيد عالية النقاوة من ($\text{HgO}, \text{Ti}_2\text{O}_3, \text{CaO}, \text{CuO}, \text{PbO}, \text{NiO}$)، و تم خلط المساحيق باستخدام الهاون اليدوي لمدة (40-60) دقيقة، ثم كبست خلطات المساحيق الناتجة باستخدام مكبس هيدروليكي تحت ضغط كبس مقدارها ($7\text{ton}/\text{cm}^2$) ولمدة دقيقتين، على شكل أقراص ذات قطر (1.5cm) وسمك يتراوح بين (0.2-0.3cm). تم تلييد العينات في الهواء الاعتيادي وتحت درجة حرارة (850°C) ولمدة (24hr) وبمعدل تسخين ($5^\circ\text{C}/\text{min}$) وذلك للحصول على مادة مترابطة ولضمان عملية انتشار تدريجي امثل بين الذرات. ثم بعد ذلك تم تبريد العينات إلى درجة حرارة الغرفة بمعدل التسخين نفسه.

اظهرت نتائج فحص حيود الاشعة السينية (XRD) أن جميع العينات تمتلك نظاما بلوريا رباعي (tetragonal)، وبيئت احتواءها على النسبة الكبرى من الطور العالي (Hg-1223)، Ti-(1223) مع نسب قليلة من الأطوار الواطئة (Hg-1212)(Ti-1212)، (Ti-1201)، (1201) مع ظهور بعض الشوائب، وان اعلى نسبة للطور (Hg-1223) كانت للعينات

$\text{HgBa}_2\text{Ca}_2\text{Cu}_{2.4}\text{Ni}_{0.6}\text{O}_{8+\delta}$ ، $\text{Hg}_{0.5}\text{Pb}_{0.5}\text{Ba}_2\text{Ca}_2\text{Cu}_{2.2}\text{Ni}_{0.8}\text{O}_{8+\delta}$ التي تساوي على التوالي (82.959%)، (81.737%) وكذلك أعلى نسبة للطور (TI-1223) كانت للعينات $\text{Tl}_{0.5}\text{Pb}_{0.5}\text{Ba}_2\text{Ca}_2\text{Cu}_{2.6}\text{Ni}_{0.4}\text{O}_{9-\delta}$ ، $\text{TlBa}_2\text{Ca}_2\text{Cu}_{2.4}\text{Ni}_{0.6}\text{O}_{9-\delta}$ وهي على التوالي (85.046%)، (83.800%). كما اظهرت نتائج قياس ثوابت الشبكة (a=b,c) تزايد في قيمة c وتم حساب النسبة (c/a) وحساب كثافة وحدة الخلية ان العينات اعلاه تمتلك اعلى قيمة

للمحور (c) وهذه القيم هي على التوالي $(c=16.2484\text{\AA})$ ، $(c=16.0635\text{\AA})$ ،
 $(c=16.0433\text{\AA})$ ، $(c=15.8110\text{\AA})$.

ومن خلال اختبار سلوك العينات من حيث تغير المقاومة الكهربائية كدالة لدرجة الحرارة باستخدام تقنية الاقطاب الاربعة (Four-Probe Technique) حصلنا على قيم درجات حرارة الانتقال الحرجة، وقيم فجوة الطاقة للعينات، حيث أظهرت جميع العينات سلوكا معدنيا فائق التوصيل و ذات درجة حرارة انتقالية عليا، حيث تم الحصول على درجة حرارة انتقالية في العينة $(\text{HgBa}_2\text{Ca}_2\text{Cu}_{2.4}\text{Ni}_{0.6}\text{O}_{8+\delta})$ حيث كانت تساوي $(T_c=138.5\text{K})$ والتي امتازت كذلك بأعلى قيمة لفجوة الطاقة $(E_g=0.0421\text{eV})$ و $(\text{Hg}_{0.5}\text{Pb}_{0.5}\text{Ba}_2\text{Ca}_2\text{Cu}_{2.2}\text{Ni}_{0.8}\text{O}_{8+\delta})$ درجة الانتقال الحرج تساوي $(T_c=139\text{K})$ وقيمة فجوة الطاقة $(E_g=0.0419\text{eV})$ ، $(\text{TlBa}_2\text{Ca}_2\text{Cu}_{2.4}\text{Ni}_{0.6}\text{O}_{9-\delta})$ $(T_c=134.6\text{K})$ وقيمة فجوة طاقة $(E_g=0.0409\text{eV})$ و كذلك للعينه $(\text{Tl}_{0.5}\text{Pb}_{0.5}\text{Ba}_2\text{Ca}_2\text{Cu}_{2.6}\text{Ni}_{0.4}\text{O}_{9-\delta})$ قيمة اعلى درجة حراره انتقال حرج تساوي $(T_c=140\text{K})$ وقيمة فجوة طاقة $(E_g=0.0425\text{eV})$.

اما الخواص العزلية للعينات التي تتضمن (ثابت العزل الحقيقي، وثابت العزل الخيالي، والفقان العزلي، والتوصيلية الكهربائية المتناوبة) فقد تمت دراستها كدالة للتردد وللمدى $(50\text{Hz}-5\text{MHz})$ في درجة حرارة الغرفة، وقد لوحظ ان هناك تغيرا واضحا في الخواص العزلية من خلال الاستبدال الجزئي ب (Pb) و (Ni)، و ان كل من ثابت العزل الكهربائي (الحقيقي و الخيالي) ومعامل فقد العزلي يقلان مع زيادة التردد ويبدأن بالاستقرار بعد تردد $(\sim 10\text{KHz})$ وان التوصيلية الكهربائية المتناوبة تزداد بازدياد التردد. ومنه نستنتج ان الخواص العزلية ولجميع العينات تعتمد بصورة كبيرة على كل من نسبة الاستبدال وكذلك على التردد.

تم حساب الخواص الميكانيكية للعينات المحضرة حيث لوحظ ان قيمة الصلادة المايكروية للعينات المحضرة تزداد بزيادة نسبة الاستبدال الجزئي بالرصاص و النيكل نسبة الى العينة النقية. ولمعرفة صفات سطح العينات من حيث خشونة اجرينا فحص AFM مجهر القوة الذرية حيث اظهرت العينات تركيبا رقائقيا مع تغيرات في التجانس و التوزيع، حيث كانت العينة $\text{Tl}_{0.5}\text{Pb}_{0.5}\text{Ba}_2\text{Ca}_2\text{Cu}_{2.6}\text{Ni}_{0.4}\text{O}_{9-\delta}$ هي الافضل بالنسبة للمركبات المحضرة معدل قطر الحبيبي يساوي 73.54 نانومتر.

وقد لوحظ ان تأثير الاستبدال الجزئي بالنيكل بدلا من النحاس بثبوت نسبة الرصاص كان ذا اثر ايجابي وعلى جميع الخواص من حيث التركيب وكذلك من حيث درجات الحرارة الحرجة ومن حيث الخواص العزلية والميكانيكية للمركبات فائقة التوصيل.



جمهورية العراق
وزارة التعليم العالي والبحث العلمي

جامعة بغداد

كلية التربية للعلوم الصرفة (ابن الهيثم)
قسم الفيزياء

دراسة و مقارنة تأثير الاستبدال الجزئي للنكل بالنحاس على الخواص الفيزيائية للمركبات الفائقة التوصيل

أطروحة قدمتها

لهيب أحمد محمد الحمداني

إلى

مجلس كلية التربية للعلوم الصرفة (ابن الهيثم) - جامعة بغداد
كجزء من متطلبات نيل درجة الدكتوراه في فلسفة علوم الفيزياء

بإشراف

أ.د. كريم علي جاسم